AN INVESTIGATION INTO THE ACCURACY OF SINGLE FREQUENCY PRECISE POINT POSITIONING (PPP)

A thesis submitted in fulfilment of the requirements for the degree of Doctor of Philosophy

Sue Lynn Choy

B. App. Sc. (Hons)

School of Mathematical and Geospatial Sciences

College of Science, Engineering and Health

RMIT University

June 2009

Declaration

I certify that except where due acknowledgement has been made, the work is that of the author alone; the work has not been submitted previously, in whole or in part, to qualify for any other academic award; the content of the thesis is the result of work which has been carried out since the official commencement date of the approved research program; and, any editorial work, paid or unpaid, carried out by a third party is acknowledged.

……..

Sue Lynn Choy

17 June 2009

Acknowledgements

I would like to thank everyone who has contributed, directly or indirectly, to the realisation of my PhD thesis.

I would like to express my sincere gratitude to my supervisors, Professor Kefei Zhang and Dr. David Silcock, who supported me, encouraged me, provided me with guidance, and kept my spirits up all through my candidature at RMIT University. Their vast knowledge and experience in conducting research are top-notch.

I would also like to thank the Geodetic Survey Department of the Natural Resources of Canada (NRCan) for kindly providing the Canadian Spatial Reference System – Precise Point Positioning (CSRS-PPP) software package. In particular Mr. Pierre Héroux, Mr. François Lahaye and Mr. Pierre Tétreault from NRCan for promptly answering questions regarding the technical aspects and usage of the software. In addition, I would like to thank Mr. Pierre Sauvé from NRCan for providing the GPSMap©76C GPS data.

To all of my colleagues at the School of Mathematical and Geospatial Sciences, who have helped me with my research and also made my time at the School so enjoyable. In particular, I would like to thank Mr. Lucas Holden and Mr. Rod Deakin for their constructive input with regard to this research.

Dr. Xingliang Huo from the Graduate School of the Chinese Academy of Sciences is thanked for his technical discussions and assistance with generating the Australia-wide Regional Ionosphere Maps. He is also acknowledged for teaching me programming in FORTRAN.

Mr. Chris Blazkow from Ultimate Positioning is thanked for providing the Trimble Geoexplorer®GeoXH (2005 series) GPS data, which were used in this study.

Finally, I would like to express my deepest gratitude to my family, for their love, patient, encouragement, understanding and support. Without them, I would not have found the courage and persistent to travel this road.

Abstract

This thesis investigates the major errors and processes affecting the performance of a viable, standalone point positioning technique known as single frequency Precise Point Positioning (PPP). The PPP processing utilises both single frequency code and carrier phase GPS observables. The mathematical model implemented is known as the *code and quasi-phase* combination. Effective measures to improve the quality of the estimated positioning solutions are assessed and proposed.

The *a priori* observations sigma (or standard deviation) ratio in the sequential least squares adjustment model plays a significant role in determining the accuracy and precision of the estimated solutions, as well as the solutions convergence time. An "optimal" observations sigma ratio is found using an empirical approach, whereby different sigma ratios are tested and evaluated. It is concluded that an *a priori* code and quasi-phase sigma ratio of 1:50 provides optimal performance irrespective of the ionospheric conditions and the location of the GPS receiver. This is an innovative attribute of the research.

The feasibility of using Regional Ionosphere Maps (RIMs) to improve the accuracy of the single frequency PPP solutions is also examined. The performance of the RIMs is evaluated as a function of geographical locations and different ionospheric conditions. The quality of the estimated point positioning solutions based on the RIMs is then compared to those using the Broadcast model and the Global Ionosphere Maps. It is concluded that the RIMs are advantageous for GPS stations located in the low latitude regions and also during periods of high ionospheric activity.

The single frequency PPP solutions convergence is investigated with respect to i) satellite clock corrections at different sampling rates, ii) varying observation sampling intervals, and iii) the different tropospheric delay mitigation methods. It is found that the clock corrections and observations sampling intervals have minimal impacts on the solutions convergence time. However, in order to improve the time of convergence, the use of a modelled tropospheric delay (instead of estimating the tropospheric delay as part of the solutions) is recommended.

The viability of using the various International GNSS Service (IGS) satellite orbit and clock corrections in single frequency PPP processing, particularly the near real-time and real-time products, is evaluated. The outcomes of this study demonstrate the potential benefits of the near real-time and real-time corrections for high accuracy point positioning. Numerical validations have been carried out using GPS data collected from different receiver types and qualities, i.e. geodetic grade, medium-cost, and low-cost receivers. The results suggest that single frequency PPP has the potential to provide 0.1m to 0.9m point positioning accuracy in post-processing mode. For real-time scenario, point positioning accuracy of about 1m to 2m can be expected. Despite the encouraging results, PPP is a challenging positioning technique and users should be aware of its limitations.

The accuracy of the PPP solutions is dependent on the quality of the GPS measurements and corrections products used, as well as the capacity of the processing engine. It is anticipated this research will provide valuable guidelines for high accuracy point positioning using a single frequency GPS receiver.

Table of Contents

List of Figures

List of Tables

Acronyms

ACs	Analysis Centres
ACC	Analysis Centre Coordinator
AFN	Australian Fiducial Network
ALGO	Algonquin GPS station
ANN	Australian National Network
ALIC	Alice Springs GPS station
ARGN	Australian Regional GPS Network
C/A	Coarse/Acquisition
C.I.	Confidence Interval
CODE	Centre of Orbit Determination in Europe
CORS	Continuously Operating Reference Stations
CSRS	Canadian Spatial Reference System
CTRS	Conventional Terrestrial Reference System
DARTS	Dynamic Ambiguities Real-Time Standalone
DARW	Darwin GPS station
DCBs	Differential Code Biases
DGPS	Differential Global Positioning System
DOY	Day Of Year
ECEF	Earth-Centred-Earth-Fixed
EOSC	European Space Operations Centre
ERPs	Earth Rotation Parameters
GDA 94	Geocentric Datum of Australia 1994
GDGPS	Global Differential GPS System
GFZ	GeoForschungsZentrum
GIMs	Global Ionosphere Maps
GIS	Geographic Information System
GNSS	Global Navigation Satellite Systems
GPS	Global Positioning System
GRS 80	Geodetic Reference System 1980
GSD	Geodetic Survey Division
HOB2	Hobart GPS station

HOFN	Hoefn GPS station
IAACs	Ionosphere Associate Analysis Centres
IAG	International Association of Geodesy
IERS	International Earth Rotation Service
IGDG	Internet-based Global Differential GPS
IGS	International GNSS Service
IISC	Indian Institute of Science GPS station
ION	Institute of Navigation
IONEX	IONsphere map EXchange
IONO-WG	Ionosphere Working Group
IPPs	Ionospheric Pierce Points
ITRF	International Terrestrial Reference Frame
ITRS	International Terrestrial Reference System
JPL	Jet Propulsion Laboratory
LEOs	Low-Earth Orbiters
LT	Local Time
MOBS	Melbourne Observatory GPS station
NAD 83	North America Datum 1983
NASA	National Aeronautics and Space Administration
NAVSTAR	NAVigation Satellite Timing And Ranging
NGA	National Geospatial-Intelligence Agency
NGS	National Geodetic Survey
NIMA	National Imagery and Mapping Agency
NOAA	National Oceanic and Atmospheric Administration
NRCan	Natural Resources of Canada
PC	Personal Computer
PCVs	Phase Centre Variations
PPP	Precise Point Positioning
PPS	Precise Positioning Service
RIMs	Regional Ionosphere Maps
RINEX	Receiver INdependent EXchange Format
RMS	Root Mean Square
RTWG	Real-Time Working Group

SA	Selective Availability
SOPAC	Scripps Orbit and Permanent Array Centre
SP3	Standard Product 3
SPS	Standard Positioning Service
STD	STandard Deviation
STR1	Stromlo (Mount) GPS station
SUTH	Sutherland GPS station
TEC	Total Electron Content
TECU	Total Electron Content Unit
TOW2	Townsville GPS station
UofC	University of Calgary
UPC	University of Catalonia
USAF	United State Air Force
UTC	Universal Time Coordinated
VTEC	Vertical Total Electron Content
WGS 84	World Geodetic System 1984
ZPD	Zenith Path Delay

CHAPTER 1

Introduction

1.1 Background

The advent of satellite geodesy is one of the greatest technological inventions. The development of Global Navigation Satellite Systems (GNSS), which is a generic term for all the satellite-based global navigation systems at the end of the twentieth century, started a new and exciting era in positioning, navigation, and timing. Accurate estimates of position, velocity, and time have become available to all virtually instantaneously, continuously, inexpensively, and effortlessly (Misra and Enge, 2006). The immediate advantages of using GNSS are high precision, high efficiency, global coverage, and all weather conditions capability.

The American NAVigation Satellite Timing And Ranging Global Positioning System (NAVSTAR GPS) is one of the most established and best known GNSS systems. Since its inception in the late 1970s, this system has revolutionised positioning and navigation along with geodesy, geospatial science and technology. Although the primary intention of GPS was for military purposes, researchers soon recognised the versatility of this system. GPS can be adapted and exploited for a myriad of civilian applications such as vehicle, air and marine navigation, machine guidance/control, search and rescue, mapping and tracking, precision farming, and land surveying.

Absolute point positioning or autonomous positioning using one single GPS receiver is the basic and simplest mode of GPS positioning. There are two levels of service provided by the GPS (Tiberius, 2003). They are the Standard Positioning Service (SPS), which is available to all users around the world, and the Precise Positioning Service (PPS), which is made exclusive to the U.S. military, certain U.S. Government agencies and civilian users who are specifically approved by the U.S. Government. The SPS is provided via the Coarse/Acquisition (C/A) code on L1 frequency, while the PPS is provided via the Precision

(P) code on both L1 and L2 frequencies. At present, the vast majority of the GPS receivers in the market are SPS receivers.

In absolute point positioning, a minimum of four ranges to four satellites and the corresponding satellite coordinates are required to determine the position of the receiver. The ranges can be measured using the code measurements, while the ephemeris of the satellites can be obtained via the broadcast navigation message. The satellite clock bias and ionospheric error can also be reduced by applying the satellite clock and ionospheric corrections available from the navigation message. The tropospheric delay, on the other hand, is often ignored in point positioning, but it can be corrected by using an existing tropospheric model, e.g. Saastamoinen model and Hopfield model (Hopfield, 1969; Saastamoinen, 1972). There are four unknown parameters in absolute point positioning, and these are the receiver coordinates (X,Y,Z) and the receiver clock bias.

The final accuracy obtainable from absolute point positioning is restricted by the limited accuracy of the corrections contained in the broadcast navigation message, as well as the nature of the code measurements. The expected horizontal point positioning accuracy from a civilian code-based GPS receiver has improved tremendously since the removal of Selective Availability (SA) in 2000. The twice-distance root mean square horizontal accuracy of the point positioning based on SPS has improved from over 100m when SA was on, to about 22m after the switch-off of SA and sometimes better than 10m (Shaw, 2000; Bisnath *et al.*, 2002; El-Rabbany, 2006). However, such accuracy is only adequate for low accuracy applications such as recreational and vehicle navigation. Highly accurate GPS positioning techniques have been developed over the last few decades by the process of relative positioning using carrier phase observables.

Relative positioning, sometimes known as differential positioning, is different from the classical point positioning technique in the sense that a minimum of two receivers are required for positioning. One is selected as a reference (base) receiver set up over an accurately known point, while the other receiver acts as a rover receiver, whereby the coordinates to be determined are relative to the reference receiver. Both the receivers are required to simultaneously observe the same set of satellites. The design of relative positioning is to take advantage of the fact that the errors associated with satellite orbit, clock, and the atmospheric propagation effects such as the ionosphere and troposphere are similar, or vary “slowly” with time at both the reference and rover receivers. In other words, the errors

exhibit spatial and temporal correlations. The shorter the separation distance between the reference and rover receivers, as well as the smaller the measurement epochs interval, the more similar the errors (Misra and Enge, 2006).

The concept of relative positioning in GPS has been utilised over the last two decades. Originally, the usage of the relative positioning technique was one reference station and one (or more) rover receivers in a local area. But this technique was soon augmented to multiple reference stations based positioning approach that is more effective and efficient. The network of reference stations could be on a regional, national, continental, or global scale.

Relative positioning provides better positioning accuracy than the classical absolute point positioning. Centimetre-level to metre-level positioning accuracy can be obtained in relative positioning and the accuracy mainly depends on whether the code and/or carrier phase measurements are used. The latter provides the highest possible positioning accuracy. Relative positioning can be performed in either static or kinematic modes, and in either real-time or post-processing modes.

One of the requirements for the relative positioning technique is the need for simultaneous observations at a minimum of two or more GPS stations, hence doubling the operational cost and complexity. The accuracy of relative positioning is also constrained by the baseline length. As the baseline length increases, the correlation between the ephemerides and atmospheric errors decreases. This limits the accuracy of the positioning solutions.

In the late 1990s, the proliferation of Continuously Operating Reference Station (CORS) networks around the world led to the introduction of precise satellite corrections. These corrections made high accuracy point positioning using a single GPS receiver possible. This novel positioning technique is known as Precise Point Positioning (PPP) (Zumberge *et al.*, 1997a; Zumberge *et al.*, 1997b). PPP has been an active research topic over the past few years, with the Institute of Navigation (ION) even introducing a separate PPP research session at their annual international technical meetings since 2004 (Beran, 2008; The Institute of Navigation, 2008).

Relative positioning is based on (single, double or triple) differencing. PPP, however, uses un-differenced carrier phase observations, in addition to the code observations, together with precise and accurate satellite orbits and clocks to achieve positioning accuracies at the

few centimetres level or better (Zumberge *et al.*, 1997b; Kouba and Hèroux, 2000; Witchayangkoon, 2000; Kouba, 2003). PPP is an attractive point positioning technique, which complements the existing relative positioning technique. It possesses the strengths of relative positioning and overcomes some of its weaknesses. PPP requires only one receiver for positioning, and eliminates the need for simultaneous observations at both the reference and rover receiver ends. In addition, this method of positioning also eliminates the need for the rover receiver to work within the vicinity of the reference receiver that only defines a locally consistent reference frame (Abdel-salam, 2005). The solutions from PPP are directly related to a global reference frame, i.e. International Terrestrial Reference Frame (ITRF).

The evolution of PPP can be dated back to a paper written by Anderle (1976), but it was not until the late 1990s that this technique was vigorously researched and studied at the Jet Propulsion Laboratory (JPL) (Zumberge *et al.*, 1997a; Zumberge *et al.*, 1997b). Since then, PPP has generated great interest among the GPS community (Hèroux and Kouba, 2001; Gao and Shen, 2002; Simsky, 2003; Abdel-salam, 2005; Wübbena *et al.*, 2005; Gao, 2006; Waypoint Products Group, 2006; NRCan, 2008b; OmniSTAR, 2008). In order to achieve high accuracy point positioning solutions, numerous research groups have used data collected from dual frequency, geodetic quality GPS receivers. Theoretical foundations and early research results on PPP can be found in Zumberge *et al.* (1997a), Zumberge *et al.* (1997b), Zumberge *et al.* (2001), Kouba and Héroux (2000), Kouba (2003), Witchayangkoon (2000), Bisnath and Langley (2002), Mullerschoen *et al.* (2000), Gao and Shen (2001), Gao and Shen (2002), Gao and Wojciechowski (2004), Colombo *et al.* (2004), and Abdel-salam (2005).

1.2 Research Motivations

Dual frequency PPP has been extensively researched within academia, governments and other scientific groups over the last decade. Several PPP software packages have been developed and it has shown that centimetre to decimetre level point positioning accuracy can be achieved in static and kinematic modes respectively using dual frequency, geodetic quality data sets (Zumberge *et al.*, 1997b; Witchayangkoon, 2000; Gao and Shen, 2002; Kouba, 2003; Leick, 2004; Abdel-salam, 2005). However, the use of a single frequency GPS receiver to achieve high accuracy point positioning poses a greater challenge due to the way the measurement errors, in particular the ionospheric effects are handled (Øvstedal, 2002; Beran, 2008). In addition, the accuracy of the positioning solutions is highly dependent on the quality of the measurements made, as well as the mathematical and stochastic models used in the

processing software. This is a relatively new research area with only a limited number of researchers investigating the possibility of using single frequency PPP to achieve high accuracy point positioning. Literatures on this topic can be found in Witchayangkoon (2000), Øvstedal (2002), Beran *et al*. (2004), Beran *et al*. (2007), Beran (2008), Le (2004), Le and Tiberius (2006), Mullerchoen *et al*. (2004), Chen and Gao (2005), Gao *et al*. (2006), Tétreault *et al*. (2005), and Simsky (2006).

The processing platform used in this research is a Personal Computer (PC) based version of the on-line Canadian Spatial Reference System PPP (CSRS-PPP) service (NRCan, 2008b). The software has been kindly provided by the Geodetic Survey Division (GSD) of Natural Resources Canada (NRCan). This service has the capability of processing dual frequency code and carrier phase observations as well as single frequency code-only observations. Single frequency PPP processing in the CSRS-PPP service using both code and carrier-phase measurements has not been made available on-line as it is not yet considered to be a robust system (Tètreault *et al.*, 2005). The problems of this processing technique are principally due to the adverse effects of the ionosphere on single frequency measurements, as well as the nature of the more precise but ambiguous carrier phase measurements. Therefore, one motivation of this research is to provide an in-depth understanding of the processes affecting the performance of single frequency PPP code and carrier phase processing, and then, to suggest desirable measures, which could help improve the quality of the estimated positioning solutions.

In recent years, the GPS community has shown a desire to have instantaneous positions without compromising the quality of the positioning solutions. With the emergence of near real-time and real-time corrections products from organisations such as National Aeronautics and Space Administration (NASA) JPL, International GNSS service (IGS) and NRCan, the prospect of real-time PPP may become a reality (Muellerschoen *et al.*, 2004; Gao *et al.*, 2006; Mireault *et al.*, 2008; Ray and Griffiths, 2008). It is well known that the quality of positioning solutions using the PPP technique is heavily dependent on the accuracy of the satellite orbit and clock corrections. It is necessary to appreciate the significance of using different correction products on the estimated positioning solutions. The NASA JPL's Global Differential GPS System (GDGPS) was designed and developed for NASA's real-time terrestrial, airborne and spaceborne applications. This system provides the unparalleled combination of real-time positioning accuracy and availability (Bar-Sever and Muellerschoen, 2003). It is reported that real-time positioning accuracy of 10cm horizontally and 20cm

vertically can be achieved anywhere around the world. However, this system is not freely accessible (Muellerschoen *et al.*, 2000; Muellerschoen *et al.*, 2001; JPL, 2007). The freely accessible Canada-wide Differential GPS Service (CDGPS, 2009) delivers, real-time GPS corrections derived from the GSD NRCan's real-time wide-area GPS correction information referred to as GPS•C. The intention of this service is to provide real-time positions with direct access to the Canadian Spatial Reference System (CSRS). These real-time corrections are only available in Canada and some parts of the United States and Greenland. On the other hand, the IGS Real-Time Working Group (RTWG) was set up in 2002 to address issues pertaining to the IGS developing real-time infrastructure and processes (IGS, 2008). This is driven by the high demand from the GPS community for real-time GPS raw data and products. The IGS has been providing the near real-time and real-time predicted GPS products such as satellite orbit and clock corrections as part of the *Ultra-Rapid* products since 2000 (Springer, 2000). Correction products are valid for all users around the world and it is offered as a free utility that is accessible by the general public through the Internet. It is of interest to examine the implications of using the IGS near real-time and real-time products on the estimated single frequency PPP solutions.

L1 data extracted from dual frequency geodetic quality receivers are routinely used in single frequency positioning research. As a result, the research findings may not necessarily represent the true capabilities of consumer grade single frequency receivers. This research also attempted to assess and conduct a comprehensive comparison of the quality of the positioning solutions using different quality single frequency GPS receivers. Single frequency GPS receivers can generally be categorised into two groups: Geographic Information System (GIS) grade receivers which have a higher price tag (medium-cost); and consumer grade (low-cost) handheld receivers which usually cost a few hundred dollars. It is expected that the results from GIS grade receivers would be better than those of low-cost receivers. Testing is undertaken in this research to evaluate the quality of the positioning results based on each receiver types using the research processing software and correction algorithms.

The basic intention of this research is to investigate an alternative, cost effective, and low positioning infrastructure technique, which could be useful for various GPS applications, including those in remote locations, where budgetary operational cost is essential. It is believed that high accuracy point positioning using a (low-cost) single frequency receiver could benefit a myriad of applications. Examples of applications include mining, airborne survey, agricultural, and off-shore oil/gas positioning. Currently, it is estimated that 75% of

all GPS receivers used globally are single frequency receiver units (Arbesser-Rastburg, 2006). Thus, any accuracy improvement in point positioning will clearly be of great practical importance. It is also anticipated that single frequency receivers will continue to be in-demand and produced due to its relatively lower price and better power utilisation (Khattanov *et al.*, 2004).

1.3 Research Aim, Scope and Questions

The aim of this research is to investigate effective measures to provide the best point positioning solutions using single frequency PPP. The final accuracy, the repeatability of results, and the time of convergence of the point positioning solutions are the main investigation. This research will predominantly deal with four aspects of single frequency PPP and the impact of each on the estimated positions. These are the *a priori* observations weighting in the adjustment model, ionospheric effects in different ionospheric conditions, the single frequency PPP convergence behaviour, and the IGS satellite orbit and clock corrections products. The performance of the single frequency PPP software will also be tested and validated using real GPS data from single frequency medium-cost and low-cost receivers.

The scope of this investigation is limited to GPS data collected from the Australian continent. The continent extends from the low latitude to middle latitude regions. The intention is to keep the scope of the research at a manageable level, particularly for the ionospheric effects assessment. Additionally, the focus of this research is purely on static single frequency PPP. It must be noted that single frequency PPP in kinematic mode was not considered in this study.

In order to achieve the research aim, the following research questions are formulated,

1. What are the limitations of the single frequency PPP?

2. Is the *a priori* code and carrier phase measurement sigma (or standard deviation) ratio important in single frequency PPP? If yes, why, and how do the settings affect the solution accuracy and convergence time?

3. Can Regional Ionosphere Maps (RIMs), with different spatial and temporal resolutions, be used to improve the accuracy of single frequency PPP?

4. Can the satellite clock correction rate, the observation sampling interval, and the use of different tropospheric delay mitigation methods affect single frequency PPP convergence time?

5. How do the various IGS satellite orbit and clock correction products perform in terms of solution accuracy and product latency?

6. What is the achievable single frequency PPP positioning accuracy using GPS data collected from a medium-cost, and low-cost handheld consumer grade receiver?

1.4 Research Approach and Contributions

The CSRS-PPP software is used as the core research processing platform. Modifications are made to the software code to accommodate the specific needs of this investigation. Besides the core processing software, an in-house coordinates transformation program is also used to transform coordinates between different datums and also to convert Earth-Centred-Earth-Fixed (ECEF) coordinates expressed in X, Y and Z to latitude (east), longitude (north) and height components.

PPP using a single frequency GPS receiver is a challenging research topic principally due to the nature of the carrier phase measurements and the adverse effects of the ionosphere. The first contribution of this research is an in-depth understanding of the contributions of *a priori* observations sigma ratios on single frequency PPP solutions, in terms of the solutions accuracy, precision and convergence behaviour. This is an innovative aspect of the research because, to the author's knowledge, this is the first report on this topic. It is discovered that the selection of an appropriate sigma ratio will significantly improve the quality of the solutions and also the time of convergence. The study is carried out based on an empirical approach using data sets collected from different receivers, different environments of the observation site, and varying atmospheric conditions. The outcome of this study is the recommendation of an "optimal" *a priori* observation sigma ratio, which could provide the best possible single frequency PPP solutions, irrespective of the location of the receiver and the ionospheric conditions.

Another integral part of this research is the study of the ionospheric effects on single frequency PPP and the mitigation methods for the error. This is because the ionospheric delay is a major error source for single frequency GPS positioning (Klobuchar, 1996; Øvstedal, 2002). The study extends the current knowledge by evaluating the feasibility of using the Broadcast model, Global Ionosphere Maps (GIMs) and Australia-wide RIMs in single frequency PPP to achieve high accuracy point positioning. The Australia-wide RIMs are created from GPS data collected locally (within the Australasia and part of the South East Asia region) and using local atmospheric models. The maps are produced using in-house software developed at RMIT University (Zhang *et al.*, 2008). Australian GPS data from stations located in different latitude zones as well as different solar conditions are used in the evaluation process. In addition, high temporal (1-hour) resolution RIMs are also created and compared to the 2-hour interval global and regional ionosphere maps. The results of the estimated positioning solutions using different ionospheric error mitigation methods under different ionospheric conditions are provided in this thesis.

Besides the adverse effects of the ionosphere, another factor that restricts the accuracy of (single frequency) PPP is the limited accuracy of the existing precise satellite orbit and clock corrections (Bisnath and Gao, 2007). The impacts of using different satellite orbit and clock corrections products with varying accuracy and latency in single frequency PPP are examined as part of this research. This is because the PPP technique greatly relies on external products to correct for these biases. This research evaluates the IGS satellite orbit and clock corrections products in terms of the achievable point positioning accuracy and precision. Special attention is given to the near real-time and real-time predicted orbit and clock corrections. Only a few preliminary studies have been undertaken to examine the quality of the estimated single frequency PPP solutions using the IGS predicted corrections products. It is hoped that the outcome of this evaluation could better demonstrate that accurate point positioning is achievable in a real-time scenario using the IGS predicted corrections products.

The fourth contribution of this research is the assessment of the influence of satellite clock correction rate, data sampling interval, and tropospheric delay mitigation methods on single frequency PPP solutions convergence time. This study is expected to provide some positive recommendations, which could be utilised to improve the convergence time in single frequency PPP static data processing.

The quality of the point positioning solutions is highly dependent upon the quality of the GPS measurements and types of receiver used. Geodetic quality, single frequency GPS measurements are used mainly to study the influence of above-mentioned components on single frequency PPP solutions accuracy, precision and convergence time. Hence the fifth contribution of this research is the investigation of the achievable point positioning accuracy in simulated real-time and post-processing modes using single frequency medium-cost and low-cost handheld consumer grade GPS receivers. This investigation was carried out by using the research software with the recommended settings suggested from the preceding studies. It is envisaged that the findings from this study could establish the possibility of using a low-cost, single receiver point positioning technique to achieve high accuracy point positions.

1.5 Thesis Outline

This thesis examines different aspects of the single frequency PPP and its implications on the estimated positioning solutions. Each Chapter concentrates on different components, investigates error sources, and notes improvements in key areas.

Chapter 1, *Introduction,* presents the introduction, background to the study, research motivation, aim and scope, as well as the research contributions.

Chapter 2, *Precise Point Positioning and Design of Research Software,* provides an account of the history and development of the PPP technique, starting from dual frequency PPP and then followed by single frequency PPP. A thorough description of the research software, which includes the implemented mathematical and adjustment models, the mathematical consideration associated with the adjustment model, the software computational flow and design is also provided.

Chapter 3, *Error Sources in PPP and Mitigation Methods,* discusses the various GPS errors sources relevant to PPP and effective mitigation methods/strategies. The effectiveness of these error mitigation methods and data processing strategies is crucial for high accuracy point positioning.

Chapter 4, *Single Frequency PPP – Setting A Priori Observations Sigma Ratio*, comprehensively details the study carried out to examine and evaluate the influence of *a*

priori observations sigma ratio in single frequency PPP. The outcomes of this study and the proposed "optimal" sigma ratio are presented.

Chapter 5, *Ionospheric Error Mitigation Strategies for Single Frequency Point Positioning*, deals with the effects of the ionosphere on single frequency point positioning, and specifically on single frequency PPP. It presents an in-depth comparison of the quality of the point positioning solutions using different ionospheric error mitigation methods. The Broadcast model, GIMs and RIMs are tested and compared for their usefulness.

Chapter 6, *Convergence Evaluation of Single Frequency PPP Solutions*, examine three aspects of PPP that could potentially influence the convergence behaviour of the single frequency PPP solutions. The three aspects investigated are the satellite clock corrections rate, observation sampling rate and the effects of either modelling the tropospheric delay using an empirical tropospheric model or estimating the delay as part of the PPP solutions.

Chapter 7, *IGS Satellite Orbit and Clock Corrections: From Post-Mission to Real-Time Point Positioning*, describes the research undertaken to examine the effects of using the various IGS satellite orbit and clock corrections on the single frequency PPP solutions. The assessment of these products focuses on the relationship between the latency and accuracy of the products with the quality of the estimated point positions. Special emphasis is placed on the near real-time and real-time correction products.

Chapter 8, *Single Frequency PPP using Medium-Cost and Low-Cost GPS Receivers*, reports on the tests undertaken to evaluate the possibilities of using a medium-cost and low-cost consumer grade GPS receiver to achieve high accuracy point positioning in both post-mission and simulated real-time static applications. The results are presented along with analyses.

Chapter 9, *Summary, Conclusions and Recommendations*, summarises the primary outcomes of this research. The implications arising from each Chapter are briefly examined and discussed. The conclusions drawn from this research are provided and a few recommendations for future work are outlined.

CHAPTER 2

Precise Point Positioning and Design of Research Software

2.1 Introduction

This Chapter presents a synopsis of the history and development of the PPP technique, starting with dual frequency PPP followed by single frequency PPP. It aims to provide readers with some background knowledge and information regarding PPP, which is necessary for the research material presented in later Chapters. A considerable amount of the literature discussed dates back to texts and journal articles that provided coverage of this topic, e.g. Zumberge *et al.* (1997a), Zumberge *et al.* (1997b), Kouba and Héroux (2000), Kouba and Héroux (2001), Kouba (2003), Witchayangkoon (2000), Gao and Shen (2001), Beran (2008) and Leick (2004). An overview of the GPS organisations that are of particular interest to this research work is also outlined. These organisations play a pivotal role in developing and producing precise corrections products and GPS data, which were used extensively in the PPP testing.

The key processing software used in this research is based on the CSRS-PPP online service. Thus, this Chapter will introduce the online processing service and further explain in details the design and architecture of the software. These include the software mathematical model, adjustment model, and the mathematical consideration associated with the sequential filter. In addition, the software computational flow and main components illustrated in a flow chart will also be presented.

2.2 Background Information

2.2.1 Dual Frequency PPP

PPP is a high accuracy, single receiver point positioning technique based on un-differenced code and carrier phase observations using precise satellite orbit and clock corrections products. The concept of point positioning using precise ephemerides was first introduced in 1970s by Richard. J. Anderle (Anderle, 1976). It was not until the late 1990s that this technique was rigorously researched. With the development and introduction of precise satellite orbit and clock corrections from the IGS and other organisations such as Centre of Orbit Determination in Europe (CODE), it is now possible to perform high accuracy point positioning without the need to difference simultaneous observations from reference and rover receivers, as with the case of relative positioning technique (Abdel-salam, 2005). In addition, the use of the more precise carrier phase measurements in PPP as primary observables could lead to high accuracy point positioning. Initial work on PPP was proposed and carried out primarily at JPL (Zumberge *et al.*, 1997b). Two publications from JPL are particularly relevant to PPP and have generated great interest among the GPS community (Zumberge *et al.*, 1997a; Zumberge *et al.*, 1997b).

The number of GPS CORS networks being established around the world is rapidly increasing, and also the computational and economical capacity associated with analysing such a large amount of data. Therefore, an efficient process to analyse these data in a consistent, robust, feasible and economical manner is essential. Zumberge *et al.* (1997b) proposed the PPP technique using un-differenced code and carrier phase observations as a method to achieve this. The adopted approach is to use post-processed data, such as the IGS precise satellite orbit and clock corrections (Zumberge *et al.*, 1997b; Leick, 2004). In addition, Zumberge *et al.* (1997b) also viewed PPP as a data compression strategy, whereby it allows the analysis of data from hundreds of GPS sites everyday with results comparable in quality to the simultaneous analysis of all data (Zumberge *et al.*, 1997b). The study documented remarkable 3D positioning results using PPP with dual frequency GPS receivers, even when SA was still active. Centimetre level (< 9cm) accuracy for single point static surveys was reported. These results were obtained using GIPSY/OASIS-II software developed at JPL.

In addition, JPL provides a free Internet processing service for PPP known as JPL's Auto-GIPSY (JPL, 2006) service. Witchayangkoon (2000) has tested the online service using various data sets with different observation lengths, from 1 hour to 24 hours. He reported that 0.1m repeatability can be generally achieved using 1 hour data, and 1cm to 2cm repeatability for data span greater than 4 hours (Leick, 2004).

The theoretical foundation of PPP using un-differenced code and carrier phase observations from dual frequency GPS receivers can be found in Kouba and Héroux (2000). The mathematical model used is termed the ionosphere-free combination of dual frequency PPP, or the so-called "Traditional" model. The emphasis of their paper was on the errors affecting PPP solutions and the ways to mitigate them. They stressed that the success of PPP depends on the consistency of the set of corrections, models and the weights applied. This included issues such as the satellite antenna offsets, phase windup, reference frames, and the Earth Rotation Parameters (ERPs) corresponding to the IGS satellite orbit, clock and stations solutions used. In their research, Kouba and Héroux (2000) used un-differenced dual frequency code and carrier phase measurements along with the IGS precise satellite orbit and clock corrections products. Comparable results to Zumberge *et al.* (1997a) were reported (Kouba and Hèroux, 2000; Hèroux and Kouba, 2001; Kouba, 2003). It is worth mentioning that they have implemented a free Internet processing service known as NRCan CSRS-PPP service. The program source codes provided by NRCan were used as the core research software in this research. Detailed description of the software architecture is presented in this Chapter.

In 2000, Muellerschoen *et al.* (2000) continued their work and developed a system for PPP using dual frequency receivers at JPL. The system was named the NASA GDGPS. JPL takes advantage of NASA's Global GPS Network (which consists of approximately 70 sites), plus other sites owned by a variety of U.S. and international partner organisations (JPL, 2007). These sites transmit data back to GDGPS Operation Centres in real-time via the Internet. The central processing site estimates the satellite orbit and clock corrections with respect to the broadcast orbit and clock parameters. Corrections to the broadcast parameters are then packed and transferred to users over the Internet, as well as via Inmarsat satellites yielding coverage over the entire globe between latitude ±75° (Sharpe *et al.*, 2002; Muellerschoen *et al.*, 2004). The GDGPS primarily services users with dual frequency receivers and there is a cost involved for accessing the NASA GDGPS real-time system.

Omnistar now also offers precise orbit and clock corrections to subscribers through the Omnistar-XP system (OmniSTAR, 2008).

The research work carried out by various authors presented so far were obtained by using the "Traditional" model. The unknown parameters of this model are the receiver position, receiver clock bias, tropospheric Zenith Path Delay (ZPD), and float ambiguity term for each satellite. Gao and Shen (2001) introduced a different dual frequency PPP mathematical model from the "Traditional" model. They named their model the University of Calgary (UofC) model. The main distinction between the two models is that the UofC uses an average of the code and phase observations on the two frequencies (i.e. L1 and L2) in addition to the ionosphere-free combination. Thus, in addition to estimating the receiver position, clock and tropospheric ZPD, the UofC model allows for the estimation of two float ambiguities for each satellite. The UofC model is made available in a commercial software package known as *P³* (Gao, 2006). However, it is worthwhile to note that both models have demonstrated comparable performance (Hèroux *et al.*, 2004).

In the past few years, substantial research on dual frequency PPP has been performed and documented in numerous literatures (e.g. Witchayangkoon (2000), Abdel-salam (2005), Gao and Shen (2002), Gao and Wojciechowski (2004), Bisnath and Langley (2002), Collins *et al.* (2001), Colombo *et al.* (2004), Ge *et al.* (2007), and Teferle *et al.* (2007)). Dual frequency PPP processing has also been implemented in the Bernese GPS software Version 5.0 (Hugentobler *et al.*, 2007).

Currently, the dual frequency PPP technique is capable of providing point positioning accuracy and precision of a few centimetres (in static mode). This is also substantiated in a preliminary analysis carried out at the start of this research to validate the achievable point positioning accuracy using dual frequency PPP (Choy *et al.*, 2007). Twenty four hours, dual frequency, static observation data from six IGS stations from various locations, namely Algonquin (ALGO), Hoefn (HOFN), Sutherland (SUTH), Indian Institute of Science (IISC), Mount Stromlo (STR1) and Melbourne Observatory (MOBS) stations were post-processed using the CSRS-PPP and AUSPOS online services. The location of the stations is illustrated in Figure 2.1.

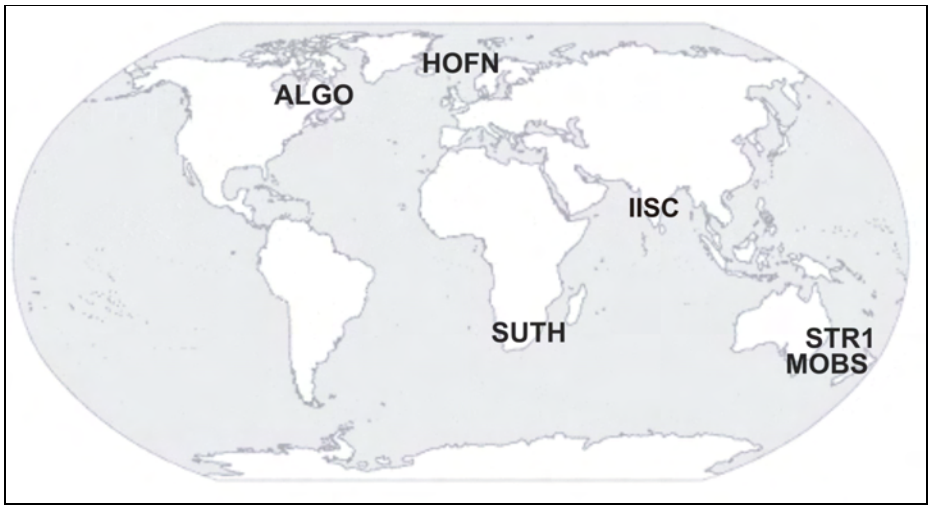

Figure 2.1: The location of ALGO, HOFN, SUTH, IISC, STR1 and MOBS IGS stations.

AUSPOS is a carrier phase based relative positioning processing service, whereby the software processes user-submitted GPS data (collected anywhere around the world) together with observations from the nearest three IGS stations. Information on AUSPOS service can be found at AUSPOS (2006). The findings from the study show that PPP positioning errors were comparable to those of the relative positioning technique and the results are presented in Figure 2.2. Less than 2cm horizontal and 8cm vertical point positioning accuracy can be expected when using dual frequency PPP.

Dual frequency PPP was initially proposed for research and scientific applications within academia, governments and other scientific groups. However, it was soon recognised for its practicality for general GPS applications. Some governments have engaged in providing PPP products and services to public users, e.g. CSRS-PPP. Private industries and companies, e.g. Navcom's StarFire and OmniSTAR-XP, have also embraced and engaged in research and development to improve PPP services, technology, and infrastructure to their clients (Bisnath and Gao, 2007; Navcom, 2008; OmniSTAR, 2008).

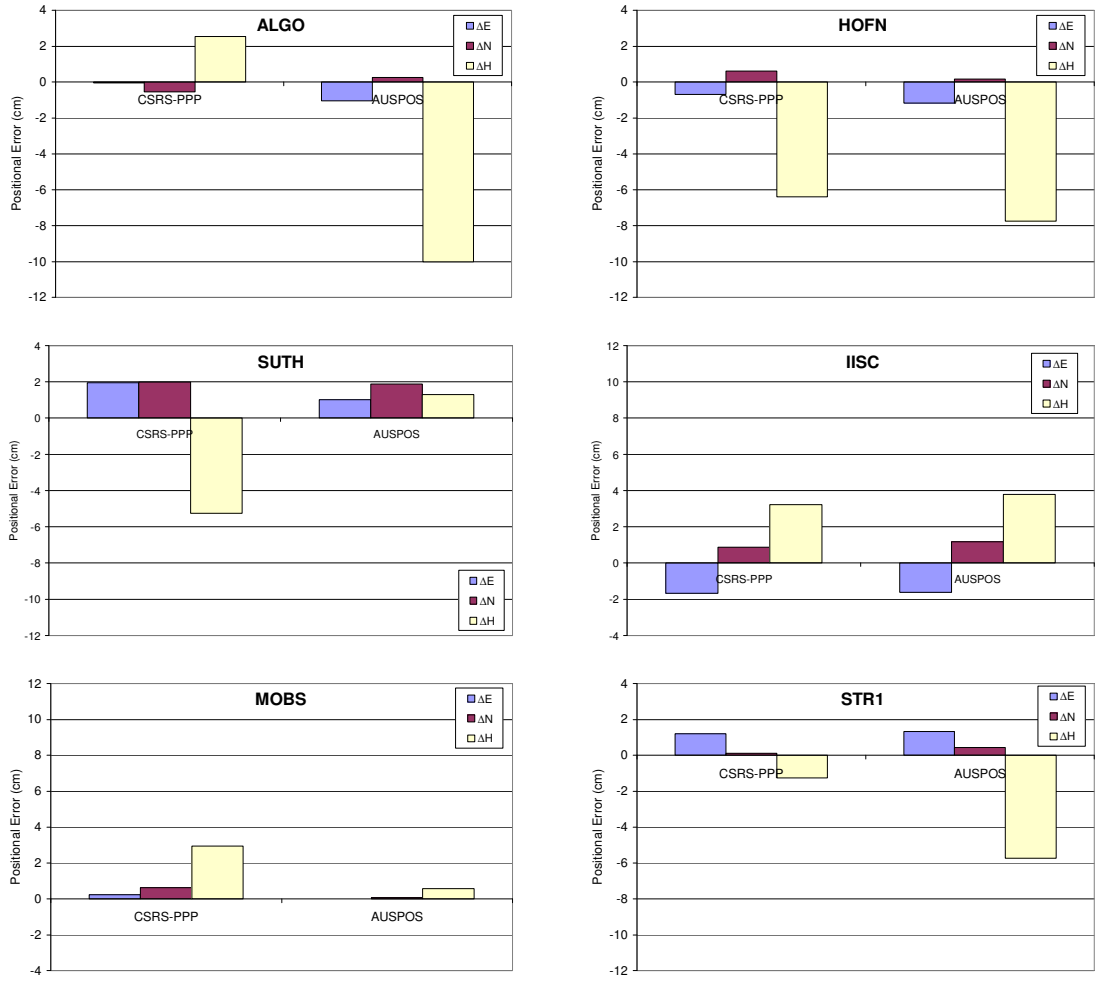

Figure 2.2: Differences between the estimated positions from the CSRS-PPP and AUSPOS online services with the accurately known coordinates of the six IGS stations, ALGO, HOFN, SUTH, IISC, MOBS and STR1. 24-hour data were used.

2.2.2 Single Frequency PPP

As mentioned in the previous section, the initial focus of the PPP research was on dual frequency PPP. However, single frequency PPP has begun to attract interest within the GPS research community. Single frequency PPP poses significant challenges as to how the atmospheric, multipath, receiver biases, *a priori* observations sigmas (or standard deviations) and other measurement error sources are handled. The positioning solutions using single frequency PPP are expected to be less accurate especially in the height estimation. An obvious reason for this degradation in accuracy is the effects of unmodeled ionospheric error (Øvstedal, 2002).

Single frequency PPP was first investigated by Witchayangkoon (2000) who proposed to use a single frequency ionosphere-free code and phase combination. Static observational data from four U.S. Naval Observatory GPS stations were used and the data were limited to the first 6 hours of the day. The evaluation was made by comparing the estimated point positioning solutions with the known coordinates. He noted that although many single frequency solutions exhibited equivalent accuracy as those obtained from dual frequency observations, single frequency PPP results did not appear to be as robust as dual frequency. Nevertheless, point positioning accuracy of about 20cm was reported. This finding was in fact quite promising.

Øvstedal (2002) examined the availability of a few empirical ionospheric models that are publicly available and quantified their usefulness for single frequency point positioning. He reported that horizontal positioning accuracy of better than 1m and a vertical accuracy of approximately 1m can be achieved when using high quality single frequency observations. The satellite orbit and clock biases were removed by using the precise ephemerides. Readers should note that no carrier phase measurements were used in this processing. The research was purely based on single frequency code-only processing.

Similarly, the NRCan CSRS-PPP online service has the ability to process single frequency GPS data, but only using single frequency code observations. The CSRS-PPP online service takes advantage of the precise satellite orbit and clock corrections, as well as the GIMs to remove the bulk of the measurement errors. Researchers at the NRCan carried out in-house testing using single frequency data. They reported that 0.2m horizontal and vertical accuracy was obtained after 2 hours of observation. These results were encouraging considering that only code observations were used.

Single frequency PPP using un-differenced code and carrier phase was studied by researchers at Delft University of Technology (Le and Tiberius, 2006). In their research, they proposed to use the phase-adjusted pseudorange algorithm, which was developed by Teunissen (1991). The filter was extensively tested using a series of static data sets. It was demonstrated that, in general, 0.5m horizontally and 1m vertically at 95% confidence interval can be achieved. In favourable conditions (e.g. low multipath environment, clean data), the horizontal and vertical positioning accuracies can be improved to 0.2m and 0.5m, respectively.

Chen and Gao (2005) investigated the performance of single frequency PPP using un-differenced code and carrier phase measurements. In their research, they proposed to estimate the ionospheric gradient parameters using un-differenced single frequency data and they compared the feasibility of these three types of ionospheric error handling methods. These were the Broadcast model with ionospheric coefficients, GIMs, and the proposed ionospheric delay estimation technique. The data used were obtained from three GPS stations located in different ionospheric regions, i.e. equatorial, middle latitude and high latitude, under different ionospheric conditions. It was found that resulting positioning solutions from both the ionospheric delay estimation technique (with the estimated ionospheric gradient parameters) and the GIMs were more accurate than those of the Broadcast model. The results obtained using the ionospheric estimation technique were comparable with those obtained with the GIMs at middle latitude stations. However, it must be noted that the former can be implemented in real-time mode, while the latter is only available in post-processing mode. Generally, a few decimetres level point positioning accuracy can be obtained at middle and high latitude stations. At equatorial stations, about one metre level point positioning can be achieved using the best ionospheric error mitigation method.

In 2006, Dr. Andrew Simsky from Septentrio Satellite Navigation presented a standalone real-time positioning algorithm for single frequency ionosphere-free positioning based on dynamic ambiguities. The system is known as Dynamic Ambiguities Real-Time Standalone Single Frequency (DARTS-SF) (Simsky, 2006). The concept of DARTS is based on the joint processing of code and carrier phase measurements in a Kalman filter. The ambiguities are estimated as unknown parameters, which can vary from epoch to epoch (Simsky, 2003). The algorithm used in DARTS-SF uses the single frequency ionosphere-free observable, whereby the ionospheric delay is accounted for. He noted that estimated ambiguities absorbed some of the measurements biases. The RMS values for the estimated positions (static applications) were about 1m horizontally and 1.5m vertically.

Single frequency PPP was also extensively researched by Dr. Tomas Beran from the University of New Brunswick. Different techniques were investigated and the code and time-differenced carrier phase filter is proposed (Beran *et al.*, 2003). The performance of this filter was first tested using single frequency measurements extracted from static, geodetic quality, dual frequency data sets. Horizontal and vertical RMS values of better than 0.2m and 0.3m, respectively, were obtained (Beran, 2008). In this research, data collected from low-cost single frequency GPS receiver in Canada was also tested. The positioning solutions obtained

were worse than those of geodetic, high quality GPS receivers. Nonetheless, the Root Mean Square (RMS) values were still within a few decimetres level horizontally and less than 2m vertically. It was found that the presence of multipath and receiver tracking capabilities were the main contributing factors limiting the quality of the estimated positioning solutions. To the best of the author's knowledge, only Beran (2008) has investigated the possibility of using data collected from low-cost single frequency GPS receivers in PPP to achieve high accuracy point positioning in post-processing mode.

Achieving high accuracy point positioning based on single frequency PPP using low-cost GPS receivers is the most desirable point positioning technique in GPS applications. This is driven by the commercial desire for low-cost receivers, ease of use in field operation process and data processing, without compromising on the quality of the estimated positioning solutions. Real-time (single frequency) PPP is also another attractive research direction. Mullerschoen *et al.* (2004), Chen and Gao (2005), and Gao *et al.* (2006) have investigated the capability of single frequency PPP using real-time precise satellite orbit and clock, as well as ionospheric products. Better than one metre level horizontal and vertical positioning accuracy was obtained using real-time single frequency PPP approach. These results were accomplished by utilising the JPL subscribed real-time service, i.e. GDGPS (Muellerschoen *et al.*, 2000; Muellerschoen *et al.*, 2001). The applicability of the IGS real-time predicted products in single frequency PPP is yet to be researched. However, there is evidence that work is constantly being carried out by the IGS to compare and evaluate the quality of their products (NGS, 2008).

2.3 Current Challenges in Single Frequency PPP

The performance of PPP is usually assessed based on its accuracy, precision, and convergence time. Research has demonstrated that dual frequency PPP is able to provide positioning solutions at an accuracy level of a few centimetres in static mode and there is usually very little difference between the accuracy and precision metrics in dual frequency PPP solutions (Bisnath and Gao, 2007). This is because the errors, in particular the ionospheric effects, are substantially mitigated in the dual frequency PPP data processing phase. In contrast, the solutions based on single frequency PPP are prone to receiver biases, as well as the adverse ionospheric effects. The ionospheric delay cannot be completely removed in single frequency PPP even with the best available ionospheric error mitigation product. As a result, the accuracy of the positioning solution decreases, particularly the height component.

Convergence time can be described, in the context of PPP, as the length of time required for the accuracy of the estimated positioning solutions to approach towards a pre-defined point or level, e.g. decimetre level. The time of convergence is highly dependent on various factors such as the quantity and geometry of the satellites, the strength and quality of the GPS measurements and the number of parameters required in the estimation process. Due to these factors, the period of convergence required for the solutions to reach a pre-defined level will vary in different applications and environments. However, in an ideal environment, an average of half an hour to one hour is required for the PPP solutions to reach convergence (Gao and Shen, 2002; Bisnath and Gao, 2007).

Single frequency PPP has not been thoroughly researched due to its challenges and limitations. PPP using single frequency GPS receivers requires a different mathematical model from that of dual frequency. Thus this involves assigning different observations weighting in the single frequency adjustment process. In addition, the biases within the single frequency PPP solutions are also larger, thus affecting the convergence behaviour and quality of single frequency PPP solutions. Therefore, this research is devoted to investigate, explore, and improve the capability and performance of single frequency PPP.

2.4 GPS Organisations Relevant to This Work

The essence of achieving high accuracy point positioning via the PPP technique is the usage of the highly precise satellite orbit and clock correction products from organisations such as the IGS. In addition, the GPS data sets that were used extensively in this research were from Geoscience Australia and the data were collected as part of the Australian Regional GPS Network (ARGN). This section provides a description of the IGS and Geoscience Australia.

2.4.1 The International GNSS Service

The IGS is a voluntary federation of more than 200 worldwide agencies in 80 countries and a global network of over 370 tracking stations (see Figure 2.3) that pool resources and data to support various applications (Dow *et al.*, 2005; Moore, 2007; IGS, 2008). The IGS was formally recognised in 1993 by the International Association of Geodesy (IAG), and officially began its routine operations on 1 January 1994 (Beutler *et al.*, 1994; Neilan, 1995). Currently, the IGS provides the highest quality GNSS data and products to support Earth science research, multidisciplinary applications, and education. In addition, the IGS contributes to the maintenance and improvement of the ITRF, and also helps to monitor the movement of the Earth's tectonic plates, assess sea-level variations, carry out precise time transfer, and determine accurate trajectories for Low-Earth Orbiters (LEO) satellites (Moore, 2007).

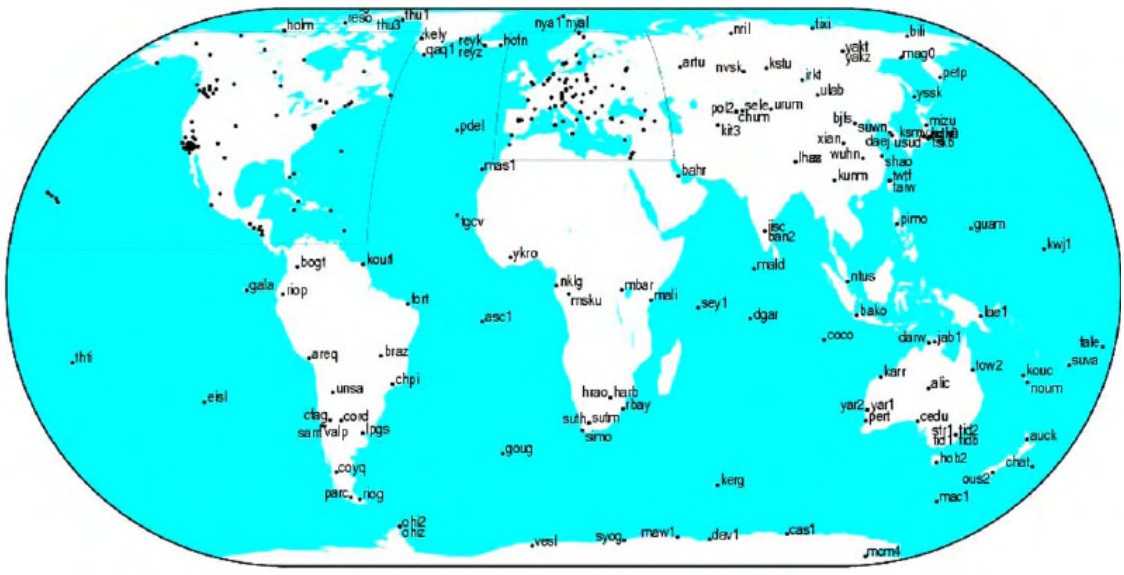

Figure 2.3: The IGS network of tracking stations (Dow et al., 2005).

Data from the permanent, continuously operating, geodetic-quality tracking stations are archived at four Global Data Centres and six Regional Data Centres. These ten Analysis Centres (ACs) regularly process the data and contribute products to the Analysis Centre Coordinator (ACC) that produces the official IGS combined products. At present, the IGS ACC functions are performed by the National Oceanic and Atmospheric Administration (NOAA), National Geodetic Survey (NGS) in USA. The ten IGS ACs are,

- CODE, AIUB, Switzerland
- European Space Operations Centre (ESOC), European Space Agency, Germany
- GeoForschungsZentrum (GFZ) Postdam, Germany
- JPL, USA
- NOAA, NGS, USA (also the ACC)
- NRCan, Canada
- Scripps Institution of Oceanography (SOPAC), USA
- U.S. Naval Observatory (USNO), USA
- Massachusetts Institute of Technology (MIT), USA
- Geodetic Observatory Pecny, Czech Republic

The Central Bureau is responsible for day-to-day management of the IGS following policies set by the International Governing Board (IGS, 2008).

IGS data are currently freely available on the Internet without charge to the public. In addition to providing GPS and GLONASS (the Russian GNSS) raw satellite measurements in Receiver-Independent EXchange (RINEX) format, the IGS also contributes a variety of products to support a wide-range of geodetic and geophysical research and applications, as well as various multidisciplinary applications. Table 2.1 presents the current IGS products made available and its characteristics. Products that are of particular interest to this research are the IGS satellite orbit and clock corrections, as well as the ionospheric Total Electron Content (TEC) grids known as the GIMs. These products were used widely in this research.

Table 2.1: The IGS products which are currently available on the Internet (Moore, 2007).

		Accuracy	Latency	Updates	Sample Interval
GPS Satellite Ephemerides/ Satellite & Station Clock					
Broadcast	Orbits	~160 cm	Real-time	--	Daily
	Satellite Clocks	~7 ns			
Ultra-Rapid (Predicted Half)	Orbits	~10 cm	Real-time	4 times daily	15 min
	Satellite Clocks	~5 ns			
Ultra-Rapid (Estimated Half)	Orbits	<5 cm	3 hours	4 times daily	15 min
	Satellite Clocks	~0.2 ns			
Rapid	Orbits	<5 cm	17 hours	Daily	15 min
	Satellite Clocks	0.1 ns			5 min
Final	Orbits	<5 cm	~13 days	Weekly	15 min
	Satellite Clocks	<0.1 ns			5 min
Note 1: IGS accuracy limits, except for predicted orbit, based on computations with independent laser ranging results. The precision is better. **Note 2:** The accuracy of all clocks is expressed relative to the IGS time scale, which is linearly aligned to GPS time in one-day segments.					
GLONASS Satellite Ephemerides					
Final		15 cm	2 weeks	Weekly	15 min
Geocentric coordinates of IGS tracking stations (>130 sites)					
Final Positions	Horizontal	3 mm	12 days	Weekly	Weekly
	Vertical	6 mm			
Final Velocities	Horizontal	2 mm/yr	12 days	Weekly	Weekly
	vertical	3 mm/yr			
Earth Rotation Parameters: Polar Motion (PM), Polar Motion Rates (PM rate) Length-of-day (LOD)					
Ultra-Rapid (Predicted Half)	PM	0.3 mas	Real-time	4 times daily	4 times daily
	PM rate	0.5 mas/day			
	LOD	0.6 ms			
Ultra-Rapid (Estimated Half)	PM	0.1 mas	3 hours	4 times daily	4 times daily
	PM rate	0.3 mas/day			
	LOD	0.03 ms			
Rapid	PM	<0.1 mas	17 hours	Daily	Daily
	PM rate	<0.2 mas/day			
	LOD	0.03 ms			
Final	PM	0.05 mas	~13 days	Weekly	Daily
	PM rate	<0.2 mas/day			
	LOD	0.02 ms			
Note: The IGS uses Very Long Baselines Interferometry results from International Earth Rotation Service Bulletin A to calibrate for long-term LOD biases					
Atmospheric Parameters					
Final Tropospheric Zenith Path Delay		4 mm	< 4 weeks	Weekly	2 hours
Ultra-Rapid Tropospheric Zenith Path Delay		6mm	2-3 hours	Every 3 hours	1 hour
Final Ionospheric TEC Grid		2-8 TECU	~11 days	Weekly	2 hours; 5 deg (long) x 2.5 deg (lat)
Rapid Ionospheric TEC Grid		2-9 TECU	< 24 hours	Weekly	2 hours; 5 deg (long) x 2.5 deg (lat)

2.4.2 Geoscience Australia

Geoscience Australia was first established in 1946 and is a national agency for geoscience research and geospatial information. The National Mapping Division of Geoscience Australia is Australia's national mapping agency, providing fundamental geographic, spatial and geodetic information in support of various applications and industries. As part of this role, the National Mapping Division of Geoscience Australia maintains a network of permanent GPS tracking stations, known as the ARGN. The ARGN consists of a network of 21 permanent, geodetic quality tracking stations in Australia and its Territories, including the Australian Antarctic Territory (Geoscience Australia, 2008). These sites are accurately coordinated and they contribute to the spatial infrastructure in Australia and its Territories, the monitoring and measurements of earth processes, e.g. plate tectonics and sea level rise. Figure 2.4 and Figure 2.5 show the location of the ARGN tracking stations in Australia and Antarctica, respectively. GPS observational data collected from a number of ARGN stations (i.e. Darwin (DARW), Townsville (TOW2), Alice Springs (ALIC), STR1, and Hobart (HOB2) stations) were used frequently in the PPP testing.

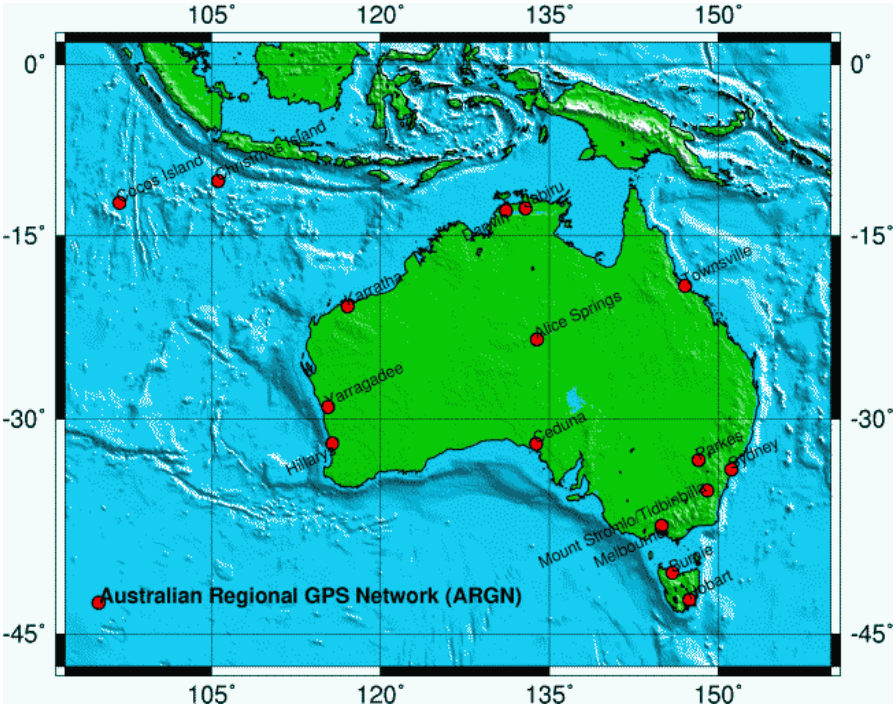

Figure 2.4: The location of the ARGN tracking stations in Australia and its Territories (Geoscience Australia, 2008).

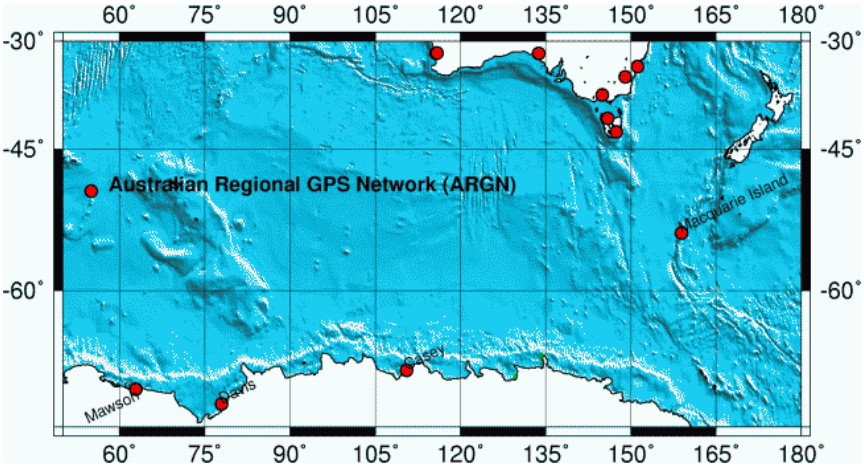

Figure 2.5: The location of the ARGN tracking stations in Antarctica (Geoscience Australia, 2008).

2.5 Research Software: An Overview of the CSRS-PPP Processing Software

The CSRS-PPP software was written and developed by the GSD of NRCan. The processing software was first introduced in October 2003 as an on-line service for the benefit of Canadian GPS users to facilitate access to the CSRS and to encourage the use of IGS products (Tètreault *et al.*, 2005). Since then, it has drawn countless attention worldwide. Drawing from its partnership with IGS, the NRCan is one of the ten IGS ACs regularly processing GPS data and contributing to the IGS combined products (refer to Section 2.4.1).

The CSRS-PPP on-line service is based on un-differenced code and carrier phase observations. The software contains all the necessary correction models, as well as conventions required to properly apply the IGS products to achieve high accuracy point positioning solutions. The CSRS-PPP service also outputs positioning solutions in ITRF coordinates, in addition to the North America Datum 1983 (NAD 83), which makes it accessible to both Canadian and worldwide GPS users. One of the key features of the CSRS-PPP on-line service is that it is designed to minimise the amount of user interaction. Users can upload and submit single frequency or dual frequency GPS RINEX data files which are then processed in either static or kinematic mode using the precise satellite orbit and clock corrections. However, only the code observations are used in CSRS-PPP single frequency data processing. Also, before submitting the GPS data file, the users can select the output

reference frame. Thus, users could either select the estimated solutions to be in NAD 83 or the ITRF reference frame. Detailed information on the CSRS-PPP on-line service can be found at the NRCan CSRS On-line Database (NRCan, 2008a).

In this research, the CSRS-PPP software version 1.04 (release version 0246) coded in Fortran 77 was used as the core research processing engine. It allows for full access, control and maximum flexibility over the entire processing process. The CSRS-PPP software version 1.04 (release version 0246) was used to process GPS data collected before the change to the new ITRF reference frame and *absolute* antenna phase centre model (refer to Section 3.5.1 for more information on the antenna phase centre corrections). For data that were collected after this change, the CSRS-PPP software version 1.04 (release version 1087) was used instead. It is also worth noting that numerous amendments were made to the original source codes in order to tailor the software to the requirements and purposes of this research.

2.6 PPP Mathematical Model

The research software is capable of processing both single and dual frequency GPS data. The software utilises both L1 and L2 code and carrier phase observations for dual frequency PPP processing. With single frequency observations data processing, the software could either process L1 code only observations, or take advantage of the more precise carrier phase measurements in the data processing process. This section describes the implemented dual frequency and single frequency mathematical models.

2.6.1 Dual Frequency PPP – Traditional Model

As discussed in Section 2.2.1, there are two PPP mathematical models that can be used for dual frequency PPP processing, i.e. the "Traditional" model and the UofC model. Both models take advantage of the ionosphere-free linear combinations of GPS code and carrier phase observations to eliminate the effects of the ionosphere so that high accuracy point positioning can be achieved. Although these two models have been well documented in various literatures (Zumberge *et al.*, 1997b; Kouba and Hèroux, 2000; Witchayangkoon, 2000; Gao and Shen, 2001; Hèroux and Kouba, 2001; Shen, 2002; Abdel-salam, 2005), the "Traditional" model will be recapitulated here as background information because this model was implemented in the software. Some dual frequency data were post-processed in this research and these positioning solutions are presented in Chapter 5.

The un-differenced code and carrier phase observation equations are expressed in Equations (2.1) and (2.2), respectively. Assuming that the PPP related errors such as phase wind-up, relativity, antenna phase centre offset and geophysical effects have been properly accounted for (see Section 3.5 for information regarding these errors), the un-differenced observation equations can be written as follows (Abdel-salam, 2005),

$$P(L_i) = \rho + c.(dt - dT) + d_{orb} + d_{ion} + d_{trop} + d_{mult/P(L_i)} + \varepsilon[P(L_i)] \tag{2.1}$$

$$\Phi(L_i) = \rho + c.(dt - dT) + d_{orb} - d_{ion} + d_{trop} + \lambda_i \cdot N_i + d_{mult/\Phi(L_i)} + \varepsilon[\Phi(L_i)] \tag{2.2}$$

where,

$P(L_i)$	-	measured pseudorange on *Li* (m)
$\Phi(L_i)$	-	measured carrier phase range on *Li* (m)
ρ	-	true geometric range (m)
c	-	speed of light (ms^{-1})
dt	-	receiver clock error (s)
dT	-	satellite clock error (s)
d_{orb}	-	satellite orbit error (m)
d_{ion}	-	ionospheric delay (m)
d_{trop}	-	tropospheric delay (m)
λ_i	-	wavelength on *Li* (m)
N_i	-	non-integer phase ambiguity on *Li* (cycle)
$d_{mult/P(L_i)}$	-	code multipath effect on *Li* (m)
$d_{mult/\Phi(L_i)}$	-	carrier phase multipath effect on *Li* (m)
$\varepsilon[\cdot]$	-	measurement noise (m)

Due to the dispersive nature of the ionosphere, the carrier phase observations on L1 and L2 frequencies can be combined to form the ionosphere-free linear combination ("Traditional" model) to eliminate the ionospheric effects. The "Traditional" model can be written as follows,

$$
\begin{aligned}
P_{IF} &= \frac{f_1^2 \cdot P(L_1) - f_2^2 \cdot P(L_2)}{f_1^2 - f_2^2} \\
&= \rho + c.(dt - dT) + d_{orb} + d_{trop} + d_{mult/P(L1+L2)} + \varepsilon[P(L_1 + L_2)] \\
&= \rho + c.(dt - dT) + d_{orb} + M \cdot ZPD + d_{mult/P(L1+L2)} + \varepsilon[P(L_1 + L_2)]
\end{aligned}
\tag{2.3}
$$

$$
\begin{aligned}
\Phi_{IF} &= \frac{f_1^2 \cdot \Phi(L_1) - f_2^2 \cdot \Phi(L_2)}{f_1^2 - f_2^2} \\
&= \rho + c.(dt - dT) + d_{orb} + d_{trop} + \frac{cf_1N_1 - cf_2N_2}{f_1^2 - f_2^2} + d_{mult/\Phi(L1+L2)} + \varepsilon[\Phi(L_1 + L_2)] \\
&= \rho + c.(dt - dT) + d_{orb} + M \cdot ZPD + \frac{cf_1N_1 - cf_2N_2}{f_1^2 - f_2^2} + d_{mult/\Phi(L1+L2)} + \varepsilon[\Phi(L_1 + L_2)]
\end{aligned}
\tag{2.4}
$$

where,

P_{IF} , Φ_{IF}	-	ionosphere-free code and carrier phase combination
f_1 , f_2	-	L1 and L2 carrier frequencies
M	-	tropospheric mapping function
ZPD	-	tropospheric zenith path delay (m)
$d_{mult/P(L1+L2)}$	-	multipath effect on the combined L1 and L2 code (m)
$d_{mult/\Phi(L1+L2)}$	-	multipath effect on the combined L1 and L2 carrier phase (m)

In Equations (2.3) and (2.4), the tropospheric delay is expressed as a function of the tropospheric mapping function and ZPD. As can be seen from these equations, the satellite orbit and clock errors, as well as the tropospheric delay play a major role in limiting the accuracy of the estimated positions. However, these errors can be compensated by using the IGS correction products and appropriate tropospheric models, which will be discussed later in Chapter 3. In addition, it is also worth noting that the ambiguity term in Equation (2.4) is a linear combination of L1 and L2, and hence, it does not preserve the integer properties of the L1 and L2 ambiguities. The combined ambiguity can only be estimated as a float solution in PPP approach.

In a dual frequency PPP solution based on the "Traditional" model, there are six unknown parameters that are required to be estimated. They are the receiver position (X^r, Y^r, Z^r), receiver clock offset, tropospheric ZPD, and the carrier phase ambiguity for each satellite in view. The complexity of the mathematical problem depends on the dynamic (static or kinematic) of the receiver. The problem would be simpler if the receiver position is fixed (static) than changing (kinematic) over time. However, kinematic PPP is not discussed in this thesis as the focus of this research is purely on static PPP applications. The receiver clock bias will drift from epoch to epoch depending on the quality of the receiver clock. The tropospheric ZPD will vary slowly, typically in the order of a few centimetres per hour. The carrier phase ambiguities will remain constant as long as the carrier tracking is continuous (Kouba, 2003; Misra and Enge, 2006).

Various researchers have shown that dual frequency PPP is capable of providing centimetre level point positioning accuracy (Zumberge *et al.*, 1997b; Kouba and Hèroux, 2000; Witchayangkoon, 2000; Kouba, 2003). The convergence time of the estimates for static applications could range between half an hour to an hour, depending of the satellite geometry and quality of the observations. Reducing the convergence time is still the main challenge for PPP (Shen, 2002; Abdel-salam, 2005; Gao and Garin, 2006; Misra and Enge, 2006; Ge *et al.*, 2007).

2.6.2 Single Frequency Point Positioning

The single frequency point positioning technique can be categorised into two approaches. They are the single frequency code-only processing, and single frequency code and carrier phase processing known as single frequency PPP. The CSRS-PPP online service only processes single frequency code measurements and it has been shown that better than a metre level point positioning accuracy can be achieved in ideal circumstances and when the precise correction products are used. This method of data processing is quite straightforward. The use of carrier phase measurements in single frequency processing, however, is far from trivial due to the ambiguous nature of the phase measurements. Nonetheless, the primary intention of this research is to investigate the feasibility of using a single frequency GPS receiver and PPP approach to achieve high accuracy point positioning.

2.6.2.1 Code-Only Processing

The classical single frequency code-only processing is the basic mode of GPS positioning and navigation. The observation equation for the code measurement is shown in Equation (2.1), and this equation can be simplified as Equation (2.5) after the satellite orbit and clock errors, atmospheric effects and multipath have been removed.

$$P(L_i) = \rho + c.dt + \varepsilon[P(L_i)] \tag{2.5}$$

The geometric range can be obtained by,

$$\rho = \sqrt{(X^s - X^r)^2 + (Y^s - Y^r)^2 + (Z^s - Z^r)^2} \tag{2.6}$$

and satellite ephemerides allows the computation of the satellite position (X^s, Y^s, Z^s). This then leaves four unknown parameters, which are the receiver position (X^r, Y^r, Z^r), and receiver clock error dt. Since there are four unknowns, observations to four different satellites will then provide a unique solution. However, if a redundant amount of observations (i.e. five or more satellites) are available, then the least squares estimation technique can be used to determine the optimal solutions.

The accuracy and precision of the position estimates using this processing method are highly dependent on the ability to eliminate and compensate the errors involved in GPS positioning, such as the satellite and atmospheric errors.

2.6.2.2 *Code and Quasi-Phase* Combination

Traditionally, the use of carrier phase observations is only common in the context of relative positioning. However, absolute point positioning using carrier phase observations have attracted significant interest from the GPS community in recent years (Beran *et al.*, 2004; Bisnath, 2004; Simsky, 2006). Carrier phase observations are used in dual frequency PPP to form the ionosphere-free linear combination, which eliminates the effects of the ionosphere (see Section 2.6.1). Single frequency point positioning, on the other hand, could also take advantage of the more precise carrier phase measurement coupled with the code measurements to compensate for the ionospheric delay.

The single frequency PPP processing strategy implemented in this research is called the *code and quasi-phase* combination. The *code and quasi-phase* combination is based on the principle that the ionosphere affects the code and carrier phase measurement at an equal magnitude but opposite in sign. Thus, the ionospheric effects can be eliminated through the combination of the code and carrier phase observations that forms the quasi-phase observable.

Recapitulating the basic code and carrier phase observables from Equations (2.1) and (2.2), the mathematical implementation of the L1 *code and quasi-phase* combination can be expressed as (ignoring the higher-order ionospheric error terms) (Choy *et al.*, 2008b),

$$\begin{aligned}\tilde{\Phi}(L_1) &= \frac{P(L_1)+\Phi(L_1)}{2} \\ &= \rho + c\cdot(dt-dT) + d_{orb} + d_{trop} \\ &\quad + \frac{\lambda_1.N_1}{2} + \frac{d_{mult/P(L_1)}}{2} + \frac{d_{mult/\Phi(L_1)}}{2} + \frac{\varepsilon[P(L_1)]}{2} + \frac{\varepsilon[\Phi(L_1)]}{2}\end{aligned} \tag{2.7}$$

where $\tilde{\Phi}(L_1)$ is the quasi-phase observable on L1 frequency.

Equation (2.7) is essentially the single frequency ionosphere-free code and phase delay proposed by Yunck (1993). The single frequency ionosphere-free code and phase delay equation is addressed in this thesis as the quasi-phase equations (Simsky, 2006), because the ionosphere-free code and phase delay equation is treated as a phase observable in the single frequency PPP processing. In fact, the quasi-phase observable is "noisier" than the original carrier phase due to the influence of the code observations. The quasi-phase observable exhibits a noise with a standard deviation of approximately half of the code noise as the carrier phase noise is negligible (Montenbruck, 2003).

$$\begin{aligned}\sigma\left(\varepsilon[\tilde{\Phi}(L_1)]\right) &= \frac{1}{2}\sqrt{\sigma^2\left(\varepsilon[P(L_1)]\right)+\sigma^2\left(\varepsilon[\Phi(L_1)]\right)} \\ &\approx \frac{1}{2}\sigma\left(\varepsilon[P(L_1)]\right)\end{aligned} \tag{2.8}$$

It is also worthwhile to note that the noise of the resulting measurement is reduced by half. Whilst, the traditional dual frequency ionosphere-free linear combination increases the code noise by a factor of three (Leick, 2004).

The benefit of using the quasi-phase observables in single frequency PPP is apparent. The ionospheric error is effectively removed in the quasi-phase equation as a consequence of the opposite ionospheric effects on the code (delay) and carrier phase observations (advance). In other words, the ionospheric delay on the signal path is essentially eliminated using the quasi-phase observables.

In the research software, Equation (2.1) is treated by the processing algorithm as code observations, while Equation (2.7) is treated as phase observations with float ambiguities.

2.7 Adjustment Model

The mathematical models described in the previous sections explicitly represent the relationship between observations and the unknown parameters. There are various adjustment models such as least squares estimation and Kalman filter, which can be used to "link" the observations with the unknown parameters. The adjustment model used in the research software is based on sequential least squares, which can adapt to varying user dynamics (Tètreault *et al.*, 2005). The sequential least squares is a step-by-step processing filter that divides a large computing burden into smaller and manageable parts, which then reduce the requirements on both computer memory and storage capabilities.

The notations describing the adjustment model used in this research closely follow those of Deakin (2005). A few good references on the basic theory of least squares are, but are not limited to, Merriman (1901), Mikhail (1976), and Krakiwsky (1976). There are two classes of variables in least squares estimation theory. The variables are observations and unknown parameters. The observations are denoted by l, and the unknown parameters are denoted by x.

$$l = [l_1 \;\; l_2 \;\; l_3 \;\; l_4 \;\; \ldots \;\; l_n] \tag{2.9}$$

$$x = [x_1 \;\; x_2 \;\; x_3 \;\; x_4 \;\; \ldots \;\; x_u] \tag{2.10}$$

For n observations with variances $\sigma_{l_1}^2$, $\sigma_{l_2}^2, \sigma_{l_3}^2, \ldots, \sigma_{l_n}^2$ and covariances $\sigma_{l_1 l_2}^2$, $\sigma_{l_1 l_3}^2, \ldots$ the variance-covariance matrix $\sum$ can be defined as,

$$\sum = \begin{bmatrix} \sigma_{l_1}^2 & \sigma_{l_1 l_2} & \cdots & \sigma_{l_1 l_n} \\ \sigma_{l_2 l_1} & \sigma_{l_2}^2 & \cdots & \vdots \\ \vdots & \vdots & \cdots & \vdots \\ \sigma_{l_n l_1} & \sigma_{l_n l_2} & \cdots & \sigma_{l_n}^2 \end{bmatrix} \tag{2.11}$$

The relationship between the variance-covariance matrix and cofactor matrix Q is expressed as,

$$Q = \frac{1}{\sigma_o^2} \sum \tag{2.12}$$

or,

$$\sum = \sigma_0^2 Q \tag{2.13}$$

where σ_0^2 is the standard unit weight of observations or also known as variance factor. The variance factor is a scalar quantity. The inverse of the cofactor matrix is known as the weight matrix W. Thus,

$$W = Q^{-1} \tag{2.14}$$

The term weight is often used to express precision by the way of an inverse relationship with the cofactor matrices. In other words, high weighting means high precision but a smaller standard deviation, and vice versa.

The linearised version of the observation equation using the Taylor's series expansion series can be written symbolically as,

$$f(x) = B\Delta x - v \tag{2.15}$$

$$f(x) = d - l \tag{2.16}$$

where,

$f(x)$	-	vector of numeric terms derived from the observations
d	-	vector of constants
B	-	matrix of coefficients
Δx	-	vector of unknown parameters
v	-	vector residuals

In the case of a dual frequency and single frequency PPP processing model, there are four types of unknown parameters, i.e. the receiver position (X^r, Y^r, Z^r), receiver clock (dt), tropospheric ZPD and (non-integer) phase ambiguities (N). Thus the corrections to the unknown parameters Δx can be expressed in a matrix form as,

$$\Delta x = \begin{bmatrix} X^r \\ Y^r \\ Z^r \\ dt \\ ZPD \\ N^i \end{bmatrix} \tag{2.17}$$

where i is the number of satellites (i.e. *1* to n).

Thus, the partial derivatives of the observation equations with respect to the parameters are as follows,

$$B = \begin{bmatrix} \frac{\delta f(x,l_p)}{\delta \Delta x_{X^r}} & \frac{\delta f(x,l_p)}{\delta \Delta x_{Y^r}} & \frac{\delta f(x,l_p)}{\delta \Delta x_{Z^r}} & \frac{\delta f(x,l_p)}{\delta \Delta x_{dt}} & \frac{\delta f(x,l_p)}{\delta \Delta x_{ZPD}} & \frac{\delta f(x,l_p)}{\delta \Delta x_{N^i}} \\ \frac{\delta f(x,l_\Phi)}{\delta \Delta x_{X^r}} & \frac{\delta f(x,l_\Phi)}{\delta \Delta x_{Y^r}} & \frac{\delta f(x,l_\Phi)}{\delta \Delta x_{Z^r}} & \frac{\delta f(x,l_\Phi)}{\delta \Delta x_{dt}} & \frac{\delta f(x,l_\Phi)}{\delta \Delta x_{ZPD}} & \frac{\delta f(x,l_\Phi)}{\delta \Delta x_{N^i}} \end{bmatrix} \tag{2.18}$$

The least squares estimation of the unknown parameters in this research is written as,

$$\Delta x = -(W_{xx} + B^T W B)^{-1}(B^T W f) \tag{2.19}$$

where, W_{xx} is the *a priori* parameter weight matrix, and W is the observation weight matrix.

The estimated unknown parameters ($\hat{x}$) with its corresponding covariance weight matrix ($\sum_x$) are,

$$\hat{x} = x^0 + \Delta x \tag{2.20}$$

$$\sum_x = (W_{xx} + B^T \sum^{-1} B)^{-1} \tag{2.21}$$

where x^0 is an approximate value of the unknown parameters.

Equation (2.19) is different from the classical least squares approach (i.e. $\Delta x = (B^T W B)^{-1}(B^T W f)$). The adjustment model in the research software is based on the general estimation technique, or also known as the combined least squares estimation technique. In the combined least squares estimation, the *a priori* weight matrix of the parameters W_{xx} is added to the solutions. The combined least squares estimation technique treats the parameters as "observables", that is, they have an *a priori* covariance matrix. This concept allows the combined least squares technique to be adapted to sequential processing of data sets where the parameters can be updated by the addition of new observations (Deakin,

2005). It should however be noted that when $W_{xx} = 0$, the combined least squares estimation is equivalent to the classical least squares approach.

As noted earlier, the implemented adjustment procedure used in the processing software is a sequential filter, which adapts to user dynamics (Tètreault *et al.*, 2005). This means that the procedure takes into account the variations in the parameters states between observation epochs, and then updates the parameters variances using appropriate stochastic models. In order to propagate the parameters' covariance information from epoch $n-1$ to n during an interval Δt, the covariance of the process noise $\sum \varepsilon_{\Delta t}$ should be updated according to the receiver dynamics, receiver clock behaviour and atmospheric conditions using (Kouba, 2003),

$$W_{xx_n} = \left(\sum_{x_{n-1}} + \sum \varepsilon_{\Delta t}\right)^{-1} \tag{2.22}$$

where,

$$\sum \varepsilon_{\Delta t} = \begin{bmatrix} \sum \varepsilon(X^r)_{\Delta t} & 0 & 0 & 0 & 0 & 0 \\ 0 & \sum \varepsilon(Y^r)_{\Delta t} & 0 & 0 & 0 & 0 \\ 0 & 0 & \sum \varepsilon(Z^r)_{\Delta t} & 0 & 0 & 0 \\ 0 & 0 & 0 & \sum \varepsilon(dt)_{\Delta t} & 0 & 0 \\ 0 & 0 & 0 & 0 & \sum \varepsilon(ZPD)_{\Delta t} & 0 \\ 0 & 0 & 0 & 0 & 0 & \sum \varepsilon(N^i)_{\Delta t} \end{bmatrix} \tag{2.23}$$

In static applications, the receiver position noise can be considered constant, $\sum \varepsilon(X^r)_{\Delta t} = \sum \varepsilon(Y^r)_{\Delta t} = \sum \varepsilon(Z^r)_{\Delta t} = 0$; in kinematic applications, the receiver position process noise depends on the receiver dynamics. The receiver clock process noise is usually set to a white noise with large $\sum \varepsilon(dt)_{\Delta t}$ values. This is because the receiver clock will drift according to the quality of its oscillator. The variation is expected to be about 0.1ns/sec, equivalent to several cm/sec, given the internal quartz clock with a frequency stability of about 10^{-10}. The tropospheric ZPD process noise $\sum \varepsilon(ZPD)_{\Delta t}$ is set to a random walk process with process noise of 5mm/√hr, since the tropospheric delay varies minimally over time. Lastly, in all instances, the ambiguity process noise $\sum \varepsilon(N^i)_{\Delta t} = 0$ since the phase ambiguity terms are constant over time provided that no cycle slips occur (Kouba, 2003).

It was discovered, during the course of this research, that the key element in achieving high accuracy point positioning solutions using the *code and quasi-phase* combination is to assign *a priori* observations weight, or sigma ratio in the adjustment model that adequately reflects the relative weight and uncertainty of the observations. The application of the *a priori* sigmas to the traditional dual frequency ionosphere-free linear combination follows the "standard" nominal values widely used in GPS processing, i.e. the carrier phase is 100 times more precise than the code measurements. In single frequency PPP, the answer to this problem is not as obvious. The code observations contain residual ionospheric delay even after the introduction of an ionospheric model, while the quasi-phase observations are free from the ionospheric delay. This complicates the relative weight ratio between the two observations. Chapter 4 will cover some basic theory behind observations weighting and describe in detail the study undertaken to understand the influence of observations weighting on single frequency PPP solutions. The recommendation of an "optimal" ratio is one of the primary objectives of this research. The corresponding results and findings will also be provided.

2.8 Computational Flow and Software Components

The PPP algorithm used in this research is summarised in Figure 2.6. This figure illustrates the software computational flow starting from the GPS observation data (input) in RINEX format to the final point positioning solutions (output). The command file is a text file consisting of all the necessary software commands and processing settings. The output results, i.e. positioning solutions, residuals and statistical results are provided in a text file format. The applications of relevant corrections and error mitigation methods implemented in the processing software are described and given in Chapter 3.

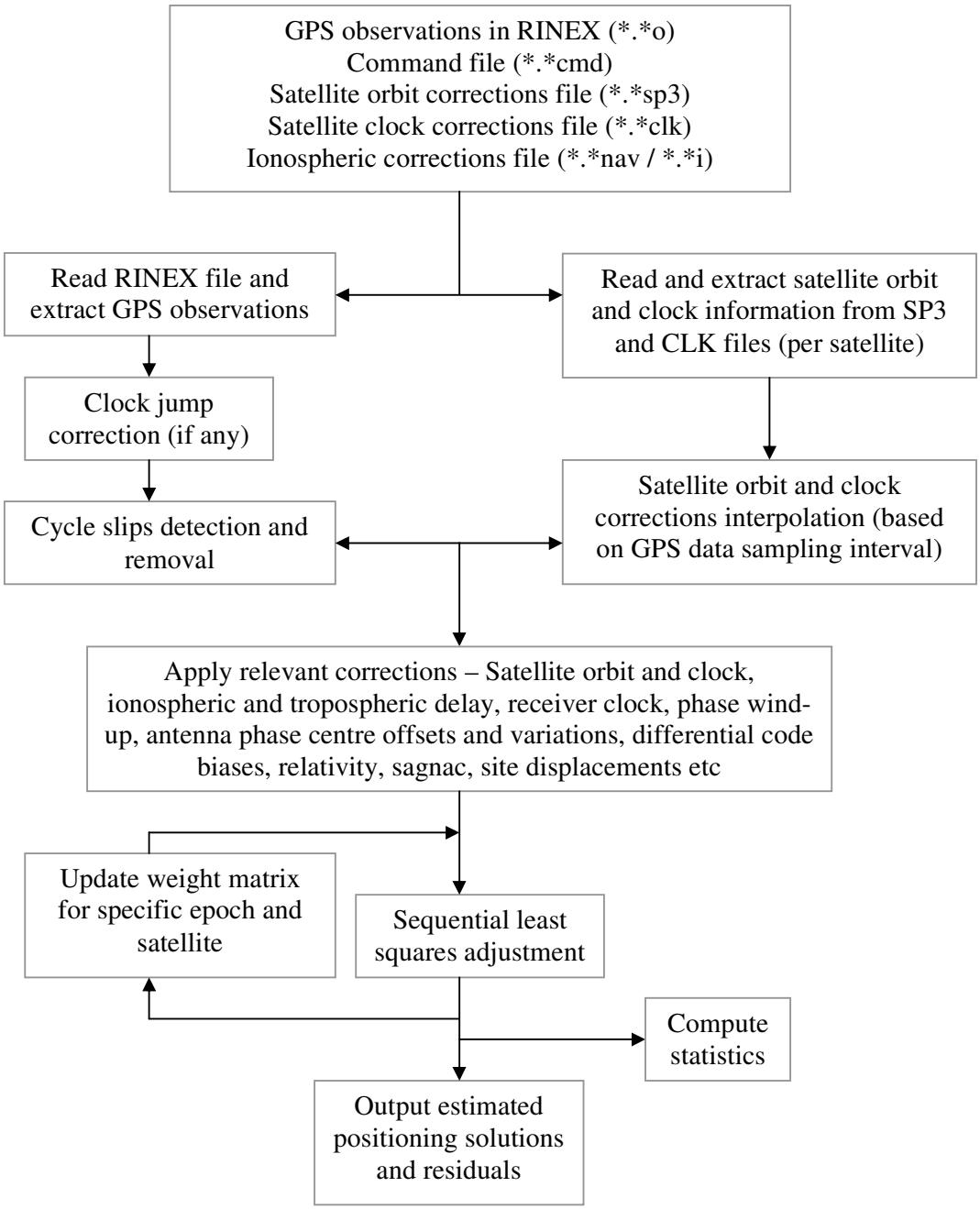

Figure 2.6: Computational flow diagram of the research software.

2.9 Summary

This Chapter has provided a thorough account of the development of the PPP technique. The idea of high accuracy point positioning using precise ephemerides was first introduced in 1970s (Anderle, 1976), but it was not until the late 1990s that this technique, in particular dual frequency PPP, was rigorously researched by the JPL researchers (Zumberge *et al.*, 1997a; Zumberge *et al.*, 1997b). The evolution of the PPP technique was a result of an innovative proposal for an efficient means to analyse large amounts of GPS data for research and scientific applications. Since then, much research has been undertaken by both academia and private industries to investigate the performance capability of this novel point positioning technique and its achievable point positioning accuracy. Numerous background literature on the topic have been suggested.

Single frequency PPP has also drawn significant attention from the GPS community in recent years due to its potential for low receiver cost plus high precision. However, it poses a challenge as to how the measurement errors, particularly the ionospheric delay are handled. Thus, this research is aimed at investigating effective measures, which could be used to help improve the quality of the single frequency PPP solutions. In addition, an overview of the CSRS-PPP software, which was used as the core processing software, has also been given. The dual frequency and single frequency PPP mathematical models that were implemented have been outlined and described. The dual frequency PPP mathematical model is essentially based on the dual frequency ionosphere-free linear combination (refer to Section 2.6.1), whilst the single frequency PPP model is based on the *code and quasi-phase* combination (refer to Section 2.6.2.2). An in-depth account of the adjustment model, i.e. sequential least squares, has been given. Although the focus of this thesis is on static mode, the adjustment procedure takes into account the variation in the parameter states between observation epochs, which means that the model can adapt to varying receiver dynamics. This review has also described the design, features and computational flow of the implemented processing software.

The next Chapter is dedicated to a comprehensive discussion on the GPS error sources that are relevant and which are required to be considered in the context of the PPP data processing process. Effective error mitigation products and strategies, which were applicable in this study, will also be presented. The key aspect to achieve high accuracy point positioning in PPP is the users' ability to effectively eliminate the adverse impacts of the existing error sources in the system.

CHAPTER 3

Error Sources in PPP and Mitigation Methods

3.1 Introduction

Point positioning using GPS technology can exhibit significant errors if the biases contained in the system are not properly and adequately accounted for. The core element to achieve high accuracy GPS positioning and navigation is the ability to accurately and precisely mitigate all these errors. An overview of the GPS error sources which are relevant to PPP, as well as the mitigation strategies that were investigated and applied in this research, form the foundation of this Chapter.

The literature in this Chapter is structured into five segments:

- **Satellite Ephemerides** – This segment aims to describe the errors caused by the GPS satellite orbit and clock. The correction strategies used in PPP processing will also be presented. These biases can be removed in relative positioning provided that the receivers are simultaneously observing to the same set of satellites. However, in single receiver point positioning like the PPP technique, these biases can only be removed by applying external correction algorithms or products from organisations like the IGS.
- **Atmospheric Errors** – The atmospheric regions that impede the propagation of GPS signals are the ionosphere and troposphere. These errors can also be removed in relative positioning provided that the baseline length between the two receivers is short. The PPP technique, on the other hand, does not have this advantage and thus needs to correct for the atmospheric effects in order to obtain high accuracy point positioning solutions. The emphasis of this section is to provide readers with an overview of the atmospheric errors affecting the propagation of GPS signals, as well as the error mitigation methods that were investigated and used in this study.

- **PPP and Associated Errors** – There are several GPS-related biases that have received little attention from the GPS community. This may be due to the small magnitude of errors with respect to the achievable GPS positioning accuracy, and/or the errors can be cancelled out in the equations as in the case of relative positioning (Abdel-salam, 2005). A few examples of these errors are the satellite and receiver antenna offsets, relativity, and the geophysical errors including the earth and atmospheric tides, as well as the plate tectonic motion. Therefore, this segment aims to describe these biases that are frequently neglected in the (relative) processing process and then their appropriate mitigation techniques. These errors need to be considered in PPP for high accuracy point positioning
- **Multipath** – This section aims to provide an overview of the errors caused by the user-defined environment known as multipath and the mitigation strategy applied in the processing software. Multipath may affect both PPP and relative positioning.
- **Reference Frames** – In reality, the reference frame should not be a source of error. However, when the wrong datum, projections or transformation parameters are applied, the computed positioning solutions will be erroneous. Therefore, it is important that GPS users understand the differences between reference frames.

3.2 Satellite Orbit and Clock Errors

Satellite orbit error is the discrepancy between the satellites' true position and the computed or "known" position. GPS satellites orbit in a pre-defined path, which are computed from the ephemerides. However, these orbits may vary from time to time due to gravitational forces and attractions, radiation pressure, particles of the Earth's atmosphere and air drag. As a result of these factors, the ephemeris data that contains the computed location of the satellites at a specific time may not agree with the true position, and this bias is known as the satellite orbit error.

GPS satellites carry highly stable atomic clocks to generate accurate timing signals. Although the onboard atomic clocks are stable, the inability of the onboard oscillator to maintain synchronisation with GPS time results in a clock error. The deviation between the atomic and GPS time is known as the satellite clock error. In addition, the GPS satellite oscillators are only adjusted occasionally, as the onboard atomic clocks will perform better if they are not constantly adjusted. As a result, the onboard atomic clocks are left to drift naturally, and their performance is closely monitored by the master control station (Roulston,

2001). The onboard atomic clocks are adjusted as required by the master control station to keep within ±1 microsecond of GPS system time (Roulston, 2001).

Precise knowledge of the satellite orbit and clock errors is crucial in un-differenced PPP solutions. Witchayangkoon (2000) stated that if the satellite orbit and clock errors are not accurately known, it would be very difficult to achieve high accuracy point positioning using PPP technique. This is because the respective solutions would be in the same "class" as the standard positioning solutions, which crudely corrects for the clock errors provided by the broadcast navigation message. Therefore, it is necessary in PPP to correct for the satellite orbit clock error as effectively as possible so that the highest possible point positioning accuracy can be achieved.

In the PPP approach, the satellite orbit and clock biases can be corrected using the IGS precise satellite corrections products. The IGS precise satellite orbit and clock corrections come in various forms and their characteristics have been illustrated in Table 2.1. The four products are the *Final*, *Rapid*, *Ultra-Rapid (Estimated Half)*, and *Ultra-Rapid (Predicted Half)* satellite orbit and clock corrections.

The IGS orbit products differ predominantly by their accuracy, latency, and the extent of the tracking stations network used in the computations. The IGS orbits can be downloaded freely from the IGS website (IGS, 2008) in SP3 format, short for Standard Product 3 (Remondi, 1993). The SP3 is an ASCII representation of the satellites position and clock corrections with their corresponding standard deviations, as well as other information such as the orbital accuracy information for each satellite. For all possible satellites, the orbit positions are given in the ITRF X, Y, Z coordinate system in kilometres. Currently, the SP3 data are provided in a 15-minute sampling interval.

Besides the tabulated 15-minute interval orbit and clock corrections in the SP3 ephemerides files, there is another clock correction file that contains satellites and monitoring stations receiver clock corrections at a higher sampling rate, i.e. 5-minute or 30-second. This file is known as the CLK file, which is a RINEX extension to record clock corrections. The satellite clock corrections can be downloaded freely from the IGS website (IGS, 2008). For all possible satellites, the clock corrections and sigma values are expressed in seconds.

The evaluation of the various IGS satellite orbit and clock corrections products in single frequency PPP was undertaken as part of this research and the findings will be given in Chapter 7. The intention of the study is to assess the quality of the estimated single frequency PPP positions using the different IGS corrections, in particular the near real-time and predicted products. Useful background information on the broadcast navigation message and the IGS satellite corrections products are presented in the following sections to provide readers with some knowledge on the quality of the satellite orbit and clock correction products.

3.2.1 Broadcast Navigation Message

The information contained in the Broadcast navigation message is computed and generated by the GPS Operational Control Segment. A Kalman filter is used to estimate the states of the satellites (position and velocity) and their clocks (phase bias, frequency bias, and frequency drift rate) (Misra and Enge, 2006). These estimated parameters are then used in a prediction model to propagate the satellite position and clock corrections into the future. The propagated parameters are entered into a set of equations and the computed coefficients are broadcast in the navigation message (Warren, 2002). The GPS Control Segment is constantly monitoring the parameter errors by comparing the broadcast estimates with the best available values. If the error for a specific satellite exceeds a specified threshold, then a contingency data upload is scheduled for that satellite (Warren, 2002; Misra and Enge, 2006). The threshold is defined by the satellite estimated range deviation and the threshold value for the contingency data upload was set at 8m prior to 1997 and 5m after that (Malys *et al.*, 1997). However, if no uploads are required, then a typical once-a-day data upload is performed.

The IGS ACC is constantly monitoring and comparing the Broadcast ephemerides with the IGS precise ephemerides. Figure 3.1 shows residuals between the Broadcast orbits with the IGS *Rapid* orbits. Figure 3.2 shows comparison between the Broadcast and precise *Rapid* clock corrections. The x-axis denotes the GPS week and the y-axis denotes the differences between the two products. In-depth description of the IGS precise satellite orbit and clock corrections will be provided in the next section.

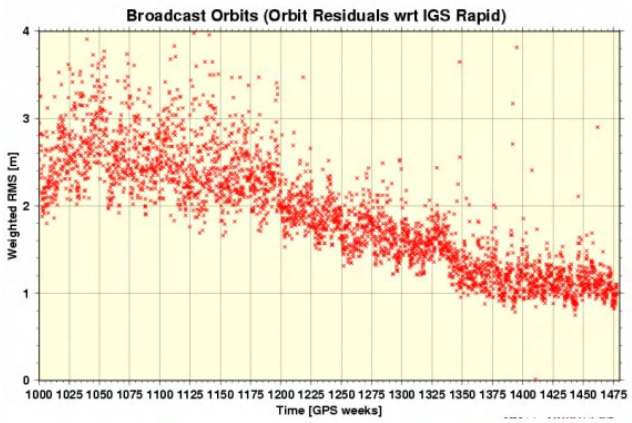

Figure 3.1: Residuals between the Broadcast and IGS *Rapid* orbits (GFZ, 2008).

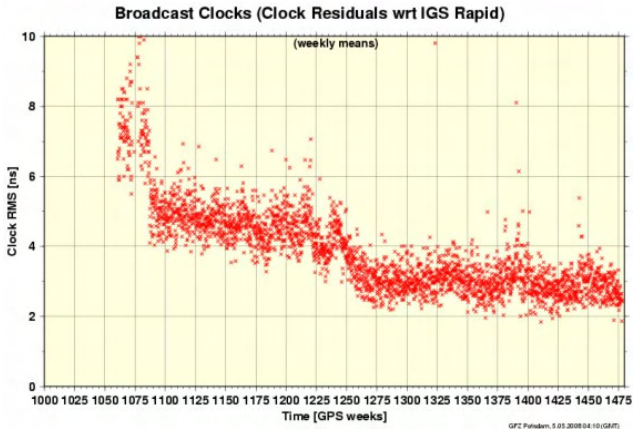

Figure 3.2: Residuals between the Broadcast and IGS *Rapid* satellite clocks (GFZ, 2008).

The quoted accuracies of the Broadcast orbit and clock corrections by the IGS are approximately 1.6m and 7ns, respectively (IGS, 2008). However, the comparison plot presented in Figure 3.2 shows that the current Broadcast satellite clock corrections are in fact more optimistic than the quoted accuracy.

3.2.2 IGS Combined Satellite Orbit and Clock Corrections

The main civilian organisation responsible for the production of precise satellite ephemerides and clock corrections is the IGS (Roulston, 2001).The products generated from the IGS are based on the combined effort from all, or most, of the IGS ACs. Each of the ACs uses data collected from numerous IGS stations around the world, which are processed using different processing software packages, algorithms, and models to generate independent solutions. These independent solutions are then weighted and combined at the IGS ACC to form the final official IGS products. The strength of this approach, as opposed to having a standard processing strategy for all ACs is that each AC has the flexibility and freedom for innovation and improvement. More importantly, this approach reduces the likelihood of errors, as it is unlikely that all ACs will be affected by the same problem at the same time (Roulston, 2001). Literature on the ACs processing procedures as well as the IGS orbit and clock corrections products combination strategies are documented at the IGS website (IGS, 2008).

3.2.2.1 IGS *Final* Satellite Orbit and Clock Corrections

The IGS *Final* satellite orbit and clock corrections are formed from the combination of seven and five ACs respectively. These ACs use different software packages like BERNESE, GAMIT, GIPSY, EPOS, BAHN and PAGES (Kouba, 2003). The IGS *Final* satellite orbit and clock corrections are usually available on the thirteenth day after the last observation. The satellite positions are sampled at 15-minute interval in SP3 format, while the clock corrections are sampled at a higher sampling rate, which is at 5-minute interval in CLK format.

At present, the IGS *Final* satellite orbit and clock corrections have the highest quality and precision among all the IGS products. The quoted accuracies of these products are better than 5cm for the orbits and better than 0.1ns for the clock corrections (IGS, 2008). The following figures, Figures 3.3 and 3.4, show residuals between the IGS ACs generated orbit and satellite clock corrections with the combined IGS *Final* products. As can be seen from these figures, the precision of the orbit and clock corrections has increased significantly in the last decade, from about 30cm to better than 3cm to 5cm, and 1.5ns to better than 0.1ns, respectively.

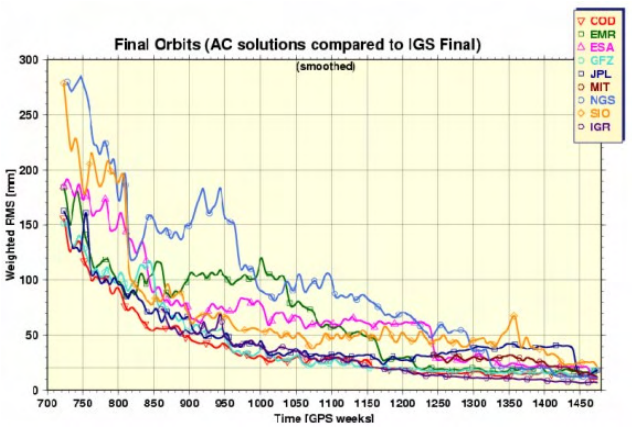

Figure 3.3: Residuals between the individual ACs generated orbits with the combined IGS *Final* orbits (GFZ, 2008).

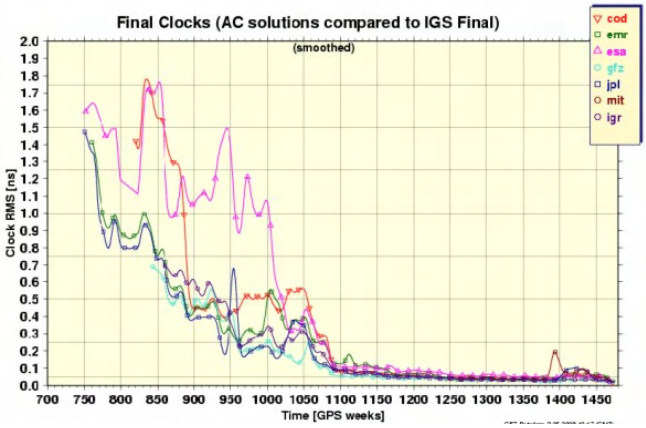

Figure 3.4: Residuals between the individual ACs generated satellite clock corrections with the combined IGS *Final* satellite clock corrections (GFZ, 2008).

3.2.2.2 IGS *Rapid* Satellite Orbit and Clock Corrections

In addition to the *Final* products, the IGS also produces precise *Rapid* orbits and clock corrections. Similar to the *Final* products, the IGS *Rapid* products are post-computed. However, they are generated with shorter latency than the *Final* products, as the number of tracking stations used in generating the *Rapid* products is less than those used in generating the *Final* products. The IGS *Rapid* satellite orbit and clock corrections are available within the next 17 hours after the end of the day of interest. It is interesting to note that the combined IGS *Rapid* orbit products, with less tracking stations, but quicker delivery times, are as precise as the best available IGS *Final* orbit products. Therefore, for most practical applications, where time and precision are priorities, the IGS *Rapid* orbit products can be used as a

substitute for the *Final* products. The published accuracies of the *Rapid* orbit and satellite clock corrections are better than 5cm and 0.1ns, respectively (IGS, 2008).

Figures 3.5 and 3.6 illustrate the residuals between the individual ACs orbit and clock corrections with the combined IGS *Rapid* products (note the different y-axis scale between Figures 3.3 and 3.5, as well as, Figures 3.4 and 3.6). From Figure 3.6, it can be seen that the quality of the satellite clock corrections has been greatly improved since the elimination of SA on 1 May 2000 (GPS week 1060). The "spike" that occurred at GPS week 1400 in the figures is caused by the IGS transition to the new *absolute* antenna phase centre model and also the change to an IGS realisation of the new ITRF 2005 (Gendt, 2006). Literature on the antenna phase centre model is provided in Section 3.5.1. The consequence of the new convention, as far as PPP users are concerned, is a general shift in the terrestrial position, station clocks, and tropospheric zenith path delay estimates. The shift will primarily have an impact on the IGS clocks (Ray, 2005b).

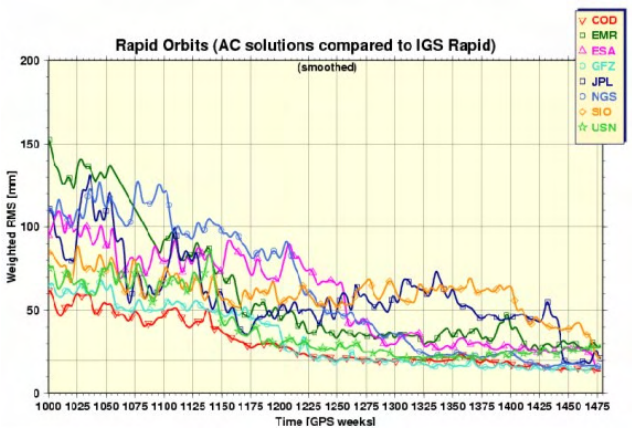

Figure 3.5: Residuals between the individual ACs generated orbits with the combined IGS *Rapid* orbits (GFZ, 2008).

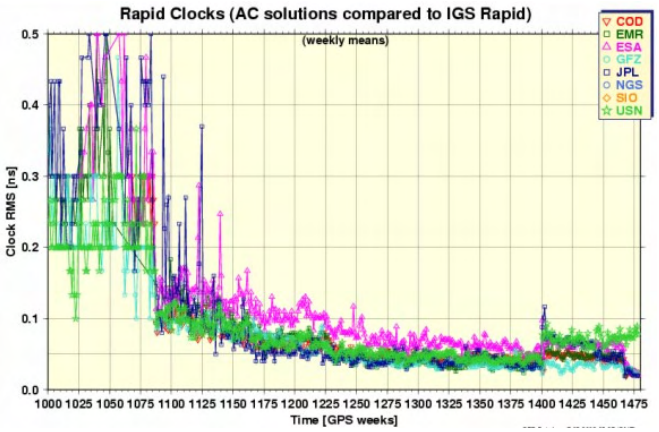

Figure 3.6: Residuals between the individual ACs generated satellite clock corrections with the combined IGS *Rapid* satellite clock corrections (GFZ, 2008).

3.2.2.3 IGS *Ultra-Rapid (Estimated Half)* Satellite Orbit and Clock Corrections

The IGS *Ultra-Rapid (Estimated Half)* orbit and clocks is another post-computed product generated by the IGS. The *Ultra-Rapid (Estimated Half)* orbit and clock corrections are near real-time products, with a latency of only three hours. The near real-time ephemerides are produced to satisfy the increasing demand from the meteorological and Low Earth Orbiters (LEOs) mission community.

The quoted accuracies of the *Ultra-Rapid (Estimated Half)* orbit and clocks are better than 5cm for the orbits and about 0.2ns for the satellite clock corrections, which are quite comparable to the more precise *Rapid* products (see Table 2.1 for comparison). Figure 3.7 shows the differences between the IGS *Ultra-Rapid (Estimated Half)* with the *Rapid* orbits. The IGS *Rapid* products are considered as "truth". The black thick line represents the smoothed IGS *Ultra-Rapid (Estimated Half)* orbits, and the pink circles denote the raw daily weighted RMS values. It can be seen from this figure that the precision of the near real-time orbits has improved over the years, as the IGS is constantly improving their spatial convergence of the global network, quality control procedures, as well as the products latency and update cycle. A graph showing the standard deviation differences between *Ultra-Rapid (Estimated Half)* with the *Rapid* clock corrections is depicted in Figure 3.8. Note that the y-axis scale is quoted in picoseconds (ps). Historical data are not available until GPS Week 1240 (NGS, 2008).

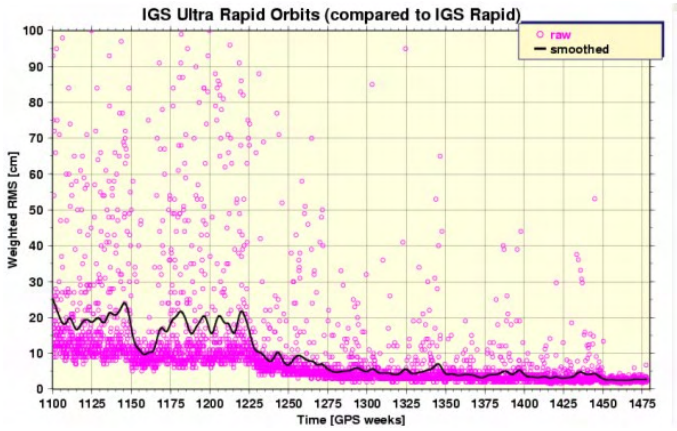

Figure 3.7: Comparison plot showing the residuals between the *Ultra-Rapid (Estimated Half)* and IGS *Rapid* orbits (GFZ, 2008).

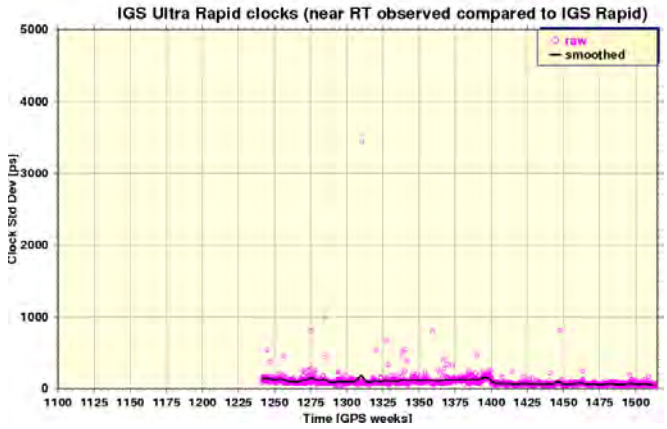

Figure 3.8: Comparison plot showing the residuals between the *Ultra-Rapid (Estimated Half)* and IGS *Rapid* satellite clock corrections (NGS, 2008).

The IGS *Ultra-Rapid (Estimated Half)* satellite orbit and clock corrections are only available in SP3 format. The file contains 48 hour orbit arc, from which 24 hours are real orbit estimates, hence known as the *Ultra-Rapid (Estimated Half)*. The remaining 24 hours are orbit predictions, known as the *Ultra-Rapid (Predicted Half)*. Since May 2004, the update cycle for the *Ultra-Rapid* products have increased from twice to four times daily (IERS, 2004). Therefore, the *Ultra-Rapid* products are released four times a day, at 03:00, 09:00, 15:00, and 21:00 Universal Coordinated Time (UTC). The *Ultra-Rapid* products, both orbits and clock corrections, are sampled at 15-minute sampling interval.

3.2.2.4 IGS *Ultra-Rapid (Predicted Half)* Satellite Orbit and Clock Corrections

The real-time IGS satellite orbit and clock corrections, better known as the *Ultra-Rapid (Predicted Half)* products, has an average prediction age of 6 hours. The predicted orbit and clock corrections are extrapolated based upon the most recent GPS observational data from the IGS hourly tracking network. Since the *Ultra-Rapid* file has a latency of 3 hours, and it contains both the observed (estimated) and extrapolated (predicted) orbits and clocks, the corrections between 3 hours to 9 hours in the predicted part of the *Ultra-Rapid* ephemerides are the most relevant for real-time applications (NGS, 2008).

Figure 3.9 shows comparison between the IGS *Ultra-Rapid (Predicted Half)* and the *Rapid* orbits. From this figure, it can be seen that the outliers of the satellite orbit predictions have reduced significantly since GPS Week 1425, and the heavy horizontal band of points is in fact within 5cm to 10cm. Figure 3.10 shows the residuals between the individual ACs generated satellite clock corrections with the combined IGS *Rapid* satellite clock corrections. The published accuracies of the *Ultra-Rapid (Predicted Half)* orbit and clock corrections are about 10cm and 0.5ns, respectively (IGS, 2008).

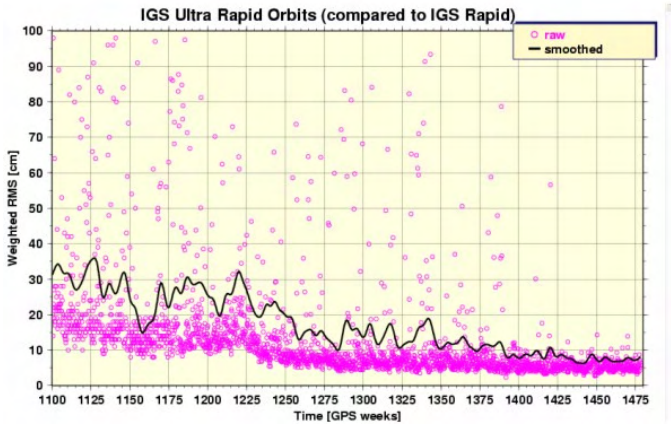

Figure 3.9: Comparison plot showing the residuals between the *Ultra-Rapid (Predicted Half)* and IGS *Rapid* orbits (GFZ, 2008).

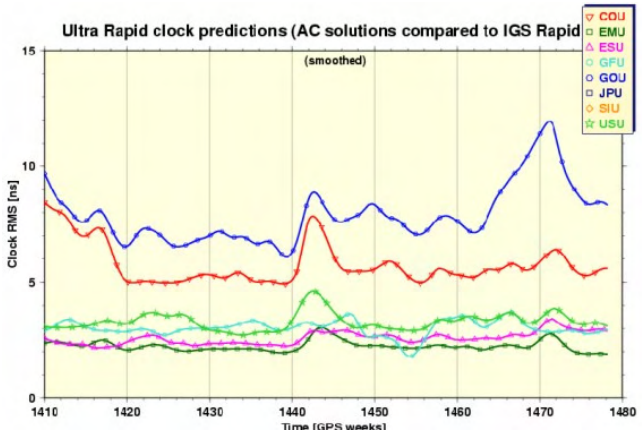

Figure 3.10: Residuals between the individual ACs generated predicted satellite clock corrections with the combined IGS *Rapid* satellite clock corrections (GFZ, 2008).

3.2.3 Satellite Orbit and Clock Interpolation Method

Most of the satellite orbit and clock corrections files are given at an evenly spaced time, e.g. 15-minute or 5-minute. A typical GPS user collects data at intervals ranging from 1-second to 30-second, and thus needs to know the satellite positions and satellite clock corrections at the times of the data when it is collected. In this research, the Chebyshev polynomial interpolation method was implemented in the software.

The Chebyshev polynomial of degree n on [-1, 1] is expressed as,

$$T_n(x) = \cos(n \arccos x) \tag{3.1}$$

The Chevyshev polynomial can be computed recursively,

$$T_n(x) = \cos(n \arccos x) \tag{3.2}$$

starting from $T_0(x) = 1$ and $T_1(x) = x$.

In addition,

$$\int_{-1}^{1} \frac{T_n(x)T_k(x)}{\sqrt{1-x^2}} = \begin{cases} 0 & \mathrm{k} \neq \mathrm{n} \\ \pi & \mathrm{k} = n = 0 \\ \frac{\pi}{2} & \mathrm{k} = \mathrm{n} \neq 0 \end{cases} \tag{3.3}$$

so that the polynomials satisfy an orthogonality relation, with respect to the weight function $w(x) = \frac{1}{\sqrt{1-x^2}}$.

The advantage of the Chebyshev polynomial expansion compared to other polynomials is that it is capable of providing a much better approximation (Seeber, 2003). In addition, the Chebyshev polynomial will not suffer from the disadvantage of higher order polynomials, that is, the error does not increase rapidly near the endpoints of the interval. In other words, the maximum deviation on the interval in the Chebyshev polynomial is minimal (Neta *et al.*, 1996).

Note: The most precise IGS Final satellite orbit and clock corrections were routinely used in this research to eliminate the biases, unless stated otherwise. An investigation into the performance of the IGS Final, Rapid, Ultra-Rapid corrections products as well as the Broadcast ephemerides in single frequency PPP was undertaken as part of this research and the corresponding findings are given in Chapter 7.

3.3 Ionospheric Effects

The ionosphere is the uppermost layer of the Earth's atmosphere between the height of 50km to 1000km above the Earth's surface. In this region, the density of free electrons and ions is high enough to influence the propagation of satellite signals (Kleusberg and Teunissen, 1996). The ionisation process is primarily driven by the Sun activity and it varies strongly with time, solar activity, the Earth's magnetic field, as well as geographical location (Camargo *et al.*, 2000; Todorova *et al.*, 2006). The effects on GPS point positioning can vary from a few metres to more than twenty metres within a day, depending on the user's location and time plus variations in the ionosphere. The day-to-day TEC variability from the monthly

mean value, at any given time and location, is approximately 20-25% (1 sigma) (Klobuchar, 1996).

The ionosphere is a dispersive medium, whereby the refraction is dependent on the signal frequency passing through it. The ionospheric delay can be defined as being inversely proportional to the square of the transmission frequency. Thus, dual frequency GPS receivers can take advantage of this property of the ionosphere to directly measure and remove the ionospheric effect by forming the dual frequency ionosphere-free linear combination (see Section 2.6.1 for the dual frequency ionosphere-free linear combination equations), sometimes referred to as the L3 combination (Klobuchar, 1996). Single frequency GPS users, on the other hand, are unable to utilise this to alleviate the ionospheric delay. Therefore, single frequency GPS users must rely on an external ionospheric product or model to correct for the delay. The accuracy of these ionospheric models is critical to achieve high accuracy PPP solutions.

The next sections describe the sunspot cycle, variability of TEC, the ionosphere in different zones of latitude, as well as the different ionospheric error mitigation methods that were investigated and applied in this research. The rationale is to provide readers with an understanding of these phenomena as they will form the basis for the design of the case studies undertaken as part of this research. The details of the case studies will be given in Chapter 5.

3.3.1 Ionospheric Variability

3.3.1.1 Sunspot Cycle

The energy source driving all solar phenomena, which affect the space weather, is known as the solar magnetic activity cycle or the sunspot (solar) cycle. A sunspot cycle is the time period from solar minimum to solar maximum as measured by the number of sunspots (dark patches on the Sun's surface). The average duration of a sunspot cycle is 11 years, although sunspot cycles as short as 9 years and as long as 14 years have been observed. The sunspot activities follow a periodic variation, and the cycles are not usually symmetric. The time from the solar minimum to maximum is shorter than the time from maximum to minimum (Leick, 2004). Figure 3.11 illustrates the daily sunspot counts from 1998 to 2008.

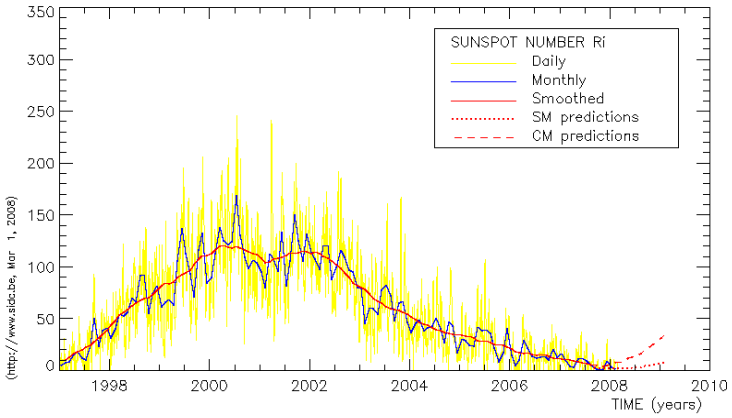

Figure 3.11: The daily sunspot counts from 1998 to 2008 (Solar Influences Data Analysis Center, 2008).

The number of sunspot counts are good indicators of solar activities, which has direct influence on the ionosphere and subsequently the GPS signals that pass through it (Leick, 2004; Wyllie, 2007). However, there is no strict mathematical relationship between them. It can happen that GPS is adversely affected even when daily sunspot counts are actually low. At the time of writing this thesis, we are approaching the end of Solar Cycle 23 (solar minimum) and are on the heels of the start of Solar Cycle 24 (solar maximum) peaking in 2011 or 2012.

3.3.1.2 Variability of Total Electron Content

The electron density integrated along the satellite signal path is called the TEC, or the slant TEC. TEC is usually quantified by the number of free electrons presented along the signal path with units of electrons per 1m². That is, 1 TEC unit (TECU) is equal to $10^{16} el/m^2$ (10^{16} electron contained in a cylinder of cross section of 1m² aligned with the signal path); and 1 TECU will cause approximately 0.163m range delay on the GPS L1 frequency (Klobuchar, 1996; Øvstedal *et al.*, 2006). Another term that is used often in ionospheric modelling and mapping is the Vertical TEC (VTEC). As the signal path length is the shortest in the zenith direction, the VTEC is the lowest. It should be remarked that irregularities in electron density can cause scintillation (fading in amplitude and changes in phase) of the radio signals, which degrade the GPS receivers tracking and navigation performance.

TEC is a function of the amount of insolation (incident solar radiation). The TEC above a particular spot on the Earth has strong diurnal variations, which is controlled by the solar radiation (Klobuchar, 1996). It is known that the daytime maximum TEC occurs at around 14:00 to 15:00 Local Time (LT), and these values are usually a factor of 2 to 4 times larger than the nighttime TEC (Skone *et al.*, 2001). The TEC variations are also associated with the sunspot cycle and seasonal variations. According to Klobuchar *et al.* (1995), the increment of the TEC values in the middle latitude region from the periods of solar minimum to maximum is by a factor of 2 to 3 times. Kunches (2000) has also reported that at a typical middle latitude station, the daily variability of TEC during the periods of solar minimum is in the order of 10 TECU; while, the daily TECU variability could sometimes reach up to 100 TECU. The seasonal TEC values in the middle latitude region are larger during the winter months than summer months (Soicher and Gorman, 1985). However, this is only true for the northern hemisphere. The southern hemisphere experiences an opposite trend (Wu *et al.*, 2006; Wyllie, 2007). Larger seasonal TEC values are observed during the summer months than the winter months. The variability of VTEC values at 14:00LT at three specific ARGN stations for the year 2006 is shown in Figure 3.12. As it can be seen from this figure, the VTEC is higher during the summer months (December to February) than the summer months (July to September).

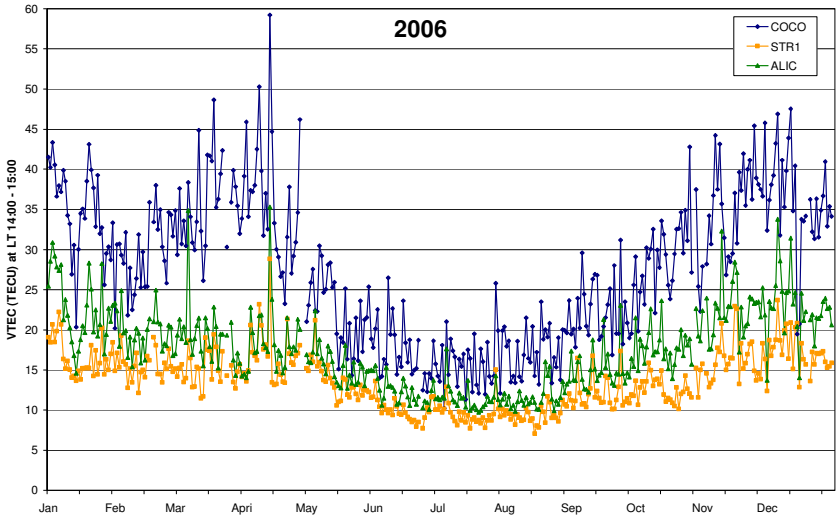

Figure 3.12: The daily VTEC at 14:00LT at Cocos Island (COCO), STR1 and ALIC ARGN stations for the year 2006.

In addition to the seasonal and diurnal variations of TEC, changes in TEC can also occur on much shorter time scales, e.g. 10 minutes. One of the phenomena responsible for

such changes is the travelling ionospheric disturbance, which is a manifestation of waves occurring in the upper atmosphere caused by severe weather and volcanic eruptions (Klobuchar, 1996).

3.3.2 The Ionosphere in Zones of Latitude

The Earth can be separated into three latitudinal regions. The three regions are the equatorial (low), middle and high latitudinal regions. Figure 3.13 denotes the latitudinal regions defined by circles of latitude.

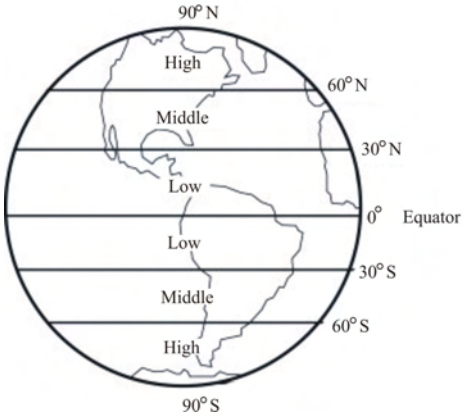

Figure 3.13: Earth's latitudinal regions used in this research.

3.3.2.1 Equatorial Region

The equatorial or low latitudinal region generally has the highest global TEC values. This is due to the stronger insolation in this region which produces enhanced ionisation along with the most disturbed ionospheric conditions caused by amplitude and phase scintillation effects (Fu *et al.*, 1999; Wyllie, 2007).

A prominent characteristic of the equatorial region is the Appleton anomaly (Appleton, 1954), or commonly known as the equatorial anomaly. This anomaly consists of two electron density maxima, located approximately 10˚ to 15˚ north and south of the equator. The daily equatorial anomaly generally starts to develop around 09:00LT to 10:00LT, reaching its maximum development at approximately 14:00LT to 15:00LT (Huang and Cheng, 1991; Skone, 2000). However during the periods of solar maximum, this anomaly may peak at about 21:00LT, with stronger scintillation effects occurring predominantly at post

sunset periods, i.e. 20:00LT to 02:00LT (Basu *et al.*, 1988). Scintillation effects are generally largest during periods of solar maximum and these degrade the GPS signals and receiver tracking capabilities.

3.3.2.2 Middle Latitude Region

The middle latitude region (or mid-latitude region) is the most studied and researched region of all the latitude zones. This is because the majority of the instruments used to observe the ionospheric conditions are located in this region. The mid-latitude region has the least variability in TEC values as compared to the equatorial and high latitude regions, which makes it stable and less disturbed. The TEC behaviour in this region has a diurnal minimum just before dawn and a diurnal maximum near 14:00LT. The standard deviation of the TEC day-to-day fluctuation about the monthly average value for any given daytime hour could generally reach 20% to 25% of the mean value (Klobuchar, 1987).

3.3.2.3 High Latitude Region

The high latitude ionosphere can be divided into the polar cap, auroral, and sub-auroral regions. The dynamic behaviour of the high latitude region has attracted many studies and research in the past decade. Different from the other zones of latitude, the unique behaviour of this region is predominately characterised by the complex interaction between the terrestrial magnetic field and charged particles flowing outwards from the Sun (solar wind) (Skone *et al.*, 2001). During the periods of enhanced solar-terrestrial interaction, energetic particles emitted from the Sun are trapped in the Earth's magnetic field, and accelerate into the high latitude ionosphere along the terrestrial magnetic field lines. These particles are energised through interactions between the Earth's magnetic field and solar wind (Nichols *et al.*, 1999), resulting in optical and ultraviolet emissions known as the aurora borealis and australis (northern and southern lights). This phenomena is common in the auroral region (Skone *et al.*, 2001). In the sub-auroral region (equatorward auroral boundary), the energetic particles are also present during the geomagnetically enhanced periods. The resulting effects can cause ionospheric range error in GPS positioning, and in severe cases, GPS receivers may lose tracking and navigation capabilities. The polar cap region, on the other hand, is enclosed by the auroral oval. The characteristics of this region are relatively less well known due to the lack of observing instruments and data.

3.3.3 Ionospheric Error Mitigation Methods Used In This Study

3.3.3.1 Broadcast Model

In the mid-1970s, a simple algorithm was developed for single frequency GPS users to correct for approximately 50% RMS of the ionospheric range error (Klobuchar, 1987; Klobuchar, 1996). This simple algorithm is called the Broadcast (ionospheric) model, or more famously known as the Broadcast Klobuchar model, named after its developer, John A. Klobuchar. The ionospheric coefficients used in the Broadcast model are available to all GPS users as part of the broadcast navigation message.

The Broadcast model is a truncated version of a much larger empirical model of TEC developed by Bent over 36 years ago (Llewellyn and Bent, 1973). The 50% correction goal was established as a compromise between, i) the number of coefficients required to be sent as part of the satellite message, ii) the coefficients update frequency, and iii) the awareness that even the state-of-the-art computationally intensive models could only remove 70% to 80% RMS of the ionospheric effects (Klobuchar, 1987; Wyllie, 2007).

The Broadcast model is based on the single-layer model or "thin shell model" of the ionosphere (see Figure 3.16). The implicit assumption of this model is that the TEC is concentrated in an infinitesimally thin spherical layer at a certain height. In the case of the Broadcast model, the single-layer model height is assumed to be 350km (Klobuchar, 1987; Leick, 2004). Another characteristic of the Broadcast model is that this model assumes the maximum daily TEC value occurs at about 14:00LT.

3.3.3.2 Global Ionosphere Maps

On 28 May 1998, the IGS Ionosphere Working Group (Iono-WG) was established by the IGS Governing Board and commenced working in June 1998 (Hernández-Pajares, 2003; Hernández-Pajares, 2005). Its main responsibility is the routine generation of the combined GIMs on a daily basis.

Currently, four IGS Ionosphere Associate Analysis Centres (IAACs) are contributing their ionospheric products to the IGS Iono-WG (Hernández-Pajares, 2008). These include the CODE, ESOC, JPL, and Technical University of Catalonia (UPC). The IAACs produce 2-

dimensional ionosphere TEC maps that refer to a 450km shell height. The mathematical approaches, as well as, the number of IGS stations used by the individual IAACs in formulating their ionospheric TEC maps are quite different. Details on the individual IAACs modelling can be found in Gao *et al.* (1994), Feltens (1998), Mannucci *et al.* (1998), Hernández-Pajares *et al.* (1999) and Schaer (1999). It should be noted that although the IAACs have different approaches in computing the TEC maps, the produced ionospheric TEC maps from individual IAAC have common spatial and temporal resolutions, as well as, daily sets of GPS satellite and IGS station receiver hardware Differential Code Biases (DCBs).

There are four validation centres, namely ESOC, JPL, NRCan and UPC. ESOC and JPL are responsible for providing IGS TEC comparison with ENVISAT and JASON altimeters TEC, while NRCan and UPC are in-charge of providing individual IAACs weight based on the geographic-dependent weighting algorithm for the production of the combined GIMs (Hernández-Pajares, 2004). Detailed information on the combination/comparison and weighting scheme can be found in Feltens (2003). The final computation of the combined IGS GIMs is processed and distributed from UPC. In addition, the combined GIMs are routinely compared and validated for its accuracy with TOPEX and JASON altimeter data. In April 2003, the IGS *Final* GIMs in IONsphere map EXchange (IONEX) format (Schaer *et al.*, 1998) became an official IGS products with a latency of 11 days. Meanwhile, a *Rapid* version of the TEC maps with a latency of less than 24 hours has been made available to the public since December 2003. Refer to Table 2.1 for products description. The GIMs can be treated as a “snapshot” of the global ionospheric TEC distribution at a specific interval. Figure 3.14 is an example of the 2-dimensional GIMs.

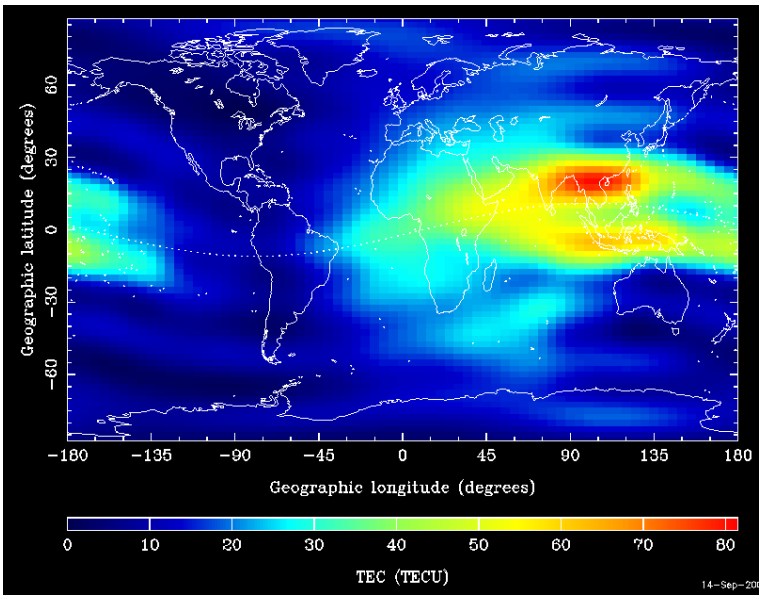

Figure 3.14: A snapshot of global TEC distribution based on the GIMs at 00:00 Universal Time (UT) on 9 September 2004 (CODE, 2007).

3.3.3.3 Australia-Wide Regional Ionosphere Maps

Besides the GIMs, single frequency GPS users may also benefit from the high spatial resolution RIMs. At present, RIMs for the Australian region are not routinely generated. In this research, an in-house software was used to create and produce the Australia-wide RIMs. The algorithm used in the software was based on a new method known as the Distance Weighted Model of Multi-Spherical Harmonic Functions. Detailed description of the development of the RIMs can be found in Zhang *et al.* (2008).

The GPS stations used to generate the Australia-wide RIMs are in Australasia and part of the South East Asia region. The north-south boundary of the generated RIMs is 12˚N to 60˚S, and the east-west boundary is 60˚E to 5˚W. This is to ensure that the Ionospheric Pierce Points (IPPs) (see Figure 3.16) for all GPS stations on the Australian continent are covered by the ionosphere maps. It should also be noted that the number of GPS stations used to generate the Australia-wide RIMs would differ for each year. As more tracking stations are established in the region, more data would be used to model the ionosphere. For example, about 80 GPS stations data were used to generate the RIMs for the year 2006, while only 30 GPS stations data were used for year 2001. Figure 3.15 shows an example of the Australia-wide RIMs at 02:00UTC on DOY 183 2006. It should be noted that the RIM has been cropped for illustration purpose.

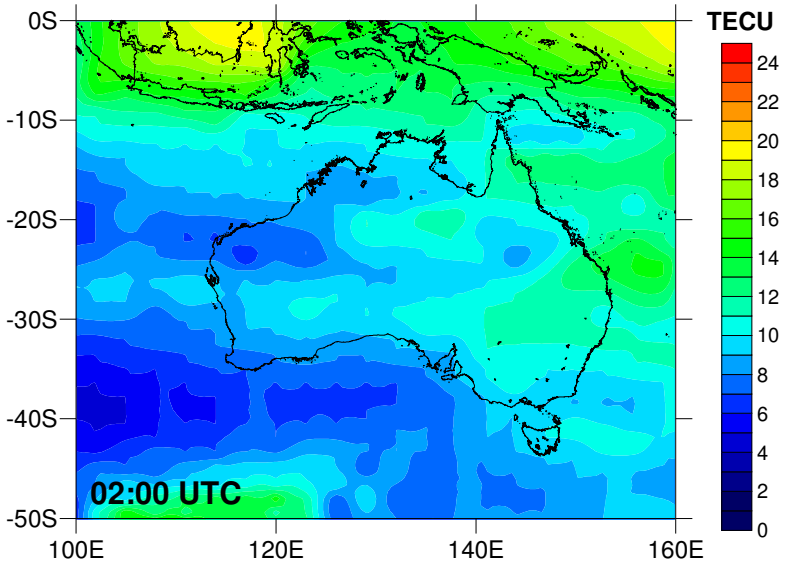

Figure 3.15: A snapshot of regional TEC distribution based on the Australia-wide RIMs at 02:00UTC on DOY 183 2006 (Choy *et al.*, 2008c).

3.3.3.4 Single Frequency Ionosphere-Free Code and Phase Delay

Perhaps the least appreciated technique for single frequency GPS users to correct for the ionospheric error is the single frequency ionosphere-free code and phase delay observables (Yunck, 1993). A beneficial characteristic of the ionosphere is that it delays the code but advances the carrier phase observations. Single frequency GPS users can take advantage of this property to eliminate the ionospheric error by taking the simple average of the code and carrier phase delay observables (Yunck, 1993; Montenbruck, 2003; Simsky, 2006). The single frequency ionosphere-free code and phase delay is implemented in this research as the quasi-phase observables.

3.3.4 Single-Layer Model and Ionospheric Mapping Function

In order to refer the VTEC to specific solar-geomagnetic coordinates, the single-layer or thin-shell model is usually adopted for the ionosphere. Figure 3.16 illustrates the single-layer model. It assumes that the TEC is concentrated in an infinitesimally thin shell at a certain altitude (H) from the surface of the Earth. The altitude, or height of the single layer model is usually from 350km to 450km, approximately corresponding to the altitude of maximum electron density (Schaer, 1999). The IGS GIMs and the Australia-wide RIMs

assume a fixed altitude of 450km for the single-layer model, while the Broadcast model assumes a single layer model height of 350km.

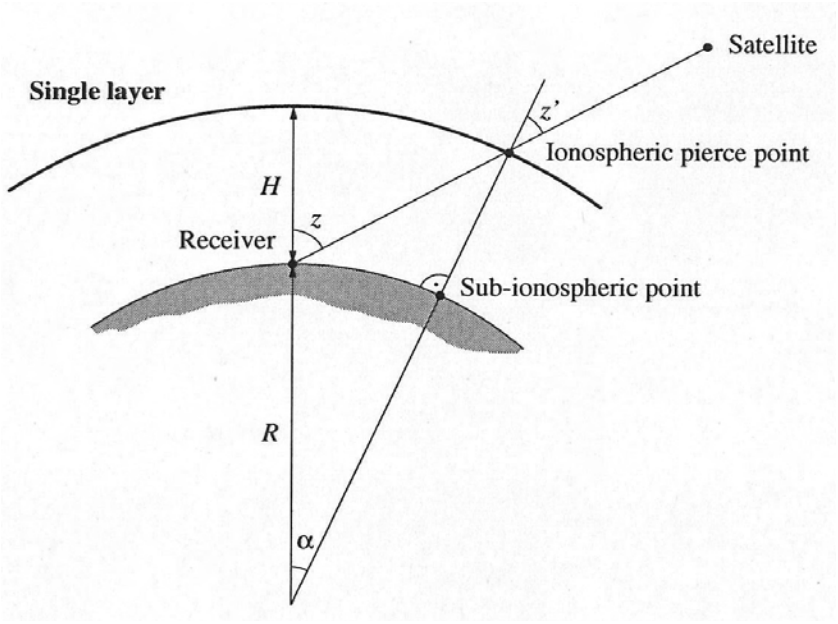

Figure 3.16: The single-layer model (Schaer, 1999)

The intersection of this shell and the satellite-receiver line of sight at a given local time is defined as the IPPs. The relationship between the satellite's zenith angle at the IPP (z'), and the zenith angle at the receiver's location is given as,

$$\sin z' = \frac{R}{R+H} \sin z \tag{3.4}$$

where R is the radius of the Earth (≈ 6371km).

As GPS always provides TEC measurements along the ray path (i.e. slant TEC), and VTEC is of main interest for absolute TEC mapping, an elevation-dependent mapping function (or ionospheric slant factor) $F(z)$ which described the ratio between the slant TEC and VTEC is required.

$$\text{Slant TEC} = \text{VTEC} \cdot F(z) \tag{3.5}$$

where,

$$F(z) = \frac{1}{\cos z'} = \frac{1}{\sqrt{1 - \sin^2 z'}} \tag{3.6}$$

Note: The GIMs were used predominantly in this research, unless stated otherwise. The feasibility of using the Broadcast model, GIMs, and Australia-wide RIMs was examined as part of this research. The results and analysis of the comparison are presented in Chapter 5.

3.4 Tropospheric Delay

The troposphere is the lower layer of the atmosphere. It extends from the surface of the Earth to about 50km into the atmosphere. Unlike the ionosphere, the troposphere is a non-ionised and a non-dispersive medium, i.e. the refraction is independent of the signals' frequency passing through it (Leick, 2004). Thus, the tropospheric delay cannot be eliminated using dual frequency observations. Another characteristic of the troposphere is that it delays both the code and carrier phase signals by the same magnitude.

It is extremely difficult to alleviate the troposphere delay completely. This is because the tropospheric effect not only depends on the satellite elevation angle and receiver altitude, but also on the atmospheric temperature, pressure and humidity. The troposphere is usually divided into two components, the dry (hydrostatic) and the wet part.

The wet component is the lower region of the troposphere, extending to about 12km from the Earth's surface. This region is highly affected by the humidity because it contains most of the water vapour. As the water vapour varies as a function of time and position, it makes it extremely difficult to model. About 10% of the tropospheric delay magnitude is caused by the wet portion of the troposphere. The dry component, on the other hand, is the higher portion of the troposphere. This component contains mostly dry gases, i.e. Nitrogen and Oxygen, which makes it easier to model. The dry component of the troposphere contributes to the remaining 90% of the total tropospheric delay.

The delay caused by the dry and wet components of the troposphere is usually modelled at the zenith angle and then scaled by an appropriate mapping function to any

satellite elevation angles. Therefore, the total tropospheric delay d_{trop} can be expressed in an equation as the combination of the delay caused by the dry and wet components (Shen, 2002),

$$d_{trop} = d_{dry} \cdot M_{dry} + d_{wet} \cdot M_{wet} \tag{3.7}$$

where d_{dry} and d_{wet} are the tropospheric ZPD caused by the dry and wet components, respectively; M_{dry} and M_{dry} are the appropriate mapping functions for the dry and wet components, respectively.

Many studies have been undertaken over the past few decades to develop robust tropospheric models. Examples of the models are Hopfield and Saastamoinen models (Hopfield, 1969; Saastamoinen, 1972). In addition to the tropospheric models, there are also different mapping functions developed to map the tropospheric ZPD as a function of elevation angles. Examples are the Chao, Herring, Lanyi, Davies and Niell mapping functions (Chao, 1974; Lanyi, 1984; Davis *et al.*, 1985; Herring, 1992; Niell, 1996; Mendes and Langley, 1998, 2000; Niell, 2000; Xu, 2003). The following sections will introduce briefly the tropospheric model (Hopfield model) and mapping function (Niell mapping function), which were used in this research. The choice of the tropospheric model and mapping function was based on several publications and recommendations, as well as its performance in both high and low elevations and its independence from surface meteorological data (Witchayangkoon, 2000; Leick, 2004; Abdel-salam, 2005).

3.4.1 Hopfield Model

The Hopfield model was developed by Helen S. Hopfield in 1963, with subsequent improvements in 1965 and 1969 (Hopfield, 1969). The model is based on a large number of meteorological radiosonde profiles made at various geographical locations over a number of years (Mekik, 1997).

The Hopfield model assumes a single polytropic (a model atmosphere in hydrostatic equilibrium) atmospheric layer that ranges from the Earth's surface to an altitude of about 11km and 40km for the wet and dry layers, respectively (Witchayangkoon, 2000; Hofmann-Wellenhof *et al.*, 2001). The dry and wet part of the tropospheric path delay can be written as,

$$\Delta_d^{Trop} = 10^{-6} N_{d,0}^{Trop} \int \left[\frac{h_d - h}{h_d} \right]^4 ds \tag{3.8}$$

$$\Delta_w^{Trop} = 10^{-6} N_{w,0}^{Trop} \int \left[\frac{h_w - h}{h_w} \right]^4 ds \tag{3.9}$$

where $N_{d,0}^{Trop}$ and $N_{w,0}^{Trop}$ are the dry and wet tropospheric refractivities for the station on the Earth's surface as a function of pressure in millibars and temperature in Kelvin, respectively; h_d and h_w are the respective polytropic thickness for the dry and wet part in metres, and h is the station height in metres above the Earth's surface.

The integral can be solved if the delay is calculated along the vertical direction and if the curvature of the signal path is neglected (Hofmann-Wellenhof *et al.*, 2001). Thus, for an observation station on the Earth's surface (i.e. $h = 0$), the tropospheric zenith path delay in metres can be expressed as,

$$\Delta^{Trop} = \frac{10^{-6}}{5} \left[N_{d,0}^{Trop} h_d + N_{w,0}^{Trop} h_w \right] \tag{3.10}$$

The Hopfield zenith tropospheric path delay Equation (3.10), can be used with a mapping function to obtain the tropospheric delay for a specific satellite elevation angle at a specific epoch.

3.4.2 Niell Mapping Function

The Niell mapping function was developed by Arthur E. Niell in 1996 (Niell, 1996). It is different from most of the other mapping functions (e.g. Lanyi, Davies and Herring mapping functions) because the Niell mapping function is essentially independent of the surface meteorology data. Niell (1996) suggested that the mapping function coefficients can be parameterised in terms of the site geographical latitude and the day of the year as studies have shown that the properties of the atmosphere are more representative than surface measurements for overall accuracy (Niell, 2001).

Based on the hydrostatic Niell mapping function, the parameter a (at tabular latitude φ_i at time t), from January 0.0 (in UTC days) is given in Equation (3.11) (Niell, 1996).

$$a(\varphi_i, t) = a_{avg}(\varphi_i) - a_{amp}(\varphi_i)\cos\left(2\pi\frac{t - T_0}{365.24}\right) \tag{3.11}$$

where, T_0 is the adopted phase, i.e. Day-Of-Year (DOY) 28 in the southern hemisphere, and the value of $a(\varphi,t)$ is obtained by linearly interpolating between the nearest $a(\varphi_i,t)$, a_{avg} and a_{amp} are the average and amplitude coefficients, respectively (see Table 3.1). A similar procedure is followed for the parameters b and c.

In addition to latitudinal and seasonal dependence, the hydrostatic mapping function is also dependent on the height above the sea level of the observation point. However, this does not apply to the wet mapping function since the distribution of the water vapour is not expected to be predictable from the station height. The coefficients for the hydrostatic and wet Niell mapping function are tabulated in Tables 3.1 and 3.2, respectively. No temporal dependence is included in the wet mapping function, thus only an interpolation in latitude for each parameter is required.

The height correction associated with the hydrostatic Niell mapping function is provided as,

$$\frac{dm(\varepsilon)}{dh} = \frac{1}{\sin(\varepsilon)} - f(\varepsilon, a_{ht}, b_{ht}, c_{ht}) \tag{3.12}$$

$$\Delta m(\varepsilon) = \frac{dm(\varepsilon)}{dh} H \tag{3.13}$$

where, $\frac{dm(\varepsilon)}{dh}$ is the mapping function height correction, $\Delta m(\varepsilon)$ is the height correction, ε is the elevation angle, H is the station height above sea level, and a_{ht}, b_{ht}, c_{ht} are also given in Table 3.1.

Table 3.1: Coefficients of the hydrostatic mapping function (Niell, 1996).

Coefficients	Latitude φ_i				
	15°	**30°**	**45°**	**60°**	**75°**
			Average		
a	1.2769934 e -3	1.2683230 e -3	1.2465397 e -3	1.2196049 e -3	1.2045996 e -3
b	2.9153695 e -3	2.9152299 e -3	2.9288445 e -3	2.9022565 e -3	2.9024912 e -3
c	62.610505 e -3	62.837393 e -3	63.721774 e -3	63.824265 e -3	64.258455 e -3
			Amplitude		
a	0.0	1.2709626 e -5	2.6523662 e -5	3.4000452 e -5	4.1202191 e -5
b	0.0	2.1414979 e -5	3.0160779 e -5	7.2562722 e -5	11.723375 e -5
c	0.0	9.0128400 e -5	4.3497037 e -5	84.795348 e -5	170.37206 e -5
			Height Correction		
	a_{ht}	2.53 e -5			
	b_{ht}	5.49 e -3			
	c_{ht}	1.14 e -3			

Table 3.2: Coefficients of the wet mapping function (Niell, 1996).

Coefficients	Latitude φ_i				
	15°	**30°**	**45°**	**60°**	**75°**
a	5.8021897 e -4	5.6794847 e -4	5.8118019 e -4	5.9727542 e -4	6.1641693 e -4
b	1.4275268 e -3	1.5138625 e -3	1.4572752 e -3	1.5007428 e -3	1.7599082 e -3
c	4.3472961 e -2	4.6729510 e -2	4.3908931 e -2	4.4626982 e -2	5.4736038 e -2

3.4.3 Estimation of Tropospheric Zenith Path Delay in PPP

The variability of the dry component is relatively low and can be estimated with a precision of approximately 1% when the surface pressure is known to mmHg (millimetres of mercury) level accuracy (Rizos, 1999). Most of the available tropospheric models can adequately and quite precisely model the dry component of the tropospheric ZPD. For the wet component, this delay is extremely difficult to estimate due to the existence of water vapour. Since the residual of the wet zenith tropospheric delay could be significant even after the use of a tropospheric model, the wet zenith tropospheric delay can be treated as an unknown and

estimated along with the other parameters in PPP processing (Kouba and Hèroux, 2000; Shen, 2002; Abdel-salam, 2005). This is implemented in the research software.

Note: The Hopfield model and Niell mapping function were used in this research to remove the bulk of the tropospheric delay. Section 6.4 will discuss the implications of modelling and estimating the tropospheric delay on the quality of the single frequency PPP solutions, as well as the convergence behaviour.

3.5 PPP and Its Associated Errors

There are several GPS errors that are frequently neglected or receive little attention from the GPS community but are relevant for PPP. The reasons are that these errors are removed in the case of relative positioning or the magnitude of these errors is insignificant with respect to the affordable GPS positioning accuracy (Abdel-salam, 2005). Since the PPP approach is based on un-differenced solutions, errors such as satellite and receiver antenna phase centre offsets, phase wind-up errors, relativity, group delay differential biases, and geophysical effects such as solid earth tides, atmospheric and ocean loading must be considered for high accuracy point positioning. The following sections briefly describe these biases.

3.5.1 Antenna Phase Centre Offsets and Variations

- **Receiver Antenna**

GPS range measurements are measured from the satellite transmitting antenna to the electrical phase centre of the receiving antenna. The receiver electrical phase centre is not a physical centre and is neither well defined nor fixed. Furthermore, for any given GPS antenna, the variation of the phase centre depends on the changing direction of the incoming GPS satellite signals, and it is a function of the antenna phase pattern, known as the Phase Centre Variations (PCVs). As a result of this, every GPS antenna will have, in addition to the antenna phase centre offset, antenna PCVs as a function of satellite elevation angle. The receiver antenna phase centre offset can cause positioning errors up to 10cm in the vertical component and a few centimetres in the horizontal component. For relative positioning over short baselines, this offset will be cancelled out provided that the users apply the correct models. However, this offset needs to be "manually" corrected in PPP.

Since 30 June 1996, the *relative* GPS antenna phase centre corrections had been applied by most of the IGS ACs to allow for a non-spherical phase response of the tracking antennas (Schmid *et al.*, 2007). The *relative* antenna phase centre correction values were derived from data collected on a short baseline. For each antenna model calibrated, a north, east, and up offset value was adopted as the mean location of the antenna electrical reference centre. Relative to the antenna phase centre offsets, the antenna PCVs were then measured as a function of elevation angle (Gendt and Schmid, 2005). The relative antenna phase centre offsets and variations are published in the *igs_01.pcv* file and the file is available from the IGS website (IGS, 2008).

The drawback of *relative* antenna PCVs is that the corrections are dependent on the assumed zero reference antenna, and that, the elevation range for the antenna PCVs has been limited to 10˚ due to the ground noise. Moreover, these systematic errors do not cancel out for long baselines even though similar antenna types are used because identical satellites may appear at different elevations at the two tracking stations. Due to these limitations, *relative* GPS antenna phase centre corrections can no longer satisfy the increasing demand for high accuracy positioning. Therefore, the only solution for this problem is the transition from *relative* to *absolute* phase centre corrections.

On 5 November 2006, the IGS has adopted the *absolute* antenna phase centre offsets and variations for its routine generation of precise satellite orbits and stations coordinates. The *absolute* antenna corrections for the receiver can be obtained from two independent methods, that is, the measurements in an anechoic chamber and the field measurements on a short baseline using a robot that is capable of tilting and rotating one of the antennas. The *absolute* receiver antenna phase centre information is contained in the file igs05_wwww.atx, where 'wwww' stands for the GPS week of the last file modification. The .atx file is available from the IGS website (IGS, 2008).

- **Satellite Antenna**

The satellite antenna phase centre offsets originate from the separation between the GPS satellite centre of mass and the electronic phase centre of its antenna. The orbital information in the broadcast navigation message refers to the satellite antenna phase centre. But the force models used by the IGS community for satellite orbit modelling refer to the satellite centre of mass. Subsequently, the resulting IGS precise satellite orbit and clock correction products also refer to the satellite centre of mass, and not the antenna phase centre.

Since the GPS range measurements are made from the antenna phase centre, users who utilise and constrain the IGS precise orbit and clock corrections in their positioning solutions need to consider the satellite phase centre offsets and monitor the orientation of the offset vectors in space as the satellite orbits the Earth (Kouba, 2003). If the offset is left uncorrected, users interested in estimating the satellite clock corrections, station height, or/and tropospheric zenith path delay will obtain erroneous results.

The separation between the GPS satellite centre of mass and the electronic phase centre of its antenna predominantly depends on the design of the satellite. The origin of the satellite coordinate system is at the satellite centre of mass. The X-coordinate axis lies in the Sun-satellite-Earth plane; the Y-coordinate axis points along the solar panel axis; and the Z-coordinate axis points toward the Earth centre (see Figure 3.17). The phase centre for most satellites are offset in the body of Z-coordinate and X-coordinate direction. Table 3.3 lists the *relative* satellite antenna phase centre offsets in metres adopted by the IGS for each satellite block. Azimuth-dependent PCVs were completely ignored in the *relative* phase centre model. Corrections from *relative* calibrations had been used until 5 November 2006.

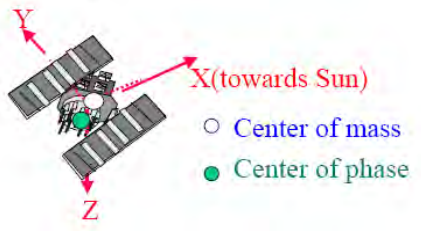

Figure 3.17: Satellite antenna phase centre offsets (Kouba, 2003).

Table 3.3: Satellite antenna phase centre offsets adopted by IGS (Kouba, 2003).

	X (m)	Y (m)	Z (m)
Block II/IIA	0.279	0.000	1.023
Block IIR	0.000	0.000	0.000

Ge and Gendt (2005) have shown that it is not sufficient to use block-specific antenna corrections, as the phase centre behaviour between certain subgroups of the satellite blocks and even between individual satellites is significant. At present, there is only one method to obtain the satellite antenna centre corrections, which is through the estimation of using global data since the official start of the IGS in 1994. Estimates from the Technische Universität

München and GFZ Potsdam using two different software packages have shown good agreement, that is, 20cm for the offsets and 1mm to 3mm for the patterns (Schmid *et al.*, 2004).

The *absolute* GPS satellite antenna centre corrections are contained in the igs05_wwww.atx file (IGS, 2008). Since the satellite antenna PCV solutions from different institutions using different software packages are generally in good agreement, the *absolute* satellite antenna PCVs are considered similar for all satellites within each block type. However, the z-offset values, which are in the direction from the satellite centre of mass towards the centre of the Earth, are satellite-specific (Gendt and Schmid, 2005; Schmid *et al.*, 2007). The IGS ACs monitor the satellite antenna models on a regular basis. As soon as significant changes are detected, an update of the IGS antenna model will be considered (Schmid *et al.*, 2007)

The IGS switch to a new *absolute* antenna phase centre was made together with the ITRF switch to the latest realisation of the new ITRF 2005 on 5 November 2006 (Gendt, 2006). Users should avoid combining results from solutions using different phase centre conventions, and the *absolute* antenna phase centre model requires corrections for both satellites and tracking receiver antennas simultaneously (Gendt, 2006; Schmid *et al.*, 2007).

Note: In this research, the relative antenna phase centre corrections were used to process all GPS data collected before the switch to absolute antenna phase centre corrections (5 November 2006). For data that were collected after the 5 November 2006, the absolute antenna phase centre corrections were utilised.

3.5.2 Phase Wind-Up

Phase wind-up error is a problem associated with the satellite and receiver antenna orientation due to the nature of circularly polarised waves intrinsic in the GPS signals (Wu *et al.*, 1993; Witchayangkoon, 2000). The phase wind-up error does not affect the code measurements, but instead, it affects the carrier phase measurements. Since PPP takes advantage of, in addition to the code, the more precise carrier phase measurements, it is therefore necessary to consider the effects of the phase wind-up error. GPS satellites transmit right circularly polarised waves, thus the observed carrier depends on the mutual orientation of the satellite and receiver antennas (Kouba and Hèroux, 2001).

In an ideal environment, the observed carrier phase at the receiver equals the geometric angle between the instantaneous electric field at the receiving antenna and some reference direction on the antenna. When the antenna orientation changes, so does the reference direction. As a result, the measured phase will also be affected. Similarly, when the satellite antenna orientation changes, so does the direction of the electric field at the transmitting antenna, and subsequently the measured phase at the receiving antenna (Witchayangkoon, 2000). This effect is called "phase wind-up".

The phase wind-up error has generally been ignored in most of the high precision GPS applications. This error is negligible in relative positioning although it has been shown that the error can reach up to 4cm for 4000km baseline (Wu *et al.*, 1993). However, this effect is quite significant for PPP positioning when constraining the IGS precise ephemerides (Kouba, 2003). Therefore, most of the IGS ACs apply the phase wind up corrections while producing their precise ephemerides. By neglecting this effect while utilising the IGS precise ephemerides, one may introduce decimetre level error in the estimated receiver position and clock errors.

Note: The phase wind-up correction was applied in this research.

3.5.3 Relativity in GPS

GPS satellites and control stations utilise highly stable and accurate atomic clocks to provide world-wide positioning and timing. These clocks have gravitational and motional frequency shifts, which are large enough that, without carefully accounting for relativistic effects, the system would not work (Ashby, 2007).

- **Periodic Clock Error Effect**

The GPS satellite orbit is not truly circular. The slight eccentricity of each satellite orbit causes an additional periodic clock error that varies with the satellite position in its orbital plane (Shen, 2002). This effect can be cancelled out in relative positioning but not in PPP approach. Therefore, it is necessary to take into account the relativistic correction to the satellite clock time suggested in the GPS Interface Control Document (ICD-GPS-200c-004, 2000) to achieve high accuracy positioning using PPP.

$$dt_{relativity} = \frac{2}{c^2} X \cdot \dot{X} \tag{3.14}$$

where c is the speed of light in a vacuum, X is the position of the satellite, and $\dot{X}$ is the velocity of the satellite at the instant of transmission.

- **Sagnac Delay**

Sagnac delay is an error associated with the Earth's rotation during the transit time of the signal from the satellite to the receiver on the ground (Ashby and Spilker Jr., 1996). The sagnac correction term can be expressed as,

$$dt_{sagnac} = \frac{2\Omega_e}{c^2} \cdot \frac{r_A \times r_B}{2} \tag{3.15}$$

where Ω_e is the earth angular rotation rate, r_A is the position vector of the satellite, and r_B is the position vector of the receiver at the instant of signal transmission.

Note: The periodic clock error offset and sagnac delay were taken into account during the data processing process.

3.5.4 Site Displacement Effects

The Earth is composed of three basic components: solid (i.e. rock), liquid (i.e. ocean) and the atmosphere, which constantly interact with each other. These "interactions" make the Earth pliable and subject to deformation. In a global sense, a station undergoes a real or apparent periodic movement reaching a few decimetres, which are generally not considered in the ITRF position (Kouba, 2003). As a consequence, accurate positioning within the ITRF frame needs to account for these periodical station displacement effects. For relative positioning with short baselines (<100km), these effects can cancel out as the effects are similar at the receivers (over broad areas of the Earth). For PPP positioning, the station displacement effects must be considered and modelled.

- **Solid Earth Tides**

The "solid" Earth is far from rigid and is pliable enough to respond to the same gravitational forces that generate the ocean tides. Tides are caused by the gravitational attraction and temporal variations of the Sun and Moon orbital motion. While the ocean tides are strongly influenced by the coastal outlines and the shape of the near-coastal ocean floor, the solid earth tides can be computed quite accurately from simple earth models (Leick, 2004). The effect of the tidal variation is larger in the vertical component and can reach as much as 30cm (Kouba, 2003). For horizontal component, its effect can reach about 5cm (Leick, 2004; Abdel-salam, 2005). Neglecting this error in point positioning would result in systematic position errors of up to 12.5cm and 5cm in the radial and north directions, respectively (Kouba, 2003).

- **Polar Tides**

Polar tides are periodical deformations caused by the changes of the Earth's spinning axis with respect to the Earth's crust, i.e. polar motion. In order to achieve sub-centimetre point positioning accuracy and be consistent with the ITRF frame, this bias is required to be considered during data processing. This is because most of the IGS ACs utilise these correction terms to generate the precise satellite orbit and clock corrections, and thus, the precise products are consistent with the station position corrections (Kouba, 2003). The polar tide displacements can reach about 7mm in the horizontal direction and 25mm in the height (Kouba, 2003).

- **Ocean Loading**

The ocean loading tides are the deformation of the sea floor and coastal land that results from the redistribution of seawater, which occurs during the ocean tides. While ocean loading is almost an order of magnitude smaller than the solid earth tides, ocean loading is more localised. For stations that are located far from the ocean (>1000km), point positioning at 5cm precision level, or static positioning over 24 hour periods, the ocean loading effects can be safely ignored (Kouba, 2003). However, for stations that are located along the coastline with observation length shorter than 24 hours, this effect needs to be taken into account. Otherwise, this error will be mapped into the tropospheric ZPD and station clock solutions (Kouba and Hèroux, 2001). The magnitude of the surface displacement caused by the ocean tide loading can reach up to 5cm in the height and 2cm in the horizontal direction (Abdel-salam, 2005).

- **Atmospheric Tides**

The gravitational forces of the Sun and Moon affect the solid earth tides, the ocean and atmosphere in different ways due to the different properties of material involved (Witchayangkoon, 2000). The atmospheric mass above the Earth's surface causes a load on the Earth's surface. This results in horizontal and vertical displacements, which can be as large as 20mm for the vertical component and 3mm for the horizontal component (Petrov and Boy, 2004; Abdel-salam, 2005). The displacement caused by the atmospheric tides varies according to the atmospheric pressure variations, as well as the geographic location.

Note: The effects of the solid earth tides, polar tides, ocean loading and atmospheric tides were modelled in the research software.

3.5.5 Differential Code Biases

- **L1-L2 (P1-P2) Differential Code Biases**

The L1-L2 (P1-P2) DCBs are the differences between L1 and L2 frequencies. They are consistent with the P1 and P2 code measurements, hence the term P1-P2. In general, the satellite DCBs are nearly constant in time but differ from satellite to satellite. The magnitude of this bias can reach up to 12 nanoseconds (ns). If left unaccounted, this may have detrimental effects on the estimated PPP solutions.

The IGS precise satellite clock correction products generated by the IGS ACs always refer to the ionosphere-free linear combination between L1 and L2 frequencies. For dual frequency PPP, no such DCB calibrations are required to be applied. However, single frequency PPP users must apply the satellite DCBs as the IGS precise satellite clock corrections are consistent with the satellite L1-L2 DCBs convention. This can be done by first correcting for the IGS satellite clocks in order to be compatible with the single frequency observations (Kouba, 2003).

The satellite DCBs are constantly computed by IGS IAACs as part of their global ionospheric TEC maps and transmitted in the broadcast ephemerides. The broadcast values are determined by the satellite manufacturer before launch and can be revised by the GPS control segments. Currently, the broadcast satellite DBCs agree with the CODE DCBs at a few nanoseconds level (CODE, 2007).

- **P1-C1 Differential Code Biases**

The P1-C1 DCBs are the differences between the code observations. As noted earlier, the L1-L2 DCBs are the differences between L1 and L2 frequencies but are consistent with the P1 and P2 code measurements. However, not all receivers output the P1 code, but are limited to C/A code. Cross correlation receivers, such as the AOA Rogue, Trimble 4000 and TurboRogue produce C/A and P2 codes in addition to the L1 and L2. The P2 code is calculated based on the summation of C/A code and the difference between P1 and P2 codes which are monitored by the receiver. On the other hand, the newer generation (non-cross correlation receivers), such as the Ashtech Z-XII and AOA Benchmark/ACT receivers, can produce C/A, P1 and P2 codes in addition to the L1 and L2. Thus, the P2 code generated from the non-cross correlation receivers are not the same as those of the cross correlation receivers (Abdel-salam, 2005). The IGS precise products are generated from a network of GPS stations using more modern receivers. They are consistent with the P1 and P2 non-cross correlation types of observations. Mixing data with different biases would degrade the IGS precise satellite clock corrections products.

The magnitude of the P1-C1 biases is quite constant, i.e. in the order of 2 nanoseconds (60cm), but they are unique for each satellite and receiver. The values of the P1-C1 biases are regularly estimated by the IGS ACs as part of their precise satellite clock corrections estimation process. The latest biases are posted on the CODE website (CODE, 2007). In addition, a converter utility (*cc2noncc*) program is also available. It can be use to transform the cross correlation receivers (Ray, 2005a).

Note: The DCB biases were considered in the data processing process.

3.6 Multipath

Multipath occurs when the GPS signal arrives at a receiver via indirect paths, i.e. two or more different paths (Wells *et al.*, 1986; Farret and Santos, 2001; Roulston, 2001; Xu, 2003). This error is often caused by reflected GPS signals from surrounding objects and terrains such as buildings, trees, canyons, and fences. The reflected signals increase the measured distance between the receiver and satellite resulting in inaccurate positions. The multipath effect provokes errors in both code and carrier phase measurements. The magnitude of range error can reach up to several metres for code measurements and up to 5cm for carrier phase measurements (Georgiadou and Kleusberg, 1988; Roulston, 2001).

Since the multipath error is *environment* dependent, the most effective mitigation technique is to locate the GPS receiver antenna away from reflecting surfaces. This may be an impractical solution for most applications. The effects of multipath can be reduced in the receiver antenna design by lowering the contribution of some types of reflections, e.g. from the ground below the antenna (Misra and Enge, 2006). An example of this is the choke ring ground plane antenna. The current GPS receivers are designed to be equipped with features, which could reduce multipath. The mitigation process is often performed during the signal processing step within the receiver itself. In addition to site selection and receiver/antenna design, multipath effects can also be reduced by setting a high elevation cut-off angle.

The elevation-dependent weighting of observations is applied in this research to mitigate the effects of multipath, as well as atmospheric errors. The observations weight to each GPS satellite was determined as a function of satellite signal paths. It is known that low elevations observations are generally more susceptible to multipath effects and atmospheric refraction than those at high elevations, thus affecting the quality of the solutions. However, low elevations observations may improve the tropospheric zenith delay estimations and consequently improve the solutions, particularly the vertical component (Rothacher *et al.*, 1997; Meindl *et al.*, 2004). Therefore, the weighting scheme used in this research quantifies the precision of the observations as a function of satellite elevation angle.

$$M(E) = \frac{1}{\sin(elevation)} \tag{3.16}$$

This weighting function was chosen based on the similarity of the cosecant function and the atmospheric effects with respect to the satellite elevations (Vermeer, 1997; Collins and Langley, 1999; Abdel-salam, 2005). Generally, the standard deviation of a satellite at about 5˚ elevation is about 10 times larger than that of a satellite at zenith.

3.7 Reference Frames

Users of GPS technology need to be aware that the coordinates of the GPS satellites computed from the parameters broadcasted in the GPS navigation message are expressed in the World Geodetic System 1984 (WGS 84) reference frame. As a consequence, the default coordinates displayed and downloaded from a GPS receiver are also expressed in the WGS 84 reference frame. In contrast, PPP technique takes advantage of the IGS precise satellite orbit and clock corrections, and the use of precise IGS products imply positioning, orientation and scale of a precise reference frame (Kouba, 2003). In this case, the estimated positioning solutions using the PPP approach are always directly in the IGS global reference frame, which conforms to the ITRF. Therefore, it is vital to understand the merits and relationships between different reference frames and use appropriate transformation tools and parameters to transform coordinates from one system, to other systems.

The following section presents a description of the ITRF, WGS 84 and Geocentric Datum of Australia (GDA 94), which are the common reference frames used for GPS positioning in Australia.

3.7.1 International Terrestrial Reference Frame

The ITRF is a global datum widely used by the scientific community and is realised by a large network for fiducial sites around the globe (Stanaway, 2007). The ITRF is a realisation of the International Terrestrial Reference System (ITRS), and is maintained by the International Earth Rotation Service (IERS). The current ITRF frame is defined by coordinates of about two hundred terrestrial stations to an accuracy at the centimetre level. In addition to the coordinates of the stations, the ITRF also takes into account the Earth crustal movements, and thus, the velocities of the movements are also estimated. Consequently, the point coordinates expressed in ITRF must always have a date (time) associated with the coordinates.

ITRF has undergone several refinements, e.g. ITRF 1989, 90, 91, 92, 94, 95, 96, 97, 2000, 2005. ITRF 2005, which was released on 5 November 2006 (GPS week 1400) is the latest realisation of the ITRF at the time of writing this thesis.

The ITRF solutions do not directly refer to a reference ellipsoid. ITRF solutions are always specified by X, Y, Z Cartesian coordinates. However, the Cartesian coordinates can be transformed to geographical coordinates (latitude, longitude and height) that refer to an ellipsoid. In this case, the Geodetic Reference System 1980 (GRS 80) ellipsoid is recommended to be used in the transformation (ITRF, 2008).

3.7.2 World Geodetic System 1984

The global geocentric reference frame known as the WGS 84 has evolved significantly since its creation in the mid-1980s. The WGS 84 continues to provide a single, common, accessible 3-dimensional coordinate system for geospatial data collected from a broad spectrum of sources (NIMA, 2004). WGS 84 is a realisation of the Conventional Terrestrial Reference System (CTRS) developed by the National Imagery and Mapping Agency (NIMA) of the U.S. Department of Defence. The NIMA was reorganised in 2004 as the National Geospatial-Intelligence Agency (NGA) (Misra and Enge, 2006). WGS 84 is the official reference system used by GPS.

WGS 84 is currently defined by the coordinates and velocities of GPS tracking stations maintained by the U.S. Air Force (USAF), NGA and a few additional IGS stations (Merrigan *et al.*, 2002). The latest realisation of the WGS 84 is WGS 84 (G1150). 'G' indicates these coordinates were obtained through GPS techniques and the number '1150' indicates the GPS week number when these coordinates were implemented in the NGA precise GPS ephemeris estimation process (NIMA, 2004; Stanaway, 2007). G1150 is the third update to the realisation of the WGS 84 reference frame. It was implemented on 20 January 2002. It followed the two previous realisations, which were WGS 84 (G730) on 29 June 1994 and WGS 84 (G873) on 29 January 1995, respectively (NIMA, 2004).

- **Relationship between WGS 84 and ITRF**

After the adjustment of a best fitting 7-parameter transformation and accounting for epoch differences, the RMS discrepancy between WGS 84 (G1150) reference frame and ITRF 2000 is about one centimetre per component (NGA, 2003). Comparisons were also made between the tracking stations maintained by USAF and NGA and a subset of IGS stations used in ITRF 2000 realisation, as well as the NGA precise ephemerides (referenced to WGS 84 (G1150)) and IGS precise ephemerides (referenced to ITRF 2000). The outcome of the comparisons indicates that the differences between WGS 84 (G1150) and ITRF 2000

reference frames are statistically insignificant to be considered (NGA, 2003). Therefore, the two reference frames are essentially identical for most applications.

3.7.3 Geocentric Datum of Australia 1994

GDA 94 is the current geodetic datum gazetted in Australia. It is based on a realisation of the ITRF 1992 fixed at epoch 1994.0 on 1 January 2004. As part of the world-wide IGS campaign, continuous GPS observations were undertaken in 1992 at eight Australian sites known as the Australian Fiducial Network (AFN). During the period of 1992 to 1994, additional GPS observations were also made at about 70 well determined GPS sites, at approximately 500km spacing across Australia. Theses sites are known as the Australian National Network (ANN) (ICSM, 1998). GPS observations collected at both the AFN and ANN sites were then combined in a single regional GPS solution to constrain the ITRF 1992 and the resulting coordinates were mapped to a common epoch of 1994. These positions, at epoch 1994, were used to form the basis for the GDA 94 (Steed, 1995; Steed and Luton, 2000). After the IGS campaign in 1992, the AFN sites were expanded into a network of permanent GPS sites, which are currently known as the ARGN (see Section 2.5.2). GDA 94 has an origin that coincides with the centre of mass of the Earth. The International Association of Geodesy recommended GRS 80 ellipsoid to be used for transformation.

- **Relationship between GDA 94 and ITRF**

According to Dawson and Steed (2004), a standard 7-parameter transformation can adequately model these differences at the cm level, provided that the 7-parameter transformation parameters are regularly updated to reflect the tectonic motion. However, a slightly more complex 14-parameter transformation, which includes the 7 parameters and their respective rates, can be used as a better long-term practical solution to these coordinate transformations. The 14 transformation parameters used to transform coordinates in ITRF 2000 to GDA 94 are listed in Table 3.4.

Table 3.4: ITRF 2000 to GDA 94 using 14-parameter transformation (Dawson and Steed, 2004).

t (years)	d_X (m)	d_Y (m)	d_Z (m)	r_X (as)	r_Y (as)	r_Z (as)	s_C (ppm)
2000.00	-0.0663	-0.0050	0.0426	0.008814	0.009127	0.009042	0.007936
/year	0.0049	0.0039	0.0049	0.001616	0.001200	0.001013	0.000096

(**Note:** the transformation parameters required to transform coordinates in ITRF 2005 to GDA 94 have yet to be published at the time of writing this thesis.)

3.7.4 Understanding Different Reference Frames

In essence, the selection of the reference frame is not a source of error. However, when the wrong datum, projections and transformation parameters are applied, the computed positioning solutions will be erroneous, and in some cases, detrimental. Thus, it is important to understand the relationships between different reference frames and use appropriate transformation tools and parameters to transform coordinates from one system to other systems.

The ITRF, WGS 84 and GDA 94 are all geocentric datums. ITRF and WGS 84 are dynamic, which means that the coordinates of a point are constantly changing to reflect the plate tectonic movement on a global scale. For most practical applications, it is safe to regard ITRF and WGS 84 coordinates as identical. However, there is a common assumption that the ITRF and WGS 84 coordinates are similar to GDA 94 at the order of less than 10cm. This assumption is incorrect (Stanaway, 2007).

The GDA 94 reference frame is static in nature. GDA 94 is a coordinate datum based on ITRF 1992 at the fixed epoch of 1994.0, which means that on 1 January 1994, GDA 94 and ITRF were aligned together. But as the Australian tectonic plate is moving at about 7cm to 8cm per year in a northeasterly direction (in an absolute sense), there is an increasing difference in positions between the two frames. This amounts to about 60cm at the start of 2001 and over a metre in 2008 (ICSM, 1998). As the Australian continent is remarkably stable and moving uniformly in the same direction, such movement is not an issue when obtaining position relative to other GDA 94 positions. But for high accuracy PPP positioning,

such movement is critical and needs to be taken into account when transforming positions expressed in ITRF to GDA 94 coordinates.

3.8 Summary

The GPS error sources that are of particular relevance in the PPP technique have been thoroughly described. The errors that are covered in this Chapter are the satellite orbit and clock errors, ionospheric and tropospheric effects, phase wind-up, satellite and receiver antenna phase centre offsets and variations, relativity, multipath, geophysical effects, which include the earth and atmospheric tides, as well as the plate tectonic motion. One of the key elements of achieving high accuracy point positioning using the PPP technique is to accurately model and effectively mitigate all of the physical phenomena affecting the measurements. The error mitigation strategies investigated and applied in this research have also been given and described. Furthermore, the merits and importance of understanding the different reference frames used in Australia have been discussed in Section 3.7.

The impacts of satellite orbit, satellite clock, ionospheric and tropospheric errors in single frequency PPP were studied as part of the research objectives. Various mitigation strategies were also explored and examined for its usefulness and practicality. The findings from the studies are presented in *Chapter 5: Ionospheric Error Mitigation Strategies for Single Frequency Point Positioning*, *Chapter 6: Convergence Evaluation of Single Frequency PPP Solutions (Section 6.4 Should Tropospheric Delay be Modelled or Estimated?)*, and *Chapter 7: IGS Satellite Orbit and Clock Corrections: From Post-Mission to Real-Time Point Positioning*.

CHAPTER 4

Single Frequency PPP – Setting *A Priori* Observations Sigma Ratio

4.1 Introduction

The previous Chapters have outlined the design of the research software, which includes the mathematical model, adjustment filter, as well as the software computational flow and components. The various error sources that affect the GPS signals and the effective mitigation methods in the context of PPP have also been described. It is important to consider these errors and take precautions to minimise those effects in order to attain the highest possible point positioning accuracy.

It was discovered during the course of this research that the *a priori* observations weighting plays a very significant role in determining the quality of the single frequency PPP solutions. It was found that the observation weighting, in particular the *a priori* observations sigma (or standard deviation) ratio between the code and quasi-phase measurements, affects the accuracy, precision, and also the convergence behaviour of the positioning solutions. Therefore, the objective of this Chapter is to evaluate the impacts of using different *a priori* code and quasi-phase measurements sigma ratios on single frequency PPP solutions. The design of the study was based on an empirical approach using static GPS data collected on the Australian continent. Five case scenarios were tested in different ionospheric conditions. The assessment of the results was undertaken by evaluating the accuracy, precision and convergence time of the position estimates. An "optimal" *a priori* sigma ratio, which would provide the best possible single frequency PPP point positioning quality, is proposed at the end of this Chapter.

4.2 Observations Weighting

The observations weight matrix has received much attention from the GPS research community in the past few years, e.g. Teunissen (1998), Hartinger and Brunner (1999), Tiberius (1999), Tiberius *et al.* (1999), Özlüdemir (2004). This is because the observation weight matrix has direct influence on the positioning solutions, ambiguity validation and quality control. In GPS point positioning, the observations are assumed to be uncorrelated. The covariance for each observation is placed on the diagonal in the variance covariance matrix. Typical factors that affect the observations noise level are the receiver dependent noise and multipath.

The receiver dependent noise is associated with the accuracy in the correlation procedures performed in a GPS receiver. In these procedures, the correlation is maximised between the receiver's generated signal and the observed signal. As a result, the correlation will not be 100% since the incoming signal is contaminated with noise. A general rule of thumb states that the signal noise level or the observation resolution is about 1% of the signal wavelength (Wells *et al.*, 1986; Seeber, 1993). Considering that the wavelength of the code and carrier phase observations are 300m and 0.2m, respectively, the noise level in the code and carrier phase observations would be 3m and 2mm, respectively (Andersson, 2006).

4.2.1 *A Priori* Sigma of Unit Weight

The observation weight is defined as being inversely proportional to the observation sigma square, or variance (Deakin, 2005),

$$W \alpha \frac{1}{\sigma^2} \tag{4.1}$$

or,

$$W = \frac{\sigma_0^2}{\sigma^2} \tag{4.2}$$

where σ^2 is the observation variance.

For un-differenced solutions, the observations weight matrix is a diagonal matrix with the diagonal terms equal to,

$$W = \begin{bmatrix} \frac{\sigma_0^2}{\sigma_{P1}^2} & & & & & & \\ & \frac{\sigma_0^2}{\sigma_{\Phi 1}^2} & & & & & \\ & & \frac{\sigma_0^2}{\sigma_{P2}^2} & & & & \\ & & & \frac{\sigma_0^2}{\sigma_{\Phi 2}^2} & & & \\ & & & & \ddots & & \\ & & & & & \frac{\sigma_0^2}{\sigma_{Pn}^2} & \\ & & & & & & \frac{\sigma_0^2}{\sigma_{\Phi n}^2} \end{bmatrix} \tag{4.3}$$

where, σ_P^2 is the variance of the code observation, σ_Φ^2 is the variance of the phase observation, and σ_P^2 and σ_Φ^2 should approximately agree with the actually measurement noise.

It is important in the GPS observation adjustment model, or any other adjustment models, to set *a priori* observations sigma values that will adequately reflect the actual observations noise and uncertainty. In addition to the standard deviation values, it is also important to have an observations ratio that is suitable to represent the mathematical relationship between the observations. Generally, the ratio of the *a priori* weights W_P and W_Φ for the L1 code and carrier phase observations are defined as (Hugentobler *et al.*, 2007),

$$\frac{W_P}{W_\Phi} = 10^{-4} \tag{4.4}$$

or more commonly,

$$\frac{\sigma_P}{\sigma_\Phi} = 100 \tag{4.5}$$

It has been established that a typical ratio of $\frac{\sigma_P}{\sigma_\Phi} = 100$ works well for dual frequency PPP using the ionosphere-free linear combination (Kouba, 2003). In fact, $\frac{\sigma_P}{\sigma_\Phi} = 100$ is the nominal ratio widely used in GPS data processing and in dual frequency PPP. This is because the error due to noise in the carrier phase observations is about one-hundredth of that in the code observations.

For single frequency PPP using ionosphere-free quasi-phase, the ratio between the *a priori* code and quasi-phase sigmas is different from the conventional dual frequency ionosphere-free linear combination. The single frequency code observation is affected by the ionospheric delay; but when combined with carrier phase observations in the quasi-phase combination, it effectively eliminates the ionospheric effects. The noise affecting the quasi-phase observations is half the effects of code multipath and tracking noise on the code as well as the carrier phase observations. Hence, the sigma ratio between the code and quasi-phase observations is difficult to determine due to the nature of the *code and quasi-phase* combination. Moreover, the noise on the code and phase observations is unknown, thus it is a challenge to produce realistic error estimates of the observations (Choy *et al.*, 2008b).

The values of the *a priori* code and quasi-phase sigmas used in the adjustment model should reflect the uncertainty of the observations. This can be determined using the *a posteriori* variance factor. However, it is noted that the values themselves are not of great important. What is more important is that the "relative" weighting between the observations should be correct (Cross, 1983; Simsky, 2006), i.e. as long as the code sigma is greater than the quasi-phase sigma. In other words, the ratio between the code and quasi-phase measurements sigma has a much more significant role in determining the optimum point positioning solutions. It is generally impossible to have guidelines for the necessary accuracy needed to determine the observations weight, or sigma value (Cross, 1983). Consequently, in this research, it was decided to test the sensitivity of different ratios on single frequency PPP by taking a few different estimates of the *a priori* sigma ratios and analysing the quality of the estimated positioning solutions.

4.2.2 Propagation of Errors

In statistics, when the dependent variables are used as observations, the stochastic characteristics of the dependent variables are associated with the uncertainty of the independent variables and the functional relationships relating the variables. This dissemination of variables uncertainty is known as propagation of errors, or also known as propagation of variances and covariances.

For many practical applications of propagation, the random variables in x and y are not linearly related, that is, $y = f(x)$. In the context of this research, the quasi-phase measurement $\tilde{\Phi}$ is a function of the code and carrier phase observations, P and Φ (refer to Equation (2.7)).

$$\tilde{\Phi} = f(P,\Phi) = \frac{1}{2}(P,\Phi) \tag{4.6}$$

The variance-covariance matrix Σ_{yy} which contains the element $\sigma^2_{\tilde{\Phi}}$ can be written as,

$$\Sigma_{yy} = J_{yx}\Sigma_{xx}J^T_{yx} \tag{4.7}$$

where, $J_{yx} = \begin{bmatrix} \frac{d\tilde{\Phi}}{dP} & \frac{d\tilde{\Phi}}{d\Phi} \end{bmatrix}$ is the Jacobian matrix of partial derivatives, and $\Sigma_{xx} = \begin{bmatrix} \sigma^2_P & \sigma_{P\Phi} \\ \sigma_{P\Phi} & \sigma^2_\Phi \end{bmatrix}$ is the variance-covariance matrix of the random variables.

Expressing the law of propagation of variance-covariance in an algebraic equation,

$$\begin{aligned}
\left[\sigma^2_{\tilde{\Phi}}\right] &= \left[\frac{d\tilde{\Phi}}{dP} \quad \frac{d\tilde{\Phi}}{d\Phi}\right] \cdot \begin{bmatrix} \sigma^2_P & \sigma_{P\Phi} \\ \sigma_{P\Phi} & \sigma^2_\Phi \end{bmatrix} \begin{bmatrix} \frac{d\tilde{\Phi}}{dP} \\ \frac{d\tilde{\Phi}}{d\Phi} \end{bmatrix} \\
&= \left[\frac{d\tilde{\Phi}}{dP}\sigma^2_P + \frac{d\tilde{\Phi}}{d\Phi}\sigma_{P\Phi} \quad \frac{d\tilde{\Phi}}{dP}\sigma_{P\Phi} + \frac{d\tilde{\Phi}}{d\Phi}\sigma^2_\Phi\right] \begin{bmatrix} \frac{d\tilde{\Phi}}{dP} \\ \frac{d\tilde{\Phi}}{d\Phi} \end{bmatrix} \\
&= \left(\frac{d\tilde{\Phi}}{dP}\right)^2 \sigma^2_P + \frac{d\tilde{\Phi}}{d\Phi}\frac{d\tilde{\Phi}}{dP}\sigma_{P\Phi} + \frac{d\tilde{\Phi}}{dP}\frac{d\tilde{\Phi}}{d\Phi}\sigma_{P\Phi} + \left(\frac{d\tilde{\Phi}}{d\Phi}\right)^2 \sigma^2_\Phi \\
&= \left(\frac{d\tilde{\Phi}}{dP}\right)^2 \sigma^2_P + 2\left(\frac{d\tilde{\Phi}}{d\Phi}\frac{d\tilde{\Phi}}{dP}\right)\sigma_{P\Phi} + \left(\frac{d\tilde{\Phi}}{d\Phi}\right)^2 \sigma^2_\Phi
\end{aligned} \tag{4.8}$$

Since $\frac{d\tilde{\Phi}}{dP} = \frac{d\tilde{\Phi}}{d\Phi} = \frac{1}{2}$ (refer Equation (4.6)), and assuming that the code and carrier phase observations are independent, i.e. their covariances are zero ($\sigma_{P\Phi} = 0$), Equation (4.8) can be rewritten as,

$$\begin{aligned}
\sigma^2_{\tilde{\Phi}} &= \left(\frac{1}{2}\right)^2 \sigma^2_P + \left(\frac{1}{2}\right)^2 \sigma^2_\Phi \\
&= \frac{1}{4}(\sigma^2_P + \sigma^2_\Phi)
\end{aligned} \tag{4.9}$$

From Equation (4.9), one can see that the quasi-phase observation variance should be four times (or two times for observation sigma) smaller than the code measurement variance. It should be remarked that the quasi-phase measurement variance only takes into account the noise and multipath effects on the code observations, as the ionospheric delay is compensated for in the quasi-phase observations; while, the code observation does contain residual ionospheric delay. Therefore, in the single frequency PPP adjustment model, the measurement variance of the quasi-phase should be at least four times smaller than the code observations variance in order to account for the ionospheric delay on the code observations (Choy *et al.*, 2008b).

4.3 Case Study

In order to study the effects of setting different *a priori* code and quasi-phase sigma ratio values on single frequency PPP solutions, five case scenarios with different ratios were formulated (see Table 4.1).

Table 4.1: The *a priori* code and quasi-phase sigmas and their corresponding observations sigma ratios.

	***A Priori* Code Sigma**	***A Priori* Quasi-Phase Sigma**	**Sigma Ratio**
Case-1	4m	0.03m	≈1 : 100
Case-2	4m	0.10m	≈ 1 : 50
Case-3	4m	0.30m	≈ 1 : 10
Case-4	4m	1m	1 : 4
Case-5	4m	-	-

Case-1 (≈1 : 100) was devised from the standard nominal ratio widely used for dual frequency ionosphere-free un-differenced code and carrier phase observations. Case-2, Case-3 and Case-4 were intermediate cases, while Case-5 was simply based on the classical L1 code-based processing. The *a priori* code sigma value was set to 4m to "sufficiently" allow for tracking noise and multipath effects. Furthermore, the *a priori* code sigma value was also chosen from the fact that the code observations do contain residual ionospheric delays. The *a priori* quasi-phase sigma, on the other hand, was scaled according to the designated ratio.

Three ARGN stations located in Australia were used, and they were DARW, STR1 and TOW2. Figure 4.1 shows the location of these stations. These stations were chosen because they represent the different latitudinal zones across Australia, i.e. low latitude and middle latitude regions. The characteristics of the latitudinal zones have been described in Section 3.3.2. DARW and TOW2 are located in the low latitude region, while STR1 is located in the middle latitude region. It should be noted that although the ARGN stations were equipped with dual frequency geodetic quality GPS receivers, only observations on L1 frequency were used in the single frequency data processing since the single frequency processing was the main focus in this study.

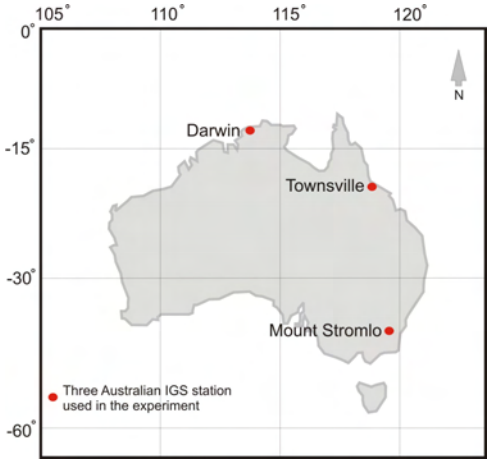

Figure 4.1: The location of the three Australian ARGN stations.

Three consecutive days were randomly selected for each year starting from 2001 to 2006 and the GPS data sets for DARW, TOW2 and STR1 were downloaded online from the SOPAC database (SOPAC, 2008). All data sets used in this study were limited to the first 4 hours of the day, starting from 14:00LT, i.e. 14:00LT to 18:00LT. It was assumed that the daily maximum ionospheric activities occur at around 14:00LT (Klobuchar, 1987), and the effects of the ionosphere is at its peak during that period. Table 4.2 outlines the data sets DOY for 2001 to 2006 that were used.

Table 4.2: The DOY of the data sets that were used.

Year	DOY
2001	336, 337, 338
2002	274, 275, 276
2003	359, 360, 361
2004	153, 154, 155
2005	149, 150, 151
2006	183, 184, 185

The IGS *Final* orbit and satellite clock corrections downloaded from the IGS website (IGS, 2008) were used in the processing. The ionospheric errors affecting the code observations were corrected by using the IGS *Final* GIMs. The tropospheric ZPD was modelled using Hopfield model with default atmospheric parameters, and the tropospheric ZPD was mapped to a slant delay by using the Niell mapping function. A cut-off elevation angle of 15° was used to reduce the data susceptibility to multipath effects, while ensuring

that a minimum of four or more satellites were always visible. The observation interval of the collected data sets was 30 seconds, similar to the majority of IGS GPS data sets.

The impacts of the different sigma ratios were evaluated based on the estimated point positioning solution accuracy and precision, as well as, the positioning convergence behaviour. The estimated solutions were basically compared to a set of known (reference) values. For all the studies and assessments carried out in this research, unless stated otherwise, the published ITRF coordinates obtained from the ITRF website (ITRF, 2008) were employed as reference points. All the ITRF coordinates that were used as reference coordinates have been brought forward to respective epochs, e.g. ITRF00 @ 03/07/2006 and ITRF00 @ 04/12/2001. Thus, the estimated coordinates from the PPP solutions in ITRF were also brought forward to correspond with the respective epochs. It is important to note that the PPP solutions and reference ITRF coordinates were originally expressed in the ECEF Cartesian coordinates X, Y, and Z. However, changes in geographical coordinates, longitude (east), latitude (north) and height components are usually used to show meaningful relations between the components. Therefore, to ease interpretation of the results, the X, Y, and Z coordinates were transformed into east, north, and height components using the GRS 80 ellipsoid recommended by ITRF team (ITRF, 2008).

4.4 Results and Discussion

Tables 4.3, 4.4 and 4.5 present the combined mean, RMS, and 95% Confidence Interval (C.I.) values for DARW, STR1 and TOW2 stations based on Case-1, Case-2, Case-3, Case-4, and Case-5 processing strategies, respectively. The mean values are computed based upon the average differences between the estimated positioning solutions with the known coordinates; while the RMS values are indications of the positioning solutions precision with regards to the known coordinates. The complete statistical analyses for each year starting from 2001 to 2006 for DARW, TOW2 and STR1 stations are presented in Tables attached in Appendix A. The numbers highlighted in pink denote the lowest values; while the numbers highlighted in green are the highest values. As expected, the accuracy of the positioning solutions at low latitude stations (DARW and TOW2) is generally lower than those of middle latitude (STR1). The Case-2 processing strategy generally provides the lowest mean and RMS values. However, it is interesting to see that the average mean and RMS positioning errors are well under 1m of the known values, which indicate that the results are quite accurate and precise.

Table 4.3: The mean, RMS and 95% confidence interval at DARW using different *a priori* observations sigma ratios.

DARW						
		Case-1	**Case-2**	**Case-3**	**Case-4**	**Case-5**
Mean (m)	**East**	-0.23	-0.07	-0.18	-0.15	-0.15
	North	0.20	0.19	0.29	0.51	0.64
	Height	-0.47	-0.15	0.01	0.20	0.60
RMS (m)	**East**	0.78	0.39	0.39	0.48	0.49
	North	0.51	0.35	0.51	0.88	1.07
	Height	1.71	0.75	0.89	1.27	1.82
95% C.I. (m)	**East**	1.53	0.76	0.77	0.95	1.03
	North	1.00	0.69	1.00	1.72	2.18
	Height	3.36	1.46	1.75	2.49	3.57

Table 4.4: The mean, RMS and 95% confidence interval at STR1 using different *a priori* observations sigma ratios.

STR1						
		Case-1	**Case-2**	**Case-3**	**Case-4**	**Case-5**
Mean (m)	**East**	-0.02	0.04	0.07	0.10	0.12
	North	0.18	0.13	0.18	0.24	0.29
	Height	0.13	0.06	0.06	-0.09	-0.17
RMS (m)	**East**	0.31	0.16	0.20	0.22	0.24
	North	0.45	0.26	0.33	0.50	0.62
	Height	0.80	0.36	0.30	0.45	0.60
95% C.I. (m)	**East**	0.61	0.31	0.38	0.44	0.47
	North	0.88	0.51	0.62	0.98	1.21
	Height	1.56	0.70	0.57	0.89	1.18

Table 4.5: The mean, RMS and 95% confidence interval at TOW2 using different *a priori* observations sigma ratios.

TOW2						
		Case-1	**Case-2**	**Case-3**	**Case-4**	**Case-5**
Mean (m)	**East**	-0.13	0.00	0.01	0.00	-0.02
	North	0.11	0.12	0.17	0.25	0.30
	Height	-0.05	0.03	0.24	0.61	0.90
RMS (m)	**East**	0.47	0.27	0.31	0.34	0.36
	North	0.41	0.28	0.39	0.55	0.62
	Height	0.78	0.46	0.53	0.88	1.39
95% C.I. (m)	**East**	0.92	0.52	0.60	0.66	0.71
	North	0.81	0.54	0.76	1.08	1.22
	Height	1.52	0.89	1.03	1.72	2.72

Note: The numbers highlighted in pink denote the minimum value, while the numbers highlighted in green are the maximum values.

Figures 4.2, 4.3 and 4.4 are the "graphical" version of the tabulated values in Tables 4.3, 4.4, and 4.5. These bar charts show the average mean and RMS values at DARW, STR1 and TOW2 stations based on all the data sets used for this study. The x-axis represents the east, north and height components, and the y-axis denotes the mean and RMS values in metres. The coloured bars represent the solutions based on different *a priori* observation sigma ratios.

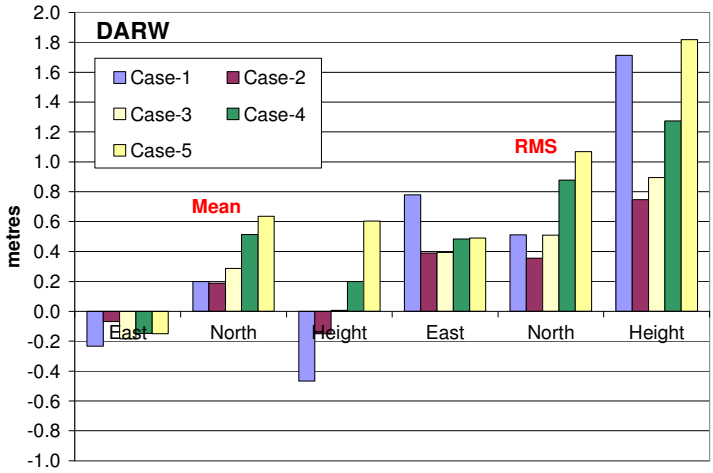

Figure 4.2: The combined mean and RMS values for DARW station.

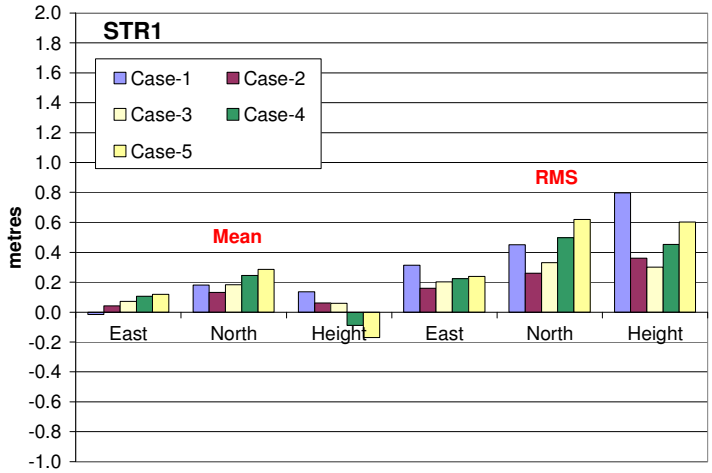

Figure 4.3: The combined mean and RMS values for STR1 station.

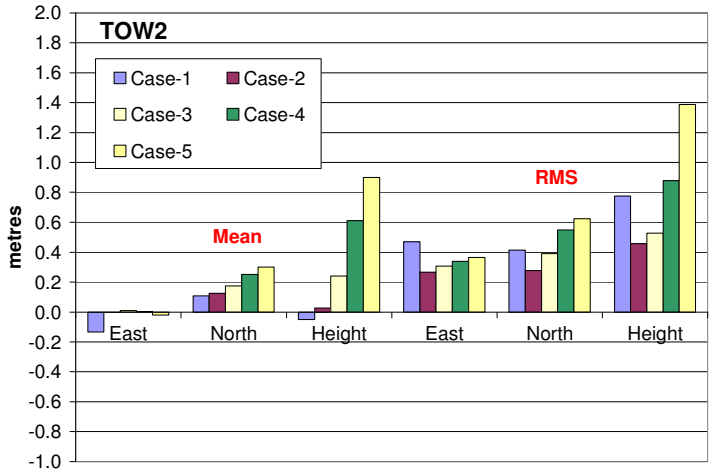

Figure 4.4: The combined mean and RMS values for TOW2 station.

From these analyses, it appears that different observations sigma ratios affect the accuracy and precision of the single frequency PPP solutions differently. Among the five sigma ratios tested, Case-2 ($\approx$ 1 : 50) has the lowest mean and RMS values, and is followed by Case-3 ($\approx$ 1 : 10) and then Case 4 (1 : 4). In comparison to the estimated solutions based on single frequency code observations (Case-5), Case-2 strategy provides approximately 50% to 60% improvement in the positioning precision. Thus, it can be said that the positioning results based on Case-2 processing strategy are the most accurate and precise. The solutions from the classical code-based processing generally have the highest mean and RMS values as only L1 code observations (no carrier phase measurements) were used in the data processing. This indicates that the solutions from Case-5 processing strategy are the least accurate and precise. However, in some cases, the solutions based on Case-1 ($\approx$ 1 : 100) have the highest mean and RMS values.

Figures 4.5, 4.6, and 4.7 show the east, north and height errors in metres as a function of local time in hours for DARW, STR1 and TOW2, respectively. These figures are divided into five rows and three columns. Each row shows the positioning errors based on the different cases, i.e., Case-1, Case-2, Case-3, Case-4, and Case-5; each column consists of graphs showing the errors of the east, north and height components. The different coloured lines denote the positioning results for the different DOY data sets. These figures are useful as they illustrate the positioning errors of the different solutions as a function of observation time.

DARW

- Case-1 (≈1 : 100)

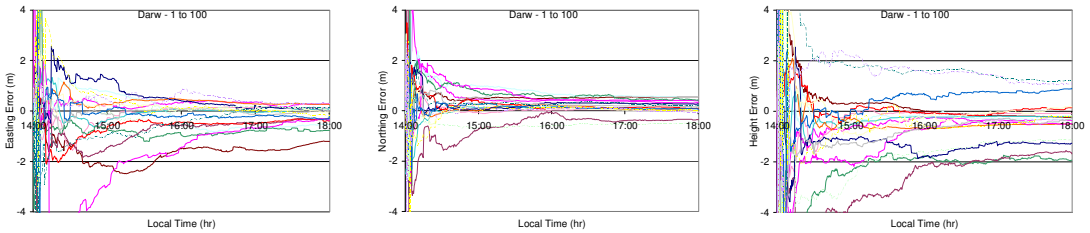

- Case-2 (≈ 1 : 50)

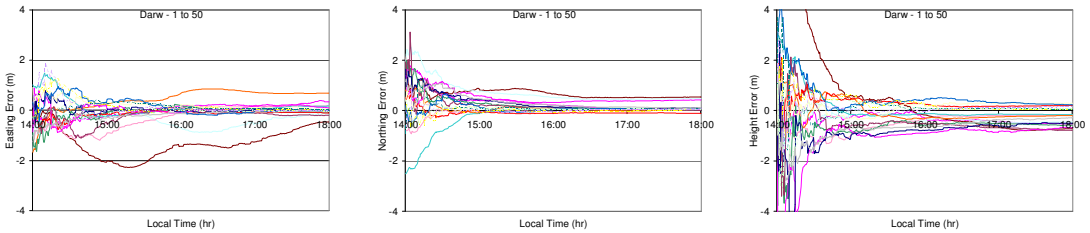

- Case-3 (≈ 1 : 10)

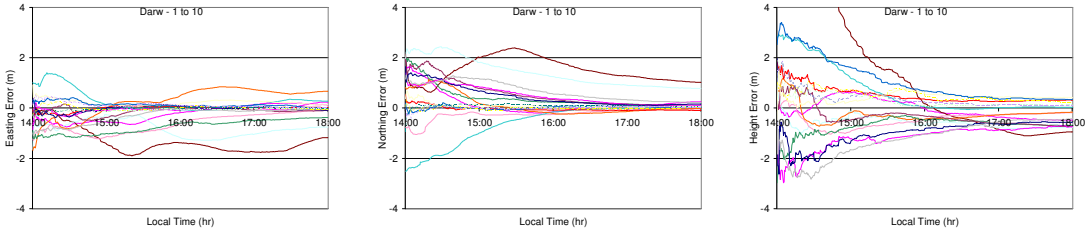

- Case-4 (1 : 4)

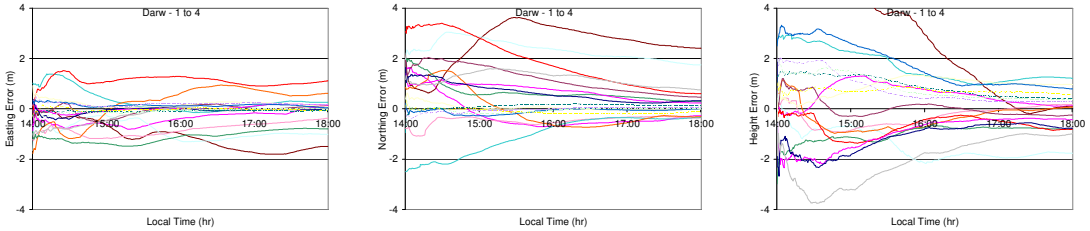

- Case-5 (code solutions)

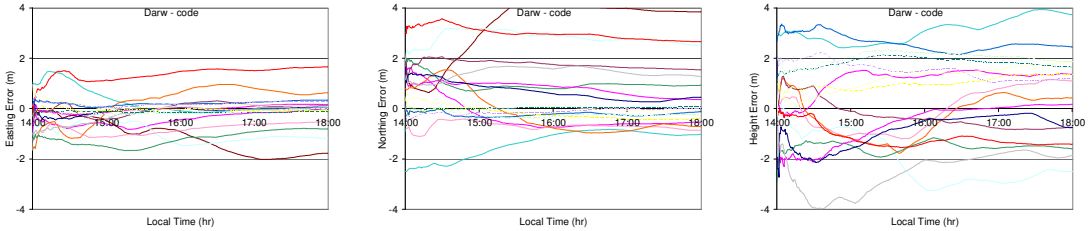

Figure 4.5: East, north and height positioning errors based on the Case-1, Case-2, Case-3, Case-4, and Case-5 processing strategies at DARW station.

STR1

- Case-1 (≈1 : 100)

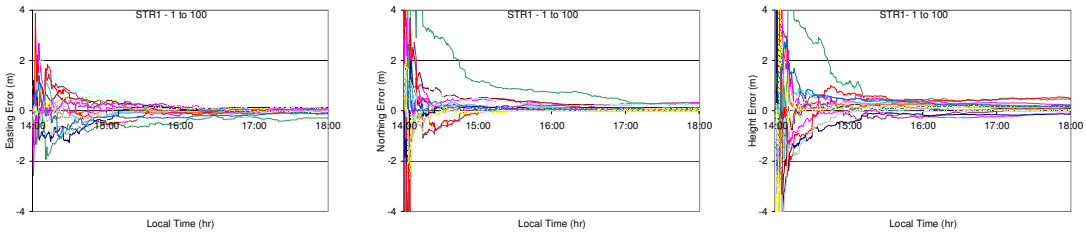

- Case-2 (≈ 1 : 50)

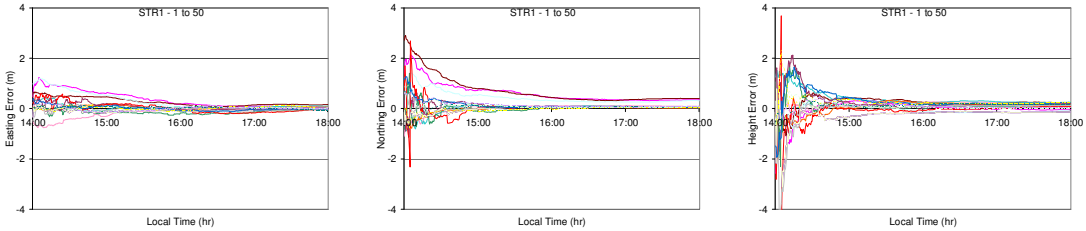

- Case-3 (≈ 1 : 10)

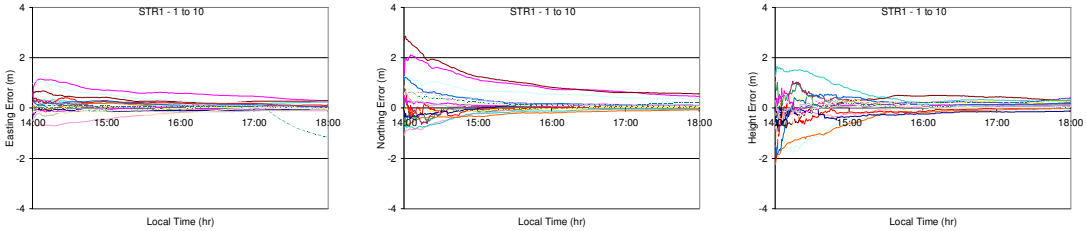

- Case-4 (1 : 4)

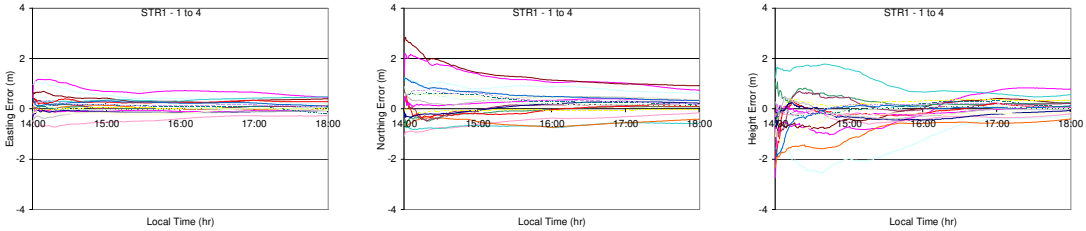

- Case-5 (code solutions)

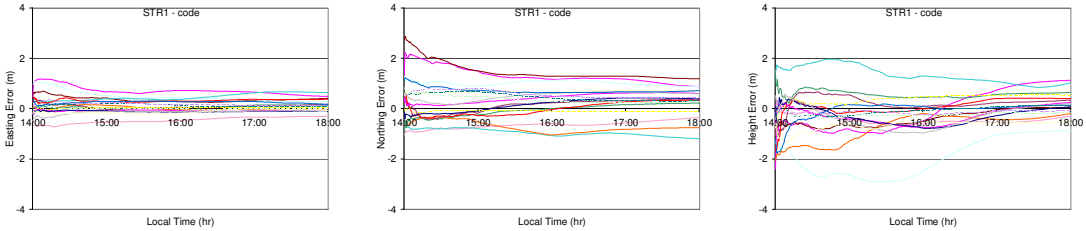

Figure 4.6: East, north and height positioning errors based on the Case-1, Case-2, Case-3, Case-4, and Case-5 processing strategies at STR1 station.

TOW2

- Case-1 (≈1 : 100)

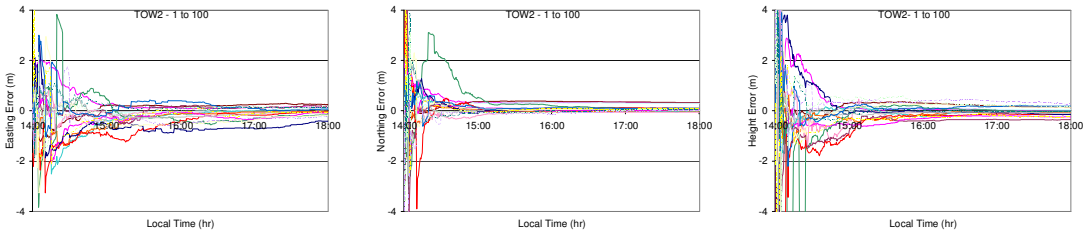

- Case-2 (≈ 1 : 50)

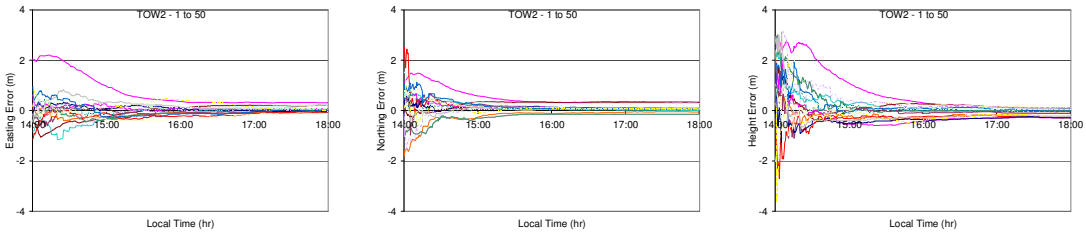

- Case-3 (≈ 1 : 10)

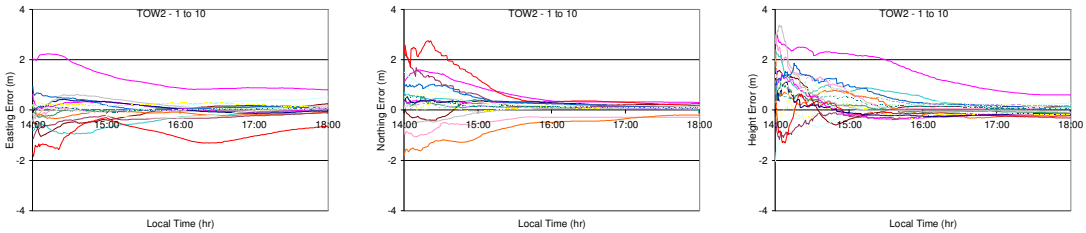

- Case-4 (1 : 4)

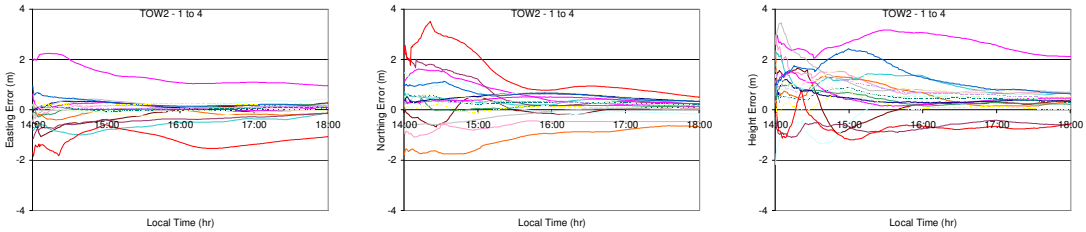

- Case-5 (code solutions)

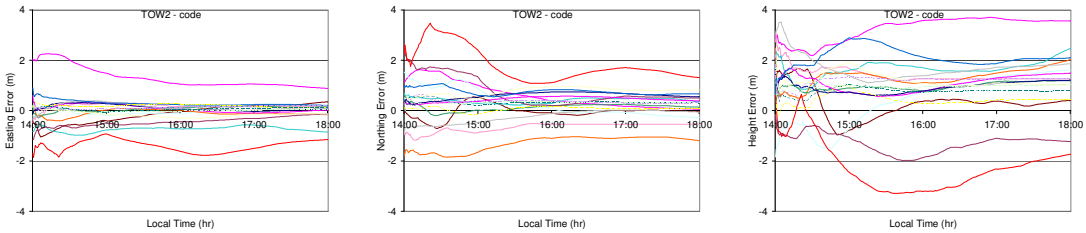

Figure 4.7: East, north and height positioning errors based on the Case-1, Case-2, Case-3, Case-4, and Case-5 processing strategies at TOW2 station.

It can be seen from these figures that the point positioning errors from Case-4 and Case-5 show comparable positioning trends. The accuracy of the horizontal and height positions did not improve with more observations. Case-5 processing strategy was essentially based on code observations only, while Case-4 was based on a code and quasi-phase observations sigma ratio of 1:4. The relative weighting between the code observations and the quasi-phase observations in Case-4 was in fact insignificant, and hence, the code observations dominated the solutions. Consequently, the Case-4 positioning results did not appear to converge and it portrays some similarities with the L1 code-based solutions.

In contrast to Case-4 and Case-5, the positioning solutions from Case-1, Case-2 and Case-3 processing strategies converged. As more observations were collected and used in the data processing, the positioning errors decreased. Thus the estimated solutions became more accurate. It can be seen from Figures 4.5, 4.6 and 4.7 that Case-2 has the best overall performance and the Case-2 solutions converged quicker than the other cases tested. When an *a priori* code and quasi-phase sigma ratio of about 1:50 was used, the variability of the horizontal and height positioning errors was lower compared to observations sigma ratios of 1:100 (Case-1), 1:10 (Case-3), 1:4 (Case-4), Case-5. It is also apparent that the single frequency PPP solutions convergence behaviour improved when Case-2 processing strategy was used. Although this pattern is consistent at the three GPS stations located in different zones of latitude, remarkable improvement can be seen at the height component at DARW station.

Figure 4.8 shows the average RMS values in metres based on all the data processed at DARW at specific observations time for Case-1, Case-2, Case-3, and Case-4 processing strategies. This figure is simply an example to demonstrate the behaviour of the positioning results for different observation lengths.

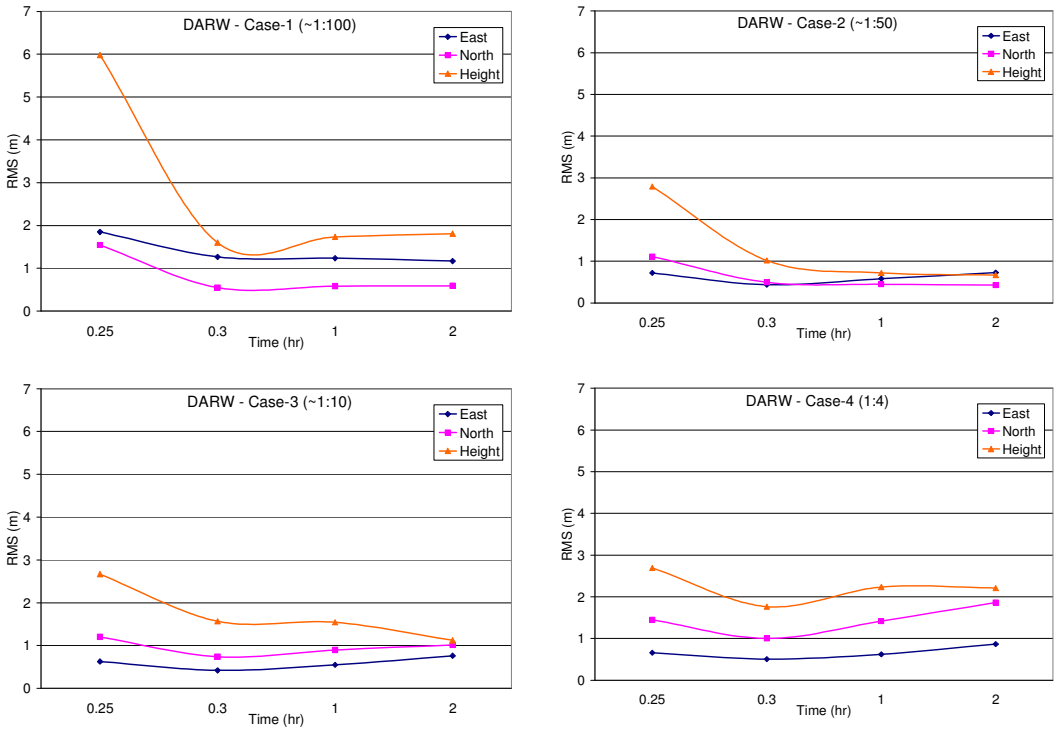

Figure 4.8: Point positioning RMS values in metres as a function of observation time in hours at DARW based on Case-1, Case-2, Case-3, and Case-4 processing strategies.

The initial positioning solutions from Case-1 strategy have the highest variability (refer to Figures 4.5, 4.6, and 4.7). However, after 15 minutes observation period, the horizontal and height errors have RMS values of about 2m and 6m, respectively. Whereas, the horizontal and height errors based on the other cases have RMS values of approximately 1m and 3m, respectively. It can also be inferred from this figure that the Case-2 solution convergence time is the shortest. About half an hour to an hour are required for Case-2 solutions to converge within a metre of the known values.

In the Case-1 processing strategy, the quasi-phase observations have a relatively smaller sigma value, or equivalently, higher weight than the quasi-phase observations in Case-2. Thus, the solutions in Case-1 are strongly influenced by the single frequency ionosphere-free combination. Since single frequency PPP is essentially based on float solutions, the ambiguity term in the quasi-phase equation needs more time for the solutions to "stabilise", which then affects the convergence behaviour of the solutions. In addition, the float ambiguity before stabilisation may also limit the accuracy and precision of the initial portion of the PPP solutions. Consequently, the variability of the positioning errors is larger in Case-1 than in the other cases tested.

In contrast to Case-1 processing strategy, the quasi-phase observations were given a relatively larger sigma value in Case-3 processing. This means that the Case-3 quasi-phase observations have lesser weight relatively to the quasi-phase observations in both Case-1 and Case-2. As a result, the code observations in Case-3 processing strategy have more influence on the estimation process. Therefore, in a relative sense, the initial estimations of the solutions in this study based on Case-3 processing strategy were not greatly affected by the ambiguities. Therefore, the estimated positions deviate minimally from the known coordinates.

Similarly in Case-4 processing strategy, the quasi-phase observations were given less weight in the adjustment model than the other processing strategies tested. The relative weighting between the code observations and the quasi-phase observations is considered insignificant. Thus, the Case-4 initial solutions do not appear to be affected by the float ambiguities, but instead, it closely followed the code-based solutions.

In order to illustrate the float ambiguities before and after stabilisation, the ambiguity values for each satellite at TOW2 on DOY359 2003 based on Case-1, Case-2 and Case-3 sigma ratios are plotted in Figure 4.9 as a function of observation time. It can be seen from this figure that the initial phase ambiguities from Case-1 vary substantially when compared to Case-2 and Case-3 strategies. In a PPP solution, the float ambiguities are estimated as part of a least squares estimation process. Therefore, any large variations in the ambiguity values will affect the accuracy and precision of the other parameters.

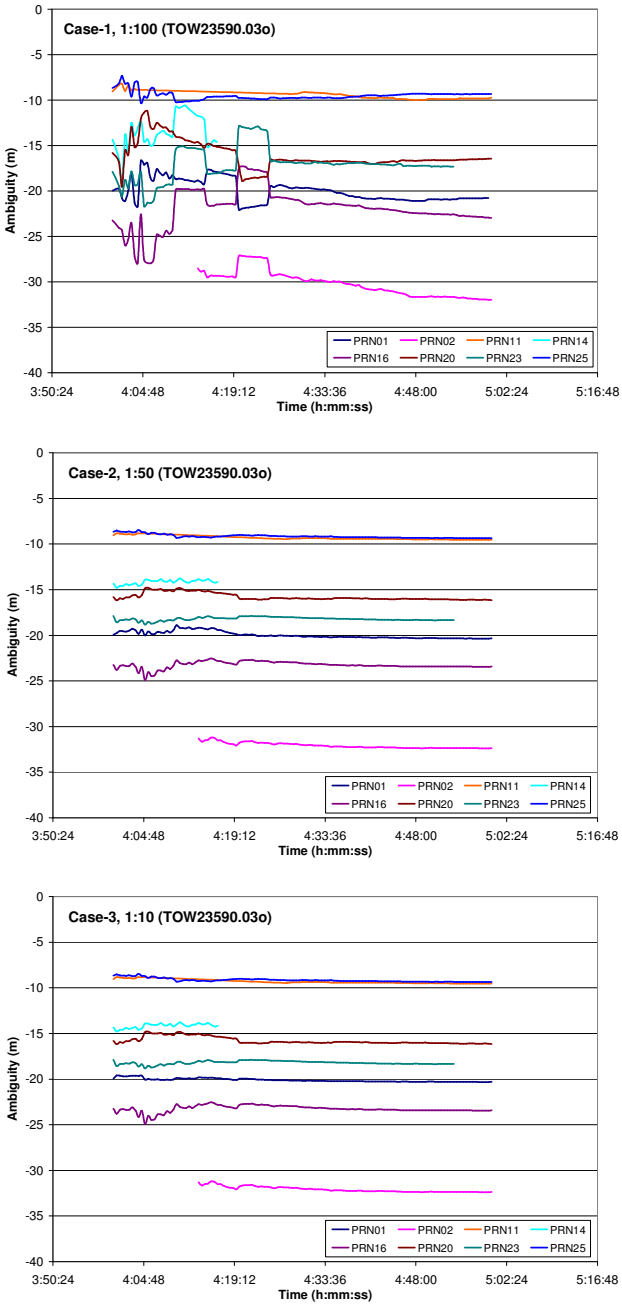

Figure 4.9: Phase ambiguity for each satellite observed at TOW2 on DOY 359 2003 using Case-1, Case-2, and Case-3 sigma ratios.

4.4.1 Relationship between Observations Sigma Ratio and Ionospheric Activities

Another point worth noting in this research is the relationship between the *a priori* single frequency PPP observations sigma ratio and the behaviour of the estimated solutions in different ionospheric conditions. Assuming that the ionosphere is the only variable considered and the local environment surrounding the GPS stations and the effects of the other GPS error sources from 2001 to 2006 remains unchanged, the relationship between the ionospheric activities and the observations sigma ratio can be established. The Sunspot Cycle 23 started in 1996; it peaked in 2001 and weakened in 2006 (Hathaway, 2008). This means that the effects of the ionosphere were the strongest in 2000 to 2001, and the ionospheric effects weaken as the year progresses. In 2006, the ionospheric activities were at its minimum (refer to Section 3.3.1).

In this study, as the quasi-phase observations in Case-3 processing strategy were given lesser weight than those in Case-1, the solutions were mostly dominated by the code observations. It is known that the code observations do contain residual ionospheric delay as the IGS *Final* GIMs are only accurate to about 2-8 TECU (see Table 2.1) (IGS, 2008). During the periods of high ionospheric activities, the residual ionospheric delay contained in the code observations is larger, which may lead to less accurate and precise point positioning solutions. Thus, single frequency point positioning using code observations, even after correcting for the ionospheric delay, is expected to provide less accurate and precise solutions typically during the periods of high ionospheric activity. To date, there are no single frequency ionospheric correction products yet to be developed, which could completely eliminate all the ionospheric effects on the code observations.

However, when the code observations are combined with the carrier phase observations, single frequency code and carrier phase ionosphere-free combination can be formed to eliminate the effects of the ionosphere (refer to Section 3.3.3.4). In this research, the quasi-phase observations in Case-3 processing strategy were assigned relatively lesser weight in the adjustment model. As a result, the solutions from this processing strategy follow the less precise code observations and the estimated solutions are relatively inaccurate and imprecise. In fact, these results are the worst during the periods of high ionospheric activity (in 2001 and 2002).

For data sets that were collected during low ionospheric activity (e.g. 2006), the positioning solutions from Case-3 processing strategy are in fact more accurate and precise than those in Case-1. Therefore, the degree of improvement using different *a priori* sigma values is highly dependent on the ionospheric activity. Case-2 processing strategy, which "fits" in between Case-1 and Case-3 is more robust and capable of providing (if not better) comparable point positioning solutions during both the periods of high and low ionospheric activities. By setting the *a priori* code and quasi-phase sigma ratio to 1:50, it possesses the strengths of Case-1 and Case-3 processing strategies, while it lacks the weaknesses of the two strategies.

4.4.2 The Use of an Ionospheric Error Mitigation Method

The use of an ionospheric product, e.g. the GIMs, improves the accuracy of the code-based single frequency point positioning (Le and Tiberius, 2006; Øvstedal *et al.*, 2006). But when an ionospheric product is used in a single frequency *code and quasi-phase* combination to correct for the ionospheric delay, it impacts only on the initial part of the single frequency PPP solutions. After the phase ambiguities stabilise, the quasi-phase observations will dominate the solutions, and the code observations will only have marginal influence in single frequency PPP solutions (Kouba and Hèroux, 2001; Simsky, 2006).

4.5 Summary

This Chapter has investigated the contributions of different *a priori* observations sigma ratios on the quality of the estimated PPP solutions. Five case scenarios were tested using GPS data collected at three ARGN stations and the results from all three stations showed similar trends. More importantly, if an appropriate observations sigma ratio is assigned in the adjustment model, the quality and performance of the single frequency PPP solutions will prevail over the classical code-based positioning solutions.

The contribution of different *a priori* code and quasi-phase sigmas is dependent on the ionospheric activities. During the periods of high ionospheric activities, more weight, or equivalently smaller sigma value should be applied to the quasi-phase observations. This is because the ionospheric errors affecting the code observations are not completely eliminated by the use of an ionospheric error mitigation product, while the ionospheric-free quasi-phase observations are free from the ionospheric effects. Alternatively, during the periods of low

ionospheric activity, the ionospheric errors affecting the code observations are relatively lower, and the code observations could provide considerably more accurate solutions after the aid of an ionospheric error mitigation product. On the other hand, the quasi-phase observations are subject to float ambiguities, which affect the solutions convergence time and the initial portion of the estimated solutions. Hence, smaller weight (or larger sigma value) should be used on the quasi-phase observations to reduce its impacts in the adjustment model.

Based on the results compiled from this study, *a priori* code and quasi-phase sigma ratio of 1:50 provided optimal performance in terms of single frequency PPP positioning accuracy, precision and convergence time despite the ionospheric conditions and the location of the GPS receivers. During the periods of high and low ionospheric activities, this ratio did not appear to have negative effects on the estimated solutions at the three ARGN stations. Therefore, it can be concluded that the *a priori* code and quasi-phase sigma ratio of 1:50 is the best ratio among all the ratios tested in this study. This sigma ratio could adequately reflect the "relative" weighting between the code and quasi-phase observations.

One of the major error sources in single frequency point positioning, after the switch-off of SA, is the adverse effects caused by the propagation of satellite signals through the ionosphere. This limits the accuracy of the estimated single frequency point positioning solutions. In order to achieve the highest possible point positioning accuracy, effective ionospheric error mitigation methods are required to minimise the impacts of the ionospheric delay. Therefore, the next Chapter will describe the study undertaken as part of this research to evaluate the effectiveness of using different ionospheric error mitigation methods in single frequency point positioning.

CHAPTER 5

Ionospheric Error Mitigation Strategies for Single Frequency Point Positioning

5.1 Introduction

The ionosphere is a critical source of error for GPS users who require high accuracy point positioning solutions, in particular single frequency receiver users. The resultant range error introduced by the ionosphere can vary from less than 1m to more than 100m depending on the time of the day, season, location of the receiver, and solar activity (Klobuchar, 1991). Thus, it is very important to understand the impacts of the ionospheric delay on single frequency positioning, and to find effective measures which can be applied to minimise the effects of the ionosphere error.

Several ionospheric error mitigation strategies have been developed in order to assist single frequency GPS users to correct for the ionospheric delay (Bent *et al.*, 1972; Chiu, 1975; Klobuchar, 1987; Anderson *et al.*, 1989; Komjathy, 1997; Bilitza, 2001). One of the more effective ionospheric error mitigation methods used in single frequency GPS point positioning is the GIMs provided by the IGS (see Section 3.3.3.2 for detailed description of the GIMs). The accuracy of the GIMs highly depends on the distribution, density and homogeneity of the GPS stations used for modelling. The location of the tracking stations around the world is not evenly distributed. As the number of tracking stations located in the northern hemisphere is higher than the southern hemisphere, the accuracy of the GIMs in the southern hemisphere may be limited. Another weakness of the GIMs is the simple mathematical model used in describing the behaviour of the ionosphere. The parameters of the model are actually determined based on the fitting of global data using a least squares technique. As a consequence, the GIMs may not be able to adequately reflect the local characteristics of the ionosphere (Yuan *et al.*, 2007; Zhang *et al.*, 2008). It is recognised that local or RIMs based

on direct GPS data collected from a regional network of tracking stations could provide a better representation of the local ionospheric behaviour (Zolesi and Cander, 1998; Gao and Liu, 2002; Ping *et al.*, 2002).

This Chapter will describe in detail the case studies undertaken to assess the feasibility of applying the RIMs in single frequency point positioning to improve the estimated positioning solutions. The estimated solutions based on the RIMs will be compared with those of the Broadcast model and GIMs. These products will be evaluated using GPS data from the low and middle latitude regions and during the periods of high and low solar activities.

5.2 Case Studies

The aim of this research is to evaluate the effectiveness of the high spatial and temporal resolution RIMs in single frequency point positioning, typically in single frequency PPP. Two case studies, Case Study 1 and Case Study 2, were formulated. Case Study 1 examines the feasibility of using RIMs, Broadcast model and GIMs in both classical single frequency code-based point positioning and PPP. Case Study 2 investigates the contribution of using higher temporal (1-hour) RIMs. The numerical results and analyses will be presented accordingly.

5.2.1 Case Study 1: Assessment of the Broadcast Model, GIMs and RIMs

The focus of the Case Study 1 is to evaluate the performance of three ionospheric error mitigation methods used in both classical code-based single frequency point positioning and PPP. The performance evaluation of the ionospheric error mitigation methods was carried out based on the accuracy and precision of the estimated positioning solutions. As the magnitude of error induced by the ionosphere is different in periods of solar maximum and minimum, GPS data collected from both periods were used in the evaluation process. The tested ionospheric error mitigation methods were the Broadcast model, GIMs and RIMs. As noted in Chapter 2, single frequency point positioning can be separated into the classical single frequency code-based solutions and single frequency PPP using *code and quasi-phase* combination. Therefore, the analyses carried out in this research were divided into two strategies as follows,

- **Strategy 1: Classical code-based single frequency point positioning**

- **Strategy 2: Single frequency PPP using *code and quasi-phase* combination**

Strategy 1 was included primarily to illustrate the quality of the estimated point positioning solutions based on the classical code-based single frequency point positioning using various ionospheric error mitigation methods. Readers should note that the emphasis of this research is on Strategy 2, that is, the feasibility of these ionospheric error mitigation methods, especially the RIMs in single frequency PPP. Each of the processing strategies was carried out using identical software configurations and settings, as well as the same set of GPS data and observation time span. The only difference between the two strategies was that the carrier phase measurements were used in Strategy 2 data processing in addition to code measurements.

In order to investigate the ionospheric effects on single frequency point positioning in Australia, the location of the GPS stations used in this study were strategically selected. The effects of the ionosphere on GPS observations strongly depend on the location of the receivers in different latitudinal zones. Observation data from five ARGN stations were strategically selected based on the location of the stations. The selected stations were DARW, TOW2, ALIC, STR1, and HOB2. The geographic location of these stations is shown and described in Figure 5.1 and Table 5.1.

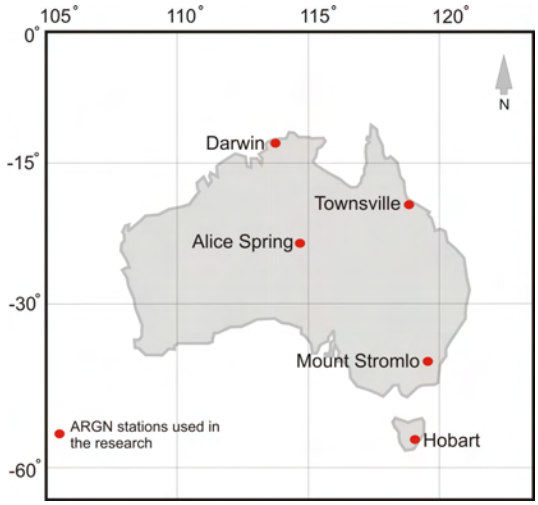

Figure 5.1: The five ARGN stations used in this study.

Table 5.1: The approximate latitude and zone of the five ARGN stations.

Station	Approx. Latitude	Latitude Region
DARW	-12˚ 51’	Low Latitude
TOW2	-19˚ 16’	Low Latitude
ALIC	-23˚ 40’	Low Latitude
STR1	-35˚ 19’	Middle Latitude
HOB2	-42˚ 48’	Middle Latitude

One of the objectives of this analysis is to test the performance of the Australia-wide RIMs during the periods of high and low ionospheric activities, i.e. solar maximum and minimum periods. Taking into account the rapid development of the ARGN stations across the Australian continent in the early 2000s, the year 2001 was selected as the period of solar maximum. For the period of solar minimum, the year 2006 was selected. Since the variations of TEC values are higher during the summer months than winter months in the southern hemisphere, GPS observation data from DOY 336 to 341 2001 were used to represent the solar maximum periods as the data were collected during the summer. For the solar minimum periods, data from DOY 183 to 188 2006 were selected as they were days during the winter months. Table 5.2 tabulates the data that are (and are not) used (or available) for this study, and Figure 5.2 denotes the daily sunspot numbers in 2001 and 2006 (SIDC, 2008). The daily sunspot number for DOY 336 to 341 2001 range between 49 and 62, whilst the daily sunspot number range between 17 and 20 for DOY 183 to 188 2006.

Table 5.2: GPS observation data that were and were not used in this study.

YEAR	2001						2006					
DOY	**336**	**337**	**338**	**339**	**340**	**341**	**183**	**184**	**185**	**186**	**187**	**188**
DARW	Y	Y	Y	Y	Y	N	Y	Y	Y	Y	Y	Y
TOW2	Y	Y	Y	Y	Y	Y	Y	Y	Y	Y	Y	Y
ALIC	NA	N	NA	N	Y	Y	Y	Y	Y	Y	Y	Y
STR1	Y	Y	Y	Y	Y	Y	Y	Y	Y	Y	Y	Y
HOB2	Y	Y	Y	Y	Y	Y	Y	Y	Y	Y	Y	Y
Legends: Y-Data was used; N-Data was not used (e.g. data was incomplete); NA-Data was not available.												

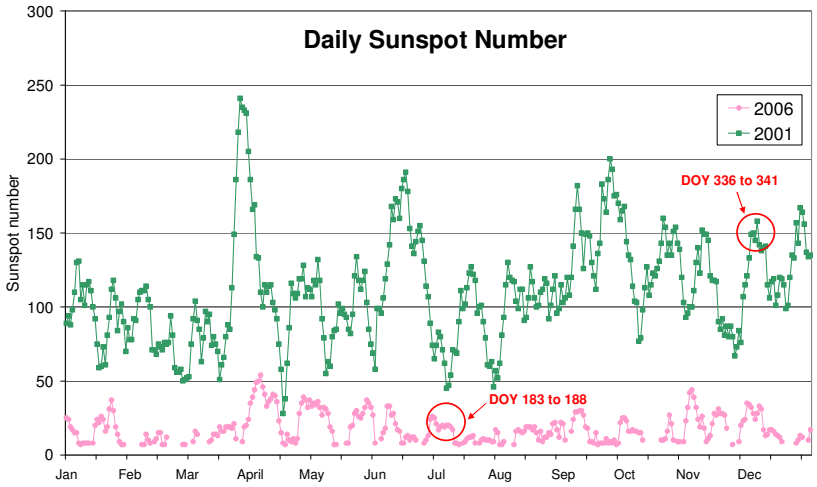

Figure 5.2: The daily sunspot number for 2001 and 2006 (SIDC, 2008).

24 hour data sets with 30 seconds observation interval for the five stations were downloaded from the SOPAC database (SOPAC, 2008). All data sets used in this experiment were windowed into a 12-hour observation period, starting from 14:00LT. A 15˚ elevation cut-off angle was applied to reduce the data susceptibility to multipath. The tropospheric ZPD was modelled and mapped using Hopfield model with default atmospheric parameters, and the Niell mapping function, respectively. The *a priori* observations sigma ratio was set to about 1:50 with a code and quasi-phase sigma value of 4m and 0.1m, respectively. The IGS *Final* satellite orbit and clock corrections were used to constrain the satellite orbit and clock errors.

In this study, the performance of the Australia-wide RIMs was compared with the "no ionospheric corrections", Broadcast model, and the GIMs. The ionospheric coefficients applied in the Broadcast model were obtained from the daily "auto" navigation file from SOPAC (SOPAC, 2008) as most of the ARGN stations did not store the daily navigation file. The "auto" file is simply a global broadcast navigation message containing all broadcast navigation messages for the 24-hour period generated using several navigation files (SOPAC, 2008). The IGS *Final* and *Rapid* GIMs used for the 2006 data processing were obtained from IGS website (IGS, 2008). However, for 2001 data processing, the CODE GIMs were used instead (CODE, 2007). This is because the IGS has only started producing the combined GIMs since 2003. Therefore, the GIMs produced from CODE were used to correct for the ionospheric effects.

Although the ARGN stations were equipped with dual frequency geodetic quality GPS receivers, only observations on L1 frequency were used for the single frequency data processing. Nonetheless, the data were also post-processed using dual frequency PPP and the results were presented in Strategy 2 along with the single frequency PPP solutions. The dual frequency PPP results were included for the purpose of comparison, as well as to demonstrate the accuracy of dual frequency PPP using the "Traditional model" described in Section 2.6.1.

5.2.1.1 Strategy 1: Single Frequency Code-Based Solutions

This section reports on the quality of the estimated point positioning solutions based on single frequency code-based processing using various ionospheric models and products. Four processing strategies, namely "no ionospheric corrections", Broadcast model, GIMs and RIMs were carried out. The "no ionospheric corrections" strategy was performed to emulate the accuracy of the estimated point positioning if no ionospheric corrections were applied. The results were separated and presented into two parts: solar maximum and solar minimum periods.

DOY 336 to 341 2001 (solar maximum)

Table 5.3 shows the combined mean and RMS values for DARW, TOW2, ALIC, STR1 and HOB2 stations based on the L1 code-only solutions for DOY 336 to 341 2001. The computed mean shows the average point positioning errors based on all the data used in this study. The RMS value indicates the dispersion of the estimated positioning solutions from the

known coordinates. From Table 5.3, one can see that the effects of the ionosphere during the periods of solar maximum, if left unaccounted for, are detrimental on the estimated point positioning solutions. The positioning errors are worse on the height component for GPS stations located in the low latitude region. The minimum and maximum RMS values for the horizontal position, if no ionospheric corrections were applied, are 1.44m and 5.72m, respectively. While, the minimum and maximum RMS values for the height component are 10.68m and 20.96m, respectively. As expected, DARW station which is located in the low latitude region portrays the largest positioning error, whilst HOB2 station that is located in the middle latitude region shows the smallest point positioning error.

Table 5.3: The statistical results for DARW, TOW2, ALIC, STR1 and HOB2 stations using single frequency code observations from DOY 336 to 341 2001 (solar maximum).

2001						
Methods	**Mean (m)**			**RMS (m)**		
	East	**North**	**Height**	**East**	**North**	**Height**
DARW						
1. No Ionospheric correction	-1.12	5.47	-20.81	1.30	5.57	20.96
2. Broadcast Model	-0.84	4.97	-2.08	1.09	5.06	2.96
3. CODE GIMs	-0.58	1.36	0.61	0.83	1.70	2.32
4. RIMs	0.11	1.99	-1.25	0.50	2.08	1.66
TOW2						
1. No Ionospheric correction	0.58	3.51	-17.31	0.65	3.62	17.44
2. Broadcast Model	0.19	3.27	1.06	0.38	3.40	2.09
3. CODE GIMs	0.35	-0.31	1.99	0.49	0.52	2.10
4. RIMs	0.31	0.25	0.98	0.57	0.75	1.15
ALIC						
1. No Ionospheric correction	-0.76	4.48	-14.56	0.82	4.61	14.64
2. Broadcast Model	-0.73	4.15	2.62	0.77	4.25	2.72
3. CODE GIMs	-0.62	1.02	1.75	0.64	1.04	1.77
4. RIMs	-0.60	1.06	1.03	0.66	1.12	1.26
STR1						
1. No Ionospheric correction	0.79	1.91	-12.01	0.80	1.97	12.06
2. Broadcast Model	0.67	2.28	3.06	0.68	2.35	3.11
3. CODE GIMs	0.37	0.44	-0.09	0.41	0.58	0.72
4. RIMs	0.36	0.62	-0.71	0.42	0.64	1.11
HOB2						
1. No Ionospheric correction	0.78	1.13	-10.63	0.79	1.20	10.68
2. Broadcast Model	0.68	1.51	2.67	0.69	1.60	2.77
3. CODE GIMs	0.41	0.10	-0.20	0.43	0.29	0.71
4. RIMs	0.37	0.40	-0.83	0.40	0.52	1.08

In this study, the benefits of using the Broadcast model are apparent in the height component. In comparison to the "no ionospheric corrections", the Broadcast model could almost correct for 90% of the height error, which is quite remarkable. However, there is only a marginal improvement in the horizontal component between no ionospheric corrections applied and using the Broadcast model.

As anticipated, the quality of the estimated solutions based on the GIMs is superior to the Broadcast model. Significant improvement can be seen on the estimated point positioning solutions when the GIMs were used. On the other hand, the developed Australia-wide RIMs are able to provide more precise height solutions at low latitude GPS stations. The biggest improvement is seen at TOW2, whereby a RMS difference of 0.95m between the GIMs and RIMs can be observed. That is, the height RMS at TOW2 based on the RIMs improves by a magnitude of two. For the middle latitude stations, the GIMs provide the best horizontal and height solutions for single frequency code-based processing.

DOY 183 to 188 2006 (solar minimum)

Table 5.4 shows the combined mean and RMS values for the five ARGN stations using data collected from DOY 183 to 188 2006.

Table 5.4: The statistical results for DARW, TOW2, ALIC, STR1 and HOB2 stations using single frequency code observations from DOY 183 to 188 2006 (solar minimum).

2006						
Methods	**Mean (m)**			**RMS (m)**		
	East	**North**	**Height**	**East**	**North**	**Height**
DARW						
1. No Ionospheric correction	0.95	0.74	-3.48	0.98	0.81	3.84
2. Broadcast Model	-0.02	1.06	1.52	0.19	1.07	1.56
3. IGS *Rapid* GIMs	0.08	0.09	1.71	0.19	0.18	1.72
4. IGS *Final* GIMs	0.10	0.10	1.78	0.19	0.18	1.78
5. RIMs	0.14	0.28	1.08	0.20	0.31	1.11
TOW2						
1. No Ionospheric correction	0.78	0.56	-1.77	0.85	0.67	2.03
2. Broadcast Model	-0.08	0.56	1.44	0.12	0.57	1.46
3. IGS *Rapid* GIMs	-0.05	0.18	1.21	0.10	0.19	1.22
4. IGS *Final* GIMs	-0.06	0.17	1.26	0.11	0.19	1.27
5. RIMs	-0.11	0.48	0.57	0.15	0.49	0.60
ALIC						
1. No Ionospheric correction	0.76	0.48	-2.62	0.78	0.74	2.99
2. Broadcast Model	0.05	0.85	1.72	0.16	0.85	1.74
3. IGS *Rapid* GIMs	0.09	0.60	1.13	0.16	0.60	1.14
4. IGS *Final* GIMs	0.08	0.45	1.17	0.15	0.54	1.18
5. RIMs	0.07	0.84	0.84	0.17	0.84	0.87
STR1						
1. No Ionospheric correction	0.65	1.25	-2.03	0.84	1.54	2.38
2. Broadcast Model	0.12	0.92	0.53	0.15	0.94	0.64
3. IGS *Rapid* GIMs	0.08	0.53	-0.04	0.10	0.54	0.15
4. IGS *Final* GIMs	0.06	0.51	-0.04	0.09	0.52	0.16
5. RIMs	0.03	0.64	0.02	0.09	0.66	0.21
HOB2						
1. No Ionospheric correction	0.46	0.86	-1.35	0.51	1.03	1.65
2. Broadcast Model	0.08	0.80	0.80	0.11	0.81	0.92
3. IGS *Rapid* GIMs	0.11	0.37	-0.16	0.12	0.37	0.24
4. IGS *Final* GIMs	0.11	0.41	-0.17	0.12	0.41	0.26
5. RIMs	0.11	0.59	0.05	0.14	0.59	0.28

The benefits of using the Australia-wide RIMs are apparent in the low latitude stations. This discovery is identical to the finding for the periods of solar maximum. The RIMs generally provide more precise height solutions than the GIMs. For example, an average height RMS value of 1.22m is obtained when using the IGS GIMs at TOW2. When the Australia-wide RIMs were used instead, the height RMS value decreases to 0.6m. This shows an improvement in the height estimations. However, for middle latitude stations, the GIMs are able to provide more precise horizontal and height solutions.

Based on the results tabulated in Tables 5.3 and 5.4, the Australia-wide RIMs have positive impacts on height estimations using single frequency code-based processing. The positive contribution is apparent at stations located in the low latitude region. Half a metre to a metre level improvement in the height estimation is achieved when using the Australia-wide RIMs instead of the GIMs. As for the horizontal component, the positioning solutions based on GIMs are slightly better. On the other hand, minimal or no improvement on both horizontal and height components is observed at the middle latitude stations. In fact, the quality of the estimated horizontal component using the RIMs is not comparable to those of GIMs. This could be attributed to the mathematical model, as well as the density and distribution of GPS stations used in modelling the regional characteristic of the ionosphere.

As a summary, single frequency code-based point positioning users should, instead of not correcting for the ionospheric errors at all, apply the Broadcast model to achieve better quality point positioning solutions in real-time. For post-processed applications, users could take advantage of the GIMs to obtain more accurate and precise positioning solutions. The benefit of using the RIMs is only apparent for height estimations at low latitude stations. Thus, the feasibility of using the RIMs (instead of GIMs) for single frequency code-based point positioning is inconclusive.

5.2.1.2 Strategy 2: Single Frequency Code and Quasi-Phase Solutions

Strategy 2 presents the evaluation of various ionospheric models and products using single frequency PPP. Similar to Strategy 1, the results are presented in two parts: the solar maximum and solar minimum periods.

DOY 336 to 341 2006 (solar maximum)

The combined mean and RMS values using data collected from DOY 336 to 341 2001 are presented in Table 5.5. A number of key points could be interpreted from the numerical values tabulated in the table.

Table 5.5: The statistical results for DARW, TOW2, ALIC, STR1 and HOB2 stations using single frequency code and carrier phase observations from DOY 336 to 341 2001 (solar maximum).

2001						
Methods	**Mean (m)**			**RMS (m)**		
	East	**North**	**Height**	**East**	**North**	**Height**
DARW						
1. No Ionospheric correction	0.38	0.55	-1.72	1.01	1.05	3.93
2. Broadcast Model	-0.04	0.49	-0.64	0.41	0.94	0.96
3. CODE GIMs	-0.17	0.24	-0.45	0.40	0.35	0.78
4. RIMs	0.06	0.31	-0.57	0.33	0.52	0.73
5. Dual Frequency PPP	0.03	0.03	-0.51	0.21	0.21	0.54
TOW2						
1. No Ionospheric correction	0.32	0.13	-0.95	0.38	0.39	2.54
2. Broadcast Model	0.04	0.31	0.07	0.27	0.71	0.49
3. CODE GIMs	0.05	0.09	0.01	0.21	0.15	0.28
4. RIMs	-0.01	0.11	-0.06	0.21	0.17	0.23
5. Dual Frequency PPP	-0.01	0.07	-0.23	0.11	0.11	0.28
ALIC						
1. No Ionospheric correction	-0.37	0.45	-1.34	0.62	0.86	2.75
2. Broadcast Model	-0.45	0.49	-0.32	0.59	0.97	1.33
3. CODE GIMs	-0.18	0.46	-0.33	0.32	0.50	0.58
4. RIMs	-0.31	0.24	-0.38	0.45	0.38	0.58
5. Dual Frequency PPP	-0.06	0.10	-0.53	0.16	0.13	0.55
STR1						
1. No Ionospheric correction	0.22	0.25	-0.28	0.32	0.62	1.47
2. Broadcast Model	0.12	0.33	0.29	0.34	0.64	0.54
3. CODE GIMs	0.03	0.14	0.05	0.19	0.22	0.23
4. RIMs	0.07	0.14	0.02	0.20	0.22	0.34
5. Dual Frequency PPP	0.03	0.10	0.07	0.13	0.13	0.20
HOB2						
1. No Ionospheric correction	0.22	0.13	-0.23	0.30	0.39	1.53
2. Broadcast Model	0.14	0.24	0.30	0.30	0.57	0.38
3. CODE GIMs	0.09	0.05	0.16	0.20	0.08	0.26
4. RIMs	0.13	0.08	0.14	0.23	0.17	0.34
5. Dual Frequency PPP	0.05	0.10	0.13	0.17	0.13	0.22

It is interesting to note that the estimated point positioning errors using single frequency PPP are smaller than the classical code-based solutions. In comparison to the solutions with "no ionospheric corrections", the level of improvement provided by the Broadcast model in single frequency PPP is not as remarkable as those based on the code-only solutions. Nonetheless, the use of the Broadcast model could still help to improve the quality of the height estimations in single frequency PPP.

During the solar maximum periods, the numerical results using the GIMs has smaller mean and RMS values than the Broadcast model. This indicates that the GIMs solutions are more accurate than those of the Broadcast model. This is true especially for the horizontal positioning component. In comparison to the Australia-wide RIMs, the GIMs also provide more accurate and precise point positioning estimations for users who are in the middle latitude region. However, for low latitude stations, the Australia-wide RIMs provide more precise height estimations, which resembles the findings from the single frequency code-based solutions.

Dual frequency PPP has the best overall performance apart from the height results for DARW and ALIC. According to Gao and Shen (2002), the tropospheric error should be estimated in dual frequency PPP as an unknown parameter in order to reduce the influence of the tropospheric error. This could help provide higher accuracy and precision point positioning estimates, in particular the height solutions. However, the tropospheric delay was modelled (instead of estimated) in this study to ensure consistency with the single frequency processing settings.

The positioning errors for each ARGN station tested in this study based on the different ionospheric correction products are plotted and attached in Appendix B. The graphs show the positioning errors versus local time at the respective GPS station. The differences between the known coordinates obtained from the ITRF website with the software computed coordinates are the positioning errors. The intention of these plots is to demonstrate the accuracy of the computed solutions as a function of observation time, and also the convergence behaviour of the positioning solutions using the GIMs and RIMs. Due to the amount of data being processed, the solutions from two stations, i.e. DARW and STR1 are used as examples for the purpose of this discussion.

Figure 5.3 presents the positioning errors at DARW station during DOY 336 to 340 2001. The x-axis shows the observation time in hours, starting from 14:00LT to 02:00LT; the y-axis shows the horizontal (2D) position errors and height position errors in metres. The horizontal component values are calculated based on the following equation,

$$\text{2D Position Error} = \sqrt{\Delta E^2 + \Delta N^2} \tag{5.1}$$

where ΔE and ΔN were the differences between the known and computed Easting and Northing. The height errors are presented as positive values to show the magnitude and the convergence feature of the errors.

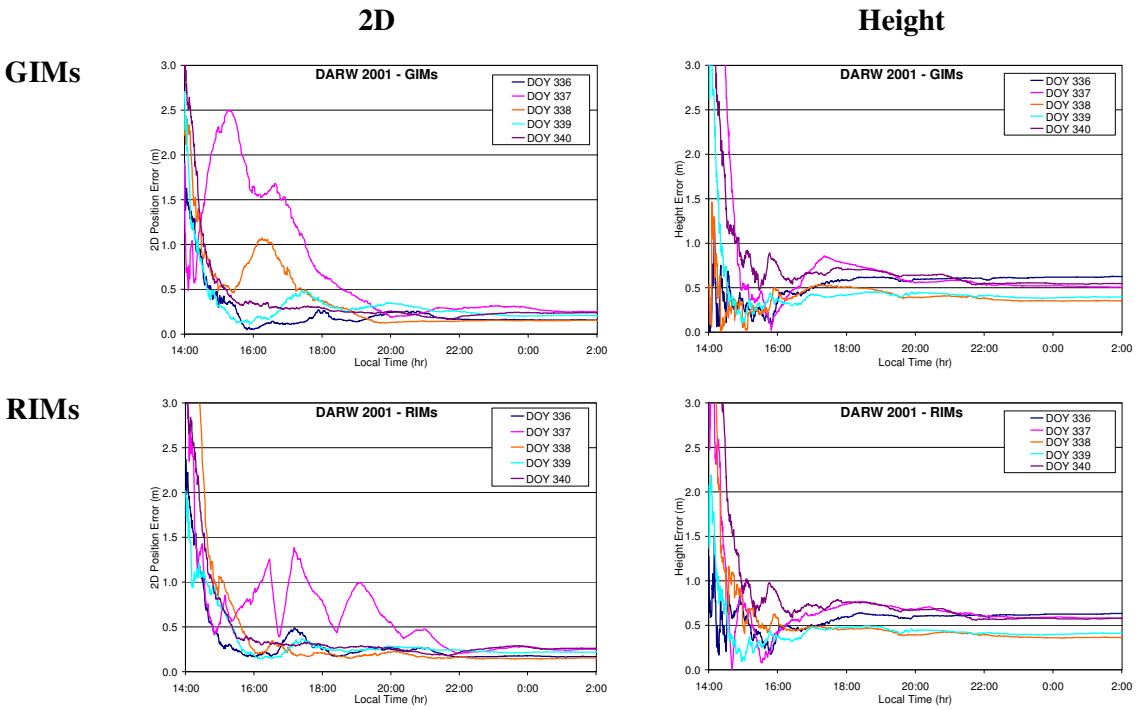

Figure 5.3: The positioning errors at DARW from DOY 336 to 341 2001 using single frequency code and carrier phase observations.

The plotted horizontal positioning errors for DOY337 2001 are unusual when compared to the other DOY data sets. Snapshots of the GIMs and RIMs at a specified time frame are plotted and compared in Figure 5.4. It can be seen from these snapshots that the GIMs have a smoother representation of the ionosphere. This is apparent in the 07:00UTC and 09:00UTC (16:30LT and 18:30LT at Darwin) snapshots, whereby differences of about 40 TECU to 60 TECU are noticeable at the northwest corner of the Australian continent. These

variations are in fact quite significant, which may have contributed to the large horizontal positioning errors in the DOY 337 2001 solutions.

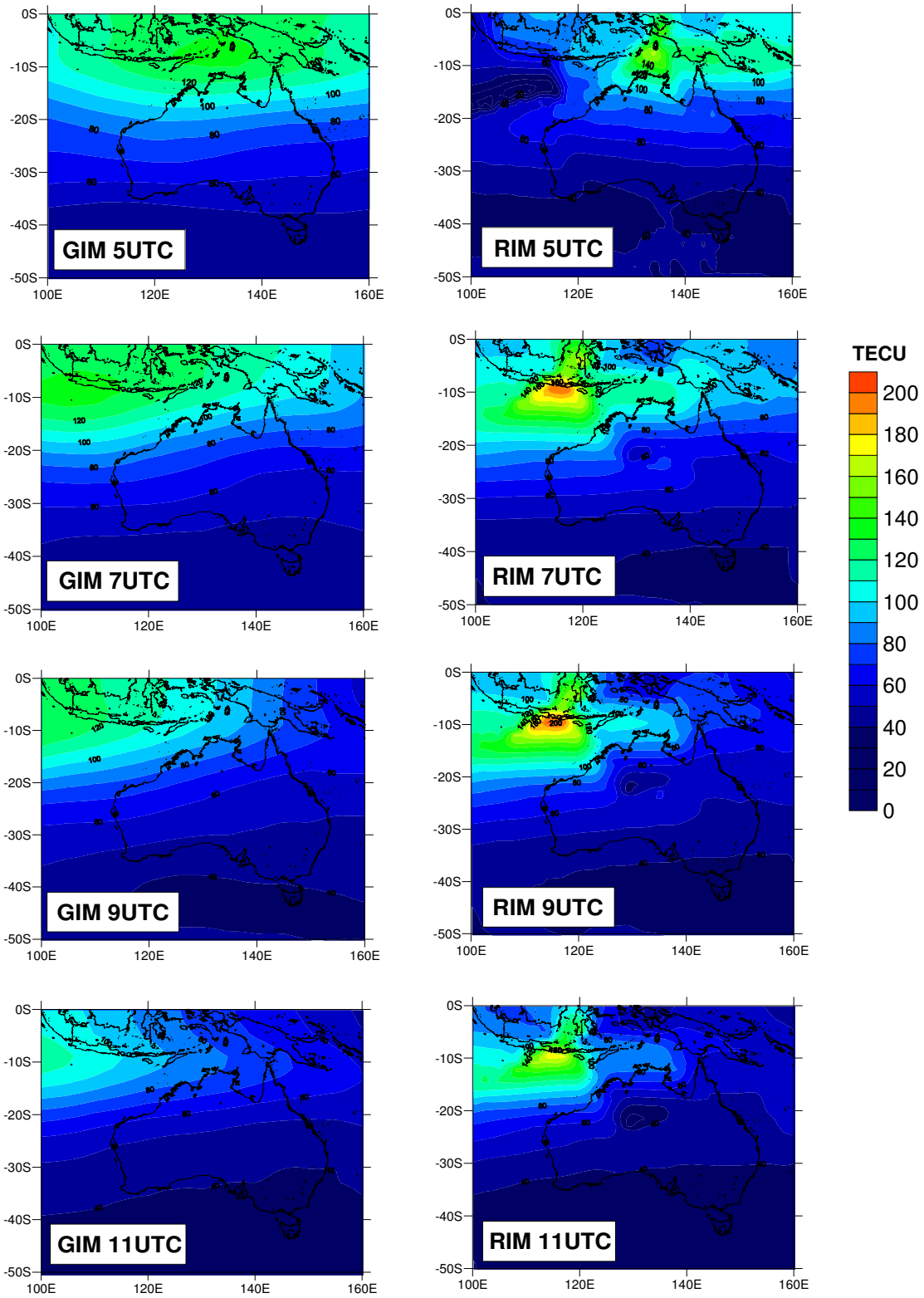

Figure 5.4: Snapshots of the GIMs and RIMs on DOY337 2001 at 05:00UTC, 07:00UTC, 09:00UTC, and 11:00UTC (05:00UTC is approximately 14:30LT at Darwin).

Figure 5.5 depicts the point positioning errors for STR1 station from DOY 336 to 341 2001. It is unclear from this figure if the higher resolution RIMs could help improve the single frequency PPP convergence time. However, it can be seen from Figures 5.3 and 5.5 that longer convergence time is required for single frequency PPP solutions in the low latitude region to converge during solar maximum periods.

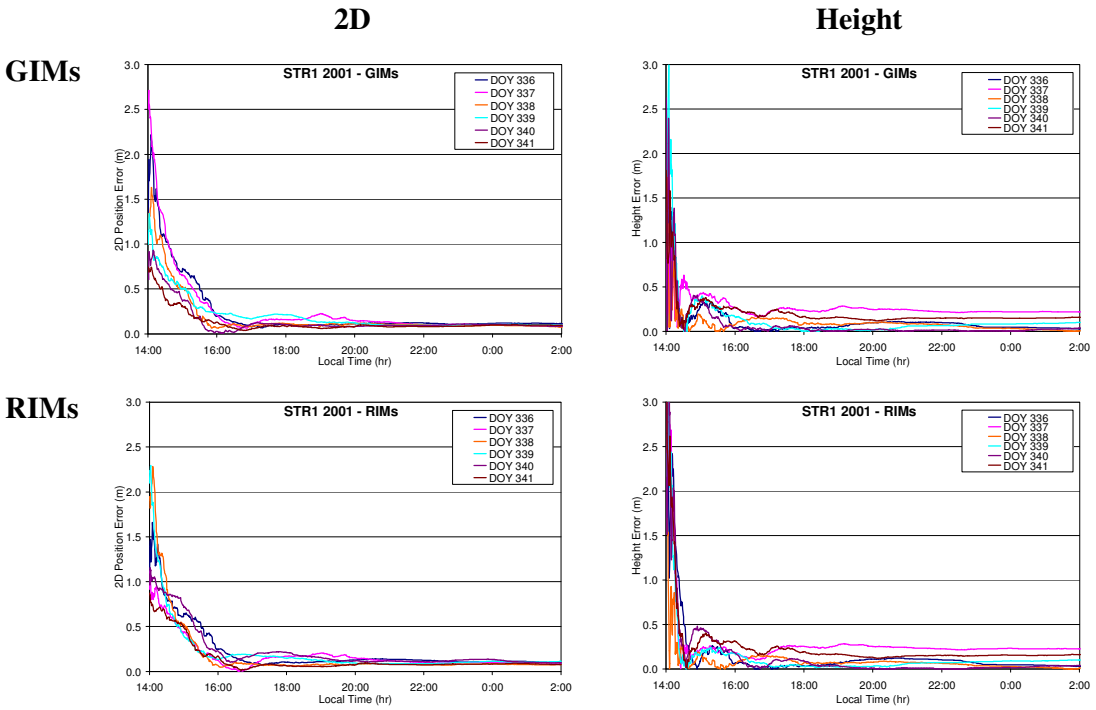

Figure 5.5: The positioning errors at STR1 from DOY 336 to 341 2001 using single frequency code and carrier phase observations.

DOY 183 to 188 2006 (solar minimum)

The combined mean and RMS values using data collected on DOY 183 to 188 2006 are presented in Table 5.6. As expected, the use of a Broadcast model will provide more accurate and precise point positioning solutions than those of no ionospheric corrections. However, it is worthwhile to point out that the combined mean and RMS values based on single frequency PPP with no ionospheric corrections applied during this period are well within 0.7m of the known values. This is attributed to the fact that the implemented single frequency PPP processing is based on the *code and quasi-phase* combination, which eliminates the ionospheric effects without the aid of an independent ionospheric error mitigation product or model.

Table 5.6: The statistical results for DARW, TOW2, ALIC, STR1 and HOB2 stations using single frequency code and carrier phase observations from DOY 183 to 188 2006 (solar minimum).

2006						
Methods	**Mean (m)**			**RMS (m)**		
	East	**North**	**Height**	**East**	**North**	**Height**
DARW						
1. No Ionospheric correction	0.12	0.06	0.00	0.24	0.10	0.62
2. Broadcast Model	0.00	0.09	0.16	0.13	0.15	0.32
3. IGS *Rapid* GIMs	-0.01	0.06	0.14	0.13	0.09	0.31
4. IGS *Final* GIMs	0.00	0.06	0.14	0.13	0.09	0.31
5. RIMs	0.00	0.07	0.13	0.13	0.10	0.28
6. Dual Frequency PPP	0.01	0.05	0.07	0.06	0.08	0.13
TOW2						
1. No Ionospheric correction	0.02	-0.19	-0.06	0.29	0.24	0.36
2. Broadcast Model	-0.14	-0.17	0.08	0.16	0.22	0.27
3. IGS *Rapid* GIMs	-0.13	-0.19	0.05	0.15	0.22	0.23
4. IGS *Final* GIMs	-0.13	-0.19	0.05	0.15	0.22	0.23
5. RIMs	-0.14	-0.19	0.04	0.17	0.22	0.24
6. Dual Frequency PPP	-0.13	-0.20	-0.01	0.15	0.21	0.12
ALIC						
1. No Ionospheric correction	0.15	0.05	0.15	0.26	0.11	0.53
2. Broadcast Model	0.01	0.10	0.33	0.12	0.16	0.52
3. IGS *Rapid* GIMs	0.02	0.09	0.31	0.11	0.14	0.49
4. IGS *Final* GIMs	0.02	0.08	0.31	0.11	0.14	0.49
5. RIMs	0.02	0.09	0.31	0.10	0.16	0.48
6. Dual Frequency PPP	0.00	0.07	0.25	0.08	0.08	0.29
STR1						
1. No Ionospheric correction	0.17	0.12	0.18	0.35	0.36	0.31
2. Broadcast Model	-0.02	0.10	0.17	0.09	0.16	0.21
3. IGS *Rapid* GIMs	-0.01	0.08	0.15	0.05	0.12	0.17
4. IGS *Final* GIMs	-0.01	0.08	0.15	0.06	0.11	0.17
5. RIMs	-0.02	0.08	0.15	0.07	0.11	0.18
6. Dual Frequency PPP	-0.02	0.08	0.11	0.07	0.11	0.13
HOB2						
1. No Ionospheric correction	0.13	0.10	0.18	0.16	0.27	0.41
2. Broadcast Model	0.02	0.09	0.22	0.13	0.15	0.44
3. IGS *Rapid* GIMs	0.03	0.07	0.18	0.10	0.12	0.38
4. IGS *Final* GIMs	0.03	0.07	0.18	0.10	0.12	0.39
5. RIMs	0.02	0.08	0.19	0.11	0.14	0.39
6. Dual Frequency PPP	-0.02	0.09	0.14	0.08	0.12	0.20

Additionally, the accuracy and precision of the estimated single frequency PPP solutions using the Broadcast model are quite similar (cm level) to that of the GIMs during the periods of solar minimum. The use of an ionospheric error mitigation method in single frequency PPP only helps to improve the accuracy of the initial code processing. This may explain the similarity in the performance between the GIMs and RIMs during the periods of low ionospheric activities. Once the float ambiguities on the phase observations stabilise, the single frequency PPP solutions will follow the more precise quasi-phase observations and the code observations will only have marginal influence on the overall solutions (Kouba and Hèroux, 2001). This is an interesting relationship because it provides an opportunity for real-

time single frequency PPP using the Broadcast model especially during ionospheric quiet days.

In order to illustrate the convergence behaviour of the single frequency PPP solutions during the solar minimum periods, the estimated point positioning errors obtained from DARW and STR1 are plotted as a function of observation time in Figures 5.6 and 5.7. Once again, it can be seen from these plots that both GIMs and RIMs have similar impacts on the single frequency PPP convergence time and the positioning accuracy. The Australia-wide RIMs did not enhance the positioning convergence time, nor did the GIMs. Nevertheless, it should be noted that, based on the statistical results provided, the RIMs could provide more precise and potentially more accurate point positioning solutions to users in the low latitude regions, especially during the periods of solar maximum.

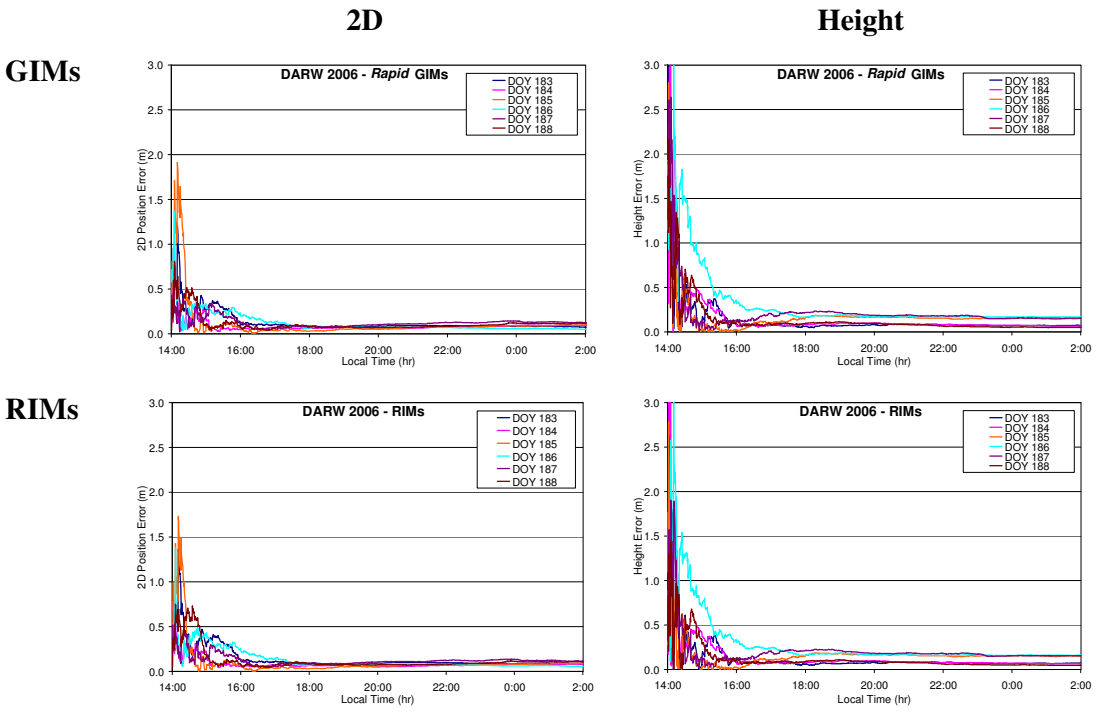

Figure 5.6: The positioning errors at DARW from DOY 183 to 188 2006 using single frequency code and carrier phase observations.

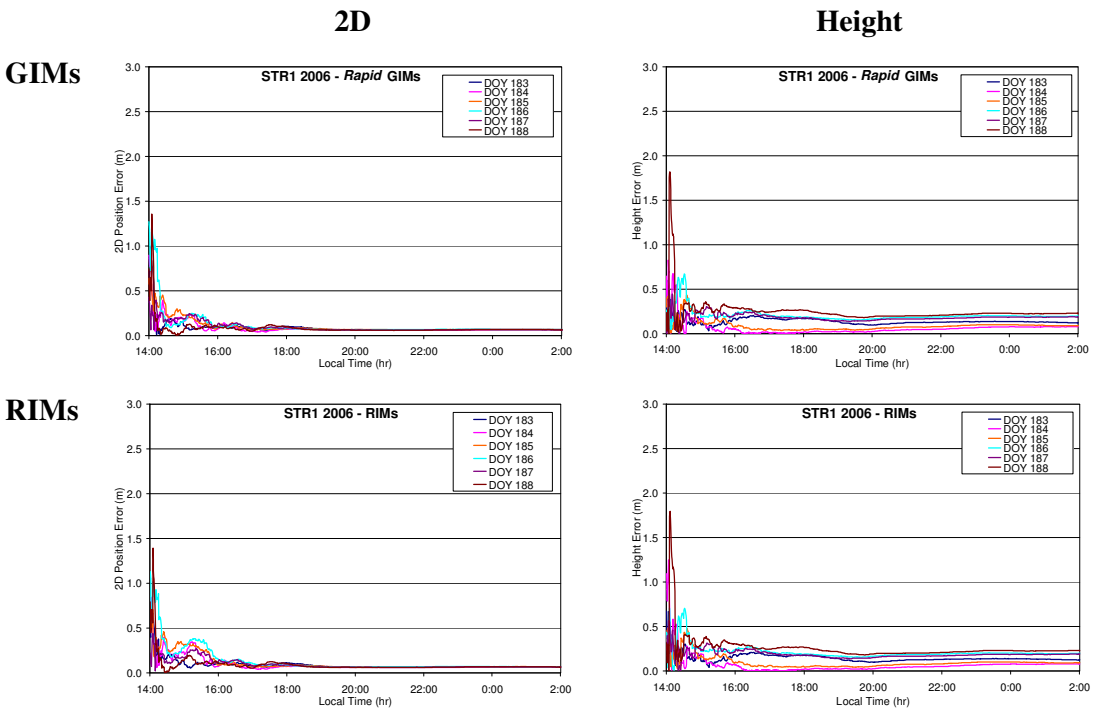

Figure 5.7: The positioning errors at STR1 from DOY 183 to 188 2006 using single frequency code and carrier phase observations.

As a summary, the RIMs are capable of providing better height estimation than the GIMs for GPS stations that are located in the low latitude regions. However, the level of improvement is more prominent in the classical single frequency code-only solutions and during the periods of solar maximum. For the horizontal component, the GIMs are able to provide more accurate point positioning estimations and there is no distinctive preference between the IGS *Rapid* and *Final* GIMs. In addition, the use of the higher spatial resolution RIMs appears to have minimal influence in speeding up the single frequency PPP convergence time. Therefore, it can be concluded that the use of the RIMs and GIMs in single frequency PPP provide comparable point positioning solutions.

The single frequency PPP solutions based on the GIMs and RIMs are slightly more accurate and precise than that of the Broadcast model. Generally, the GIMs and RIMs could better compensate for the ionospheric effects than the Broadcast model. However, during the absence of the more accurate ionospheric error mitigation products, the Broadcast model is recommended to be used in order to enhance the accuracy of the single frequency point positioning.

5.2.2 Case Study 2: High Temporal Resolution RIMs

The objective of the Case Study 2 is to examine the impacts of higher temporal resolution Australia-wide RIMs on single frequency point positioning. Daily 1-hour interval RIMs were created, in addition to the 2-hour interval RIMs, for DOY 336 to 341 2001 and DOY 183 to 188 2006. Identical software settings and products described in Case Study 1 were applied. The following section reports on the numerical results and statistical analyses undertaken in this study. Comparison between the positioning errors based on the 1-hour RIMs and the nominal 2-hour interval RIMs and GIMs from Case Study 2 will also be made.

5.2.2.1 Strategy 1: Single Frequency Code-Based Solutions

DOY 336 to 341 2001 (solar maximum)

Table 5.7 outlines the combined mean and RMS values for the classical code-based single frequency point positioning errors using 2-hour interval GIMs and RIMs, as well as 1-hour interval RIMs for the five ARGN stations tested. The numerical values in this table are based on data collected during the solar maximum periods, DOY 336 to 341 2001.

DOY 183 to 188 2006 (solar minimum)

Table 5.8 presents the combined mean and RMS values for the two 2-hour GIMs, RIMs and the 1-hour interval RIMs using single frequency code observations collected from DOY 183 to 188 2006.

Table 5.7: The statistical results of the point positioning errors based on single frequency code observations using two hour interval GIMs, RIMs and one hour interval RIMs for DOY 336 to 341 2001 (solar maximum).

2001						
Methods	**Mean (m)**			**RMS (m)**		
	East	**North**	**Height**	**East**	**North**	**Height**
DARW						
1. CODE GIMs	-0.58	1.36	0.61	0.83	1.70	2.32
2. RIMs	0.11	1.99	-1.25	0.50	2.08	1.66
3. RIMs (1hr)	-0.05	1.48	-0.53	0.46	1.57	1.25
TOW2						
1. CODE GIMs	0.35	-0.31	1.99	0.49	0.52	2.10
2. RIMs	0.31	0.25	0.98	0.57	0.75	1.15
3. RIMs (1hr)	0.38	0.44	0.53	0.65	0.66	0.86
ALIC						
1. CODE GIMs	-0.62	1.02	1.75	0.64	1.04	1.77
2. RIMs	-0.60	1.06	1.03	0.66	1.12	1.26
3. RIMs (1hr)	-0.82	0.65	0.37	0.84	0.75	1.76
STR1						
1. CODE GIMs	0.37	0.44	-0.09	0.41	0.58	0.72
2. RIMs	0.36	0.62	-0.71	0.42	0.64	1.11
3. RIMs (1hr)	0.38	0.50	-0.71	0.45	0.54	0.96
HOB2						
1. CODE GIMs	0.41	0.10	-0.20	0.43	0.29	0.71
2. RIMs	0.37	0.40	-0.83	0.40	0.52	1.08
3. RIMs (1hr)	0.44	0.30	-0.81	0.47	0.45	1.00

Table 5.8: The statistical results of the point positioning errors based on single frequency code observations using two hour interval GIMs, RIMs and one hour interval RIMs for DOY 183 to 188 2006 (solar minimum).

2006						
Methods	**Mean (m)**			**RMS (m)**		
	East	**North**	**Height**	**East**	**North**	**Height**
DARW						
1. IGS *Rapid* GIMs	0.08	0.09	1.71	0.19	0.18	1.72
2. RIMs	0.14	0.28	1.08	0.20	0.31	1.11
3. RIMs (1hr)	0.10	0.18	0.72	0.17	0.25	0.73
TOW2						
1. IGS *Rapid* GIMs	-0.05	0.18	1.21	0.10	0.19	1.22
2. RIMs	-0.11	0.48	0.57	0.15	0.49	0.60
3. RIMs (1hr)	-0.16	0.38	0.48	0.18	0.39	0.52
ALIC						
1. IGS *Rapid* GIMs	0.09	0.60	1.13	0.16	0.60	1.14
2. RIMs	0.07	0.84	0.84	0.17	0.84	0.87
3. RIMs (1hr)	0.10	0.81	0.42	0.18	0.81	0.45
STR1						
1. IGS *Rapid* GIMs	0.08	0.53	-0.04	0.10	0.54	0.15
2. RIMs	0.03	0.64	0.02	0.09	0.66	0.21
3. RIMs (1hr)	0.10	0.58	-0.03	0.12	0.59	0.21
HOB2						
1. IGS *Rapid* GIMs	0.11	0.37	-0.16	0.12	0.37	0.24
2. RIMs	0.11	0.59	0.05	0.14	0.59	0.28
3. RIMs (1hr)	0.08	0.49	-0.04	0.12	0.50	0.27

There are some similarities between the numerical results tabulated in Tables 5.7 and 5.8. The mean and RMS values for the height component using the 1-hour interval RIMs are the lowest at DARW, TOW2 and ALIC stations. This is true for both solar maximum and minimum periods. In comparison to the GIMs, a remarkable improvement (47%) in height estimation is achieved when higher temporal resolution RIMs were used. However, the horizontal component estimations do not seem to benefit from the higher temporal resolution ionospheric maps. The GIMs still provide the best point positioning solutions for the middle latitude stations. Nonetheless, the higher temporal resolution RIMs will generally provide better positioning solutions than the standard 2-hour sampling interval RIMs.

5.2.2.2 Strategy 2: Single Frequency Code and Quasi-Phase Solutions

DOY 336 to 341 2006 (solar maximum)

This section presents the statistical analysis based on single frequency PPP *code and quasi-phase* combination solutions using the 2-hour GIMs and RIMs, as well as the 1-hour interval RIMs. The combined mean and RMS values for data collected from DOY 336 to 341 2001 are tabulated in Table 5.9.

It can be inferred from this table that the level of improvement provided by the higher resolution RIMs to single frequency PPP solutions is not as significant as those using code-based processing. The positioning solutions at DARW station, which is located in the low latitude region, benefited the most from the high temporal resolution RIMs. In order to illustrate the convergence behaviour of the single frequency PPP solutions using the higher temporal resolution RIMs, the horizontal and height errors for DARW station are plotted in Figure 5.8. The 2-hour RIMs plots are also included for comparison purposes. From this figure, it is apparent that the positioning solutions based on the higher temporal RIMs converge quicker. Furthermore, the DOY 337 2001 positioning solutions using the 1-hour RIMs does not have the same trend as those of the 2-hour RIMs and the positioning errors are indeed smaller when the 1-hour RIMs was used.

Table 5.9: The statistical results of the point positioning errors based on single frequency code and carrier phase observations using two hours interval GIMs, RIMs and one hour interval RIMs for DOY 336 to 341 2001 (solar maximum).

2001						
Methods	**Mean (m)**			**RMS (m)**		
	East	**North**	**Height**	**East**	**North**	**Height**
DARW						
1. CODE GIMs	-0.17	0.24	-0.45	0.40	0.35	0.78
2. RIMs	0.06	0.31	-0.57	0.33	0.52	0.73
3. RIMs (1hr)	0.02	0.25	-0.48	0.25	0.39	0.62
TOW2						
1. CODE GIMs	0.05	0.09	0.01	0.21	0.15	0.28
2. RIMs	-0.01	0.11	-0.06	0.21	0.17	0.23
3. RIMs (1hr)	0.00	0.11	-0.07	0.22	0.17	0.23
ALIC						
1. CODE GIMs	-0.18	0.46	-0.33	0.32	0.50	0.58
2. RIMs	-0.31	0.24	-0.38	0.45	0.38	0.58
3. RIMs (1hr)	-0.39	0.20	-0.44	0.49	0.27	0.62
STR1						
1. CODE GIMs	0.03	0.14	0.05	0.19	0.22	0.23
2. RIMs	0.07	0.14	0.02	0.20	0.22	0.34
3. RIMs (1hr)	0.04	0.13	0.02	0.19	0.18	0.30
HOB2						
1. CODE GIMs	0.09	0.05	0.16	0.20	0.08	0.26
2. RIMs	0.13	0.08	0.14	0.23	0.17	0.34
3. RIMs (1hr)	0.18	0.09	0.07	0.25	0.13	0.38

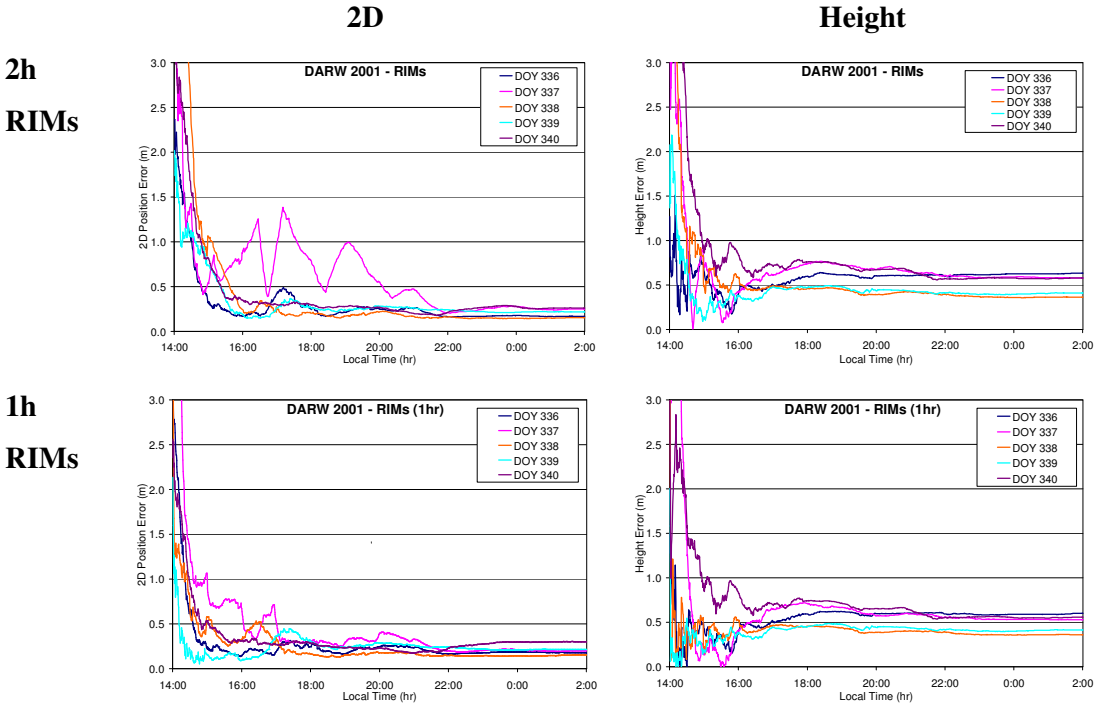

Figure 5.8: The positioning errors at DARW from DOY 336 to 341 2001 using single frequency code and carrier phase observations.

Figure 5.9 depicts the positioning errors at STR1 station using the 2-hour and 1-hour RIMs from DOY 336 to 341 2001. It can be seen from this figure that the initial portion of the positioning errors based on the higher temporal resolution RIMs are lower. This is because the high temporal resolution RIMs could better capture the characteristics of the ionosphere. However, once the phase ambiguities are stabilised, the quasi-phase observations will prevail and consequently the RIMs will have little impact on the overall solutions.

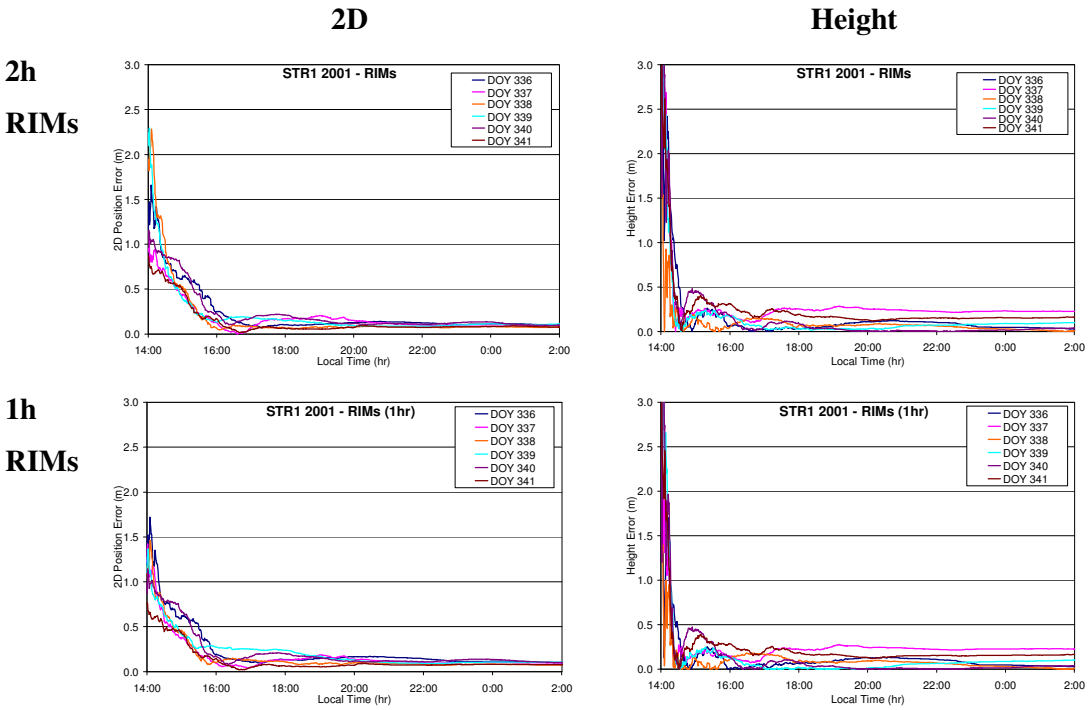

Figure 5.9: The positioning errors at STR1 from DOY 336 to 341 2001 using single frequency code and carrier phase observations.

DOY 183 to 188 2006 (solar minimum)

Table 5.10 presents the combined mean and RMS values based on data collected from DOY183 to 186 2006.

Table 5.10: The statistical results of the point positioning errors based on single frequency code and carrier phase observations using two hour interval GIMs, RIMs and one hour interval RIMs for DOY 183 to 188 2006 (solar minimum).

2006						
Methods	**Mean (m)**			**RMS (m)**		
	East	**North**	**Height**	**East**	**North**	**Height**
DARW						
1. IGS *Rapid* GIMs	-0.01	0.06	0.14	0.13	0.09	0.31
2. RIMs	0.00	0.07	0.13	0.13	0.10	0.28
3. RIMs (1hr)	0.00	0.06	0.11	0.13	0.09	0.28
TOW2						
1. IGS *Rapid* GIMs	-0.13	-0.19	0.05	0.15	0.22	0.23
2. RIMs	-0.14	-0.19	0.04	0.17	0.22	0.24
3. RIMs (1hr)	-0.14	-0.19	0.04	0.17	0.22	0.23
ALIC						
1. IGS *Rapid* GIMs	0.02	0.09	0.31	0.11	0.14	0.49
2. RIMs	0.02	0.09	0.31	0.10	0.16	0.48
3. RIMs (1hr)	0.02	0.09	0.30	0.11	0.15	0.47
STR1						
1. IGS *Rapid* GIMs	-0.01	0.08	0.15	0.05	0.12	0.17
2. RIMs	-0.02	0.08	0.15	0.07	0.11	0.18
3. RIMs (1hr)	-0.01	0.08	0.15	0.06	0.11	0.18
HOB2						
1. IGS *Rapid* GIMs	0.03	0.07	0.18	0.10	0.12	0.38
2. RIMs	0.02	0.08	0.19	0.11	0.14	0.39
3. RIMs (1hr)	0.01	0.08	0.19	0.11	0.14	0.39

It can be seen from Table 5.10 that the RIMs with a higher temporal resolution have similar impacts on the single frequency PPP solutions as with the standard 2-hour RIMs. In the middle latitude region, all PPP solutions computed using the 2-hour GIMs, RIMs and the 1-hour RIMs have comparable accuracy and precision.

Figures 5.10 and 5.11 show the positioning errors at DARW and STR1 stations respectively using different temporal resolution RIMs for DOY 183 to 188 2006. It appears that both the positioning solutions show a similar trend.

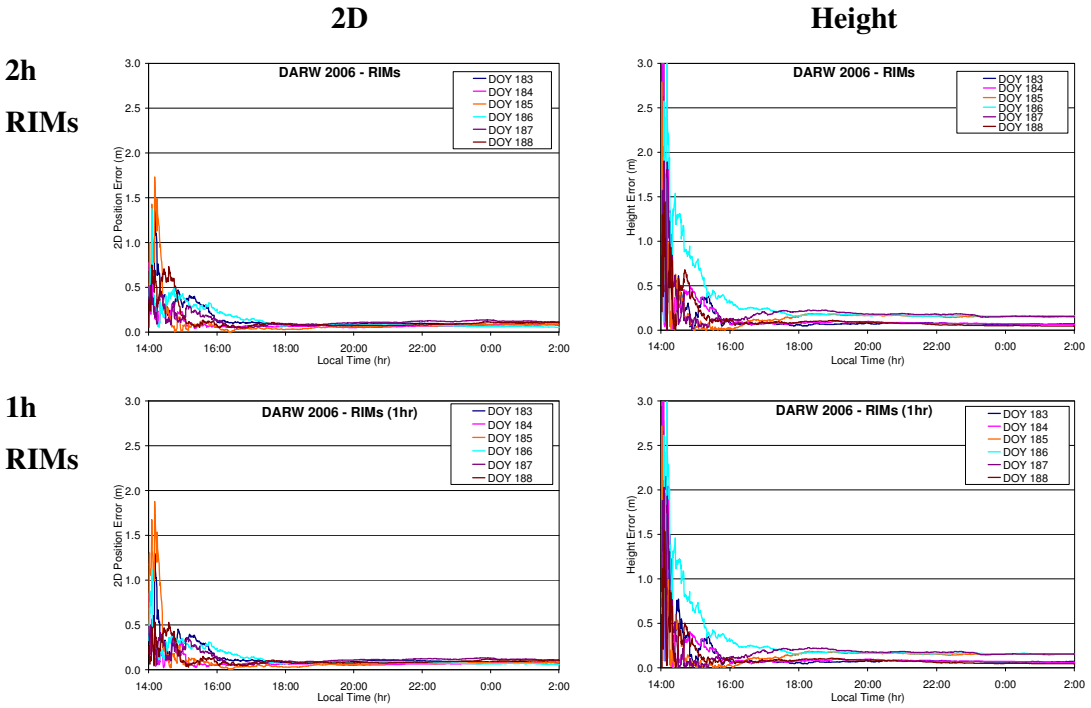

Figure 5.10: The positioning errors at DARW from DOY 183 to 188 2006 using single frequency code and carrier phase observations.

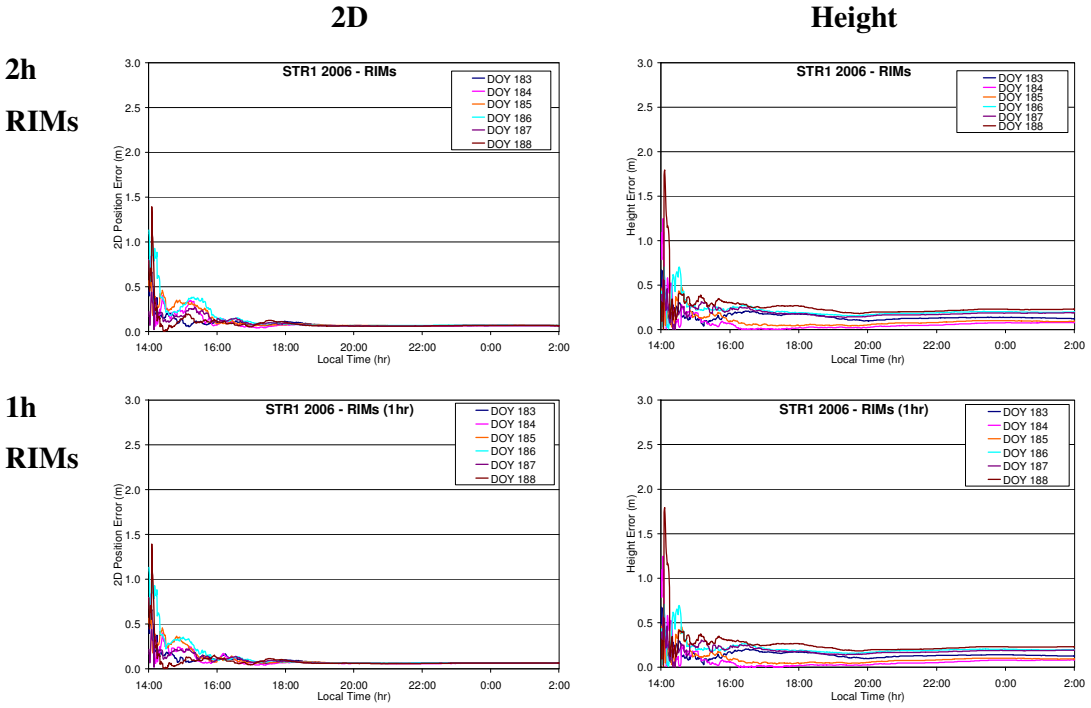

Figure 5.11: The positioning errors at STR1 from DOY 183 to 188 2006 using single frequency code and carrier phase observations.

Based on the results from Case Study 2, it can be concluded that the higher temporal resolution RIMs could help to improve the single frequency point positioning solutions, particularly in the low latitude region and during the ionospheric disturbed periods. However, it should be noted that the degree of improvement will not be significant in the implemented single frequency PPP algorithm. This is because single frequency PPP is based on the *code and quasi-phase* combination which eliminates the ionospheric delay. The higher temporal resolution RIMs will help improve the initial portion of the single frequency PPP solutions that relies heavily on the code observations. As the carrier phase ambiguities stabilise over time and the carrier phase observations are added to the solutions, the ionosphere-free quasi-phase observations will dominate the solutions. Consequently, the use of an external ionospheric error mitigation model or product will have minimal contribution.

5.3 Summary

This Chapter has detailed the two case studies undertaken in this research to examine the impacts of the ionospheric delay on single frequency point positioning and to evaluate effective measures that can be applied to reduce the adverse effects. The numerical results have also been analysed, presented and discussed. The first case study, Case Study 1, aimed to evaluate the performance of the Broadcast model, GIMs and Australia-wide RIMs using the single frequency code-based and single frequency *code and quasi-phase* combination. The effectiveness of these products was assessed as a function of solar maximum and minimum periods, as well as the geographical locations of the GPS receiver in the Australian region. Among the three ionospheric products tested, the GIMs and RIMs are the most effective products that can be used to minimise the ionospheric delay followed by the Broadcast model. In comparison with the GIMs, the Australia-wide RIMs have positive impacts on the height estimation using the classical single frequency code-based point positioning for stations located in the low latitude region and during the periods of solar maximum. However, due to the nature of the ionosphere-free quasi-phase observations in the single frequency PPP algorithm, the performance of the RIMs and GIMs is in fact quite similar, and the level of improvement provided by the RIMs on single frequency PPP estimated solutions is marginal. Additionally, it is also interesting to discover from this research that the single frequency PPP solutions using the Broadcast model is not substantially worse than that of the GIMs and RIMs. This is true for data collected in the middle latitude region and during the periods of solar minimum. This finding is encouraging as the broadcast ionospheric coefficients are transmitted by the GPS navigation message and are available to all GPS users in real-time.

The second case study, Case Study 2, aimed to assess the feasibility of applying higher temporal (1-hour) RIMs in single frequency point positioning. In this study, RIMs with an hour sampling interval were created and assessed in addition to the nominal 2-hour sampling interval GIMs and RIMs. It was discovered that the RIMs with higher temporal resolution could help improve the height estimations in single frequency code-based processing. However, only marginal improvement on the height component could be achieved when the single frequency PPP (*code and quasi-phase* combination) algorithm is used.

Based on the results compiled from both case studies, it can be concluded that the use of higher spatial and temporal ionospheric maps could help improve the accuracy of the code observations, typically in the low latitude region and during the periods of high solar activities. For single frequency PPP, only marginal improvement can be expected. The ionospheric products or models will only reduce the ionospheric biases on the code observations and the quality of the code observations is only evident in the initial part of single frequency PPP solutions. This is attributed to the nature of the single frequency PPP algorithm used. When the phase ambiguities stabilise, the solutions will follow the more precise ionosphere-free quasi-phase observations and the code measurements will have marginal impacts on the solutions. As a result of this, the ionospheric products like the GIMs, RIMs and Broadcast model will only have trivial influence in the overall point positioning solutions.

CHAPTER 6

Convergence Evaluation of Single Frequency PPP Solutions

6.1 Introduction

The preceding Chapter has discussed the impact of the ionospheric effects pertinent to the single frequency point positioning solutions during both the solar disturbed and benign periods. Ionospheric error mitigation methods like the Broadcast model, GIMs and Australia-wide RIMs were tested and their performances were assessed via the quality of the estimated positioning solutions. RIMs with different temporal resolutions were also assessed and the corresponding results were concisely presented. The magnitude of the error was evaluated in both classical single frequency code-only and single frequency PPP based on the *code and quasi-phase* combination.

The objective of this Chapter is to study the relationship between satellite clock corrections, observation sampling rate and tropospheric delay with single frequency PPP solutions convergence behaviour. The first part of this Chapter investigates the implications of using different IGS satellite clock corrections sampling intervals on the time of convergence. The second section, which is covered in Section 6.3, looks at the effects of different observation sampling rates on single frequency PPP convergence time. The third part examines the viability of either modelling the tropospheric delay using an empirical model or estimating the delay as part of the single frequency PPP solutions. The analysis of the results is carried out by evaluating the time required by the solutions to converge, and also the quality of the estimated positioning solutions.

6.2 Satellite Clock Corrections Sampling Intervals

Various researches have shown that the high-rate satellite clock corrections improves the time of convergence in dual frequency PPP solutions (Kouba and Hèroux, 2000, 2001; Abdel-salam, 2005; Waypoint Products Group, 2006). However, the contributions of utilising the high-rate satellite clock corrections to speed up the solutions convergence time in single frequency PPP are yet to be researched and validated. Therefore, the purpose of this study is to evaluate the effects of the clock corrections sampling intervals on single frequency PPP convergence behaviour. It aims to test whether the high-rate satellite clock corrections could improve the single frequency PPP convergence time.

6.2.1 CODE High-Rate Satellite Clocks

In this study, two satellite clock corrections files with different sampling intervals were used and compared. They were the IGS combined 5 minute satellite clock corrections and the 30 second (high-rate) satellite clock corrections from CODE. Data from STR1 stations with observations sampling interval of 30 seconds were collected from DOY 187 to 189 2006. Although observation data were collected using a dual frequency, geodetic quality GPS receiver, only single frequency observations were extracted and processed in this investigation.

Figure 6.1 shows the satellite clock corrections for satellite PRN02 on DOY 188 2006 from the IGS 5 minute and CODE 30 second clock corrections. It can be seen from this figure that the clock corrections from the IGS and CODE do not agree because the different IGS ACs generally refer to different reference clocks. As a result, the satellite clock corrections should always be used in conjunction with the precise satellite orbit corrections from the same AC to eliminate these biases. This is because the errors from the precise orbit and clock solutions from the same AC (or combined solutions) are tightly correlated, and thus, the errors tend to cancel out when the orbit and clock corrections from the same AC are used together (Colombo, 2007). In this instance, the IGS combined orbit product “igs13825.sp3’’ was used with the IGS combined satellite clock correction “igs13825.clk”; and the CODE orbit “cod13825.eph” was used with the CODE 30 second clock correction “cod13825.clk”.

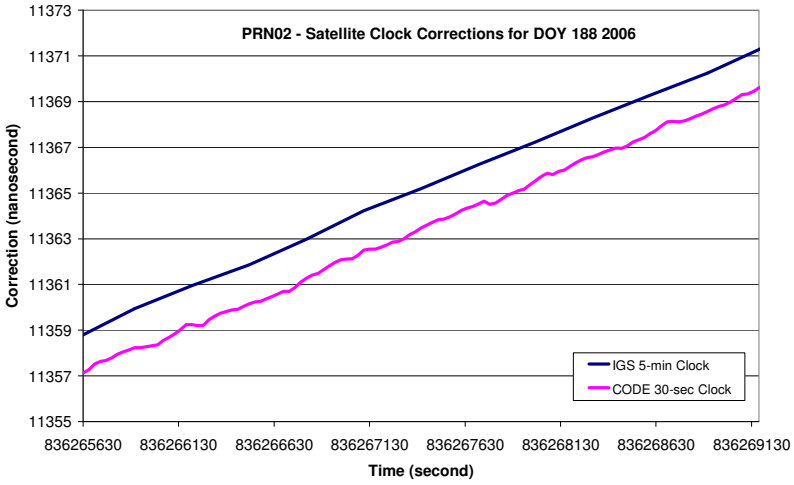

Figure 6.1: Satellite clock corrections from the IGS and CODE for satellite PRN02 on DOY 188 2006.

It is also interesting to point out that the 5 minute satellite clock corrections portrayed a more linearised pattern, while the CODE 30 second satellite clock corrections have a more tremulous characteristic. This was caused by the different interpolation methods used by CODE and also the research software. The high-rate 30 second CODE satellite clock corrections were produced based on an efficient phase-consistent interpolation of 5 minute clock results using phase time differences (Hugentobler, 2004; Hugentobler, 2005). Whereas, the CSRS-PPP software uses a simple linear interpolation method to "up-sample" the 5 minute satellite clock corrections.

The ionospheric delay affecting the single frequency positioning solutions was corrected using the IGS *Final* GIMs. *A priori* code and quasi-phase sigmas were set to 4m and 0.1m respectively. A 15˚ cut-off elevation angle was applied. Since no satellite clock bias sigmas were provided by the 30 second clock file, a constant sigma value of 3cm was assigned in this study unless noted otherwise.

The use of the satellite clock correction products was divided into three case scenarios in accordance with the satellite clock sampling intervals. Table 6.1 lists the three different scenarios. Case-1 and Case-2 used the IGS combined products. In Case-2, the 5 minute IGS satellite clock corrections were interpolated to a 30 second interval using a simple linear interpolation method. Case-3 takes advantage of the CODE satellite orbit and high-rate 30 second satellite clock corrections products.

Table 6.1: The three case studies that are formulated for the purpose of the study.

	Products	Accuracy	Sampling Interval	Clock Interpolation
Case-1	Orbit	< 5cm	15 min	No
	Clock	< 0.1 ns	5 min	
Case-2	Orbit	< 5cm	15 min	Yes
	Clock	< 0.1 ns	5 min	
Case-3	Orbit	< 5cm	15 min	No
	Clock	< 0.1 ns	30 sec	

Case-1

The convergence behaviour of the Case-1 positioning solutions is shown in Figures 6.2 and 6.3. Figure 6.2 shows the horizontal (2D) positioning errors in metres as a function of time, while Figure 6.3 illustrates the height errors. The different coloured lines represent the positioning errors for the different DOY datasets. Since Case-1 did not apply any clock interpolation process, the solutions can only be computed at 5 minute interval and hence the estimated positioning errors were plotted at every 5 minute.

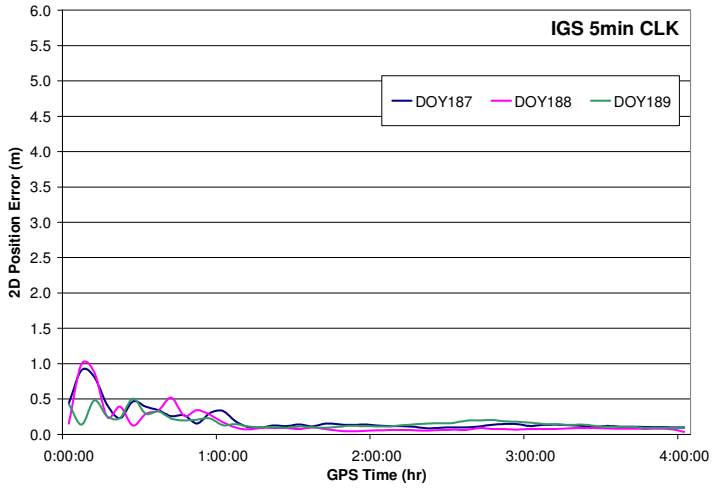

Figure 6.2: Case-1, Horizontal errors as a function of time using the IGS 5 minute satellite clock corrections without interpolation.

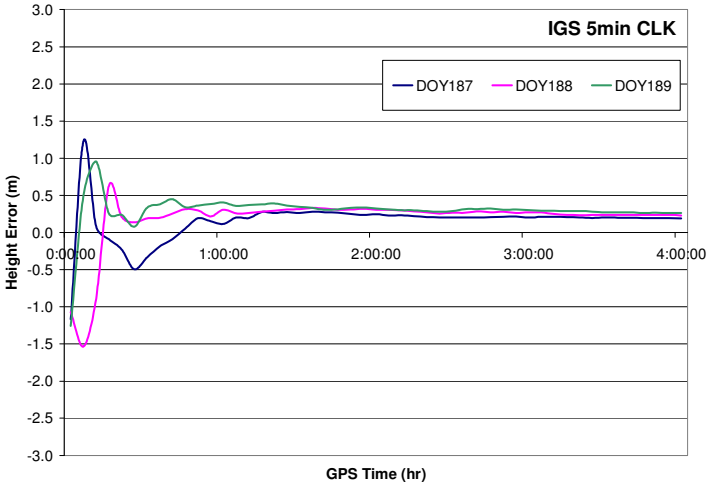

Figure 6.3: Case-1, Height errors as a function of time using the IGS 5 minute satellite clock corrections without interpolation.

Table 6.2 shows the time required by the horizontal and height components to converge to better than 50cm, 30cm and 20cm of the known position. The numerical values in the second, third and fourth columns (from the left) represent the number of epochs required for the solutions to converge for DOY 187, 188 and 189 2006, respectively. The fifth column lists the average epochs calculated from the number of epochs required for DOY 187, 188 and 189; and the last column shows the average observation time in hours and nearest minutes based upon the average epochs and observations sampling interval. The numbers shown in the table depict the absolute number of epochs, that is, no single epoch of positioning errors exceeded the threshold limits. When interpreting the numbers, one should understand that the number of epochs shown in the table are estimates of the convergence time. The positioning errors may fluctuate with small amplitude around the thresholds (Abdel-salam, 2005).

Table 6.2: Case-1, Convergence statistic using the IGS 5 minute satellite clock without interpolation.

	DOY 187	DOY 188	DOY 189	Average Epochs	Average Time (h:mm)
2D position <50cm	6	9	3	6	0:30
2D position <30cm	13	12	8	11	0:55
2D position <20cm	21	13	37	24	1:58
Height <50cm	6	4	3	4	0:22
Height <30cm	22	38	-	30	2:30
Height <20cm	-	-	-	-	-

Note: 1 epoch is equivalent to 5 minutes; dash line denotes no solutions fell under the threshold limit.

Case-2

Figures 6.4 and 6.5 illustrate the behaviour of the estimated positions as a function of time based on Case-2 processing scenario. In this case, the clock interpolation process was performed and the solutions were computed according to the observations interval, i.e. 30 second. The time required for Case-2 solutions to converge to better than 50cm and 20cm for both horizontal and height components is tabulated in Table 6.3.

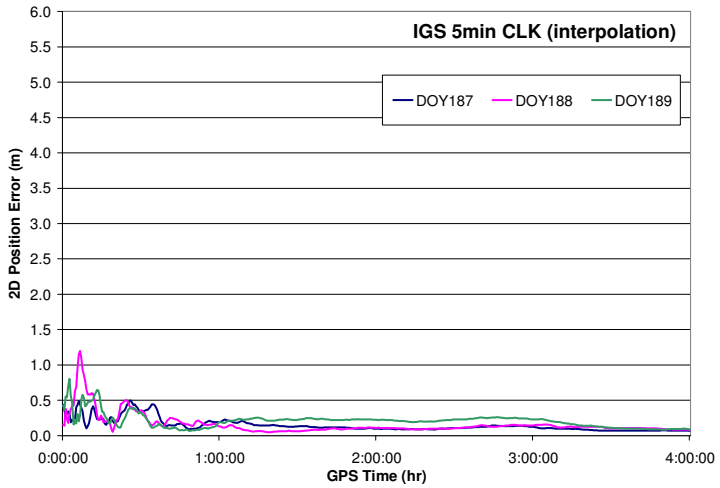

Figure 6.4: Case-2, Horizontal errors as a function of time using the IGS 5 minute satellite clock corrections with interpolation.

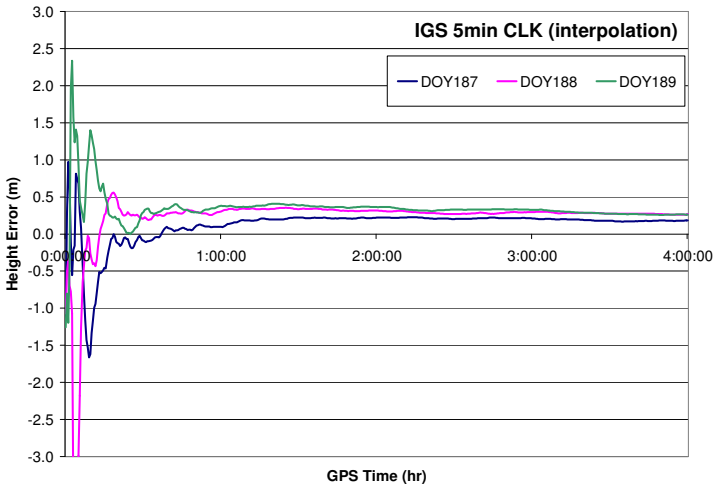

Figure 6.5: Case-2, Height errors as a function of time using the IGS 5 minute satellite clock corrections with interpolation.

Table 6.3: Case-2, Convergence statistic using the IGS 5 minute satellite clock with interpolation

	DOY 187	DOY 188	DOY 189	Average Epochs	Average Time (h:mm)
2D position <50cm	54	51	29	45	0:22
2D position <30cm	75	84	348	169	1:25
2D position <20cm	146	372	394	304	2:32
Height <50cm	32	41	32	35	0:18
Height <30cm	33	-	-	33	0:17
Height <20cm	-	-	-	-	-

Note: 1 epoch is equivalent to 30 seconds; Dash line denotes no solutions fell under the threshold limit.

Case-3

Figures 6.6 and 6.7 depict the convergence behaviour of the horizontal and height components when using the high-rate 30 second satellite clock corrections from CODE. The convergence behaviour is summarised in Table 6.4.

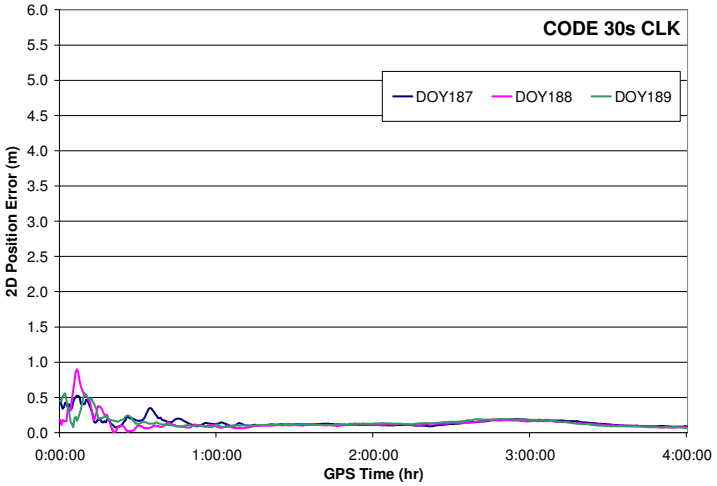

Figure 6.6: Case-3, Horizontal errors as a function of time using the CODE 30 second satellite clock corrections.

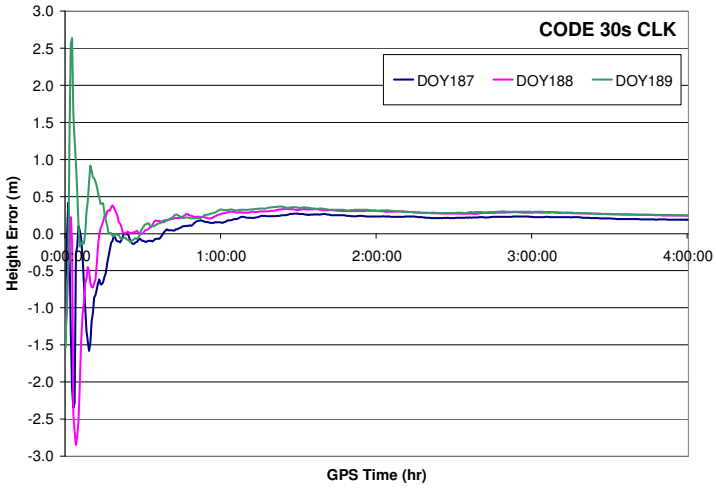

Figure 6.7: Case-3, Height errors as a function of time using the CODE 30 second satellite clock corrections.

Table 6.4: Case-3, Convergence statistic using the CODE 30 second satellite clock.

	DOY 187	DOY 188	DOY 189	Average Epochs	Average Time (h:mm)
2D position <50cm	22	23	25	23	0:12
2D position <30cm	74	36	29	46	0:23
2D position <20cm	399	389	384	391	3:15
Height <50cm	32	24	27	28	0:14
Height <30cm	214	456	472	381	3:10
Height <20cm	-	-	-	-	-

Note: 1 epoch is equivalent to 30 seconds; Dash line denotes no solutions fell under the threshold limit.

Based on the numerical values tabulated in Tables 6.2, 6.3 and 6.4, it can be concluded that high-rate satellite clock corrections may potentially improve the initial solution convergence time. In this study, an average time of 12 minutes is required for the horizontal positions and 14 minutes for the vertical positions to be better than half a metre of the known positions, when the high-rate clock corrections were used. This is followed by the 5 minute clock corrections with interpolation (Case-2) and without interpolation (Case-3). This shows that less time (i.e. less epochs) is required for both the horizontal and height components to converge to be within half a metre of the known values. However, this trend can not be validated using the higher threshold limits, i.e. <30cm and <20cm.

6.2.2 IGS Combined High-Rate Satellite Clocks

Starting from GPS week 1406 (17th December 2006), the IGS has since provided the combined high-rate 30 second satellite clock corrections, in parallel with the standard 5 minute satellite clock file. The combined high-rate satellite clock corrections are based on the submissions from four of the IGS ACs. However, it must be noted that the IGS high-rate satellite clock corrections have not been declared as an official IGS product at the time of writing this thesis.

Figures 6.8 and 6.9 compare the satellite clock corrections for satellites PRN17 and PRN08 respectively, using the IGS 5 minute and the IGS high-rate 30 second clock corrections. The blue line represents the IGS 5 minute clock corrections while the pink line denotes the IGS 30 second corrections. Once again, the 5 minute clock corrections plotted in

these figures are based on a simple linear interpolation, and thus, have a more linearised pattern.

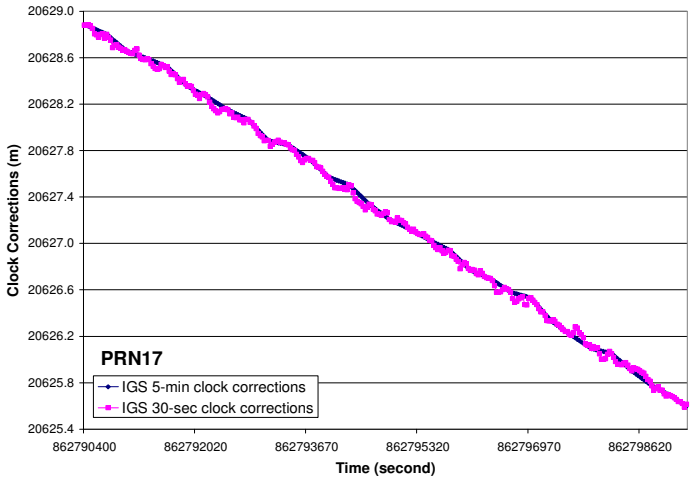

Figure 6.8: Satellite clock corrections in metres for PRN17 on DOY 130 2007 using the 5 minute clock corrections and 30 second clock corrections.

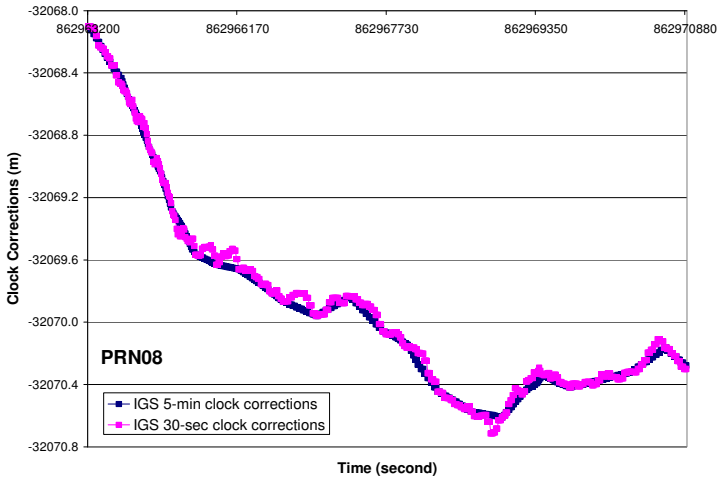

Figure 6.9: Satellite clock corrections in metres for PRN08 on DOY 132 2007 using the 5 minute clock corrections and 30 second clock corrections.

The following study was conducted to evaluate the feasibility of using the new IGS combined high-rate satellite clock corrections (Case-3). The results from Case-3 processing were compared to those of the standard 5 minute satellite clock corrections with interpolation (Case-2). Note that Case-1 processing strategy was not undertaken as it was not necessary (i.e. analysis of the 5 minute satellite clock corrections without interpolation has been done in Section 6.2.1). The same GPS station (STR1), software and processing scheme described in the previous section were implemented, except for the clock bias sigma settings and the date of the data used in this experiment. The satellite clock bias sigma settings used in this study originated from the satellite clock files and the dates of the collected data were DOY 130 to 132 2007.

Case-2

Figures 6.10 and 6.11 show the convergence behaviour of the single frequency PPP solutions using the IGS 5 minute satellite clock corrections. Figure 6.10 depicts the horizontal positioning errors, while Figure 6.11 depicts the height errors as a function of time. The convergence behaviour is numerically summarised and given in Table 6.5.

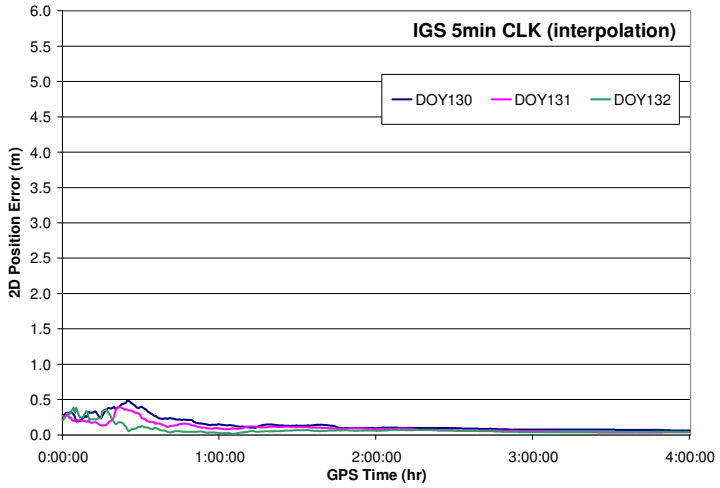

Figure 6.10: Case-2, Horizontal errors as a function of time using the IGS 5 minute satellite clock corrections with interpolation.

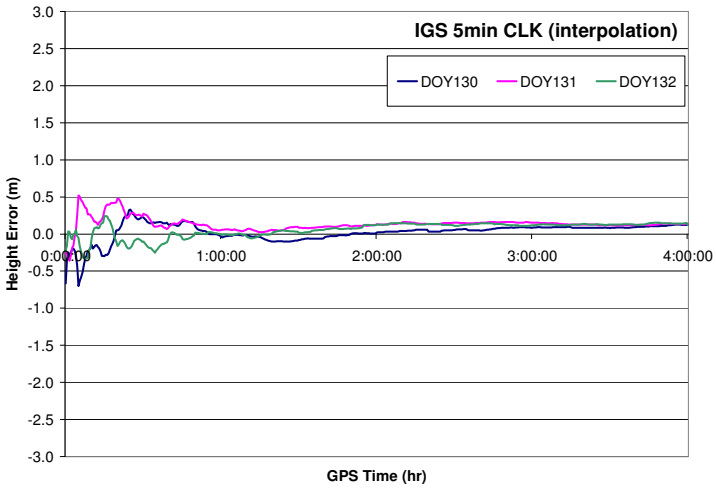

Figure 6.11: Case-2, Height errors as a function of time using the IGS 5 minute satellite clock corrections with interpolation.

Table 6.5: Case-2, Convergence statistic using the IGS 5 minute satellite clock with interpolation.

	DOY 130	DOY 131	DOY 132	Average Epochs	Average Time (h:mm)
2D position <50cm	53	1	1	18	0:09
2D position <30cm	73	60	37	57	0:28
2D position <20cm	120	97	47	88	0:44
Height <50cm	14	42	1	19	0:10
Height <30cm	34	64	70	56	0:28
Height <20cm	99	367	459	308	2:34

Note: 1 epoch is equivalent to 30 seconds; Dash line denotes no solutions fell under the threshold limit.

Case-3

Figures 6.12 to 6.13 illustrate the single frequency PPP horizontal and height component convergence behaviour using the IGS combined high-rate 30 second satellite clock corrections. Table 6.6 summarises these figures.

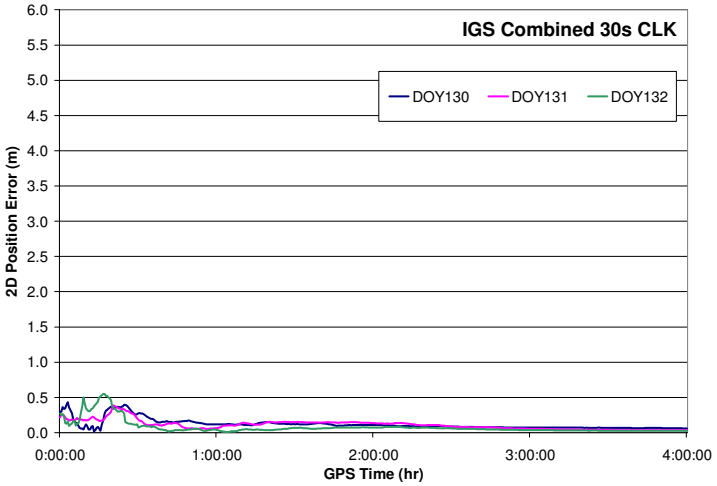

Figure 6.12: Case-3, Horizontal errors as a function of time using the IGS 30 second satellite clock corrections.

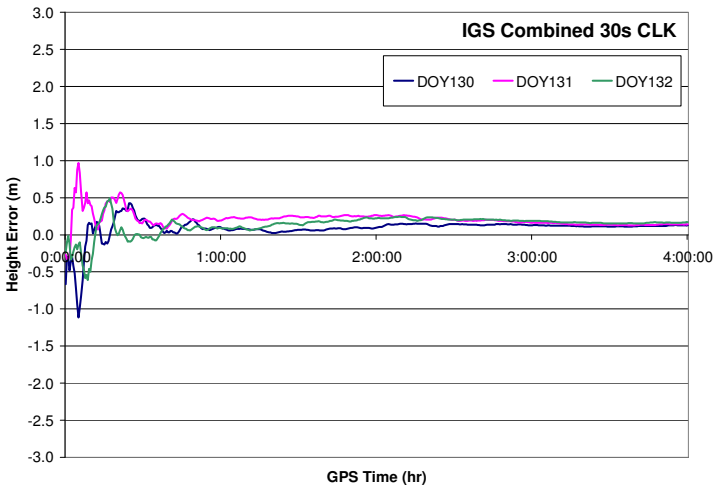

Figure 6.13: Case-3, Height errors as a function of time using the IGS 30 second satellite clock corrections.

Table 6.6: Case-3, Convergence statistic using the IGS 30 second satellite clock.

	DOY 130	DOY 131	DOY 132	Average Epochs	Average Time (h:mm)
2D position <50cm	1	1	40	14	0:07
2D position <30cm	65	58	50	58	0:29
2D position <20cm	103	183	50	112	0:56
Height <50cm	14	46	35	32	0:16
Height <30cm	55	267	37	120	1:00
Height <20cm	279	383	-	331	2:46

Note: 1 epoch is equivalent to 30 seconds; Dash line denotes no solutions fell under the threshold limit.

The amplitude of the positioning errors is generally smaller when 5 minute satellite clock corrections with interpolation were applied. On closer inspection on the statistical values in Tables 6.5 and 6.6, it appears that the IGS high-rate 30 second clock corrections did not enhance the single frequency PPP solutions convergence time.

Discussion

In theory, the satellite clock corrections based on interpolation is not as accurate as those of the orbits. This is not a consequence of the interpolation method used, but instead, it is attributed to the high irregularities in the clock corrections which are quite unpredictable. Therefore, the objective of this study is to investigate whether satellite clock corrections with high sampling interval could help improve the time of convergence of the single frequency PPP solutions.

By examining the figures and numerical results presented in this section, it is not apparent that the satellite clock corrections sampling interval have a significant impact on single frequency PPP convergence behaviour. The clock corrections with higher sampling intervals may assist with the convergence time if the definition of convergence is set at half a metre level of the known values. However, for a longer observation session, the solutions did not seem to benefit from the high-rate satellite clock corrections.

According to Abdel-salam (2005), satellite clock corrections at a higher sampling interval, e.g. 30 second, is recommended for dual frequency PPP as it will speed up the

solution convergence time. However, the results from this study based on single frequency PPP processing show otherwise. The use of high-rate satellite clock corrections could not improve the convergence of the single frequency PPP solutions. One of the main reasons for this may be due to the nature of the single frequency PPP mathematical model. The model behind single frequency PPP is different to that of dual frequency. As explained in Chapter 2, dual frequency PPP takes advantage of the traditional ionosphere-free linear combination to remove 99% of the ionospheric error. Assuming that all the other major sources of errors have been considered in dual frequency PPP solutions, any improvement in the system or products, e.g. high-rate clock corrections with no (or minimal) interpolation error, will have positive impacts on the overall solutions.

Single frequency PPP processing, on the other hand, is dependent on the code observations, in particular the initial portion of the estimated solutions. Consequently, single frequency PPP solutions may contain residual ionospheric errors. The magnitude of the residuals may vary from decimetre level to a few metres, depending on the receiver location, time of observation as well as the solar cycle. These residuals are, in most cases, larger than the clock interpolation error. For instance, the average difference between the interpolated 5 minute and 30 second clock corrections for PRN08 is about 2cm (see Figure 6.9). Therefore, any small improvement in the satellite clock correction interpolation method may not be obvious in the single frequency PPP solutions. Other reasons which may possibly explain this phenomenon are the GPS satellite geometry, irregularities of the clock corrections in some of the satellites observed at STR1, and the quality of the observations (Abdel-salam, 2005).

In conclusion, the findings from this study could not justify that the satellite clock corrections with high sampling intervals will have significant impacts on single frequency PPP solutions. The high-rate satellite clock corrections could be used if they are available as they may help to enhance the initial solutions convergence behaviour. The downside of the high-rate clock corrections is that it could not guarantee positive improvement over a long observation period. Therefore, the IGS precise 5 minute satellite clock corrections file with a simple in-built interpolation method is adequate for single frequency PPP static processing.

6.3 Effects of Different Observation Rates

The second part of this Chapter studies the relationship between GPS observation sampling interval with the solutions convergence time and also the quality of the positioning solutions. 1 second observation interval data sets were collected at STR1 station for 4 hours each day, starting from DOY 184 to 189 2006. The 1 second data sets were "down-sampled" to yield 15 second and 30 second data sampling intervals. Similar processing schemes as per Section 6.2 were applied and the IGS *Final* precise orbit, clock corrections, and GIMs were used in this study.

Figures 6.14 and 6.15 plot the horizontal and height positioning errors respectively from post-processing 1, 15 and 30 second GPS observation data. Note the different y-axis scales used in the horizontal and height graphs. From these figures, one can see that the trend of the positioning errors using the different sampling intervals is generally equivalent, but the magnitude is different on certain days.

The time required for the horizontal and height components to converge to better than 50cm, 30cm and 20cm is provided in Table 6.7. In this table, the number of epochs required by the solutions to converge is presented, and an average number is also calculated and provided. The numerical values presented in the last column are the average time in hours and minutes required by the solutions to converge. These values were calculated based upon the average epoch and the observation rate.

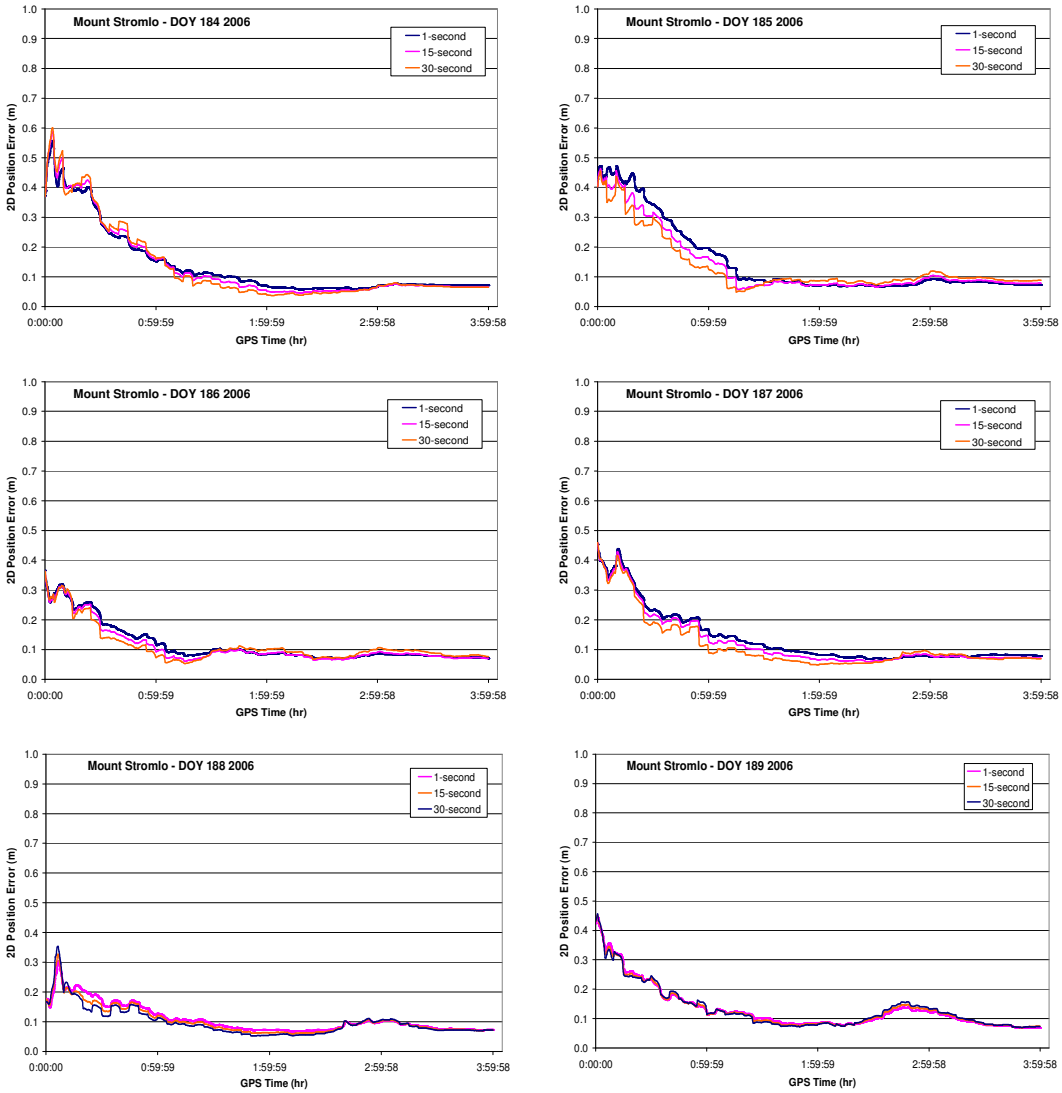

Figure 6.14: 2D position errors for six days using 1, 15 and 30 second observation sampling intervals.

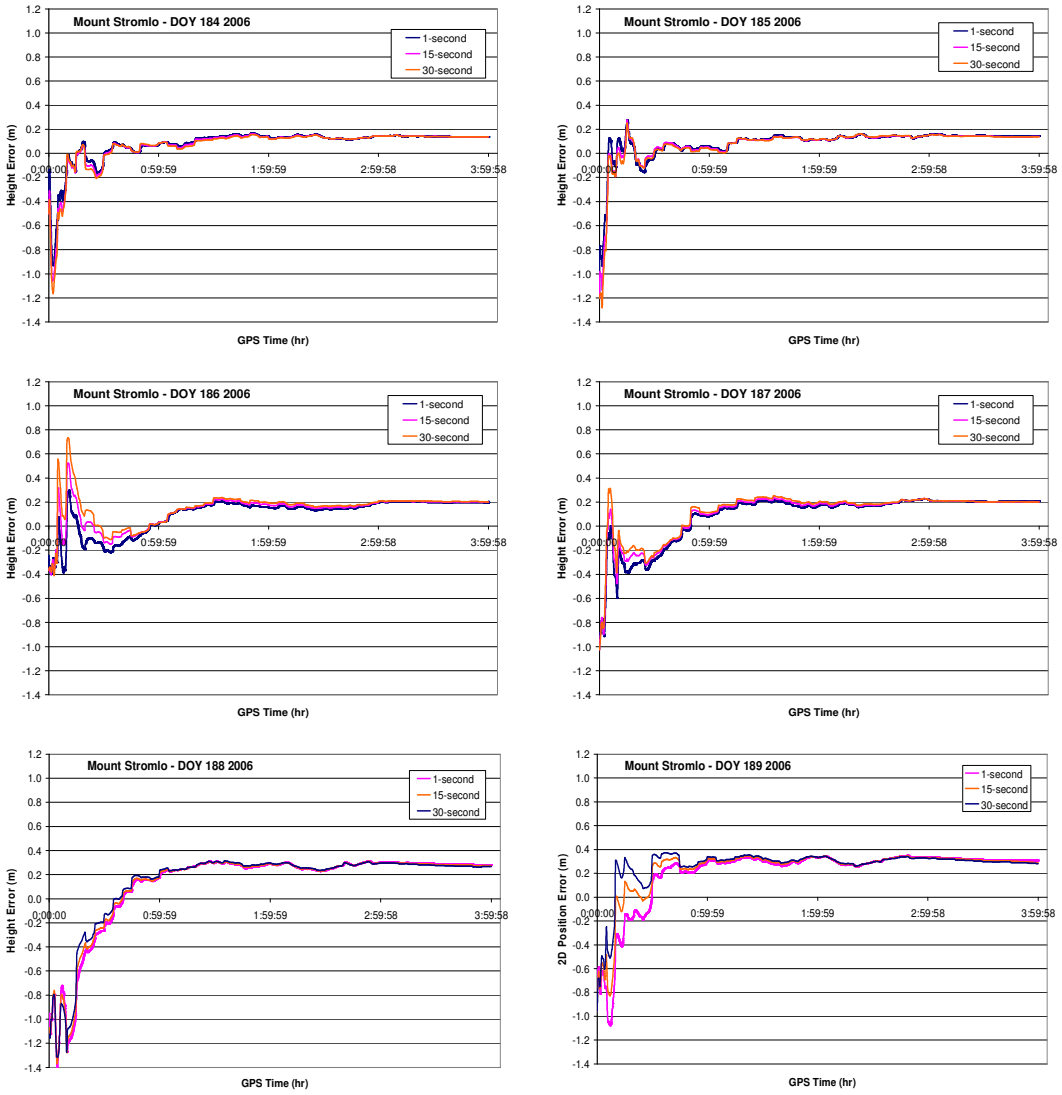

Figure 6.15: Height errors for six days using 1, 15 and 30 second observation sampling intervals.

Table 6.7: Convergence statistics based on the different observation rates.

1-second Observation Rate								
DOY	**184**	**185**	**186**	**187**	**188**	**189**	**Average Epochs**	**Average Time (h:mm)**
2D position <50cm	599	661	1	12	1	1	213	0:04
2D position <30cm	2036	2693	1503	1515	499	1301	1591	0:27
2D position <20cm	3901	4194	3291	3971	3072	3172	3600	1:00
Height <50cm	601	680	559	1189	1391	859	880	0:15
Height <30cm	2226	2696	2115	2536	-	-	2393	0:40
Height <20cm	-	-	-	-	-	-	-	-
15-second Observation Rate								
2D position <50cm	40	42	1	1	1	5	15	0:04
2D position <30cm	180	160	99	100	34	80	109	0:27
2D position <20cm	260	250	160	221	200	223	219	0:55
Height <50cm	40	42	49	66	75	40	52	0:13
Height <30cm	180	161	99	147	-	-	147	0:37
Height <20cm	-	-	-	-	-	-	-	-
30-second Observation Rate								
2D position <50cm	20	4	1	1	1	3	5	0:03
2D position <30cm	90	70	30	49	18	31	48	0:24
2D position <20cm	130	100	60	110	100	340	140	1:10
Height <50cm	50	10	30	20	32	18	27	0:13
Height <30cm	90	70	192	200	-	-	138	1:09
Height <20cm	-	-	-	-	-	-	-	-

Note: Dash line denotes no solutions fell under the threshold limit.

It appears that GPS observations with a higher sampling interval would not necessarily enhance the single frequency PPP solutions convergence time. In fact, the different sampling rates do not exhibit superiority from one to the other in terms of improving the solutions convergence time. In order to further analyse the relationship between observation rate and the positioning errors, the statistical properties of the positioning errors were calculated. Table 6.8 lists the mean and RMS values for the east, north and height errors. The results tabulated in the table show that the horizontal and height positioning accuracy and precision are not greatly affected by the observation sampling rate. The maximum difference is only 3cm in the height component.

Table 6.8: The mean and RMS of the east, north and height errors at STR1 station based on 1, 15 and 30 seconds data sampling intervals.

Average statistics		**Sampling Interval**		
		1s	**15s**	**30s**
East	**Mean (m)**	0.07	0.05	0.04
	RMS (m)	0.13	0.12	0.12
North	**Mean (m)**	0.06	0.06	0.06
	RMS (m)	0.09	0.08	0.08
Height	**Mean (m)**	0.11	0.13	0.14
	RMS (m)	0.24	0.24	0.25

Discussion

It is a common misconception that the positioning accuracy as well as the time of convergence could be improved when GPS observations are recorded at a high sampling rate. The results from this study, however, show that there is no connection between higher observation sampling interval and the quality of single frequency PPP static solutions. GPS observations with higher sampling rate do not necessarily guarantee shorter convergence time and more accurate positioning solutions. This is because observations with higher sampling interval only act as correlated or redundancy measurements and may, in some instances, improve (slightly) the precision of the solutions (Beran *et al.*, 2007). However, it should be noted that observations with higher sampling intervals do not add much strength to the solutions. This is also the case in high accuracy relative GPS positioning. The implemented single frequency PPP filter takes advantage of the system knowledge from previous epoch estimates and also the between-epoch satellite geometry change. Hence, the changes between

epochs play an imperative role in the single frequency PPP processing. In static single frequency PPP processing, high-rate observation data would not help to improve the quality of the positioning estimates as the changes in satellite geometry are minimal between two subsequent epochs.

In summary, there appears to be no relationship between observations sampling interval with single frequency PPP static performance. Observations with a higher sampling rate would not improve the performance of the solutions, but instead, act as redundancies in the solutions. GPS Observation data recorded at 30 second sampling interval is sufficient for single frequency PPP static applications.

6.4 Should Tropospheric Delay be Modelled or Estimated?

In this study, the relationship between the tropospheric delay and single frequency PPP convergence behaviour was investigated. Two questions were raised in this study:-

1. Should the tropospheric delay be modelled using an empirical model or estimated as part of the PPP solutions?
2. What are the implications of using surface meteorological observations as initial parameters to model the troposphere?

Four case scenarios were formulated and their descriptions were presented in Table 6.9. Case-1 used an empirical model to model the tropospheric ZPD. In this instance, the Hopfield model was applied and the Niell mapping function was used to map the ZPD to a slant delay. The selection of Hopfield model and Niell mapping function was based on the merits of several recommendations, and the ability of the Niell mapping function to perform optimally in low and high elevation angles, as well as its independence from meteorological parameters (Niell, 1996; Mendes and Langley, 2000; Leick, 2004). In the Case-2 strategy, the tropospheric delay was estimated as part of the single frequency PPP solutions. Details on the tropospheric delay estimation process in a PPP solution have been presented in Chapter 3. It is important to note that only the wet component of the tropospheric delay was estimated as an unknown parameter with the receiver position, receiver clock offset and ambiguity terms. The nature of the Case-3 and Case-4 strategy was similar to that of Case-1 and Case-2 respectively. The only difference between them was the settings of the initial surface parameters. Case-1 and Case-2 utilised the software default surface parameters while Case-3 and Case-4 applied the observed surface meteorological parameters at the beginning of the data processing.

Table 6.9: Description of the case scenarios.

	Tropospheric Delay	**Surface Parameters**
Case-1	Empirical model	Default
Case-2	Estimation	Default
Case-3	Empirical model	Meteorological
Case-4	Estimation	Meteorological

30 second GPS observation data from TOW2 station from DOY 182 to 189 2006 were used in this study. Surface meteorological measurements were downloaded from the IGS website (IGS, 2008). The required initial parameters were the surface temperature, pressure and humidity. The default surface parameters, on the other hand, were adjusted based on the receiver height. The IGS *Final* precise satellite orbit, clock corrections, and GIMs were utilised. Similar processing settings applied in the study described in Section 6.2 were used.

One of the characteristics of GPS positioning is the correlation between the tropospheric error and the estimated height (see Figure 6.16) (Mendes and Langley, 1998; Vollath *et al.*, 2003). Therefore, the height errors were the main focus in this study as the horizontal component will not be greatly affected by the tropospheric delay.

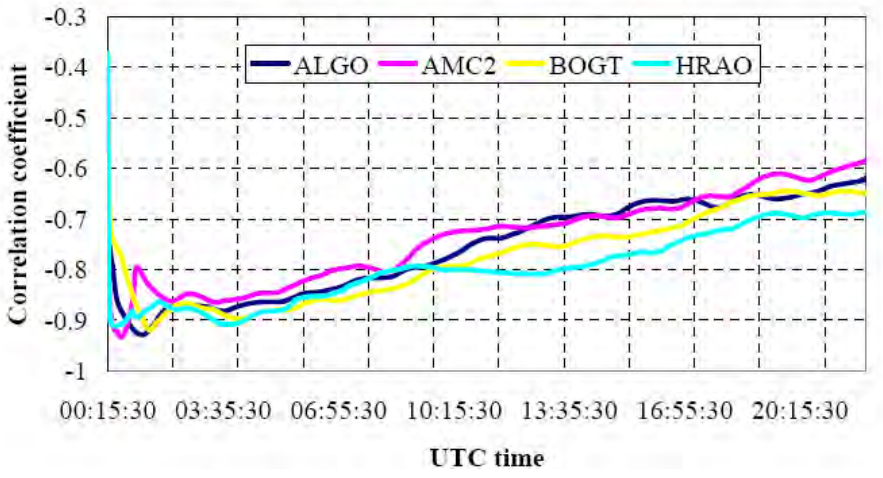

Figure 6.16: The correlation between tropospheric delay and height for the four IGS stations, ALGO, AMC2, BOGT and HRAO (Abdel-salam, 2005).

Figure 6.17 depicts the convergence behaviour of the single frequency PPP height solutions based on Case-1 (Modelled), Case-2 (Estimated), Case-3 (Modelled (met)) and Case-4 (Estimated (met)) processing scenarios.

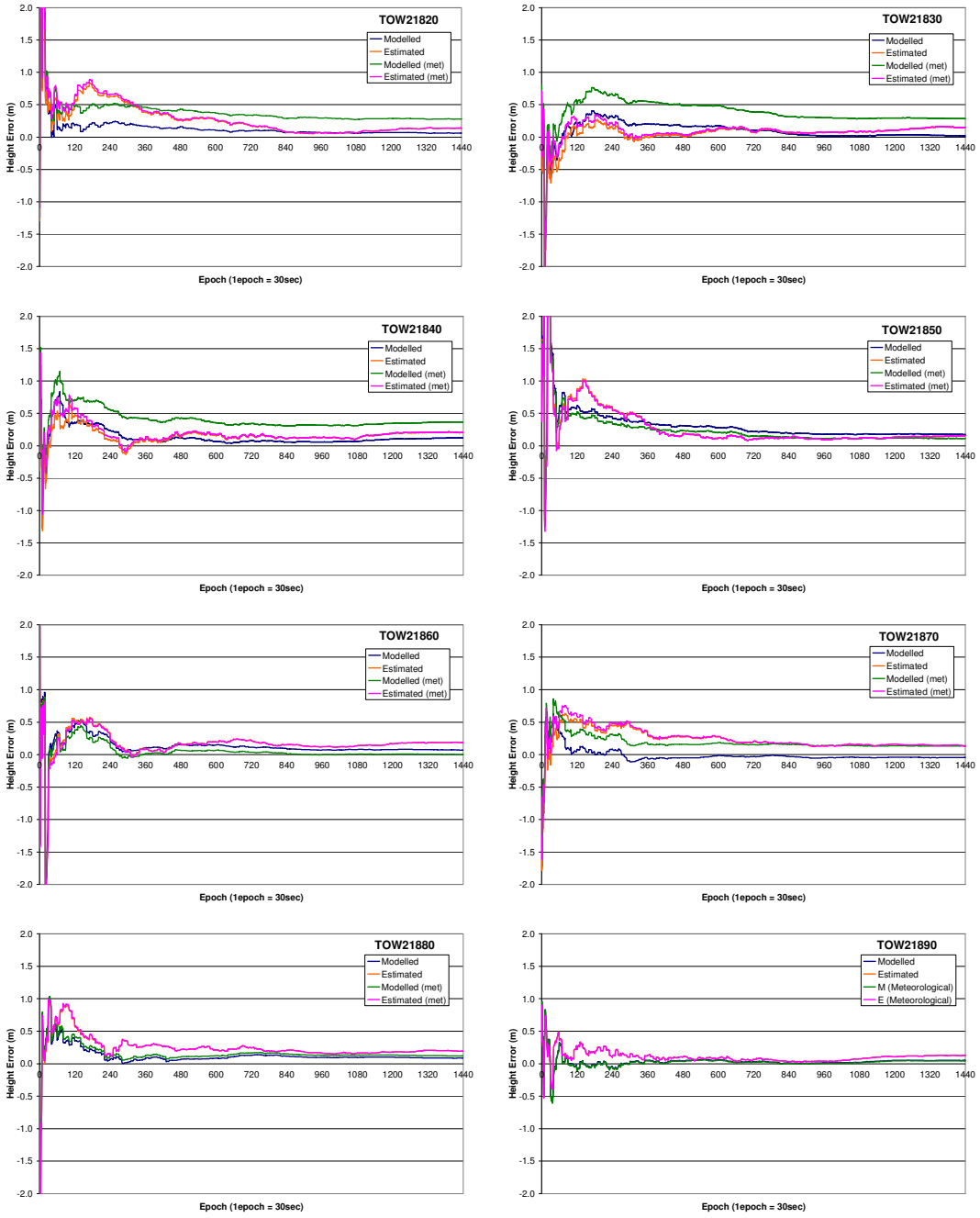

Figure 6.17: The height errors plotted against the number of epochs, for TOW2 from DOY 182 to 189 2006.

The x-axis in Figure 6.17 represents the number of epochs, whereby 1 epoch is equivalent to 30 second. 12 hour GPS observation data were post-processed; hence there were a total of 1440 epochs. The y-axis represents the height errors in metres for DOY 182 to 189 data sets. From this figure, it can be seen that the height errors based on Case-2 and Case-4 strategies were quite equivalent. However, the errors from Case-1 and Case-3 strategies were quite different. Case-1 provided more accurate height estimations than Case-3 processing strategy.

Table 6.10 summarises the convergence behaviour of the height solutions. Once again, the calculation of the convergence epoch or time was performed in such a way that no single epoch of height error exceeded the defined thresholds, i.e. 50cm, 30cm and 20cm. The last column presents the average number of epochs required for the height error to converge within the threshold limits. The average epochs were calculated based on the solutions from the DOY 182 to 189 2006. Readers should note that the figures in the table only act as an estimation because the positioning errors may fluctuate with a small amplitude around the threshold limits.

Table 6.10: Convergence behaviour: the number of epochs required for the height component to converge to better than 50cm, 30cm and 20cm.

Case-1: Modelled										
DOY	**182**	**183**	**184**	**185**	**186**	**187**	**188**	**189**	**Avg**	**Avg Time (h:mm)**
Height <50cm	57	35	86	239	157	51	80	40	93	0:47
Height <30cm	60	280	231	681	240	80	150	69	224	1:52
Height <20cm	490	627	279	-	610	80	220	70	339	2:50
Case-2: Estimated										
Height <50cm	340	58	130	339	210	300	147	60	198	1:39
Height <30cm	610	193	200	390	240	620	729	220	400	3:20
Height <20cm	780	1401	-	-	-	1306	-	279	942	7:51
Case-3: Modelled (meteorological observations)										
Height <50cm	370	629	280	180	30	80	119	40	216	1:48
Height <30cm	-	-	-	400	208	272	190	69	228	1:54
Height <20cm	-	-	-	767	240	900	846	70	565	4:43
Case-4: Estimated (meteorological observations)										
Height <50cm	340	32	159	335	208	300	175	60	201	1:41
Height <30cm	630	220	214	390	240	621	729	220	408	3:28
Height <20cm	785	-	-	-	-	1412	-	307	835	6:58

Note: Dash line denotes no solutions fell under the threshold limit; Avg is an acronym of average.

The number of epochs required for the solutions to converge within the thresholds is the lowest for Case-1 strategy. When comparing Case-1 with Case-2, it appears that the convergence time was improved by an average of about 53% when the tropospheric delay was modelled instead of using default surface meteorological measurements. 46 minutes were required in Case-1 for the height positioning errors to be within half a metre of the known value; while Case-2 required 1 hour and 39 minutes. As a result, it can be concluded that the modelling of the tropospheric delay using an empirical model in single frequency PPP could ensure quicker solutions convergence. In contrast, the results from Case-3 and Case-4 strategies are worse than those of Case-1 and Case-2. Therefore, the surface meteorological measurements are not essential for single frequency PPP processing. In some instances, it may even prolong the convergence process.

In order to validate the accuracy and precision of the solutions from the Case-1, Case-2, Case-3 and Case-4 processing strategies, the average mean and RMS values for each positioning components were computed based on all the estimated solutions from the eight DOY data sets. The results are presented in Table 6.11. It is evident from these numerical results that the different tropospheric delay mitigation strategies do not play an important role in affecting the quality of the estimated horizontal positions. Figure 6.18 shows an example of the horizontal positioning errors using different tropospheric delay mitigation strategies. From Table 6.11, it can be seen that the height error for Case-1 has the lowest mean and RMS values, while Case-4 has the highest values. This indicates that among all the case scenarios tested, the highest positioning accuracy and precision is achieved in Case-1, that is, when the tropospheric error is modelled using default surface parameters.

Table 6.11: The average mean and RMS values for the east, north and height components in the four cases.

		Case-1	Case-2	Case-3	Case-4
East	**Mean (m)**	0.01	0.00	0.00	0.00
	RMS (m)	0.10	0.10	0.10	0.10
North	**Mean (m)**	0.02	0.02	0.02	0.01
	RMS (m)	0.07	0.07	0.07	0.07
Height	**Mean (m)**	0.12	0.19	0.19	0.20
	RMS (m)	0.22	0.28	0.28	0.29

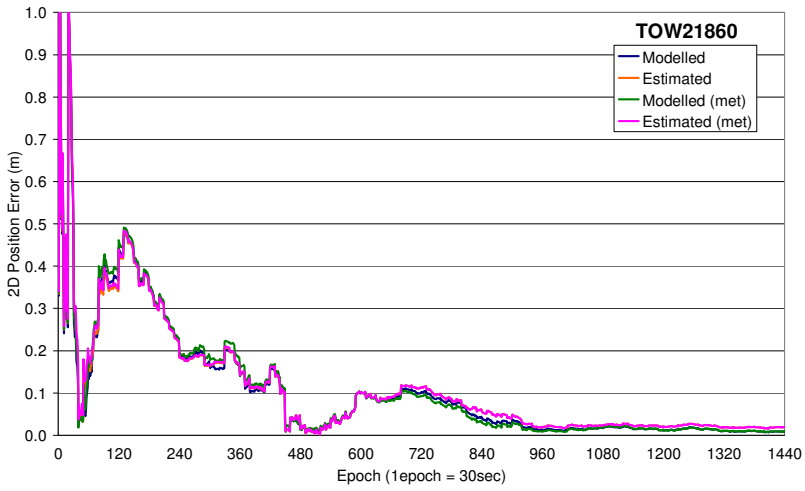

Figure 6.18: Horizontal errors for TOW2 on DOY186 using different tropospheric delay mitigation strategies.

Discussion

The quality of the horizontal positions and convergence time are not influenced by the tropospheric delay mitigation strategies. The height estimation is, however, prone to the effects of the troposphere. The following conclusions may be drawn:

- **The convergence behaviour** – The wet part of the tropospheric delay is difficult to model due to the unpredictable and complex nature of the troposphere. Hence, this delay should be treated as an unknown parameter in the PPP solutions estimation process for centimetre positioning applications, i.e. dual frequency PPP (Gao and Shen, 2002). It was discovered from this study that modelling the tropospheric delay in single frequency PPP, instead of estimation, can provide an average of 53% improvement in convergence time. The single frequency PPP mathematical model is different from those of dual frequency PPP. Unlike dual frequency PPP, the solutions based on single frequency PPP may contain larger residual errors, which are mainly caused by the ionospheric delay. As a result, the single frequency PPP approach could only provide decimetre to metre level point positioning accuracy. The estimation of an additional tropospheric parameter in the solution may also add strain to the data processing process, which may then affect the solutions convergence time. Therefore, the tropospheric delay is recommended to be modelled (instead of estimated) in single frequency PPP using an empirical model.
- **Accuracy and precision** – Based on the numerical results presented in Table 6.11, the mean and RMS values from Case-1 (modelling) are 0.12m and 0.22m, respectively. On the other hand, Case-2 (estimation) has higher mean and RMS values, i.e. 0.19m and 0.28m, respectively. These values indicate that modelling the tropospheric delay instead of estimation will help improve the height accuracy and precision.
- **Default surface meteorological parameters** – The preceding discussion focussed on either modelling or estimating the tropospheric delay using default surface meteorological parameters. In this research, it is also of interest to understand the implications of applying observed surface meteorological parameters on single frequency PPP solutions. Graphical and numerical comparisons have been presented. It appears that the solutions based on the default surface parameters are more accurate, precise and have a quicker convergence. The use of surface meteorological parameters may not necessarily guarantee better positioning quality. This is because meteorological parameters observed on the surface of the Earth are not always good indicators of the atmospheric conditions a few kilometres above (Brunner and Tregoning, 1994; Roberts and Rizos, 2001). This finding is encouraging as single

frequency PPP users do not need to worry about deploying meteorological sensors during a survey to achieve better positioning results and quicker convergence.

6.5 Summary

This Chapter has described the three case studies undertaken to understand the relationships between the satellite clock corrections rate, observation interval and tropospheric delay in terms of the quality of the single frequency PPP solutions and also the convergence behaviour. The first test compared the 5 minute satellite clock corrections with the high-rate 30 second clock corrections. The results of this test indicated that the 5 minute satellite clock corrections file with interpolation is adequate for single frequency PPP static processing. It was discovered that high-rate satellite clock corrections will not significantly enhance the solutions convergence time. In some instances, they may even prolong the convergence time.

The second study was carried out to investigate the effects of observation sampling intervals on single frequency PPP convergence behaviour and the quality of the estimated positioning solutions. It was found that GPS observations with higher sampling intervals would not enhance the solutions convergence time, but instead, act as redundancies in the solutions.

The third part of the study assessed the feasibility of using two different tropospheric delay mitigation strategies in improving the quality and convergence time of estimated single frequency PPP solutions. The effects of using either the default or observed surface meteorological measurements as initial parameters were also analysed. The results showed that the recommended method to correct for the tropospheric delay is to model the error using an empirical model, in parallel with the software default meteorological parameters. Estimating the tropospheric delay as part of the solutions would not only add strain to the solutions convergence behaviour, but also degrade the accuracy and precision of the positioning solutions. Therefore, it is recommended for single frequency PPP users to model the tropospheric delay using an empirical model with default surface meteorological parameters.

The use of various satellite orbit and clock corrections products from the IGS and their influence on the quality of the estimated single frequency PPP solutions will be the focus of the next Chapter.

CHAPTER 7

IGS Satellite Orbit and Clock Corrections: From Post-Mission to Real-Time Point Positioning

7.1 Introduction

In recent times, there has been an increased interest in obtaining accurate satellite ephemerides with short latency and frequent updates in order to support real-time and near-real-time GPS applications. Members of the IGS have been discussing for several years the creation of a real-time component (i.e. infrastructure and processes) for the IGS to support an increasing demand for real-time products and corrections. The IGS RTWG was established to govern and address issues pertaining to the development of the IGS real-time infrastructure and processes (IGS Real-Time Working Group, 2007).

It has been revealed, in the preceding studies, that single frequency PPP is able to provide 0.1m to 0.9m level point positioning accuracy in a post-processing mode. In many instances, point positioning accuracy of better than 0.5m could be achieved by taking advantage of the precise IGS *Final* and *Rapid* products. This finding is impressive considering that GPS data from one single frequency receiver is required for processing. The next objective of this research is to explore and address the potential benefits of using the IGS *Ultra-Rapid*, in particular the predicted orbit and clock corrections for real-time single frequency PPP. This forms the underlying foundation of Chapter 7.

The IGS has been producing *Ultra-Rapid* products for near real-time and real-time applications since November 2000. The products include satellite orbits, clocks, and ERPs. The *Ultra-Rapid* ephemerides have a window of 48 hours and consist of two parts, i.e. the first part contains the observed data, and the second part contains the predicted data (see

Sections 3.2.2.3 and 3.2.2.4). The timely availability of these real-time products has created new opportunities for GPS users and applications.

This Chapter aims to assess the feasibility of applying the IGS *Ultra-Rapid* products for real-time and near real-time single frequency PPP static applications. A simulation of a real-time and near real-time PPP scenario will be undertaken and the position estimates will be compared with those of the precise products. A performance evaluation of various IGS precise satellite orbit and clock correction products in a single frequency PPP static mode will also be performed.

7.2 Evaluation of the Satellite Orbit and Clock Corrections

At present, no work has been undertaken to assess the quality of the estimated positioning solutions using the IGS *Ultra-Rapid* correction products in the PPP approach. It was decided, as part of this research, to analyse and evaluate the viability of utilising different satellite orbit and clock corrections products on the estimated single frequency PPP results. It is believed that the findings will be of practical benefits as the correction products are freely accessible over the Internet to the public.

This section will cover an in-depth discussion of the investigation. This study has two objectives:

1. to explore the strengths and possibilities of using the IGS *Ultra-Rapid* satellite orbits and clocks for real-time and near real-time single frequency PPP static applications, and
2. to evaluate the feasibility of using the various IGS satellite orbits and clocks besides the *Ultra-Rapid* products in single frequency PPP by examining the accuracy and precision of the estimated point positioning.

The relevant satellite orbit and clock corrections are the broadcast satellite corrections, the IGS *Ultra-Rapid (Predicted Half)*, *Ultra-Rapid (Estimated Half)*, *Rapid*, and *Final* orbit and clock corrections. The performance of each product was assessed based on the accuracy of the estimated point positioning solutions with respect to the station known coordinates, which were treated as “true” coordinates. Raw GPS data collected at five ARGN stations located in different latitudinal zones across the Australian continent were used. They were DARW, TOW2, ALIC, STR1 and HOB2 stations (see Figure 5.7 for their locations).

A total of twelve daily GPS data sets were downloaded from the years 2004 to 2007. Table 7.1 outlines the dates (DOY) of the selected data sets. All data sets used in this study were windowed into 6 hours observation sessions, starting from 00:00 GPS time (i.e. 00:00 to 06:00 GPS time). The sampling interval of the data was 30 second.

Table 7.1: The DOY of the data sets that were used in the study.

Year	DOY
2004	357, 358, 359
2005	355, 356, 358
2006	187, 188, 189
2007	130, 131, 132

The Broadcast and IGS products for each DOY were downloaded from the SOPAC and IGS websites, respectively (IGS, 2008; SOPAC, 2008). There are two important points regarding the Broadcast and IGS *Ultra-Rapid (Predicted Half)* correction products that are worth addressing. As no broadcast navigation message files were stored at DARW, TOW2, ALIC, STR1 and HOB2 stations, the SOPAC "auto" navigation files were used as a replacement (SOPAC, 2008). A description of the "auto" navigation files has been given in Chapter 5. For the IGS *Ultra-Rapid (Predicted Half)* corrections, users should note that the *Ultra-Rapid* products have a latency of 3 hours. As a result, the orbit and clock corrections within 3 hours to 9 hours in the predicted part of the *Ultra-Rapid* files are most relevant for real-time point positioning. Therefore, the appropriate portion of the predictions was extracted for the use of this study.

The Broadcast model with the ionospheric coefficients contained in the broadcast navigation message was used in all of the data processing (in this study) to mitigate the effects of the ionosphere. This is to maintain consistency in the data processing. The Broadcast model was used because the ionospheric coefficients are available in real-time to all GPS users. The tropospheric zenith path delay was corrected using the Hopfield model with default atmospheric parameters, and the tropospheric ZPD was mapped to the slant delay by using the Niell mapping function (Hopfield, 1969; Niell, 1996). In addition to the single frequency PPP solutions, the estimated point positions based on the classical single frequency code-only point positioning technique using the broadcast corrections are also presented. This method of point positioning is essentially the same as the SPS. The rationale behind this is to provide readers with a point of reference of the achievable point positioning accuracy using single

frequency PPP technique in relation to the classical single frequency code-based point positioning.

7.3 Numerical Analysis and Discussion

Due to the quantity of data being processed, a series of line graphs and statistical data illustrating the accuracy and precision of the estimated positions for all the stations evaluated in this study are attached in Appendix C. These graphs depict the time series of the east, north and height errors for each station and day using different satellite orbit and clock corrections. The positioning results were categorised as follows:

i) Single frequency code-based processing using the Broadcast orbits, clock corrections, and Broadcast ionospheric model.
ii) Single frequency PPP processing using the Broadcast orbits, clock corrections, and Broadcast ionospheric model.
iii) Single frequency PPP processing using the IGS *Ultra-Rapid (Predicted Half)* orbits, clock corrections, and Broadcast ionospheric model.
iv) Single frequency PPP processing using the IGS *Ultra-Rapid (Estimated Half)* orbits, clock corrections, and Broadcast ionospheric model.
v) Single frequency PPP processing using the IGS *Rapid* orbits, clock corrections, and Broadcast ionospheric model.
vi) Single frequency PPP processing using the IGS *Final* orbits, clock corrections, and Broadcast ionospheric model.

In addition to the line graphs, the mean and RMS values for each station were computed and are also presented in Appendix C.

In order to aid the interpretation of the results, the positioning errors for DARW, TOW1, ALIC, STR1 and HOB2 stations for all of the twelve DOY datasets are computed as averages, and presented here in Figures 7.1, 7.2, 7.3, 7.4 and 7.5, respectively. The different coloured lines symbolise different satellite orbit and clock corrections used in the data processing. The left graphs depict the 2D horizontal errors as a function of time; while the graphs on the right plot the absolute value of the height errors (i.e. positive only). The horizontal positioning errors were calculated using Equation (5.1).

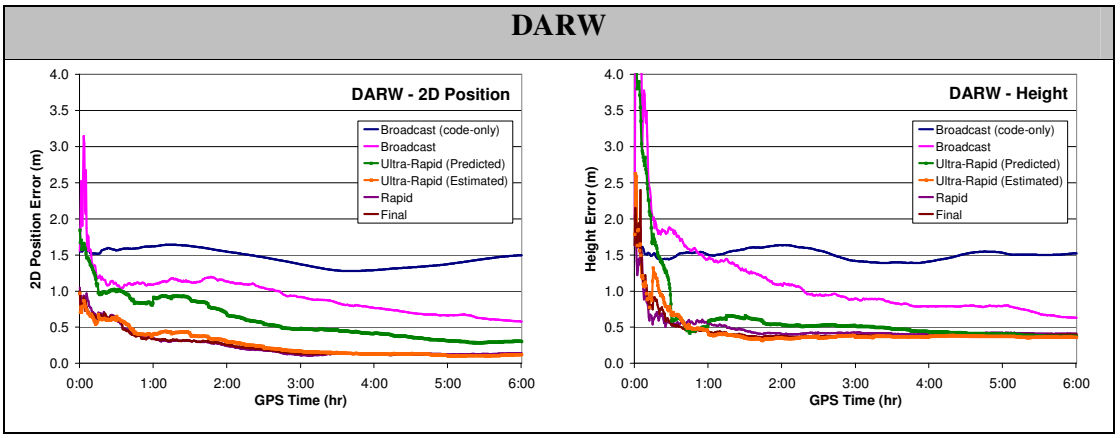

Figure 7.1: Point positioning results at DARW station using different satellite orbit and clock correction products. Time series of the 2D positioning errors on the left, and the height errors on the right.

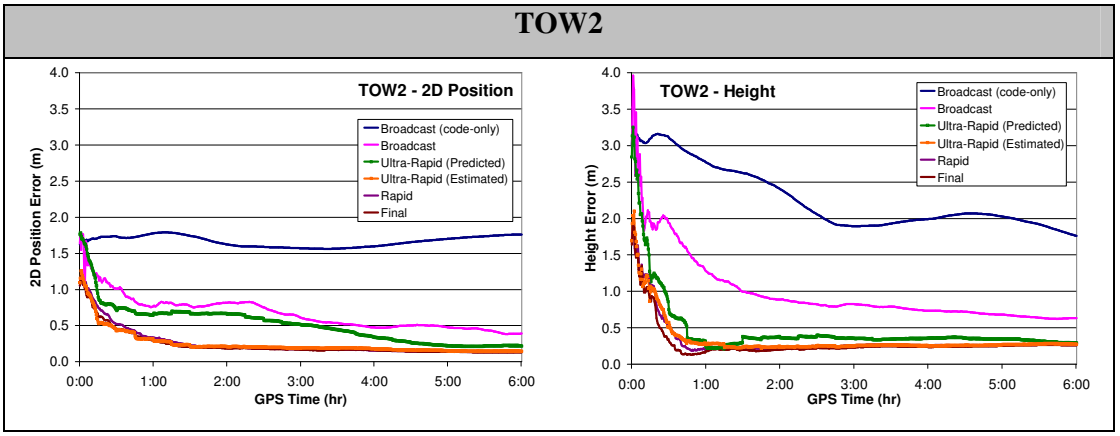

Figure 7.2: Point positioning results at TOW2 station using different satellite orbit and clock correction products. Time series of the 2D positioning errors on the left, and the height errors on the right.

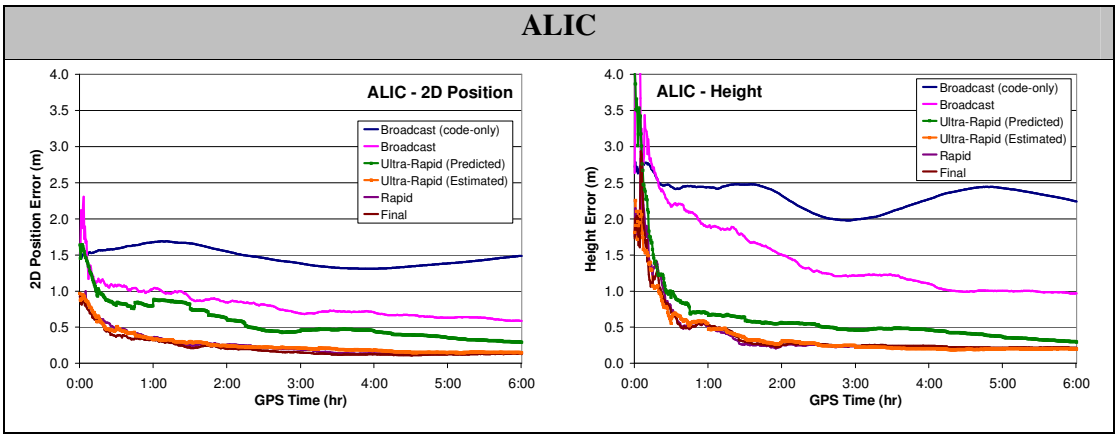

Figure 7.3: Point positioning results at ALIC station using different satellite orbit and clock correction products. Time series of the 2D positioning errors on the left, and the height errors on the right.

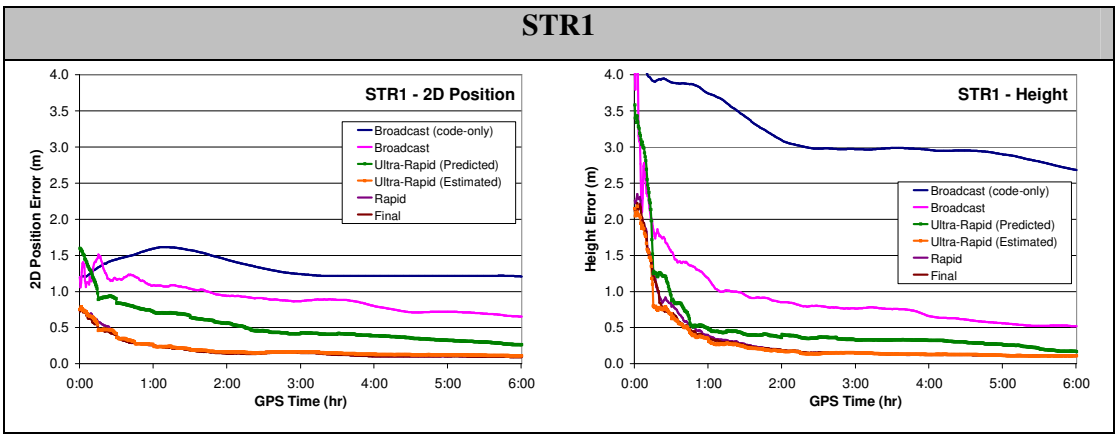

Figure 7.4: Point positioning results at STR1 station using different satellite orbit and clock correction products. Time series of the 2D positioning errors on the left, and the height errors on the right.

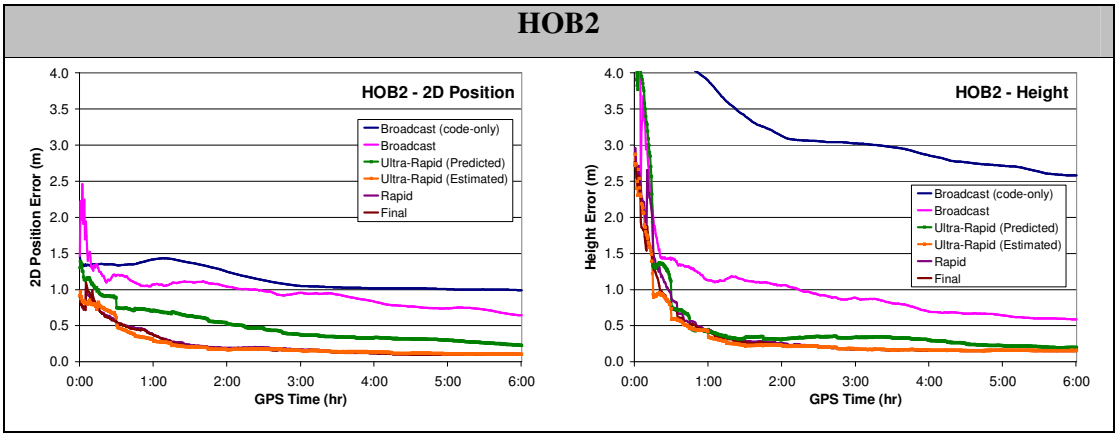

Figure 7.5: Point positioning results at HOB2 station using different satellite orbit and clock correction products. Time series of the 2D positioning errors on the left, and the height errors on the right.

From these figures, it can be seen that the errors associated with the horizontal positions are lower than the errors from the height estimates. This is due to the propagation of GPS signals through the ionosphere, as well as the nature and design of the GPS system. However, as more data are collected and processed, the errors associated with the ionospheric delay cancel out, and subsequently, the errors in the height estimates diminish. In addition, it can be inferred from Figures 7.1, 7.2, 7.3, 7.4, and 7.5 that the characteristic of the positioning errors based on various ephemerides at the five ARGN stations is basically similar. The accuracy of the position estimates (after ambiguities stabilisation) using single frequency PPP are often higher than those of the SPS. This is because single frequency PPP takes advantage of the more precise carrier phase measurements. Moreover, the implemented single frequency PPP mathematical model is essentially reliant on the ionosphere-free *code and quasi-phase* combination, which eliminates the ionospheric error (refer to Section 2.6.2.2). However, as noted in Chapter 4, the use of the carrier phase measurements to achieve high accuracy point positioning is subjected to the ambiguous nature of the phase measurements, which could potentially limit the quality of the PPP solutions. Thus, the initial portion of the estimated solutions before phase ambiguities stabilisation is often inaccurate and imprecise. Nevertheless, once the phase ambiguities stabilise as more observations are collected, and provided that no cycle slips occur, the solutions will follow the more precise single frequency ionosphere-free quasi-phase observables.

The combined mean and RMS of the positioning errors for DARW, TOW2, ALIC, STR1 and HOB2 stations using the different satellite orbit and clock corrections are presented in Figures 7.6, 7.7, 7.8, 7.9, and 7.10, respectively.

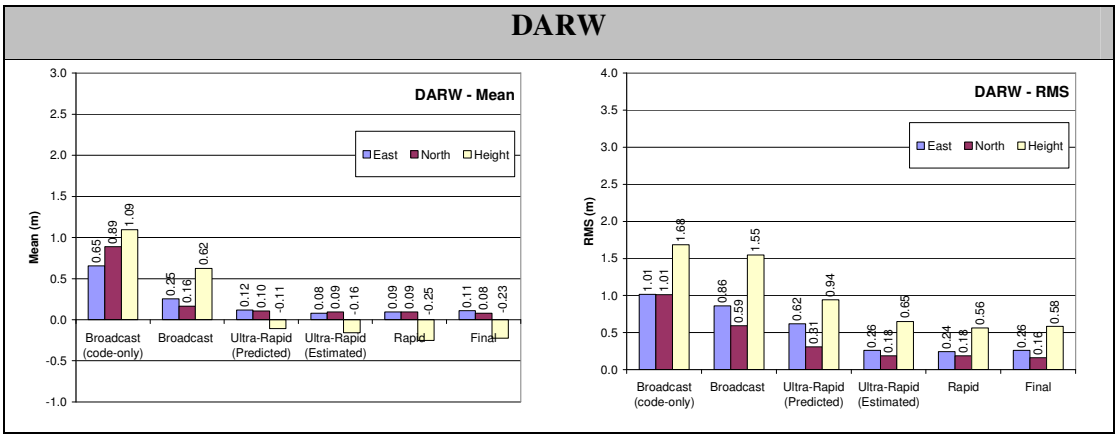

Figure 7.6: Statistical analysis of the estimated positioning solutions at DARW using different satellite orbit and clock correction products. The left bar chart shows the mean, while the bar chart on the right shows the RMS value.

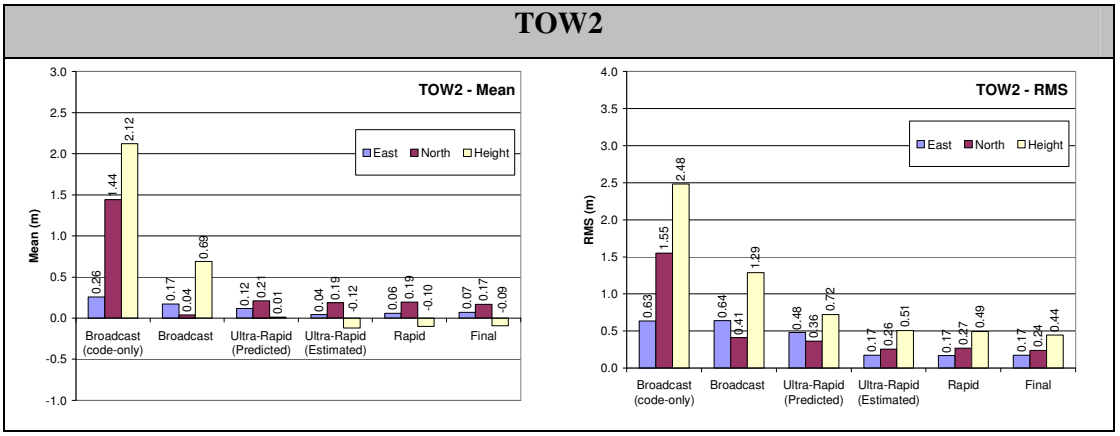

Figure 7.7: Statistical analysis of the estimated positioning solutions at TOW2 using different satellite orbit and clock correction products. The left bar chart shows the mean, while the bar chart on the right shows the RMS value.

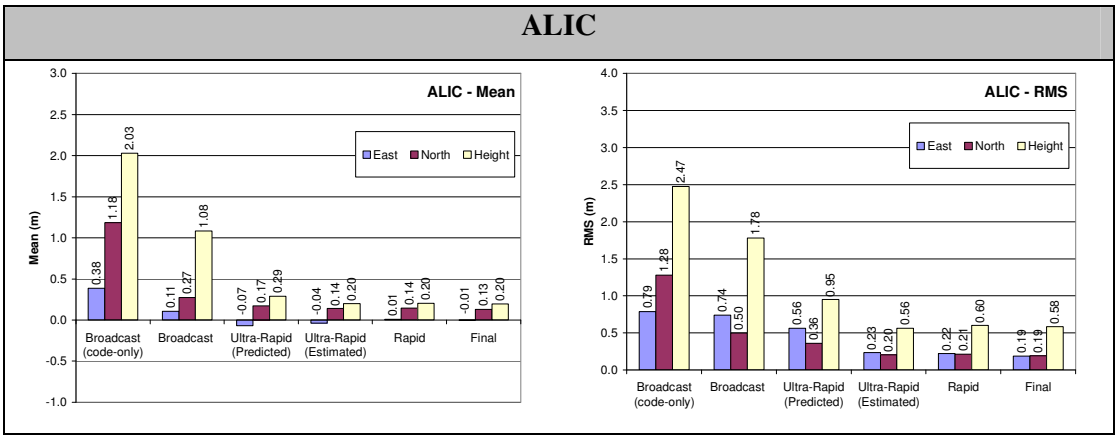

Figure 7.8: Statistical analysis of the estimated positioning solutions at ALIC using different satellite orbit and clock correction products. The left bar chart shows the mean, while the bar chart on the right shows the RMS value.

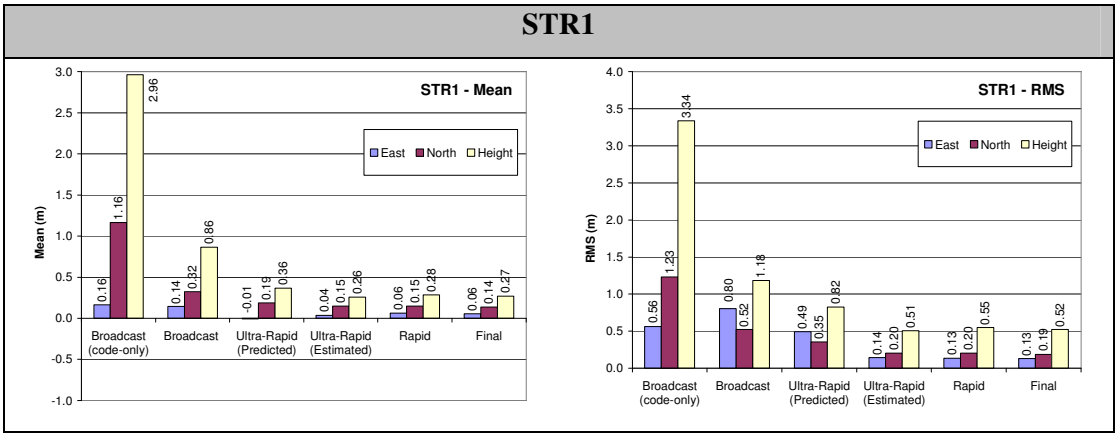

Figure 7.9: Statistical analysis of the estimated positioning solutions at STR1 using different satellite orbit and clock correction products. The left bar chart shows the mean, while the bar chart on the right shows the RMS value.

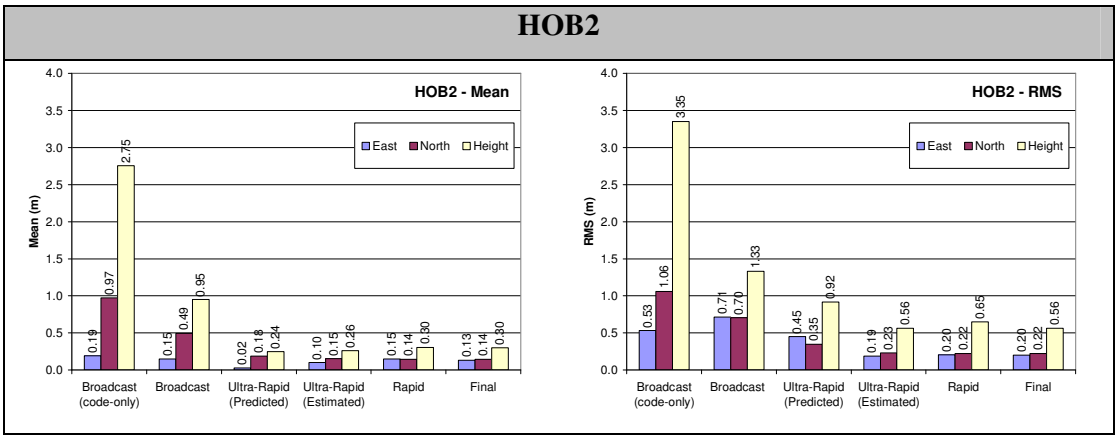

Figure 7.10: Statistical analysis of the estimated positioning solutions at HOB2 using different satellite orbit and clock correction products. The left bar chart shows the mean, while the bar chart on the right shows the RMS value.

Based on the positioning results and statistical analysis obtained from this study, it can be seen that the use of the IGS *Ultra-Rapid (Predicted Half)* orbit and clock corrections in single frequency PPP (represented by the green lines in Figures 7.1 to 7.5), in comparison to the Broadcast ephemerides (represented by the pink lines in Figures 7.1 to 7.5), could enhance the accuracy and precision of the real-time position estimates. After half an hour (60 epochs) of observation, the 2D horizontal and height positioning solutions using the IGS predicted orbits and clocks converged to be within 1m of the known values. The PPP solutions using the Broadcast ephemerides, on the other hand, required more than an hour (1 – 2 hours) before the solutions converge within the required limit. The average mean and RMS (RMS are noted in brackets) values of the position errors from the five ARGN stations using the *Ultra-Rapid (Predicted Half)* products are 0.18m (0.63m) horizontally and 0.16m (0.87m) vertically. The mean and RMS of the position errors based on the Broadcast ephemerides are 0.31m (0.92m) horizontally and 0.84m (1.43m) vertically. These results are promising as the IGS predicted satellite orbit and clock corrections can be used in real-time (instead of the Broadcast ephemerides) to obtain more accurate point positioning solutions.

The use of the near real-time *Ultra-Rapid (Estimated Half)* orbit and clock corrections in single frequency PPP also provided promising results. In fact, the single frequency PPP solutions using the near real-time *Ultra-Rapid (Estimated Half)* orbit and clock corrections, which have a short latency of just 3 hours, were quite comparable to those of the more precise

IGS *Rapid* products (refer to Figures 7.1, 7.2, 7.3, 7.4, and 7.5). The deviation was only a few centimetres. The RMS of the horizontal and height errors are 0.29m and 0.59m, respectively. As expected, the use of the *Ultra-Rapid (Estimated Half)* corrections in single frequency PPP could provide more accurate position estimates than the predicted orbits and clocks. This is evident particularly in the horizontal positioning estimates (see Figures 7.1, 7.2, 7.3, 7.4, and 7.5) and the level of improvement provided by the *Ultra-Rapid* is about a factor of two. Ray and Griffiths (2008) from NOAA NGS reported the current status of the IGS *Ultra-Rapid* products. They noted that the performance of the IGS satellite orbit and clock products for real-time and near real-time applications has improved dramatically, in particular the *Ultra-Rapid (Estimated Half)* products. Up to seven ACs contribute to the production of the IGS *Ultra-Rapid (Estimated Half)* satellite orbit and clock corrections. This gives redundancy in the solutions, which helps to enhance the reliability and accuracy of the orbit and clock corrections. Moreover, they also noted that the precision of the IGS *Ultra-Rapid (Estimated Half)* orbits is closely approaching to those of the *Rapid* orbits.

In parallel to the advancement of the *Ultra-Rapid* products, the quality of the *Rapid* satellite orbit and clock corrections has also increased in the last few years. This is attributed to the timely advancement of new technology such as software algorithms, data acquisition and communication schemes. Currently, the *Rapid* service provides satellite orbit and clock solutions within a day (17 hours) and has almost the same precision as the *Final* solutions, which has a latency of almost 2 weeks. According to Kouba (2003), the *Rapid* products are in fact as precise as the *Final* products. In addition, there is also good agreement between satellite clock estimates produced by IGS ACs. These estimates agree within 0.1-0.2ns (Kouba, 2003). The findings in this study have shown that the use of the *Rapid* and *Final* orbit and clock corrections products in single frequency PPP would provide, for all practical purposes, comparable (i.e. within a few centimetres variation) point positioning accuracy.

It is encouraging to identify from this study that the use of the IGS *Ultra-Rapid* orbit and clock corrections, which are available to all users in real-time and near real-time, in single frequency PPP can provide point positioning accuracy better than 0.5m (after phase ambiguities stabilisation). In comparison with the classical SPS technique, this improvement is quite remarkable. However, it is important to acknowledge the limitations of real-time single frequency PPP.

One of the limitations of real-time single frequency PPP is the long convergence time. The phase ambiguities on L1 frequency are not of integer values because they are "corrupted" by the satellite and receiver phase biases (Gao and Garin, 2006). As a consequence, the integer ambiguities of the phase measurements cannot be resolved. Instead, the ambiguities are estimated in PPP as float solutions, which require a long convergence period. The time of convergence varies depending on the number and geometry of visible satellites, observation quality, and users' defined environment. Furthermore, it can be established from this study that the position convergence also depends on the quality of the ephemerides used to constrain the satellite orbit and clock errors. When precise satellite orbit and clock corrections such as the *Final* corrections are used, the errors (caused by the satellite orbits and clocks) contained in the least squares solutions are minimal. Thus, lesser epochs are required by the float ambiguity solutions to stabilise. In contrast, the point positions computed using real-time satellite orbit and clock corrections, i.e. the broadcast and predicted ephemerides, are subjected to longer convergence times. This is owing to the same "principle" that the errors contained in the solutions are larger and hence affecting the stabilisation process of the float ambiguity solutions. It can be seen from Figures 7.1, 7.2, 7.3, 7.4, and 7.5 that the errors based on the real-time ephemerides continually decrease as more observations were collected and processed. Nevertheless, the accuracy of the position estimates using single frequency PPP technique is still encouraging in comparison to the classical code-based processing.

The second challenge of real-time PPP is the quality of the predicted satellite clock corrections. The precision of the satellite clock corrections is generally lower than those of the orbits. This is because the stochastic behaviour of the satellite atomic clock variations is virtually impossible to predict. Currently, only four IGS ACs contribute the estimates of the satellite clock biases, which limits the robustness and quality of the *Ultra-Rapid* clock products (Ray and Griffiths, 2008). Although the *Ultra-Rapid* observed clocks have typical errors about twice of the *Rapid*, the quality of the *Ultra-Rapid* predicted clocks is worse, i.e. almost the same level as the broadcast navigation values. In order to improve the quality of the clock predictions, the IGS is currently developing a system for true real-time clock monitoring and broadcast capability (Ray and Griffiths, 2008).

The dissemination of the precise satellite orbits and clocks corrections is another challenge for real-time PPP. In this study, the point positions were estimated based on the simulation of real-time single frequency PPP. This is due to the limitation of the research software platform, which was not designed for real-time data processing. At present, there are

governments and private organisations providing real-time precise orbit and clock data via the Internet or communication satellites. Examples of these real-time services are the JPL real-time data known as Internet-based Global Differential GPS (IGDG), the NRCan real-time data known as the GPS•C, OmniSTAR-XP, and Navcom's StarFire (Lahaye *et al.*, 1997; Muellerschoen *et al.*, 2000; Muellerschoen *et al.*, 2004; Dixon, 2006; JPL, 2007; Mireault *et al.*, 2008; OmniSTAR, 2008). The JPL IGDG, OmniSTAR-XP, and Navcom's StarFire are available through subscription services, while the NRCan GPS•C real-time corrections are only distributed nationally through the Canadian-wide Differential GPS System (DGPS). The IGS predicted orbit and clock corrections, on the other hand, are freely accessible on the Internet to all users. The move towards real-time GNSS data and derived products have been a strategic objective of the IGS for several years, and this has been reaffirmed in the IGS Strategic Plan for the years 2008 to 2012 (Caissy, 2007). Recently, the IGS RTWG has been established to govern the IGS Real-time Pilot Project (Dow *et al.*, 2005; IGS, 2008). An important theme of this pilot project is to promote and support the development of real-time applications by shortening the latency while improving the quality of the associated products. It is envisioned that with the improved products together with the integration of GPS and wireless technology, the applicability of real-time PPP in different applications can soon be revolutionised.

7.4 Summary

This Chapter has provided a description of the study undertaken to evaluate the feasibility of using different satellite orbit and clock corrections for single frequency PPP static applications. The study has two objectives. The first objective was to investigate the potential of using the IGS *Ultra-Rapid* ephemerides for real-time and near real-time point positioning. The second objective was to compare the performance of various IGS satellite orbit and clock and products (besides the *Ultra-Rapid* corrections) in single frequency PPP. The assessment was carried out based upon the accuracy and precision of the estimated single frequency PPP solutions.

The results have demonstrated that the *Ultra-Rapid (Predicted Half)* satellite orbit and clock corrections can be used to achieve high accuracy point positions. It has been shown that after half an hour of observations (60 epochs), the 2D horizontal and height solutions converged to better than 1m of the known values. This is encouraging because the results can be treated as simulation of the achievable point positioning accuracy in real-time using single

frequency PPP. The PPP solutions using the near real-time *Ultra-Rapid (Estimated Half)* orbit and clock corrections were also favourable. In fact, the deviation between the positioning solutions using the *Ultra-Rapid (Estimated Half)* and *Rapid* products were minimal, i.e. at the level of a few centimetres. In comparison to the *Ultra-Rapid (Predicted Half)* products, the time required by the *Ultra-Rapid (Estimated Half)* solutions to convergence within 1m of the known values was shorter. However, this was compromised by the slightly longer (3 hours) product latency. Nevertheless, the quality of the positioning results obtained from this study was promising considering that less than 1m positioning accuracy can be achieved in real-time and near real-time positioning scenarios.

It can be summarised from this investigation that the quality of the estimated PPP solutions improves as a function of the corrections latency. The *Final* and *Rapid* satellite orbit and clock correction products would provide the best point positioning accuracy, and are then followed by the *Ultra-Rapid (Estimated Half)* and *Ultra-Rapid (Predicted Half)* products. It should be noted that although the IGS *Final* products with a latency of about 13 days have the highest quality and consistency, the shorter latency *Rapid* products, with a latency of only 17 hours, are in fact capable of providing comparable positioning results. Therefore, for most practical purposes, the users will not notice any significant discrepancy between the point positioning results from using the IGS *Final* or *Rapid* satellite orbit and clock products.

CHAPTER 8

Single Frequency PPP using Medium-Cost and Low-Cost GPS Receivers

8.1 Introduction

In Chapter 7, the accuracy and precision of the estimated single frequency PPP solutions using various IGS satellite orbit and satellite corrections products have been assessed and evaluated. The corresponding results and discussions were also presented. It has been shown that the use of the precise IGS *Rapid* and *Final* satellite orbit and clock corrections in single frequency PPP could provide the best point positioning solutions. However, the trade-off in achieving high accuracy positioning solutions is the long latency of the corrections. For example, in order to apply the precise corrections in GPS processing, it is necessary to wait for 17 hours to 2 weeks after the data are collected. This method of GPS processing is recommended when the quality of the estimated positions is critical and time is not a restraining factor. Alternatively, users who wish to obtain their positions in real-time could opt to apply either the Broadcast corrections or the IGS *Ultra-Rapid (Predicted Half)* orbit and clock corrections. It has been shown that the IGS predicted orbit and clock corrections could provide better point position estimates than the Broadcast corrections. When the IGS predicted corrections are used, the estimated position errors are within 1m of the known values.

All single frequency GPS measurements used in the previous studies were extracted from datasets collected from geodetic quality dual frequency GPS receivers in static mode. It is of much interest to validate independently the capability of PPP using GPS observation data collected from various single frequency receivers. This Chapter will present the study undertaken to examine the achievable point positioning accuracy using single frequency GPS receivers. Single frequency GPS receivers of varying costs will be tested. The performance of

these receivers will be assessed via the quality of the estimated point positioning solutions. It is envisaged that the findings from these analyses could, in addition to validating the performance of the implemented single frequency PPP algorithm, provide some indications of the achievable point positioning accuracy using different receiver types.

8.2 Types of GPS Receiver

GPS technology is used in various applications that require different accuracy, performance, and availability levels. The selection of the appropriate receiver type for a particular project or application should be made from a sound analysis of the following criteria (American Society of Civil Engineers, 2000):

1. the required accuracy for which the receiver is to be used,
2. the nature of the applications,
3. operational environments,
4. technical and signal processing requirements,
5. human resources,
6. power consumption requirements, and
7. budgetary limitations

As a general rule, the more accurate a GPS receiver positions and navigates, then the more the receiver will cost. At present, the price of a GPS receiver unit ranges between a few hundred dollars to tens of thousands of dollars (Australian Dollar – AUD).

The GPS receiver market, in particular the handheld and low-cost GPS receiver market, has grown rapidly in the last two decades. Magellan introduced the first low-cost handheld GPS receiver for consumer market in 1989 (Xiao *et al.*, 2002; Magellan Navigation Incorporation, 2008). Ever since, the demand for low-cost handheld GPS receivers has constantly increased. According to Stansell *et al.* (2006), the intensive GPS market penetration and usage has been primarily driven by low-cost, low power, and high sensitivity receivers. The vast majority of worldwide GPS enabled consumer devices are cost driven. Therefore, any improvement in the quality of the point positioning solutions, especially for low-cost handheld GPS receivers, will be beneficial.

The two generic types of GPS receiver in the market, at present, are the single frequency and dual frequency receivers. Within GPS receiver types, there are three different classifications of receivers, namely the geodetic grade, medium-cost (usually GIS grade), and low-cost receivers. The classification of receivers is defined by the unit cost, accuracy level, and navigation capabilities. Table 8.1 outlines the receivers' classifications as defined by these parameters.

Table 8.1: The classification of GPS receiver units.

Receiver Classification	Approximate Price (AUD)	Signal	Accuracy	Applications
Low-cost	<$1,000	Code or/and carrier phase; single frequency	~3 – 15m (absolute)	Tracking, navigation, positioning and location based services
Medium-cost (GIS grade)	$1,000 - $10,000	Code or/and carrier phase; single frequency	~0.5 – 3m (relative)	GIS applications such as asset mapping
Geodetic grade	> $10,000	Code and carrier phase; dual frequency	Centimetre level (relative)	Precise navigation, surveying and geodesy applications

8.3 Point Positioning Quality Investigation: A Cost-Benefit Analysis

A number of researchers have investigated the potential of using low-cost single frequency receivers to achieve high accuracy positioning and for geodetic applications. For example, Masella *et al.* (1997), Rizos *et al.* (1998), Masella (1999), Janssen *et al.* (2002), Roberts *et al.* (2004), Söderholm (2005), Alkan *et al.* (2006), Saeki and Hori (2006), and Alkan *et al.* (2007) have studied the performance of low-cost receivers using relative positioning techniques. They have reported a differential positioning accuracy of around a few centimetres to 1.5m (for a 20km baseline).

The use of a low-cost GPS receiver to obtain accurate point positioning creates a major challenge because it is highly dependent on how the measurement error sources are handled (Beran *et al.*, 2007). Researchers such as Tiberius (2003) and Milbert (2005) have

investigated the performance of low-cost receivers using the SPS and attained point positioning accuracy of a few metres (5m to 15m). According to the latest U.S. Government's GPS SPS standard performance report, it is possible to provide a global average positioning accuracy of 9m horizontally and 13m vertically (at 95% confidence interval) (U.S. Assistant Secretary of Department of Defence, 2008). It should, however, be noted that the quoted values are usually quite pessimistic because they did not account for the atmospheric errors, multipath and receiver noise (Tiberius, 2003). The potential of the PPP technique using a low-cost receiver, to date, is still a relatively new research area. Only Beran *et al.* (2007) have investigated the performance of a low-cost handheld GPS receiver using their implemented single frequency PPP filter. They reported that a low-cost receiver could provide horizontal and height positioning accuracy of better than 1m and 2m, respectively, in post-processing mode.

This study aims to test various low-cost single frequency GPS receivers for high accuracy point positioning in post-processing and real-time scenarios. The intention is to examine an alternative, cost-effective positioning technique for applications that are restricted by budgetary and operational limitations, without compromising on the quality of the estimated positioning solutions. The proposed technique would be useful for applications in remote areas such as Central Australia. Static tests were undertaken to demonstrate the positioning capabilities of both medium-cost and low-cost GPS receivers. The selection of the receiver model was limited by the availability of the units. Table 8.2 and Figure 8.1 describe the model, features and specifications of the receivers used in this study.

Table 8.2: Classification and specifications of the GPS receivers used in this study.

Receiver Classification	Receiver Name	Approx. Price (AUD)	Brief Description
Low-cost	Garmin GPS 12 XL (discontinued product since 2001)	~$400	• 12 channels (L1 code and carrier phase) • Quoted GPS accuracy: 15m RMS • DGPS capable • External antenna connection (optional) • Size: 5.3 x 14.7 x 3.1cm • Weight: 269 grams with 4 AA batteries
Low-cost	Garmin GPSMap®76C	~$400	• 12 channels (L1 code and carrier phase) • Quoted GPS accuracy: <15m (95% confidence interval) • WAAS and DGPS capable • External antenna connection (optional) • Size: 6.9 x 15.7 x 3.5cm • Weight: 216 grams with 2 AA batteries
Medium-cost: GIS grade (with internal antenna)	Trimble Geoexplorer® GeoXH (2005 series)	~$9,400	• 12 channels (L1 code and carrier phase) • Quoted accuracy: 30cm (H-Star post-processed) • SBAS (including WAAS and EGNOS) and DGPS capabilities • Internal antenna with optional Zephyr antenna • Size: 21.5 x 9.9 x 7.7cm • Weight: 780 grams with battery (internal 6800 mAH lithium-ion battery)
Medium-cost: GIS grade (with external antenna)	Trimble Pathfinder® Pro XRS	~$15,000 (purchase price in 2001)	• 12 channels (L1 code and carrier phase) • Quoted accuracy: submetre (post-processed) • SBAS (including WAAS and EGNOS) and DGPS capabilities • External combined L1 GPS/beacon/satellite differential antenna • Size: 11.1 x 5.1 x 19.5cm • Weight: 760 grams (receiver), 550 grams (antenna)

Garmin 12 XL

Garmin GPSMap® 76C

Trimble Geoexplorer®
GeoXH (2005 series)

Trimble Pathfinder®
Pro XRS

Figure 8.1: The GPS receivers that were used in this research (Garmin Limited, 2008; Trimble Navigation Limited, 2008).

GPS observation data from four different stations collected using different receiver units were tested. Information of each station and the DOY during which the data were collected are given in Table 8.3.

Table 8.3: Station information and DOY during which the data used in this research were collected.

Station Name and Location	Receiver Model	DOY	Approximate WGS 84 Coordinates (latitude, longitude, and height)
Point YB3, Victoria, Australia	Garmin 12 XL	356 2008	37˚ 48’ S 145˚ 01’ E 30m
Point PIER13, Ottawa, Canada	Garmin GPSMap®76C	095 2005	45˚ 24’ N 75˚ 55’ W 45m
Point ULTIMATE, Victoria, Australia	Trimble Geoexplorer® GeoXH (2005)	266 2008	37˚ 52’ S 145˚ 05’ E 56m
Point LR31, Victoria, Australia	Trimble Pathfinder® Pro XRS	260 2006	37˚ 18’ S 145˚ 50’ E 290m

As the objective of this study was to investigate the real-time and post-processing capabilities of these receivers using single frequency PPP, the collected data sets were processed both in simulated real-time and post-processing modes. For simulated real-time processing, the IGS *Ultra-Rapid (Predicted Half)* satellite orbit and clock corrections were applied. The selection of the *Ultra-Rapid (Predicted Half)* was adopted because of the positive findings from the preceding investigation described in Chapter 7. It was found that the IGS predicted corrections could provide more accurate point position estimates than the Broadcast ephemerides. The ionospheric error was partially eliminated by using the Broadcast model with the broadcast ionospheric coefficients. For post-mission processing, the precise IGS *Rapid* satellite orbit and clock products, as well as the IGS *Rapid* GIMs were used to remove the bulk of the satellite orbit, clock and ionospheric errors. The tropospheric ZPD was corrected in both scenarios using the Hopfield model with default atmospheric parameters, and the tropospheric ZPD was mapped to the slant delay by using the Niell mapping function (Hopfield, 1969; Niell, 1996). The *a priori* code and quasi-phase sigma ratio was set to 1:50 and a 15º elevation mask was applied.

The following sections provide the results of the analyses, commencing with the medium-cost GPS receivers followed by the low-cost units. Numerical results in both graphical and tabular formats, as well as discussion will be presented.

8.3.1 Medium-Cost GPS Receiver

8.3.1.1 Trimble Pathfinder® Pro XRS

GPS data were collected at Point LR31 in Victoria, Australia, on DOY 260 2006 for four hours using the Trimble Pathfinder® Pro XRS receiver. As the Pathfinder® Pro XRS receiver uses an external L1 antenna, the antenna was accurately mounted on top of a tripod (tribrach) over the point. The height offset between the marker on the ground and the approximate antenna phase centre was measured and recorded in the observation file. The data were collected at 1 second sampling interval, but the data were "down-sampled" to a 30 second interval for consistency and comparison purposes.

The known coordinates of Point LR31 used in this analysis were obtained from previous surveys using traditional surveying techniques, as well as GPS multi-receiver baseline processing. The accuracy of the known coordinates is quoted to be to the nearest

centimetre for the horizontal component and to the nearest decimetre for the height component. The accuracy is considered adequate for the purpose of this study.

The trajectory or sky plot of the visible satellites throughout the observation period at Point LR31 is illustrated in the left plot in Figure 8.2. The bar chart on the right in Figure 8.2 depicts the number of satellites processed as a function of observation period. An average of eight satellites was observed throughout the survey. However, there were a few occasions when only five satellites were available and processed.

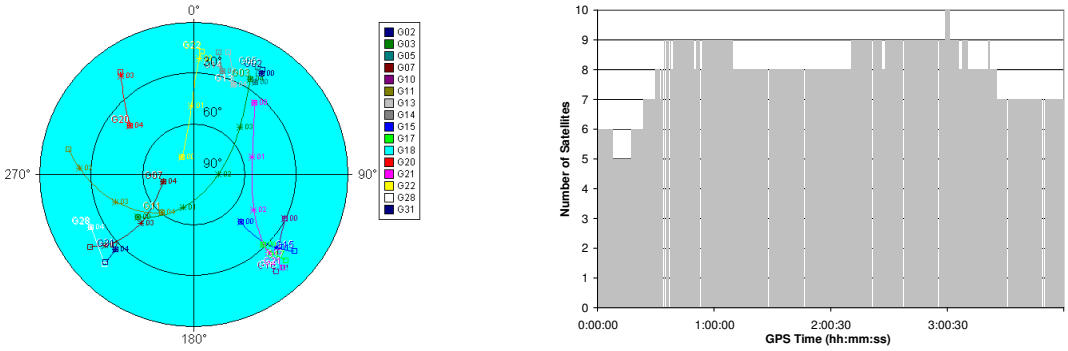

Figure 8.2: The trajectory of the visible satellites over the sky at Point LR31 (left plot); the number of satellites processed as a function of observations period (right plot).

IGS *Rapid* Products (latency of about 17 hours)

Figure 8.3 shows the differences (or positioning errors) between the estimated east, north and height positions with the accurately known coordinates of Point LR31. Note that the local time in Victoria when these data were collected was 10:00LT (i.e. 10:00LT to 14:00LT). It is encouraging to see that, although the PPP solutions required half an hour to converge, all estimated point positions (including the initial estimates) are within 1m of the known coordinates. No apparent atmospheric effects, particularly the ionospheric delay can be observed. After one hour of observation, the positioning solutions are accurate to about 0.4m.

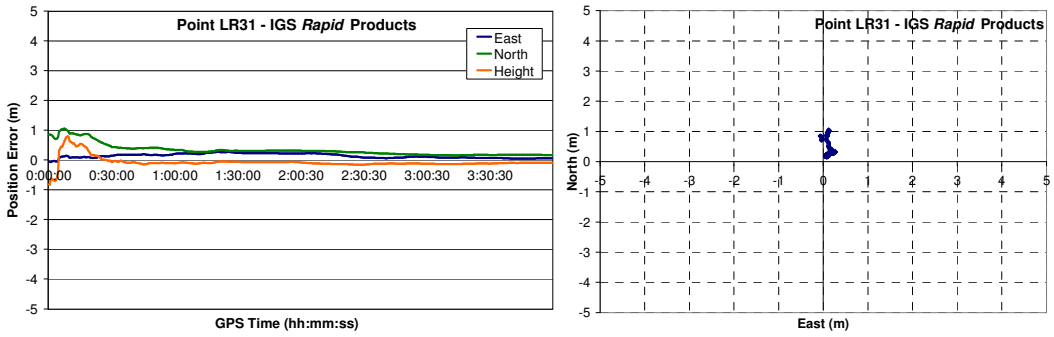

Figure 8.3: Point positioning results at Point LR31 in post-processing mode. Time series of the east, north and height errors on the left; scatter plot of the horizontal errors on the right.

Figure 8.4 depicts the magnitude of the code and quasi-phase observations residuals for all the observed satellites. The residuals were plotted as a function of time. In general, the observation residuals are caused by factors that are not considered in the data processing software, e.g. the residuals multipath effects, the receiver antenna type, and the receiver internal tracking mechanism (Beran *et al.*, 2007).

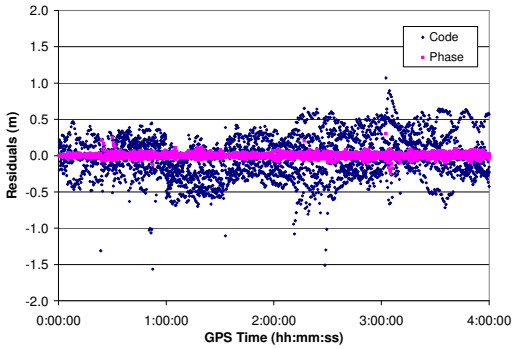

Figure 8.4: Code and quasi-phase residuals at Point LR31 in post-processing mode.

In order to assist with the interpretation of the results, the mean, STandard Deviation (STD) and RMS values were computed using all of the positioning solutions (480 epochs) obtained from the test. The statistical values are presented in Table 8.4. As noted previously in Chapter 4, the RMS values are indications of the precision of the estimated positions with regards to the "ground truth" (i.e. the "accepted value" used in the RMS calculation was zero). Whilst, the STD provides an indication of the spread of the estimated positioning solutions from the mean (i.e. the "accepted value" used in the STD calculation was the computed mean). From Table 8.4, it can be seen that the mean positions are in good

agreement with the known coordinates. The deviation between the mean and the known coordinates is less than 0.4m.

Table 8.4: Mean, STD and RMS of the estimated positions at Point LR31 in post-processing mode.

Point LR31 – IGS *Rapid* Products			
	Mean (m)	**STD (m)**	**RMS (m)**
East	0.14	0.07	0.16
North	0.33	0.20	0.38
Height	-0.07	0.18	0.19

IGS *Ultra-Rapid (Predicted Half)* Products (Real-time)

In contrast to Figure 8.3, Figure 8.5 plots the east, north and height positioning errors at Point LR31 using the IGS *Ultra-Rapid (Predicted Half)* satellite orbit and clock corrections. The estimated positions are indications of the achievable single frequency PPP accuracy in real-time using a medium-cost receiver. Although the numerical results presented here were based on a simulation (i.e. the data were first collected in the field and then processed later using the predicted satellite orbit and clock corrections), they could still be considered as good representatives of the achievable positioning accuracy in a real-time scenario.

It can be seen that the initial portion (first half an hour of the observation time span) of the north and height errors ranged between 3m to 6m of the known values. This is mainly attributed to the phase ambiguities. As more observations were collected and processed, the more accurate the solutions became. After one to one and the half hour of observations, the single frequency PPP errors converged to be within 1m of the known values.

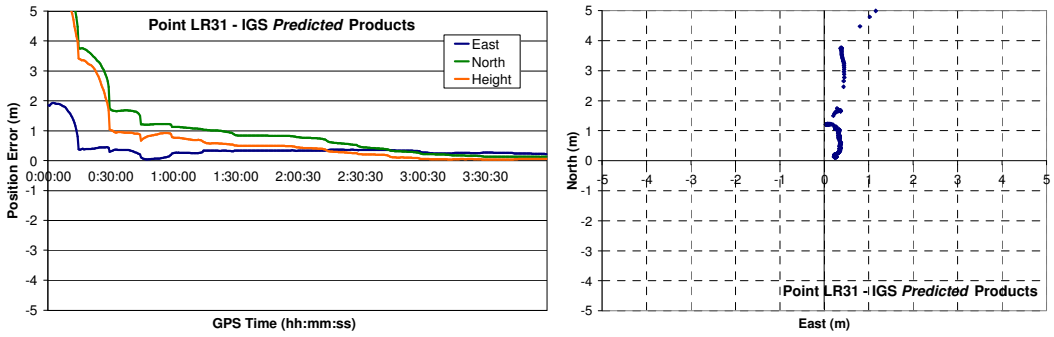

Figure 8.5: Point positioning results at Point LR31 in real-time mode. Time series of the east, north and height errors on the left; scatter plot of the horizontal errors on the right.

The code and quasi-phase measurement residuals using the IGS *Ultra-Rapid (Predicted Half)* satellite orbit and clock corrections are plotted in Figure 8.6. The measurements residuals portrayed larger variations than those in Figure 8.4, which were generally caused by the less accurate predicted orbit and clock corrections.

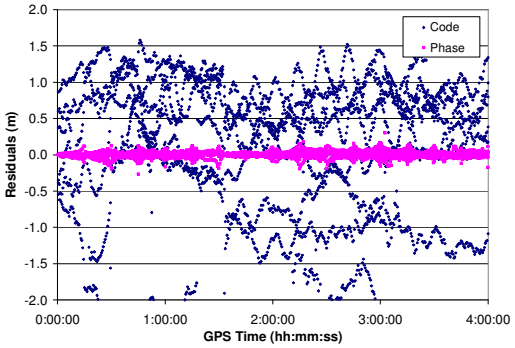

Figure 8.6: Code and quasi-phase residuals at Point LR31 in real-time mode.

The satellite orbit and clock corrections from the IGS *Rapid* and *Ultra-Rapid (Predicted Half)* products on DOY 260 2006 were compared for the purpose of this assessment. The differences between the two products are plotted in Figure 8.7. The *Rapid* corrections are considered as "truth" because the corrections are more accurate than the predicted corrections. Therefore, the differences between these two products are assumed to be the predicted orbit and clock errors. The points on the graphs represent the orbit (left graph) and clock biases (right graph), respectively, for each satellite.

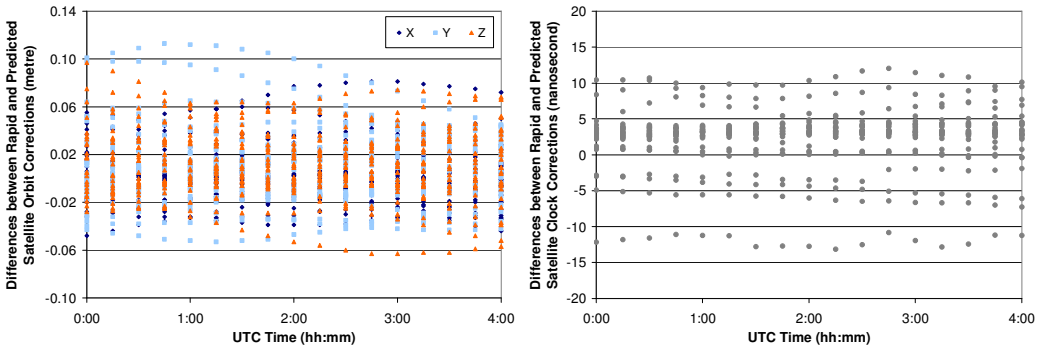

Figure 8.7: Comparison plots between the IGS *Rapid* and *Ultra-Rapid (Predicted Half)* satellite orbit (left graph) and clock corrections (right graph) for all the satellites on DOY 260 2006.

It appears from this figure that most of the discrepancies in the predicted orbit are within the IGS quoted accuracy, i.e. 5cm-10cm (refer Table 2.1). However, the variations between the *Rapid* and predicted clock corrections are quite large, which may have resulted in the large positioning errors. For some satellites, the differences between the *Rapid* and predicted clock corrections are about 10ns (equivalent to 3m in the range error). This is significantly greater than the 5ns accuracy quoted by IGS for the clock predictions.

Table 8.5 tabulates the statistical results of the estimated positioning solutions at Point LR31 using the IGS *Ultra-Rapid (Predicted Half)* satellite orbit and clock corrections. As anticipated, the positioning results based on the predicted orbit and clock corrections are not as accurate as those using the *Rapid* corrections. The mean position estimates based on the predicted orbit and clock corrections are approximately 1.2m horizontally and 0.9m vertically. The deviation of the horizontal and height components from the "ground truth" is within 2m of the known values. These results are quite impressive and they are representative of the achievable point positioning accuracies and precisions in real-time using a medium-cost single frequency GPS receiver.

Table 8.5: Mean, STD and RMS of the estimated positions at Point LR31 in real-time mode.

Point LR31 – IGS *Ultra-Rapid (Predicted Half)* Products			
	Mean (m)	**STD (m)**	**RMS (m)**
East	0.38	0.35	0.51
North	1.14	1.43	1.83
Height	0.85	1.42	1.65

8.3.1.2 Trimble Geoexplorer® GeoXH (2005 Series)

The Trimble Geoexplorer® GeoXH (2005 series) is also a medium-cost receiver. Unlike the Pathfinder® Pro XRS, this receiver has an inbuilt internal antenna. The receiver was placed on a tripod set up over Point ULTIMATE in Melbourne, Australia. The height from the marker to the approximate antenna phase centre was measured and noted in the observation file. One second interval data were collected for 4 hours on DOY 266 2008, but the data were "down-sampled" to a 30 second interval. The "true" coordinates of Point ULTIMATE were determined based on GPS multi-receiver baseline processing and the coordinates are accurate to one centimetre. Figure 8.8 shows the trajectory of the visible satellite over the sky at Point ULTIMATE on DOY 266 2008 and the number of satellites used in the data processing.

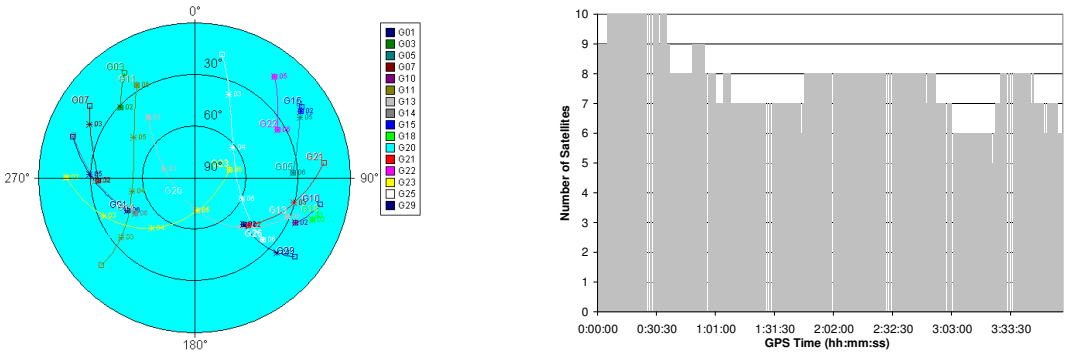

Figure 8.8: The trajectory of the visible satellites over the sky at Point ULTIMATE (left plot); the number of satellites processed as a function of observations period (right plot).

IGS *Rapid* Products (latency of about 17 hours)

The left graph in Figure 8.9 illustrates the east, north and height errors as a function of observation time. The right graph in Figure 8.9 is a scatter plot of the horizontal positioning errors. It can be inferred from this figure that the estimated horizontal positions are well within 1m of the "ground truth". The initial height solutions, on the other hand, vary between 1m to 2m. However, as more data were collected, the accuracy of the height solutions improved to be better than 1m of the "ground truth".

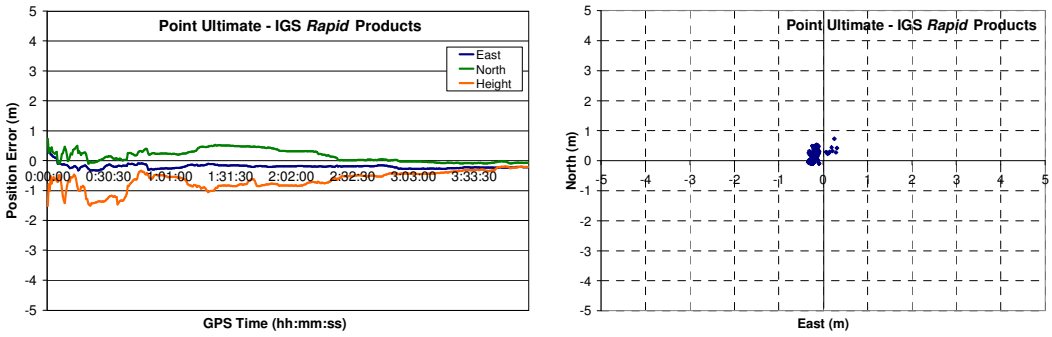

Figure 8.9: Point positioning results at Point ULTIMATE in post-processing mode. Time series of the east, north and height errors on the left; scatter plot of the horizontal errors on the right.

Figure 8.10 plots the code and quasi-phase residuals. The noise of the handheld Trimble Geoexplorer® GeoXH receiver was larger than those of the Pathfinder® Pro XRS receiver. This may be attributed to the quality of the receiver antenna.

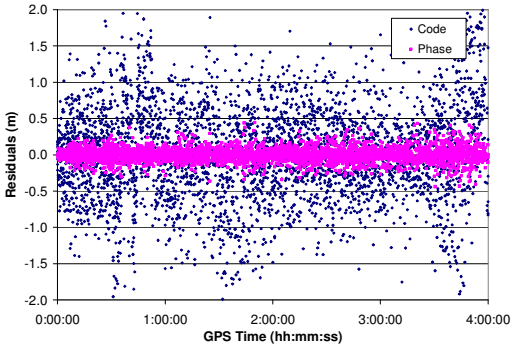

Figure 8.10: Code and quasi-phase residuals at Point ULTIMATE in post-processing mode.

The mean, STD and RMS of the estimated positions are summarised in Table 8.6. The accuracy of the east and north positions are better than 0.3m, while the accuracy of the height estimation is about two times worse than the horizontal position.

Table 8.6: Mean, STD and RMS of the estimated positions at Point ULTIMATE in post-processing mode.

Point ULTIMATE – IGS *Rapid* Products			
	Mean (m)	**STD (m)**	**RMS (m)**
East	-0.20	0.08	0.21
North	0.16	0.20	0.25
Height	-0.66	0.31	0.72

IGS *Ultra-Rapid (Predicted Half)* Products (Real-time)

The following figures, Figures 8.11 and 8.12, show the accuracy of the positioning solutions and its residuals using the IGS *Ultra-Rapid (Predicted Half)* orbit and clock corrections. The results presented here were simulation of the achievable point positioning solutions in real-time using single frequency PPP. The 2m horizontal errors and 4m height errors in the first 30 minutes of observation can be attributed to the phase ambiguities. After one hour of observation, the real-time positioning solutions converged to be better than 2m of the known values.

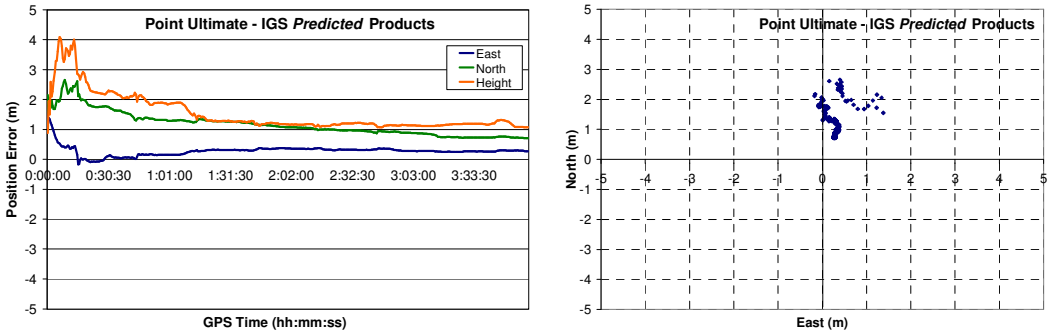

Figure 8.11: Point positioning results at Point ULTIMATE in real-time mode. Time series of the east, north and height errors on the left; scatter plot of the horizontal errors on the right.

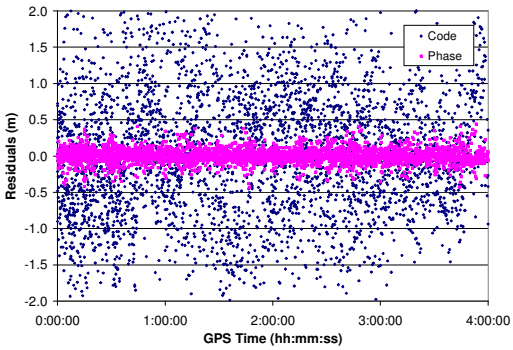

Figure 8.12: Code and quasi-phase residuals at Point ULTIMATE in real-time mode.

Table 8.7 shows the statistics of the estimated point positioning solutions. The horizontal and height positioning errors using the predicted corrections are about 1.2m and 1.5m, respectively. Although the spread of the estimated positions from the mean is less than 1m, the precision of the estimated position are between 1m to 2m of the "ground truth". These results are still favourable as they are comparable to the solutions obtained using the code-based relative positioning technique.

Table 8.7: Mean, STD and RMS of the estimated positions at Point ULTIMATE in real-time mode.

Point ULTIMATE – IGS *Ultra-Rapid (Predicted Half)* Products			
	Mean (m)	**STD (m)**	**RMS (m)**
East	0.28	0.17	0.32
North	1.18	0.43	1.24
Height	1.53	0.65	1.64

Discussion

Although the observation data collected at Point LR31 and Point ULTIMATE were from two different GPS receiver models, locations, and days, the results from both are quite consistent. The estimated point positioning solutions using the medium-cost receivers are generally in good agreement with the known values. As anticipated, the positioning solutions using the IGS *Rapid* orbit, clock corrections and GIMs are better than those using the predicted products. Accuracies and precisions better than 0.3m horizontally and 0.7m vertically are obtained in post-processing mode. For real-time point positioning, coordinate accuracies and precisions of about 1.5m to 2m are obtained. These results are significant

considering that only one receiver is required and also the cost of a GIS grade receiver is significantly lower than those of geodetic quality, and hence the term medium-cost. Moreover, the data collection and processing procedures involved with single receiver point positioning is less complex than those of relative positioning techniques.

8.3.2 Low-Cost GPS Receiver

8.3.2.1 Garmin 12 XL

The previous section focused on the quality of the point positioning solutions provided by medium-cost receivers. Since a vast majority of GPS users are using low-cost receivers, it will be interesting to investigate the real-time and post-processing capabilities of single frequency PPP using a low-cost handheld receiver.

Low-cost GPS receivers generally do not output RINEX data. However, there is software available, which can be used to convert (Garmin) binary data into RINEX format (Gálan, 2002; Milbert, 2005; The University of Nottingham, 2008). In this study, the Garmin 12 XL unit with an external antenna was placed on a tripod set up accurately over a coordinated point, Point YB3 in Melbourne, Australia. The offset in height between the marker on the ground and the approximate antenna centre was measured and recorded in the observation file. A Garmin binary stream was collected by a PC and the binary data was converted into RINEX format using Professor Antanio Gálan's RINEX converter software (Gálan, 2002). 4 hours worth of data were collected on DOY 356 2008 at a sampling rate of 1 second, but were "down-sampled" to 30 second for consistency and comparison purposes.

The known coordinates of Point YB3 were determined using GPS multi-receiver baseline processing and also traditional surveying methods. The quoted accuracy of the position is to the nearest centimetre on the horizontal component and to the nearest decimetre on the height. This is considered sufficient for the intention of this assessment.

Figure 8.13 illustrates the sky plot of the satellites during the survey at Point YB3 on DOY 356 2008 and the number of satellites that were used for the data processing. The average number of satellites observed during the survey was eight.

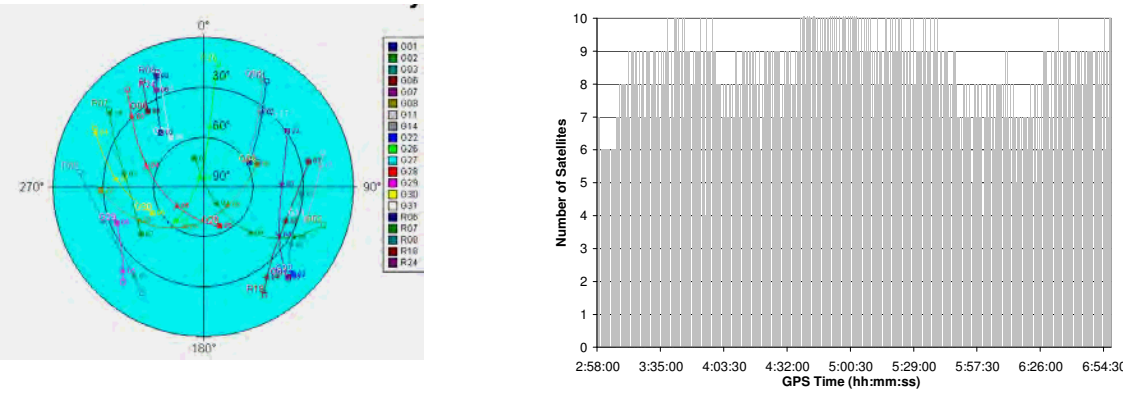

Figure 8.13: The trajectory of the visible satellite over the sky at Point YB3 (left plot); the number of satellites processed as a function of observations period (right plot).

IGS *Rapid* Products (latency of about 17 hours)

Figures 8.14 and 8.15 show the east, north and height errors with respect to the known coordinates for Point YB3 and the code and phase residuals using the IGS *Rapid* satellite orbit, clock and ionospheric corrections. Note that Figure 8.14 has a different scale from previous plots. Point YB3 is situated on open field with an unobstructed view of the sky. When these data were collected, the local time in Melbourne was around 14:00LT (i.e. 14:00LT to 18:00LT).

It can be inferred from this figure that the initial estimates vary greatly in the first 15 minutes of observations, which result in outliers in the scatter plot. This is caused by the initial (float) phase ambiguities and also the nature of the receiver used. Once the phase ambiguities stabilise, i.e. after 30 minutes into the observations, the solutions converge to be within 2m of the "ground truth". From Figures 8.14 and 8.15, it is apparent that the noise and residuals of the low-cost handheld receiver are quite large. This is not surprising as the quality of a low-cost handheld receiver is less than a GIS grade receiver. Even so, these results are very encouraging. It must be remembered that these data were collected in a very open environment. Therefore, there is no reason to suspect severe multipath effects.

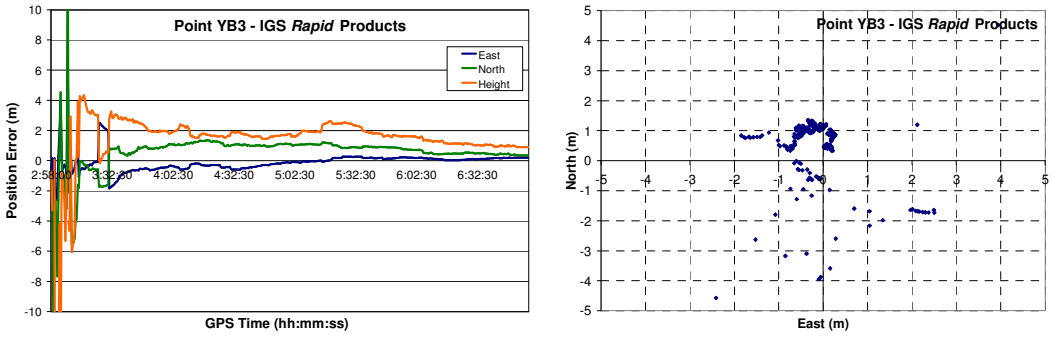

Figure 8.14: Point positioning results at Point YB3 in post-processing mode. Time series of the east, north and height errors on the left; scatter plot of the horizontal errors on the right.

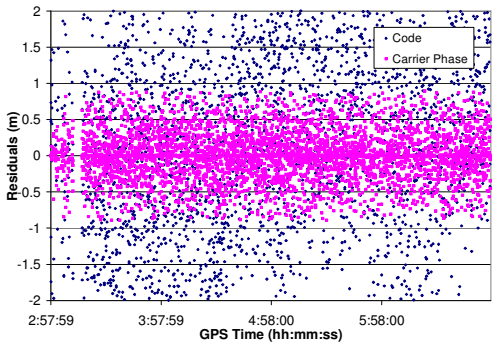

Figure 8.15: Code and carrier phase residuals at Point YB3 in post-processing mode.

The mean, STD and RMS values were calculated based on all the positioning results observed from the test and are tabulated in Table 8.8. There are a few decimetre biases on the east and north components and a metre level height bias, which were probably caused by the residual atmospheric errors. The deviation (RMS value) of the estimated positioning solutions based on the known values is 1.7m horizontally and 3.3m vertically. These results are quite remarkable considering the cost and type of receiver used.

Table 8.8: Mean, STD and RMS of the estimated positions at Point YB3 in post-processing mode.

Point YB3 – IGS *Rapid* Products			
	Mean (m)	**STD (m)**	**RMS (m)**
East	-0.11	0.79	0.79
North	0.55	1.44	1.54
Height	1.36	2.99	3.29

IGS *Ultra-Rapid (Predicted Half)* Products (Real-time)

In contrast to Figure 8.14, Figure 8.16 depicts the simulated real-time point positioning errors using the IGS *Ultra-Rapid (Predicted Half)* satellite orbit and clock corrections. The ionospheric effects were partially mitigated by utilising the Broadcast model with the broadcast ionospheric coefficients. The variation of the initial positioning solutions from the known values is quite significant. This finding is identical to those based on *Rapid* products. However, when using the predicted corrections, which are extrapolated from the observed orbits and clock information, a longer convergence time is needed for the solutions to be within 2m of the known values. Additionally, one can infer from the scatter plot presented in Figure 8.17 that the horizontal solutions using the Garmin 12 XL receiver are neither accurate nor precise. Nonetheless, the majority of the positioning estimates are within 2m of the known values. Figure 8.17 plots the code and phase measurement residuals.

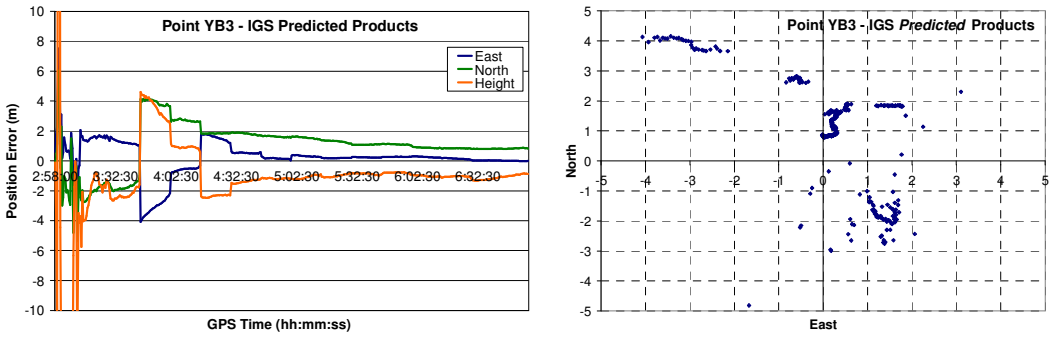

Figure 8.16: Point positioning results at Point YB3 in real-time mode. Time series of the east, north and height errors on the left; scatter plot of the horizontal errors on the right.

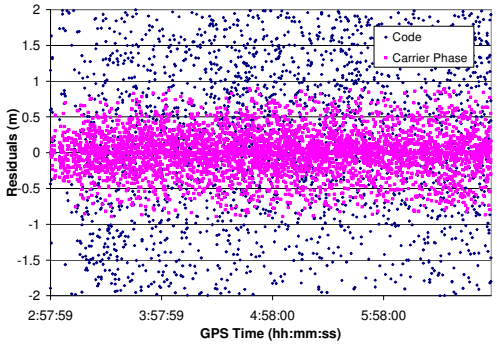

Figure 8.17: Code and carrier phase residuals at Point YB3 in real-time mode.

The statistics of the estimated positioning solutions at Point YB3 are tabulated in Table 8.9. The statistical results in this table reflect the real-time point positioning accuracy and precision, which are achievable by using a low-cost receiver. The quality of the estimated positioning solutions (in particular the height estimates) from a low-cost receiver is lower than those of using a medium-cost GIS grade receiver. This is due to the nature and capability of the GPS receivers to provide quality observation data, as well as the inefficiency of the Broadcast ionospheric model to completely model the ionospheric delay. The mean of the positioning solutions are accurate to about 1m from the known values. The deviation of the estimated positions from the known coordinates is 2.2m horizontally and about 3.6m vertically. These values can be considered comparable to the values obtainable from conventional code-based real-time DGPS. Of course, the results compiled from this study will not necessarily be typical for all low-cost handheld GPS types and the environments at which the data are collected. Nonetheless, these results can be considered as representative of the achievable point positioning accuracy based on single frequency PPP using low-cost handheld GPS receivers.

Table 8.9: Mean, STD and RMS of the estimated positions at Point YB3 in real-time mode.

Point YB3 – IGS *Ultra-Rapid (Predicted Half)* Products			
	Mean (m)	**STD (m)**	**RMS (m)**
East	0.24	1.18	1.20
North	1.00	1.58	1.87
Height	-1.38	3.32	3.59

8.3.2.2 Garmin GPSMap®76C

Data collected from a Garmin GPSMap®76C unit provided by NRCan were also analysed for this study. The 3 hour data were collected in Canada, on a stable pillar located in a fairly open area. The coordinates were determined using multi-receiver baselines processing and the coordinates are accurate to centimetre level. Although the data were collected in Canada, the numerical results were included in this thesis to further validate the attainable point positioning accuracy using a low-cost GPS receiver.

The low-cost GPS data were collected on DOY 095 2005. Although the data were collected at a sampling rate of 5 seconds, the data were “down-sampled” to 30 seconds.

Figure 8.18 shows the trajectory of the visible satellite at Point PIER13 during the survey (left plot), and the number of satellites used in the data processing (right plot). An average of five satellites was processed although there were a few occasions where only three GPS satellites were processed. It should be noted that a minimum of four satellites is required to compute positions in 3-dimensions, but as more satellites are observed, more redundancy in the solution will occur.

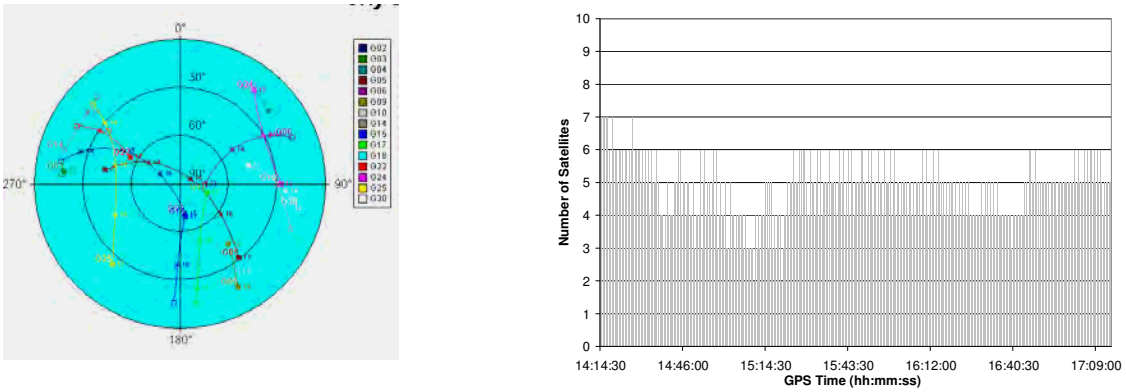

Figure 8.18: The trajectory of the visible satellites over the sky at Point PIER13 (left plot); the number of satellites processed as a function of observations period (right plot).

IGS *Rapid* Products (latency of about 17 hours)

The east, north and height errors and the code and phase residuals were computed and plotted in Figures 8.19 and 8.20. When these data were collected, the local time in Ottawa, Canada, is 5 hours behind UTC. These data were collected in the late morning (i.e. about 09:00LT to 12:00LT).

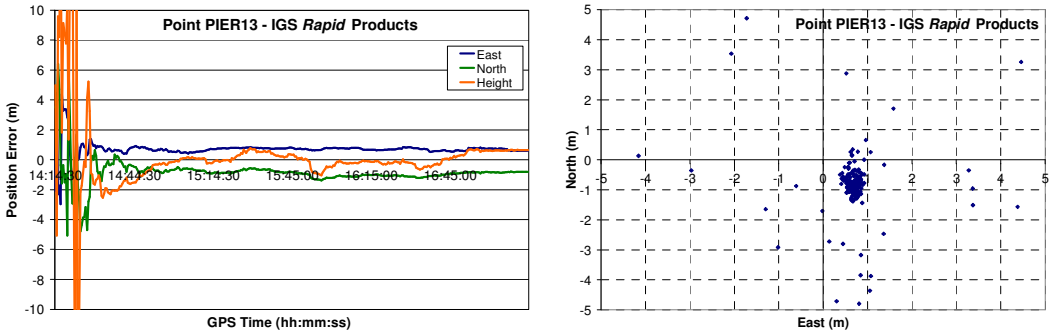

Figure 8.19: Point positioning results at Point PIER13 in post-processing mode. Time series of the east, north and height errors on the left; scatter plot of the horizontal errors on the right.

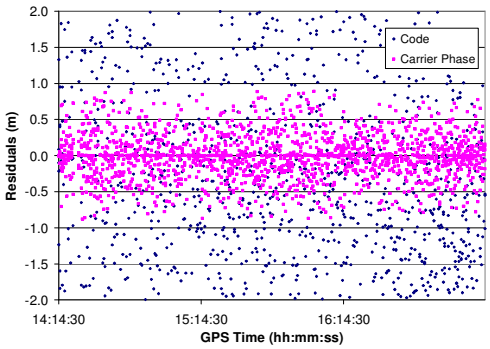

Figure 8.20: Code and carrier phase residuals at Point PIER13 in post-processing mode.

The statistical results for the estimated positions at Point PIER13 are presented in Table 8.10. The precision of the horizontal solutions is about 1m level, while the precision of the height solutions are about 3m. The mean of the horizontal and height components are well within 1m of the known coordinates.

Table 8.10: Mean, STD and RMS of the estimated positions at Point PIER13 in post-processing mode.

Point PIER13 – IGS *Rapid* Products			
	Mean (m)	**STD (m)**	**RMS (m)**
East	0.70	0.61	0.92
North	-0.83	0.94	1.26
Height	0.10	2.57	2.57

IGS *Ultra-Rapid (Predicted Half)* Products (Real-time)

Figure 8.21 and 8.22 illustrate the accuracy of the estimated positions and the code and phase residuals using the *Ultra-Rapid (Predicted Half)* products and the Broadcast model. The spread in the horizontal position solution ranges between 1m to 2 m with a few outliers.

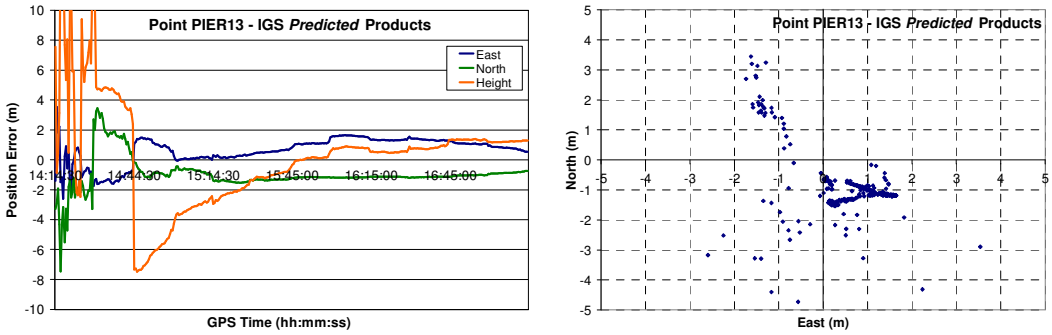

Figure 8.21: Point positioning results at Point PIER13 in real-time mode. Time series of the east, north and height errors on the left; scatter plot of the horizontal errors on the right.

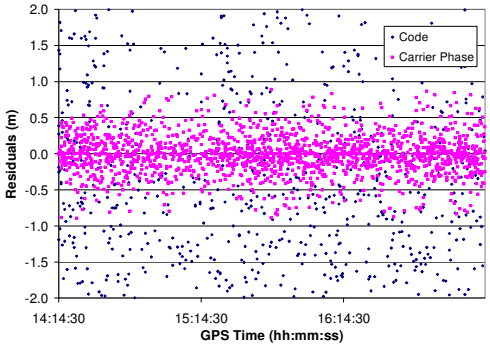

Figure 8.22: Code and carrier phase residuals at Point PIER13 in real-time mode.

The mean, STD and RMS were computed and tabulated in Table 8.11. The positioning bias is within 1m of the known values. The precision of the individual positioning estimates from the "true" values is less than 2m for the horizontal component and about 3.5m for the height component.

Table 8.11: Mean, STD and RMS of the estimated positions at Point PIER13 in real-time mode.

Point PIER13 – IGS *Ultra-Rapid (Predicted Half)* Products			
	Mean (m)	**STD (m)**	**RMS (m)**
East	0.64	0.89	1.09
North	-0.98	1.09	1.47
Height	0.21	3.44	3.45

8.4 Discussion

In order to aid with the discussion of the results, the statistical analysis of all the positioning results obtained from the single frequency GPS receivers tested in this study are combined and presented in Table 8.12 (next page). The numerical results are grouped into post-processing and real-time processing modes.

As expected, the estimated point positions using the medium-cost GPS receivers are more accurate and precise than those using the low-cost GPS receivers. This is mainly attributed to the quality of the receivers and antennas used. In addition, the accuracy of the positioning solutions in post-processing mode is generally higher than those of real-time. This can be explained by the quality of the satellite orbit and clock corrections, as well as the ionospheric corrections used. It can be inferred from Table 8.12 that the mean and RMS of the estimated horizontal and height positions (in post-processing mode) using the medium-cost receivers are within 0.1m to 0.8m of the known value. In the real-time processing scenario, the accuracy of the estimated positions decreases, particularly the horizontal positioning estimates. The mean and RMS values of the horizontal and height components using medium-cost receivers are around 1.2m to 2m. Nevertheless, these results are remarkable considering that only a single GPS receiver unit is required, and yet it is capable of providing comparable positioning accuracy as the code-based relative positioning technique.

One of the questions raised in this research is if it is possible to take advantage of a low-cost single frequency GPS receiver to achieve high accuracy point positioning using the single frequency PPP technique. Two low-cost, handheld, consumer grade GPS receivers that have a price tag of about AUD$400 were tested. The receivers were the Garmin 12 XL and Garmin GPSMap®76C. Observation data were collected at different locations and on different dates. The data from Garmin 12 XL (Point YB3) were collected in Australia, while

the data from Garmin GPSMap®76C (Point PIER13) were collected in Canada. The data analysis from the latter was included in this thesis to confirm the attainable point positioning accuracy using a low-cost receiver.

Table 8.12: Mean, STD and RMS of the horizontal and height components in both post-processing and real-time scenarios using the medium-cost and low-cost single frequency GPS receivers.

Statistical Results \ Receiver Type		Mean (m)			
		Post-Processing		Real-Time Processing	
		2D	Height	2D	Height
Medium-cost	Pathfinder®Pro XRS	0.36	-0.07	1.20	0.85
	Geoexplorer®GeoXH	0.26	-0.66	1.21	1.53
Low-cost	12 XL	0.56	1.36	1.03	-1.38
	GPSMap®76C	1.09	0.10	1.17	0.21
Statistical Results \ Receiver Type		**STD (m)**			
		Post-Processing		**Real-Time Processing**	
		2D	**Height**	**2D**	**Height**
Medium-cost	Pathfinder®Pro XRS	0.21	0.18	1.47	1.42
	Geoexplorer®GeoXH	0.22	0.31	0.46	0.65
Low-cost	12 XL	1.64	2.99	1.97	3.32
	GPSMap®76C	1.12	2.57	1.41	3.44
Statistical Results \ Receiver Type		**RMS (m)**			
		Post-Processing		**Real-Time Processing**	
		2D	**Height**	**2D**	**Height**
Medium-cost	Pathfinder®Pro XRS	0.41	0.19	1.90	1.65
	Geoexplorer®GeoXH	0.33	0.72	1.28	1.64
Low-cost	12 XL	1.73	3.29	2.22	3.59
	GPSMap®76C	1.56	2.57	1.83	3.45

It can be seen from Table 8.12 that the quality of the estimated positions at Point PIER13 (GPSMap®76C) is better than those from Point YB3 (12 XL) although fewer satellites were processed at Point PIER13. A few extreme outliers in the Point YB3 solutions are detected, which may have been a result of the receiver tracking and filtering mechanisms (refer to Figures 8.14 and 8.19 (post-processing mode); Figures 8.16 and 8.21 (real-time processing scenario) for comparison purposes). It is worth noting that the Garmin 12 XL receivers were discontinued as a commercial product a few years ago, and were replaced by the Garmin GPSMap®76c receivers. If the outliers are removed from the statistical computation and analysis, the results for Point YB3 would be comparable to those of Point PIER13. Nevertheless, it is encouraging to note that the low-cost handheld GPS receivers

tested in this study are quite capable of providing point positioning accuracy of about 1m (with a precision of better than 1.8m) in the horizontal component; and 1.4m vertical accuracy (with a precision of 3.3m) in post-processing mode. For real-time single frequency PPP using a low-cost handheld unit, the accuracy of the horizontal positions is 1.2m (with a precision of 2.2m) and the accuracy of the height component is about 1.4m (with a precision of 3.6m). In comparison with the quoted SPS accuracy, these results show an improvement of about one order of magnitude.

The results compiled in this study have been encouraging and appear to confirm the potential of using either medium-cost or low-cost single frequency GPS receiver to achieve high accuracy precise point positioning. It is interesting to discover that the low-cost receiver tested in this research, which has a price tag of approximately AUD$400, is quite capable of providing reasonably accurate point positioning solutions. It should be acknowledged that the numerical results would not necessarily be typical for all GPS data. The results may vary depending on factors such as the environment, time and date of the collected data, receiver model, quality of the antenna, and geometry of the satellites. Nevertheless, the results presented in this Chapter can be treated as plausible representatives of the achievable point positioning accuracy using the single frequency PPP technique.

8.5 Summary

As the global GPS market is becoming more competitive, high performance yet cost effective GPS positioning techniques and technologies will be desirable and be highly in demand. This study aimed to investigate the possibilities of using a single frequency GPS receiver and PPP, particularly a low-cost receiver unit, to achieve high accuracy precise point positioning in both real-time and post-processing modes. Since the quality of the point positions was the key focus in this study, the assessment of the results was performed by comparing the estimated point positions with the accurately known coordinates, which were treated as the “true” coordinates. The numerical results have been analysed, and discussions have been presented. As a general rule, the more accurate a GPS receiver positions and navigates, the more the receiver costs. Therefore, GPS users should note that the accuracy of the estimated positioning solutions is highly dependent on the cost and the quality of the receivers and antennas.

CHAPTER 9

Summary, Conclusions and Recommendations

9.1 Summary

This thesis has investigated numerous aspects of single frequency PPP, which may potentially improve the point positioning accuracy, precision, and time of convergence of this technique. A detailed account of the findings has also been presented. As described in Section 1.3, the primary aim is to examine effective measures and methodologies to provide the best point positioning solutions using the single frequency PPP technique. The aim has been met.

The specific contributions of this research can be summarised as follows:

- A comprehensive study of the impacts of setting different *a priori* observations sigma ratios on the overall point positioning accuracy and convergence behaviour.
- The identification and recommendation of an "optimal" *a priori* observations sigma ratio for single frequency PPP.
- The development of Australia-wide RIMs. These were tested for their effectiveness in improving the accuracy of the estimated point positioning solutions.
- A comprehensive analysis of single frequency PPP convergence behaviour and its relation to satellite clock correction rates, data sampling intervals, and tropospheric delay mitigation methods.
- The development of a procedure for single frequency PPP, which could provide the best possible point positioning quality.
- An assessment of the effects of applying various IGS satellite orbit and clock products in single frequency PPP. The products were assessed in terms of the effects of the product latency and accuracy on the quality of the estimated single frequency PPP solutions.

- The evaluation of the IGS real-time and near real-time satellite orbit and clock corrections for high accuracy point positioning.
- A better understanding of the possibilities of using medium-cost and low-cost GPS receivers to achieve high accuracy point positioning in simulated real-time and post-processing modes.

9.2 Conclusions

9.2.1 *A Priori* Observations Sigma Ratio

It was discovered that the *a priori* code and quasi-phase measurements sigma ratio has a significant effect on the accuracy and precision of the estimated single frequency PPP solutions, as well as the solutions convergence time. The processing software utilises the single frequency ionosphere-free quasi-phase measurements, in addition to the code measurements. This complicates the weighting process of the code and quasi-phase measurements in the adjustment model.

A comprehensive study was undertaken to examine the contributions of setting a range of different *a priori* observations sigma ratios in the single frequency PPP adjustment model. It is concluded that if the quasi-phase measurements are given a high weighting, the solutions will follow the more precise but ambiguous quasi-phase measurements, which then affects the time of convergence. However, such a setting appears to be beneficial in terms of the solutions accuracy and convergence behaviour during high ionospheric activity periods. This is attributed to the ionosphere-free quasi-phase measurements, which dominate the PPP solutions.

In contrast, if the quasi-phase measurements are given a low weighting, the positioning solutions will follow the less precise but unambiguous code measurements. This is desirable during the ionospheric benign periods, but not during the periods of high ionospheric activities. Nonetheless, an *a priori* code and quasi-phase sigma ratio of ~1:50 is found to be an optimal ratio regardless of the receiver location and varying ionospheric conditions. This ratio has been demonstrated to provide the best positioning accuracy without sacrificing the solution convergence time.

9.2.2 Ionospheric Effects

Australia-wide RIMs with different temporal resolutions were developed to validate the effectiveness of applying the RIMs to improve the accuracy of the estimated point positions. The evaluation of the ionosphere maps was done by comparing the positioning solutions from using the RIMs to those based on the Broadcast model and also the GIMs. The results from this study indicated that the Australia-wide RIMs could help to improve the accuracy of the height estimations for low latitude stations. However, for most practical purposes, the use of the GIMs is still preferred as it provides better horizontal positioning accuracy regardless of the location of the receiver.

9.2.3 Convergence Analysis

A comprehensive analysis of the impacts of using different satellite clock correction rates, data sampling intervals, and tropospheric delay mitigation methods on single frequency PPP convergence behaviour has been conducted. There was no evidence to show that high rate satellite clock corrections will have a significant impact on the single frequency PPP solutions convergence time. The standard 5-minute satellite clock corrections with a simple, in-built satellite clock interpolation method are sufficient. In addition, it was also discovered that, for single frequency PPP in static mode, data with high sampling intervals only act as redundancies, and thus, have minimal effects on the solutions convergence behaviour. For this reason, a data sampling interval of 30-seconds is adequate for single frequency PPP static applications.

Another component of this analysis examined the implications of either modelling the tropospheric delay using an empirical model or estimating the delay as an unknown as part of the PPP solutions. The effects of using either the default or observed surface meteorological measurements as initial parameters were also analysed. It was concluded that the preferred method to correct for the tropospheric delay in single frequency PPP is to model the error using an empirical model, in parallel with the software default meteorological parameters. Estimating the tropospheric delay as part of the solutions adds strain to the solutions convergence behaviour, and also degrades the accuracy and precision of the estimated positioning solutions.

9.2.4 Impacts of using Different IGS Satellite Orbits and Clocks

The quality of the satellite positions and clock corrections plays a vital role in determining the accuracy of the PPP solutions. At present, the IGS orbit and clock correction products come in four types, namely the *Final*, *Rapid*, *Ultra-Rapid (Estimated Half)*, and *Ultra-Rapid (Predicted Half)*. These products vary in the accuracy and the latency of the corrections. The quality of the IGS precise *Final* and *Rapid* satellite orbit and clock corrections has proven to be excellent, providing the best point positioning accuracy. For most practical purposes, the users will not notice any significant discrepancy between the point positioning results from using the IGS *Final* or *Rapid* satellite orbit and clock products. The *Ultra-Rapid (Estimated Half)* and *Ultra-Rapid (Predicted Half)* products, which have been made available by the IGS since late 2000, allow PPP processing in near real-time and real-time modes. The results from this study have demonstrated that the IGS predicted orbit and clock corrections can be used to obtain high accuracy point positioning in real-time. It was shown, in a simulated real-time scenario that, horizontal and height positioning accuracy of 1m can be obtained after a one hour observation period. The single frequency PPP positioning solutions based on the near real-time *Ultra-Rapid (Estimated Half)* satellite orbit and clock corrections were also favourable. The deviation of the positioning solutions based on the *Ultra-Rapid (Estimated Half)* and *Rapid* products were in fact minimal.

9.2.5 Single Frequency PPP Accuracy and Performance

As the global GPS market is becoming more competitive, high performance yet cost effective GPS positioning techniques and technologies will be desirable and be highly in demand. The capability of single frequency PPP was validated in this research using single frequency GPS data collected from three different types of receiver, namely geodetic grade, medium-cost (GIS grade) and low-cost receivers. It has been shown that single frequency PPP is capable of achieving 0.2m-0.3m horizontal accuracy and 0.5m-1m height accuracy. These results were accomplished by using single frequency data from geodetic quality GPS receivers. PPP is an attractive point positioning technique because it is autonomous, seamless, consistent, and the procedures are independent of the location of the GPS receiver.

The performance of single frequency PPP using medium-cost and low-cost consumer grade GPS receivers has been investigated. The point position estimates based on PPP processing has been compared with a set of accurately known coordinates. The positioning

solutions from the medium-cost GIS grade receivers were generally in good agreement with the known coordinates. Point positioning accuracy better than 0.3m horizontally and 0.7m vertically was obtained in post-processing mode using a medium-cost receiver. For real-time positioning, coordinates accuracy of about 1m to 2m was achieved. These findings are encouraging as the price of the medium-cost GIS grade receivers is fairly economical for a myriad of GPS applications. In addition, remarkable point positioning results have also been obtained when using a low-cost GPS receiver in single frequency PPP. Point positioning accuracy of about 1m to 1.5m was achieved in both real-time and post-processing modes. However, it should be noted that the precision of the estimated positioning solutions in the real-time scenario are generally worse than the post-processed solutions.

The quality of the estimated single frequency PPP solutions has also been evaluated based upon the number of epochs required before the solutions converge to decimetre level accuracy. This is a result of the phase ambiguity terms, which are estimated in PPP as float values. In general, half an hour to an hour is required for the static single frequency PPP to converge within 1m of the known values.

9.3 Recommendations

The single frequency PPP approach has demonstrated promising results in the field of high accuracy GPS point positioning. This thesis has also examined numerous facets of single frequency PPP, which could potentially improve the performance of this technique. There are many future research topics in single frequency PPP, which are worthwhile to explore. A few recommendations are as follows:

- ***A priori* measurements sigma value and ratio.** It is recommended to test the feasibility of the *a priori* code and quasi-phase measurements sigma ratio of ~1:50 using GPS data collected from around the world. Additionally, the selection of realistic measurements weighting for different receiver types and locations requires further study. This can be done by analysing the effects on the residuals, the estimated parameters, and the *a posteriori* variance covariance matrix in the adjustment model.
- **Single frequency PPP in kinematic mode.** The emphasis of this research has been purely on single frequency PPP processing in static mode. A similar study needs to focus on kinematic applications. It has been demonstrated that a sequential least squares filter could generate optimal results for static processing. However, for (real-time) kinematic processing, the Kalman filter may be more suitable.

- **Quality control.** Dealing with carrier phase measurements typically in real-time kinematic applications, requires robust quality control algorithms. These include cycle slip detection and correction, as well as multipath reduction. It is strongly recommended to undertake an in-depth investigation on the quality control algorithms.
- **Ionospheric effects.** The ionospheric delay remains as a major error source in achieving high accuracy point positioning using a single frequency GPS receiver. Any improvement in the ionospheric error mitigation methods will clearly be beneficial to single frequency PPP users. Recommended work includes, but is not limited to, residual ionospheric delay estimation, and improving the latency and accuracy of the ionospheric maps by increasing the spatial and temporal resolution of the maps.
- **Real-time implementation.** It has been shown that point positioning accuracy of 1m - 2m can be achieved using real-time (simulated) single frequency PPP. It is anticipated that PPP implementation for real-time applications will have a high demand in the near future. Additional testing is strongly recommended to further validate the performance of single frequency PPP, typically in real-time scenario using data streaming from wireless Internet. An effective satellite clock interpolation strategy is also considered necessary to effectively interpolate the 15-minute and 5-minute clock corrections from the IGS.
- **Future generation GNSS systems and modernisations.** With the emergence of new GNSS systems like the "modernised" GLONASS and Galileo (the European GNSS) systems, it will be interesting to investigate the possible signal combinations in order to enhance the performance of both dual frequency and single frequency PPP.

As a final commentary, this research has been a unique study of a novel standalone point positioning technique, which takes advantage of the more economical single frequency GPS receivers to achieve high accuracy point positioning. There is no doubt that future development in algorithms, functional and stochastic modelling, as well as advancement in GPS technology and its associated products will continue to improve the PPP solutions integrity, convergence, accuracy, and precision.

References

Abdel-salam M. (2005) Precise Point Positioning Using Un-Differenced Code and Carrier Phase Observations, *PhD thesis*, The University of Calgary, Canada.

Alkan R. M., El-Rabbany A. and Saka M. H. (2006) Assessment of Low-Cost Garmin OEM GPS Receiver for Surveying Applications, *Ontario Professional Surveyor*, vol. 49, no. 4, pp. 14-16.

Alkan R. M., El-Rabbany A. and Saka M. H. (2007) Low Cost, Single-Frequency GPS For Surveying, *Location*, vol. March-April.

American Society of Civil Engineers (2000) *NAVSTAR Global Positioning System Surveying*, American Society of Civil Engineers Publications.

Anderle R. J. (1976) Point Positioning Concept Using Precise Ephemeris, *Proceedings of International Geodetic Symposium*, Las Cruces, New Mexico, 12-14 October, pp. 47-75.

Anderson D. N., Forbes J. M. and Codrescu M. (1989) A Fully Analytical, Low-and Middle-Latitude Ionospheric Model, *Journal of Geophysical Research*, vol. 94.

Andersson J. V. (2006) Undifferenced GPS for Deformation Monitoring, *PhD thesis*, Royal Institute of Technology, Stockholm, Sweden.

Appleton E. V. (1954) The Anomalous Equatorial Belt in The F2-Layer, *Journal of Atmospherics and Terrestrial Physics*, vol. 5, pp. 348-351.

Arbesser-Rastburg B. (2006) *The Galileo Single Frequency Ionospheric Correction Algorithm*, <http://sidc.oma.be/esww3/presentations/Session4/Arbesser.pdf> (January 2007).

Ashby N. (2007) *Relativity in the Global Positioning System*, <http://relativity.livingreviews.org/Articles/lrr-2003-1/> (April 2008).

Ashby N. and Spilker Jr. J. (1996) *Introduction to Relativistic Effects on the Global Positioning System*, in BW Parkinson, JJ Spilker Jr., P Axelrad and P Enge, *Global Positioning System: Theory and Applications Volume 1*, American Institute of Aeronautics and Astronautics, Inc., Washington, DC, vol. 1, pp. 623-715.

AUSPOS (2006) *AUSPOS-Online GPS Processing Service*, <http://www.ga.gov.au/bin/gps.pl> (November 2006).

Bar-Sever Y. and Muellerschoen R. (2003) NASA's Global Differential GPS System, *Geophysical Research Abstract*, vol. 5, no. 07885.

Basu S., MacKenzie E. and Basu S. (1988) Ionospheric Constraints on VHF/UHF Communications Links During Solar Maximum and Minimum Periods, *Radio Science*, vol. 23, no. 3, pp. 363-378.

Bent R. B., Llewellyn S. K. and Walloch M. K. (1972) *Description and Evaluation of the Bent Ionospheric Model*, DBA Systems, Melbourne, Florida.

Beran T. (2008) Single-frequency, Single-receiver Terrestrial and Spaceborne Point Positioning, *PhD thesis*, University of New Brunswick, Canada.

Beran T., Kim D. and Langley R. (2003) High-Precision Single-Frequency GPS Point Positioning, *Proceedings of ION GNSS 16th International Technical Meeting of the Satellite Division*, Portland, Oregon, 9-12 September.

Beran T., Bisnath S. B. and Langley R. B. (2004) Evaluation of High-Precision, Single-Frequency GPS Point Positioning Models, *Proceedings of ION GNSS 17th International Technical Meeting of the Satellite Division*, Long Beach, CA, pp. 1893-1901.

Beran T., Langley R., Bisnath S. B. and Serrano L. (2007) High-Accuracy Point Positioning With Low-Cost GPS Receivers, *Journal of Navigation*, vol. 54, no. 1, pp. 53-63.

Beutler G., Mueller I. and Niell A. (1994) The International GPS Service for Geodynamics (IGS): Development and Start of Official Service on 1 January 1994, *Manuscripta Geodaetica*, vol. 68, pp. 43-51.

Bilitza D. (2001) International Reference Ionosphere 2000, *Radio Science*, vol. 36, no. 2, pp. 261-275.

Bisnath S. B. (2004) Precise Orbit Determination of Low Earth Orbiters With a Single GPS Receiver-Based, Geometric Strategy, *PhD thesis*, University of New Brunswick, Canada.

Bisnath S. B. and Gao Y. (2007) Current State of Precise Point Positioning and Future Prospects and Limitations, *Proceedings of International Union of Geodesy and Geophysics (IUGG) 24th General Assembly*, Perugia, Italy, 2-13 July.

Bisnath S. B. and Langley R. B. (2002) High-Precision, Kinematic Positioning with a Single of GPS Receiver, *NAVIGATION: Journal of The Institute of Navigation*, vol. 49, no. 3, pp. 161-169.

Bisnath S. B., Langley R. and Beran T. (2002) Precise Platform Positioning with a Single GPS Receiver, *GPS World*, vol. 13, no. 4, pp. 42-49.

Brunner F. K. and Tregoning P. (1994) Tropospheric Propagation Effects in GPS Height Results Using Meteorological Observations, *Australian Journal of Geodesy, Photogrammetry and Surveying*, vol. 60, pp. 49-65.

Caissy M. (2007) *[IGSMAIL-5616]: Announcing A Call for Participation in the IGS Real-time Pilot Project*, <http://igscb.jpl.nasa.gov/mail/igsmail/2007/msg00096.html> (May 2007).

Camargo P. O., Monico J. F. G. and Ferreira L. D. D. (2000) Application of Ionospheric Corrections in the Equatorial Region for L1 GPS Users, *Earth Planets Space*, vol. 52, pp. 1083-1089.

CDGPS (2009) *Canada-wide Differential GPS (CDGPS)*, <http://www.cdgps.com> (January 2009).

Chao C. C. (1974) The Tropospheric Calibration Model for Mariner Mars 1971, *JPL Technical Report*, pp. 61-76.

Chen K. and Gao Y. (2005) Real-Time Precise Point Positioning Using Single Frequency Data, *Proceedings of ION GNSS 18th International Technical Meeting of the Satellite Division*, Long Beach, CA, 13-16 September, pp. 1514-1523.

Chiu Y. T. (1975) An Improved Phenomenological Model of Ionospheric Density, *Journal of Atmospheric and Terrestrial Physics*, vol. 37.

Choy S, Zhang K, Silcock D. and Wu F. (2007) Precise Point Positioning - A Case Study in Australia, *Proceedings of the Spatial Sciences Institute Biennial International Conference*, Hobart, Australia, 14-18 May.

Choy S., Zhang K. and Silcock D. (2008a) An Evaluation of Various Ionospheric Error Mitigation Methods used in Single Frequency PPP, *Journal of Global Positioning Systems*, vol. 7, no. 1, pp. 62-71.

Choy S., Zhang K., Silcock D. and Holden L. (2008b) An Empirical Approach to Study the Effects of *A Priori* Observations Sigma Ratio in Single Frequency Precise Point Positioning, *Proceedings of The International Symposium of GPS/GNSS*, Odaiba, Tokyo, Japan, 11-14 November.

Choy S., Zhang K., Silcock D. and Holden L. (2008c) Feasibility of Using Regional Ionosphere Maps in Single Frequency Precise Point Positioning: A Case Study in Australia, *Proceedings of The International Symposium of GPS/GNSS*, Odaiba, Tokyo, Japan, 11-14 November.

CODE (2007) *Global Ionosphere Maps Produced by CODE*, <http://www.aiub.unibe.ch/content/research/gnss/code___research/igs/global_ionosphere_maps_produced_by_code/index_eng.html> (January 2007).

Collins P. and Langley R. (1999) Possible Weighting Scheme for GPS Carrier Phase Observations in the Presence of Multipath, *Contract report DAAH04-96-C-0086/TCN 98151 for the United States Army Corps of Engineers Tropographic Engineering Centre*.

Collins P., Lahaye F., Kouba J. and Héroux P. (2001) Real-Time WADGPS Corrections from Undifferenced Carrier Phase, *Proceedings of ION National Technical Meeting*, Long Beach, California, 22-24 January.

Colombo O. L. (2007) *Canadian Space Geodesy Forum: Problem of Using IGS Precise Satellite Orbit Data*, <https://listserv.unb.ca/cgi-bin/wa?A2=ind0705&L=canspace&P=2291> (May 2008).

Colombo O. L., Sutter A. W. and Evans A. G. (2004) Evaluation of Precise, Kinematic GPS Point Positioning, *Proceedings of ION GNSS 17th International Technical Meeting of the Satellite Division*, Long Beach, CA, 21-24 September 2004, pp. 1423-1430.

Cross P. (1983) *Advanced Least Squares Applied to Position-Fixing*, Working Paper No.6, Department of Land Surveying, North East London Polytechnic, London.

Davis J. L., Herring T. A., Shapiro I. I., Rogers A. E. E. and Elgered G. (1985) Geodesy by Radio Interferometry: Effects of Atmospheric Modeling Errors on Estimates of Baseline Length, *Radio Science*, vol. 20, no. 6, pp. 1593-1607.

Dawson J. and Steed J. (2004) *International Terrestrial Reference Frame (ITRF) to GDA94 Coordinate Transformations*, <http://www.ga.gov.au/image_cache/GA3795.pdf> (November 2007).

Deakin R. E. (2005) *Notes of Least Squares*, School of Mathematical and Geospatial Science, RMIT University, Melbourne, Australia.

Dixon K. (2006) StarFire: A Global SBAS for Sub-Decimetre Precise Point Positioning, *Proceedings of 19th International Technical Meeting of the Satellite Division*, Fort Worth, Texas, 26-29 September 2006, pp. 2286-2296.

Dow J. M., Neilan R. E. and Gendt G. (2005) The International GPS Service (IGS): Celebrating the 10th Anniversary and Looking to the Next Decade, *Advances in Space Research*, vol. 36, no. 3, pp. 320-326.

El-Rabbany A. (2006) *Introduction to GPS: The Global Positioning System* (2nd edition), Artech House, Boston, MA.

Farret J. and Santos M. (2001) An Alternative Method for Detection and Mitigation of Static Multipath in L1 Carrier Phase Measurements, *Proceedings of ION National Technical Meeting*, Long Beach, USA, 22-24 January.

Feltens J. (1998) Chapman Profile Approach For 3D Global TEC Representation, *Proceedings of the IGS Analysis Centres Workshop*, Darmstadt, Germany, 9-11 February, pp. 285-297.

Feltens J. (2003) The Activities of the Ionosphere Working Group of the International GPS Service (IGS), *GPS Solutions*, vol. 7, no. 1, pp. 41-46.

Fu W., Han S. and Rizos C. (1999) Real-Time Ionospheric Scintillation Monitoring, *Proceedings of ION GPS 12th International Technical Meeting of The Satellite Division of The Institute of Navigation*, Nashville, Tennessee, 14-17 September.

Gálan A. T. (2002) *Obtaining Raw Data From Some Garmin Units*, <http://artico.lma.fi.upm.es/numerico/miembros/antonio/async/> (December 2008).

Gao Y. (2006) *P³ Software Package*, <http://www.ucalgary.ca/~ygao/p3.htm> (January 2007).

Gao Y., Hèroux P. and Kouba J. (1994) Estimation of GPS Receiver and Satellite L1/L2 Signal Delay Biases Using Data From CACS, *Proceedings of The International Symposium on Kinematic Systems in Geodesy, Geomatics and Navigation*, Banff, Canada, pp. 109-117.

Gao Y. and Shen X. (2001) Improving Ambiguity Convergence in Carrier Phase-Based Precise Point Positioning, *Proceedings of ION GPS 2001*, Salt Lake City, UT, 11-14 September 2001, pp. 1532-1539.

Gao Y. and Shen X. (2002) A New Method for Carrier-Phase-Based Precise Point Positioning, *Journal of the Institute of Navigation*, vol. 49, no. 2, pp. 109-116.

Gao Y. and Liu Z. (2002) Precise Ionosphere Modelling Using Regional GPS Network Data, *Journal of Global Positioning Systems*, vol. 1, no. 1, pp. 18-24.

Gao Y. and Wojciechowski A. (2004) *High Precision Kinematic Positioning using Single Dual-Frequency GPS Receiver*, <http://www.isprs.org/istanbul2004/comm3/papers/387.pdf> (October 2006).

Gao Y. and Garin L. (2006) *GNSS Solution: Precise Point Positioning and Its Challenges, Aided-GNSS and Signal Tracking*, <http://www.insidegnss.com/pdf/12-06-GNSSSol.pdf> (December 2006).

Gao Y., Zhang Y. and Chen K. (2006) Development of a Real-Time Single Frequency Precise Point Positioning System and Test Results, *Proceedings of ION GNSS 19th International Technical Meeting of the Satellite Division*, Fort Worth, Texas, pp. 2297-2303.

Garmin Limited (2008) *GPSMAP® 76C*, <https://buy.garmin.com/shop/shop.do?pID=251> (September 2008).

Ge M. and Gendt G. (2005) Estimation and Validation of The IGS Absolute Antenna Phase Center Variations, *Proceedings of the IGS 2004 Workshop and Symposium*, Berne, Switzerland, pp. 209-219.

Ge M., Gendt G., Rothacher M., Shi C. and Liu J. (2007) Resolution of GPS Carrier-Phase Ambiguities in Precise Point Positioning (PPP) with Daily Observations, *Journal of Geodesy*, vol. 82, no. 7, pp. 389-399.

Gendt G. (2006) *[IGSMAIL-5438]: IGS Switch to Absolute Antenna Model and ITRF 2005*, <http://igscb.jpl.nasa.gov/mail/igsmail/2006/msg00161.html> (November 2006).

Gendt G. and Schmid R. (2005) *[IGSMAIL-5189]: Planned Changes to IGS Antenna Calibrations*, <http://igscb.jpl.nasa.gov/mail/igsmail/2005/msg00111.html> (May 2008).

Georgiadou Y. and Kleusberg A. (1988) On Carrier Signal Multipath Effects in Relative GPS Positioning, *Manuscripta Geodaetica*, vol. 13(3), pp. 172-179.

Geoscience Australia (2008) *Australian Regional GPS Network*, <http://www.ga.gov.au/geodesy/argn/> (January 2008).

GFZ (2008) *IGS Analysis Center Coordinator (ACC) at GFZ Potsdam*, <http://www-app2.gfz-potsdam.de/pb1/igsacc/> (June 2008).

Hartinger H. and Brunner F. K. (1999) Variance of GPS Phase Observations: the Sigma Model, *GPS Solutions*, vol. 3, no. 4, pp. 39-47.

Hathaway D. (2008) *Solar Physics - The Sunspot Cycle*, <http://solarscience.msfc.nasa.gov/SunspotCycle.shtml> (January 2008).

Hernández-Pajares M. (2003) *Performance of IGS Ionosphere TEC Maps - IGS Iono WG Report (March 2003)*, <http://maite152.upc.es/~ionex3/doc/IGS_IONO_report_April2003_7.pdf> (March 2008).

Hernández-Pajares M. (2004) IGS Ionosphere WG Status Report: Performance of IGS Ionosphere TEC Maps (Position Paper), *Proceedings of International GNSS Service Workshop and Symposium*, Berne, Switzerland, 1-5 March.

Hernández-Pajares M. (2005) *International GNSS Service Working Group: Ionospheric Products*, <http://gage152.upc.es/~ionex3/igs_iono/igs_iono.html> (October 2008).

Hernández-Pajares M. (2008) *Private Communication (Email)*, Research Group of Astronomy and Geomatics, Technical University of Catalonia, 3 June.

Hernández-Pajares M., Juan J. M., Sanz J. and Colombo O. L. (1999) Precise Ionospheric Determination and its Application to Real-Time GPS Ambiguity Resolution, *Proceedings of ION GPS 1999*, Nashville, TN, 14-17 September 1999, pp. 1409-1417.

Hèroux P. and Kouba J. (2001) GPS Precise Point Positioning Using IGS Orbit Products, *Physics and Chemistry of the Earth Part A*, vol. 26, no. 6-8, pp. 573-578.

Hèroux P., Gao Y., Kouba J., Lahaye F., Mireault Y., Collins P., Macleod K., Tétreault P. and Chen K. (2004) Products and Applications for Precise Point Positioning - Moving Towards Real-Time, *Proceedings of ION GNSS 17th International Technical Meeting of the Satellite Division*, Long Beach, CA, 21-24 September 2004, pp. 1832-1843.

Herring T. A. (1992) Modelling Atmospheric Delays in the Analysis of Space Geodetic Data, *Proceedings of ION GPS-97*, Kansas City, Missouri, pp. 251-259.

Hofmann-Wellenhof B., Lichtengegger H. and Collins J. (2001) *GPS Theory and Practice* (5th edition), Springer-Verlag Wien New York.

Hopfield H. S. (1969) Two-Quartic Tropospheric Refractivity Profile for Correcting Satellite Data, *Journal of Geophysical Research*, vol. 74, no. 18, pp. 4487-4499.

Huang Y. N. and Cheng K. (1991) Ionospheric Disturbances at the Equatorial Anomaly Crest Region During the March 1989 Magnetic Storm, *Journal of Geophysical Research*, vol. 96, no. A8, pp. 13953-13965.

Hugentobler U. (2004) *CODE High Rate Clocks (IGSmail-4913)*, <http://igscb.jpl.nasa.gov/mail/igsmail/2004/msg00136.html> (May 2007).

Hugentobler U. (2005) *High-Rate GPS Satellite Clock Corrections*, <https://listserv.unb.ca/cgi-bin/wa?A2=ind0510&L=canspace&T=0&P=3776> (January 2007).

Hugentobler U., Dach R., Fridez P., and Meindl M. (2007) *Bernese GPS Software Version 5.0*, Astronomical Institute, University of Berne.

ICD-GPS-200c-004 (2000) *GPS Interface Control Document*, ARINC Research Corporation, CA, USA.

ICSM (1998) *Geocentric Datum of Australia Technical Manual, Version 2.2*, < http://www.icsm.gov.au/gda/gdatm/gdav2.3.pdf> (December 2006).

IERS (2004) IERS Annual Report 2004, W Dick and B Richter, International Earth Rotation and Reference System Service, Verlag des Bundesamts für Kartographie und Geodäsie, Frankfurt am Main, Germany.

IGS (2008) *International GNSS Service*, <http://igscb.jpl.nasa.gov/> (June 2008).

IGS Real-Time Working Group (2007) *The IGS Real-time Working Group Terms of Reference*, <http://www.rtigs.net/pdf/charter.pdf> (November 2008).

ITRF (2008) *International Terrestrial Reference Frame*, <http://itrf.ensg.ign.fr/> (March 2008).

Janssen V., Roberts C., Rizos C. and Abidin H. (2002) Low-cost GPS-based Volcano Deformation Monitoring at Mt. Papandayan, Indonesia, *Journal of Volcanology and Geothermal Research*, vol. 115, no. 1-2, pp. 139-151.
JPL (2006) *The Automated GIPSY Interface for the Mail-in User*, <http://milhouse.jpl.nasa.gov/ag/> (May 2007).

JPL (2007) *The NASA Global Differential GPS System*, <http://www.gdgps.net/index.html> (July 2008).

Khattanov B., Murphy M., Gnedin M., Cruickshank B., Boisvert J., Sheffel J., Jayaraman V., Yudin V. and Fuller-Rowell T. (2004) An Ionospheric Forecasting System, *Proceedings of ION GNSS 17th International Technical Meeting of the Satellite Division*, Long Beach, CA, 21-24 September, pp. 408-419.

Kleusberg A. and Teunissen P. (1996) *Lecture Notes In Earth Sciences: GPS For Geodesy,* Springer Verlag, Berlin.

Klobuchar J. A. (1987) Ionospheric Time-Delay Algorithm for Single-Frequency GPS Users, *IEEE Transactions on Aerospace and Electronic Systems*, vol. AES-23, no. 3, pp. 325-331.

Klobuchar J. A. (1991) Ionospheric Effects on GPS, *GPS World*, vol. 2, no. 4, pp. 43-51.

Klobuchar J. A. (1996) *Ionospheric Effects on GPS*, in BW Parkinson, JJ Spilker Jr., P Axelrad and P Enge, *Global Positioning System: Theory and Applications Volume 1*, American Institute of Aeronautics and Astronautics, Inc., Washington, DC, vol. 1, pp. 485-516.

Klobuchar J. A., Doherty P. and El-Arini B. (1995) Potential Ionospheric Limitations to GPS Wide-Area Augmentation System, *Journal of the Institute of Navigation*, vol. 42, no. 2, pp. 353-370.

Komjathy A. (1997) Global Ionospheric Total Electron Content Mapping Using The Global Positioning System, *PhD thesis*, University of New Brunswick, Canada.

Kouba J. (2003) *A Guide to using International GPS Service (IGS) Products*, <ftp://igscb.jpl.nasa.gov/igscb/resource/pubs/GuidetoUsingIGSProducts.pdf> (April 2006).

Kouba J. and Hèroux P. (2000) *GPS Precise Point Positioning Using IGS Orbit Products*, <http://www.geod.nrcan.gc.ca/publications/papers/abs3_e.php> (April 2006).

Kouba J. and Hèroux P. (2001) Precise Point Positioning Using IGS Orbit and Clock Products, *GPS Solutions*, vol. 5, no. 2, pp. 12-28.

Krakiwsky E. (1976) A Synthesis of Recent Advances in the Method of Least Squares, Technical Report No.42, Department of Surveying Engineering, University of New Brunswick, Fredericton, Canada.

Kunches J. M. (2000) In the Teeth of Cycle 23, *Proceedings of 13th International Technical Meeting of The Satellite Division of The Institute of Navigation*, Salt Lake City, Utah, 19-22 September.

Lahaye F., Caissy M., Héroux P., Macleod K. and Popelar J. (1997) Canadian Active Control System Real-Time GPS*Correction Service Performance Review, *Proceedings of National Technical Meeting of the Institute of Navigation*, Santa Monica, California, 14-16 January.
Lanyi G. (1984) Tropospheric Delay Effects in Radio Interferometry, *Telecommunication and Data Acquisition (TDA) Progress Report 42-78*, Jet Propulsion Laboratory, Pasadena, California, pp. 152-159.

Le A. Q. (2004) Achieving Decimetre Accuracy with Single Frequency Standalone GPS Positioning, *Proceedings of ION GNSS 17th International Technical Meeting of the Satellite Division*, Long Beach, CA, pp. 1881-1891.

Le A. Q. and Tiberius C. C. J. M. (2006) Single-Frequency Precise Point Positioning with Optimal Filtering, *GPS Solutions*, vol. 11, no. 1, pp. 61-69.

Leick A. (2004) *GPS Satellite Surveying* (3rd edition), John Wiley & Sons, Inc., New Jersey.

Llewellyn S. K. and Bent R. B. (1973) Documentation and Description of The Bent Ionospheric Model, Technical Report AFCRL-TR-73-0657.

Magellan Navigation Incorporation (2008) *Magellan Professional, News and Events: Magellan and Ashtech to become a new $125 Million Satellite Navigation, Positioning and Communications Products Company*, <http://pro.magellangps.com/en/news/releases/viewRelease.asp?id=179> (September 2008).

Malys S., Larezos M., Gottschalk S., Mobbs S., Winn B., Feess W., Menn M., Swift E., Merrigan M. and Mathon W. (1997) The GPS Accuracy Improvement Initiative, *Proceedings of ION GPS-97*, Kansas City, Missouri, 16-19 September, pp. 375-384.

Mannucci A. J., Wilson B. D., Yuan D. N., Ho C. H., Lindqwister U. J. and Runge T. F. (1998) A Global Mapping Technique for GPS-Derived Ionospheric Total Electron Content Measurements, *Radio Science*, vol. 33, pp. 565-582.

Masella E. (1999) Achieving 20 cm Positioning accuracy in Real Time Using GPS - the Global Positioning System, *GEC Review*, vol. 14, no. 1, pp. 20-27.

Masella E., Gonthier M. and Dumaine M. (1997) The RT-Star: Features and Performance of a Low-Cost RTK OEM Sensor, *Proceedings of ION GPS 1997 International Technical Meeting of the Satellite Division of the ION*, Kansas City, Missouri, pp. 53-59.

Meindl M., Schaer S., Hugentobler U. and Beutler G. (2004) Tropospheric Gradient Estimation at CODE: Results from Global Solutions, in Applications of GPS Remote Sensing to Meteorology and Related Fields, *Journal of the Meteorological Society of Japan*, vol. 82, no. 1B, pp. 331-338.

Mekik Ç. (1997) Tropospheric Delay Models in GPS, *Proceedings of International Symposium on GIS/GPS*, Istanbul, Turkey, 15-19 September, pp. 156-170.

Mendes V. and Langley R. (1998) Optimization of Tropospheric Delay Mapping Function Performance for High-Precision Geodetic Applications, *Proceedings of DORIS Days*, Toulouse, France, 27-29 April.

Mendes V. and Langley R. (2000) An Analysis of High-Accuracy Tropospheric Delay Mapping Functions, *Physics and Chemistry of the Earth*, vol. 25, no. 12, pp. 809-812.

Merrigan M., Swift E., Wong R. and Saffel J. (2002) A Refinement to the World Geodetic System 1984 Reference Frame, *Proceedings of ION GNSS 15th International Technical Meeting of the Satellite Division 2002*, Portland, Oregon, September.

Merriman M. (1901) *Method of Least Squares* (8th edition), John Wiley & Sons, New York.

Mikhail E. (1976) *Observations and Least Squares*, IEP-A Dun-Donnelley Publisher, New York.

Milbert D. (2005) *Dennis Milbert's GPS Software Index Page*, <http://home.comcast.net/~dmilbert/softs/> (December 2008).

Mireault Y., Tétreault P., Lahaye F., Collins P. and Caissy M. (2008) Real-Time and Near Real-Time GPS Products and Services from Canada, *Proceedings of IGS Analysis Centre Workshop*, Miami Beach, Florida, USA, 2-6 June.

Misra P. and Enge P. (2006) *Global Positioning System - Signals, Measurements, and Performance* (2nd edition), Ganga-Jamuna Press, Massachusetts.

Montenbruck O. (2003) Kinematic GPS Positioning of LEO Satellites using Ionosphere-Free Single Frequency Measurements, *Aerospace Science and Technology*, vol. 7, pp. 396-405.

Moore A. W. (2007) The International GNSS Service Any Questions?, *GPS World*, <http://sidt.gpsworld.com/gpssidt/article/articleDetail.jsp?id=408374> (January 2007).

Muellerschoen R., Bertiger W. I., Lough M. F., Stowers D. and Dong D. (2000) An Internet-Based Global Differential GPS System, Initial Results, *Proceedings of ION National Technical Meeting*, Anaheim, USA, 26-28 January.

Muellerschoen R., Reichert A., Kuang D., Heflin B. and Bar-Sever Y. (2001) Orbit Determination with NASA's High Accuracy Real-Time Global Differential GPS System, *Proceedings of ION GPS 2001*, Salt Lake City, UT, 11-14 September.

Muellerschoen R., Iijima B., Meyer R., Bar-Sever Y. and Accad E. (2004) Real-Time Point-Positioning Performance Evaluation of Single-Frequency Receivers Using NASA's Global Differential GPS System, *Proceedings of ION GNSS 17th International Technical Meeting of the Satellite Division*, Long Beach, CA, 21-24 September, pp. 1872-1880.

Navcom (2008) *The StarFire Network*, <http://www.navcomtech.com/StarFire/> (July 2008).

Neilan R. E. 1995. The Organisation of the IGS, IGS 1994 Annual Report, IGS Central Bureau, Pasadena, California, USA.

Neta B., Clynch J. R., Danielson D. A. and Sagovac C. P. (1996) Fast Interpolation for Global Positioning System (GPS) Satellite Orbits, *Proceedings of AIAA/AAS Astrodynamics Specialist Conference*, San Diego, USA.

NGA (2003) Addendum to NIMA TR8350.2: Implementation of the World Geodetic System 1984 (WGS 84) Reference Frame G1150 < http://earth-info.nga.mil/GandG/publications/tr8350.2/Addendum%20NIMA%20TR8350.2.pdf> (July 2007).

NGS (2008) *IGS Analysis Center Coordinator (ACC) at NOAA/NGS*, <http://www.ngs.noaa.gov/igsacc/WWW/> (June 2008).

Nichols J., Hansen A., Walter T. and Enge P. (1999) Observations of Equatorial Scintillation using GPS Receivers, *Proceedings of ION GPS 12th International Technical Meeting of the Satellite Division of the Institute of Navigation*, Nashville, Tennessee, 14-17 September.

Niell A. (1996) Global Mapping Functions for the Atmosphere Delay at Radio Wavelengths, *Journal of Geophysical Research*, vol. 101, no. B2, pp. 3227-3246.

Niell A. (2000) Improved Atmospheric Mapping Functions for VLBI and GPS, *Earth Planets Space*, vol. 52, no. 6, pp. 415-423.

Niell A. (2001) Preliminary Evaluation of Atmospheric Mapping Functions Based on Numerical Weather Models, *Physics and Chemistry of the Earth*, vol. 26, pp. 475-480.

NIMA (2004) Department of Defence World Geodetic System 1984: Its Definition and Relationships with Local Geodetic Systems, Technical Report, NIMA TR8350.2.

NRCan (2008a) *Canadian Spatial Reference System Online Database*, <http://www.geod.nrcan.gc.ca/online_data_e.php> (May 2006).

NRCan (2008b) *Earth Science Sector: CSRS-PPP (Precise Point Positioning) Service*, <http://ess.nrcan.gc.ca/2002_2006/gnd/csrs_e.php> (July 2008).

OmniSTAR (2008) *OmniSTAR: The Global Positioning System*, <http://www.omnistar.com/> (July 2008).

Øvstedal O. (2002) Absolute Positioning with Single-Frequency GPS Receivers, *GPS Solutions*, vol. 5, no. 4, pp. 33-44.

Øvstedal O., Kjorsvik N. S. and Gjevestad J. G. O. (2006) Surveying Using GPS Precise Point Positioning, *Proceedings of XXIII FIG Congress*, Munich, Germany, 8-13 October.

Özlüdemir T. (2004) The Stochastic Modelling of GPS Observations, *Turkish Journal of Engineering and Environmental Science*, vol. 28, pp. 223-231.

Petrov L. and Boy J. (2004) Study of The Atmospheric Pressure Loading Signal In Very Long Baseline Interferometry Observations, *Journal of Geophysical Research*, vol. 109, no. B03405.

Ping J., Kono Y., Matsumoto K., Otsuka Y., Saito A., Shum C., Heki K. and Kawano N. (2002) Regional Ionosphere Map Over Japanese Islands, *Earth Planets Space*, vol. 54, pp. 13-16.

Ray J. (2005a) *[IGSMAIL-5078]: Updated P1-C1 Bias Values*, <http://igscb.jpl.nasa.gov/mail/igsmail/2005/msg00001.html> (May 2008).

Ray J. (2005b) *Planned Changes to IGS Antenna*, <https://listserv.unb.ca/cgi-bin/wa?A2=ind0508&L=canspace&P=3523> (April 2007).

Ray J. and Griffiths J. (2008) Status of IGS Ultra-Rapid Products for Real-Time Applications, *American Geophysical Union, Fall Meeting*, vol. 89, no. 52.

Remondi B. (1993) *NGS Second Generation ASCII and Binary Orbit Formats and Associated Interpolation Studies*, Permanent Satellite Tracking Networks for Geodesy and Geodynamics (Symposium No. 109 held 11-24 August, 1991, in Vienna, Austria), Springer-Verlag.

Rizos C. (1999) *Principles and Practice of GPS Surveying - Tropospheric Delay*, <http://www.gmat.unsw.edu.au/snap/gps/gps_survey/chap6/628.htm> (May 2007).

Rizos C., Han S. and Han X. (1998) Performance Analysis of a Single-Frequency, Low-Cost GPS Surveying System, *Proceedings of ION GPS 1998 International Technical Meeting of the Satellite Division of ION*, Nashville, Tennessee, pp. 427-435.

Roberts C. and Rizos C. (2001) Mitigating Differential Troposphere Effects For GPS-Based Volcano Monitoring, *Proceedings of 5th International Symposium on Satellite Navigation Technology & Application*, Canberra, Australia, 24-27 July.

Roberts C., Seynat C., Rizos C. and Hooper G. (2004) Low-cost Deformation Measurement System for Volcano Monitoring, *Proceedings of 3rd FIG Regional Conference, "Surveying the Future - Contributions to Economic, Environment and Social Development*, Jakarta, Indonesia, 3-7 October.

Rothacher M., Springer T. A., Schaer S. and Beutler G. (1997) Processing Strategies for Regional GPS Networks, *Proceedings of IAG General Assembly*, Rio de Janeiro, Brazil, 3-9 September.

Roulston A. (2001) An Evaluation of Predicted Ephemerides for High Precision Real-Time GPS Positioning, *Master thesis*, RMIT University, Melbourne, Australia.

Saastamoinen J. (1972) Contributions to The Theory of Atmospheric Refraction, *Bulletin Geodesique*, pp. 105-107.

Saeki M. and Hori M. (2006) Development of an Accurate Positioning System Using Low-Cost L1 GPS Receivers, *Computer-Aided Civil and Infrastructure Engineering*, vol. 21, no. 4, pp. 258-267.

Schaer S. (1999) Mapping and Predicting the Earth's Ionosphere using the Global Positioning System, *PhD thesis*, University of Berne, Switzerland.

Schaer S., Gurtner W. and Feltens J. (1998) IONEX: The IONosphere Map EXchange Format Version 1, *Proceedings of IGS AC Workshop*, Darmstadt, Germany, 9-11 February.

Schmid R., Mader G. L. and Herring T. A. (2004) From Relative to Absolute Antenna Phase Centre Corrections, *Proceedings of IGS 2004 Workshop and Symposium*, Berne, Switzerland, pp. 209-219.

Schmid R., Steigenberger P., Gendt G., Ge M. and Rothacher M. (2007) Generation of A Consistent Absolute Phase Centre Correction Model for GPS Receiver and Satellite Antennas, *Journal of Geodesy*, vol. 81, no. 12, pp. 781-798.

Seeber G. (1993) *Satellite Geodesy* (1st edition), Walter de Gruyter GmbH & Co., Berlin.

Seeber G. (2003) *Satellite Geodesy* (2nd edition), Walter de Gruyter GmbH & Co., Berlin.

Sharpe T., Hatch R. and Nelson F. (2002) StarFire and Real-Time GIPSY: A Global High-Accuracy Differential GPS System, *Proceedings of 4th International Symposium on GPS/GNSS*, Wuhan University, China, 6-8 November.

Shaw M. (2000) Modernization of The Global Positioning System, *GPS World*, vol. 11, no. 9, pp. 36-44.

Shen X. (2002) Improving Ambiguity Convergence in Carrier Phase-based Precise Point Positioning, *Master thesis*, The University of Calgary, Canada.

SIDC (2008) *Solar Influences Data Analysis Centre: Daily Sunspot Number*, <http://sidc.oma.be/sunspot-data/dailyssn.php> (March 2008).

Simsky A. (2003) Standalone Real-Time Positioning Algorithm Based on Dynamic Ambiguities (DARTS), *Proceedings of ION GNSS 16th International Technical Meeting of the Satellite Division 2003*, Portland, Oregon, 12-19 September.

Simsky A. (2006) Standalone Real-Time Navigation Algorithm for Single-Frequency Ionosphere-Free Positioning Based on Dynamic Ambiguities (DARTS-SF), *Proceedings of ION GNSS 18th International Technical Meeting of the Satellite Division*, Fort Worth, Texas, pp. 301-308.

Skone S. (2000) GPS Receiver Tracking Performance Under Ionospheric Scintillation Conditions, *Proceedings of IGS Network Workshop*, Soria Moria, Oslo, Norway, 12-14 July.

Skone S., El-Gizaway M. and Shrestha S. M. (2001) Limitations in GPS Positioning Accuracies and Receiver Tracking Performance During Solar Maximum, *Proceedings of KIS 2001 The International Symposium on Kinematics System in Geodesy, Geomatics and Navigation*, Banff, Canada, 5-8 June, pp. 129-143.

Söderholm S. (2005) GPS L1 Carrier Phase Double Difference Solution Using Low Cost GPS Receivers, *Proceedings of ION GNSS 18th International Technical Meeting of the Satellite Division*, Long Beach, CA, pp. 376-380.

Soicher H. and Gorman F. (1985) Seasonal and Day-to-Day variability of Total Electron Content at Mid-Latitude Near Solar Maximum, *Radio Science*, vol. 20, no. 3, p. 383.

Solar Influences Data Analysis Center (2008) *Sunspot Index Graphics*, <http://sidc.oma.be/html/wolfjmms.html> (January 2008).

SOPAC (2008) *Scripps Orbit and Permanent Array Center*, <http://sopac.ucsd.edu/> (May 2008).

Springer T. A. (2000) *[IGSMAIL-3088]: IGS Ultra Rapid Products*, <http://igscb.jpl.nasa.gov/mail/igsmail/2000/msg00427.html> (January 2009).

Stanaway R. (2007) GDA94, ITRF, WGS84: What's The Difference? Working With Dynamic Datums, *Proceedings of Spatial Science Institute Biennial International Conference (SSC2007)*, Hobart, Tasmania, pp. 216-222.

Stansell T., Fenton P., Garin L., Hatch R., Knight J., Rowitch D., Sheynblat L., Stratton A., Studenny J. and Weill L. (2006) BOC or MBOC? The Common GPS/Galileo Civil Signal Design: A manufacturer Dialog Part 1, *Inside GNSS*, vol. 1, no. 5, pp. 28-43.

Steed J. (1995) The Geocentric Datum of Australia, *Surveying World*, vol. 4, no. 1, pp. 14-17.

Steed J. and Luton G. (2000) WGS84 and the Geocentric Datum of Australia 1994, *Proceedings of ION GPS 2000*, Salt Lake, Utah, 25-29 September.

Teferle F. N., Orliac E. J. and Bingley R. M. (2007) An Assessment of Bernese GPS Software Precise Point Positioning Using IGS Final Products For Global Site Velocities, *GPS Solutions*, vol. 11, no. 3, pp. 205-213.

Tètreault P., Kouba J., Hèroux P. and Legree P. (2005) CSRS-PPP: An Internet Service For GPS User Access To The Canadian Spatial Reference Frame, *GEOMATICA*, vol. 59, no. 1, pp. 17-28.

Teunissen P. (1991) The GPS Phase-Adjusted Pseudorange, *Proceedings of The 2nd International Workshop on High Precision Navigation*, Stuttgart/Freudenstadt, Germany, pp. 115-125.

Teunissen P. (1998) Weighting GPS Dual Frequency Observations: Bearing the Cross of Cross-Correlation, *GPS Solutions*, vol. 2, no. 2, pp. 28-37.

The Institute of Navigation (2008) *The Institute of Navigation*, <http://www.ion.org/> (December 2008).

The University of Nottingham (2008) *Gringo Software*, <http://www.bigf.ac.uk/gringo/index.html> (August 2008).

Tiberius C. C. J. M. (1999) The GPS Data Weight Matrix: What Are the Issues?, *Proceedings of ION 1999 National Technical Meeting "Vision 2010: Present and Future"*, San Diego, California, USA, pp. 219-227.

Tiberius C. C. J. M. (2003) Handheld GPS Receiver Accuracy: Standard Positioning Service, *GPS World,* <*http://www.gpsworld.com/gpsworld/Innovation/Standard-Positioning-Service---Handheld-GPS-Receiv/ArticleStandard/Article/detail/46415*> (August 2008).

Tiberius C. C. J. M., Jonkman N. and Kenselaar F. (1999) The Stochastics of GPS Observables, *GPS World*, vol. 10, no. 2, pp. 49-54.

Todorova S., Hobiger T. and Schuh H. (2006) Combination of GPS and Satellite Altimetry Data for Global Ionosphere Maps, *Proceedings of International Scientific Conference SGEM 2006*, Albena, Bulgaria, pp. 265-277.

Trimble Navigation Limited (2008) *GeoXH Handheld*, <http://www.trimble.com/geoxh.shtml> (September 2008).

U.S. Assistant Secretary of Department of Defence (2008) *Global Positioning System Standard Positioning Service Performance Standard*, <http://www.navcen.uscg.gov/GPS/geninfo/2008SPSPerformanceStandardFINAL.pdf> (April 2009).

Vermeer M. (1997) The Precision of Geodetic GPS and One Way of Improving It, *Journal of Geodesy*, vol. 71, pp. 240-245.

Vollath U., Brockmann E. and Chen X. (2003) Troposphere: Signal or Noise?, *Proceedings of ION GNSS 16th International Technical Meeting of the Satellite Division 2003*, Portland, Oregon, 9-12 September.

Warren D. (2002) Broadcast vs Precise GPS Ephemerides: A Historical Perspective, *Master thesis*, Air University, Ohio, USA.

Waypoint Products Group (2006) *Airborne Precise Point Positioning (PPP) in GrafNav 7.80 with Comparisons to Canadian Spatial Reference System (CSRS) Solutions*, <http://www.novatel.com/Documents/Waypoint/Reports/PPPReport.pdf> (July 2007).

Wells D., Beck N., Delikaraoglou D., Kleusberg A., Krakiwsky E., Lachapelle G., Langley R., Nakiboglu M., Schwarz K., Tranquilla J. and Vanícek P. (1986) *Guide to GPS Positioning*, Canadian GPS Associates, Fredericton, N.B., Canada.

Witchayangkoon B. (2000) Elements of GPS Precise Point Positioning, *PhD thesis*, The University of Maine, USA.

Wu J. T., Wu S. C., Hajj G. A., Bertiger W. I. and Lichten S. M. (1993) Effects of Antenna Orientation on GPS Carrier Phase, *Manuscripta Geodaetica*, vol. 18, pp. 91-98.

Wu S., Zhang K., Yuan Y. and Wu F. (2006) Spatio-temporal Characteristics of the Ionospheric TEC Variation for GPSnet-based Real-time Positioning in Victoria, *Journal of Global Positioning Systems*, vol. 5, no. 1, pp. 52-57.

Wübbena G., Schmitz M. and Andreas B. (2005) PPP-RTK: Precise Point Positioning Using State-Space Representation in RTK Networks, *Proceedings of ION GNSS 18th International Technical Meeting of the Satellite Division*, Long Beach, CA, 13-16 September, pp. 2584-2594.

Wyllie S. (2007) Modelling The Temporal Variation of The Ionosphere In A Network-RTK Environment, *PhD thesis*, RMIT University, Australia.

Xiao B., Zhang K., Grenfell R. and Norton T. (2002) Handheld GPS - Today and Tomorrow, *Proceedings of FIG XXII International Congress*, Washington D. C., USA, 19-26 April.

Xu G. (2003) *GPS Theory, Algorithms and Applications* (1st edition), Springer-Verlag, Berlin, Germany.

Yuan Y., Huo X. and Ou J. (2007) Models and Methods for Precise Determination of Ionospheric Delay using GPS, *Progress in Natural Science*, vol. 2, no. 17, pp. 187-196.

Yunck T. (1993) Coping With the Atmosphere and Ionosphere in Precise Satellite and Ground Positioning, *Geophysical Monograph 73*, vol. 13.

Zhang K., Wu F., Huo X. and Wu S. (2008) Development of a Grid Ionospheric Model and Characterisation of Spatio-Temporal Ionospheric Variations of Australia, *Journal of Spatial Science (currently under review).*

Zolesi B. and Cander L. (1998) Advances in Regional Ionospheric Mapping Over Europe, *Annali Di Geofisica*, vol. 41, no. 5-6, pp. 827-842.

Zumberge J. F., Watkins M. M. and Webb F. H. (1997a) Characteristics and Applications of Precise GPS Clock Solutions Every 30 Seconds, *Journal of Navigation*, vol. 44, no. 4, pp. 449-456.

Zumberge J. F., Heflin M. B., Jefferson D. C., Watkins M. M. and Webb F. H. (1997b) Precise Point Positioning for The Efficient and Robust Analysis of GPS Data From Large Networks, *Journal of Geophysical Research*, vol. 102, no. B3, pp. 5005-5017.

Zumberge J. F., Webb F. H. and Bar-Sever Y. (2001) Precise Post Processing of GPS Data Products and Services from JPL, *Proceedings of ION National Technical Meeting*, Long Beach, CA, 22-24 January.

Papers Produced as Part of This Thesis

Choy S, Zhang K., Silcock D. and Wu F. (2007) Precise Point Positioning - A Case Study in Australia, *Proceedings of the Spatial Sciences Institute Biennial International Conference*, Hobart, Australia, 14-18 May.

Choy S, Zhang K. and Silcock D. (2007) Single Frequency Precise Point Positioning, *Proceedings of the Joint International Symposium and Exhibition on Geoinformation and GPS/GNSS 2007,* Johor Bahru, Malaysia, 5-7 November.

Choy S, Zhang K. and Silcock D. (2007) Single Frequency Precise Point Positioning using Different Ionospheric Error Mitigation Methods, *Proceedings of the IGNSS Symposium 2007*, Sydney, Australia, 4 - 6 December.

Choy S., Zhang K. and Silcock D. (2008) An Evaluation of Various Ionospheric Error Mitigation Methods used in Single Frequency PPP, *Journal of Global Positioning Systems*, vol. 7, no. 1, pp. 62-71.

Choy S., Zhang K., Silcock D. and Holden L. (2008) An Empirical Approach to Study the Effects of *A Priori* Observations Sigma Ratio in Single Frequency Precise Point Positioning, *Proceedings of The International Symposium of GPS/GNSS*, Odaiba, Tokyo, Japan, 11-14 November.

Choy S., Zhang K., Silcock D. and Holden L. (2008) Feasibility of Using Regional Ionosphere Maps in Single Frequency Precise Point Positioning: A Case Study in Australia, *Proceedings of The International Symposium of GPS/GNSS*, Odaiba, Tokyo, Japan, 11-14 November.

Choy S, Silcock D. and Zhang K. (2009) Single Frequency Precise Point Positioning Using A Low-Cost GPS Receiver, *Proceedings of the Surveying & Spatial Sciences Institute Biennial International Conference*, Adelaide, Australia, 28 September – 2 October.

Appendix A: Statistical Analyses of using Different *A Priori* Observations Sigma Ratios

Note: Numerical values in pink are the minimums, while those in green are the maximums.

High Ionospheric Activity → Low Ionospheric Activity

DARW							
Case-1: 1 to 100		**2001**	**2002**	**2003**	**2004**	**2005**	**2006**
Mean (m)	**East**	-0.49	0.07	-0.72	-0.41	0.16	-0.02
	North	0.66	0.04	0.11	0.39	0.04	-0.07
	Height	-0.10	-0.34	-1.69	-1.15	-0.02	0.49
RMS (m)	**East**	0.91	0.42	0.93	1.18	0.63	0.61
	North	0.78	0.24	0.73	0.53	0.37	0.43
	Height	1.17	0.71	2.39	2.16	1.31	2.54
Case-2: 1 to 50		**2001**	**2002**	**2003**	**2004**	**2005**	**2006**
Mean (m)	**East**	-0.57	0.10	-0.15	-0.04	0.19	0.07
	North	0.63	-0.06	0.13	0.33	0.04	0.06
	Height	0.03	-0.13	-0.29	-0.90	0.31	0.08
RMS (m)	**East**	0.73	0.52	0.29	0.23	0.33	0.23
	North	0.72	0.34	0.32	0.45	0.16	0.13
	Height	1.09	0.57	0.67	1.15	0.53	0.47
Case-3: 1 to 10		**2001**	**2002**	**2003**	**2004**	**2005**	**2006**
Mean (m)	**East**	-0.80	-0.03	-0.29	-0.11	0.12	0.01
	North	1.03	-0.23	0.30	0.54	0.03	0.05
	Height	0.33	0.00	-0.17	-1.12	0.67	0.33
RMS (m)	**East**	0.89	0.61	0.36	0.23	0.17	0.11
	North	1.19	0.57	0.48	0.65	0.08	0.08
	Height	1.51	0.72	0.64	1.26	0.79	0.45
Case-4: 1 to 4		**2001**	**2002**	**2003**	**2004**	**2005**	**2006**
Mean (m)	**East**	-0.79	-0.09	-0.01	-0.10	0.10	0.00
	North	1.57	-0.51	1.23	0.84	-0.06	0.01
	Height	0.80	0.35	-0.54	-1.37	1.12	0.84
RMS (m)	**East**	0.87	0.70	0.82	0.22	0.15	0.14
	North	1.91	0.83	1.38	0.90	0.14	0.12
	Height	2.22	0.97	0.72	1.54	1.21	0.97
Case-5: code		**2001**	**2002**	**2003**	**2004**	**2005**	**2006**
Mean (m)	**East**	-0.84	-0.10	0.07	-0.10	0.10	-0.04
	North	1.95	-0.75	1.90	0.97	-0.14	-0.11
	Height	1.61	0.92	-0.99	-1.32	1.62	1.79
RMS (m)	**East**	0.94	0.70	0.95	0.22	0.16	-0.04
	North	2.35	1.01	1.92	1.01	0.22	-0.11
	Height	3.13	1.63	1.13	1.56	1.66	1.79

High Ionospheric Activity

Low Ionospheric Activity

STR1							
Case-1: 1 to 100		**2001**	**2002**	**2003**	**2004**	**2005**	**2006**
Mean (m)	**East**	0.16	-0.05	-0.09	-0.03	-0.08	0.00
	North	0.42	0.07	0.38	0.09	0.03	0.09
	Height	-0.06	0.24	0.44	-0.06	0.18	0.06
RMS (m)	**East**	0.39	0.18	0.49	0.31	0.29	0.23
	North	0.57	0.28	1.12	0.27	0.26	0.22
	Height	0.75	0.42	1.33	1.27	0.72	0.30
Case-2: 1 to 50		**2001**	**2002**	**2003**	**2004**	**2005**	**2006**
Mean (m)	**East**	0.29	-0.01	-0.02	-0.03	0.00	0.01
	North	0.59	0.00	0.03	0.02	0.03	0.12
	Height	0.03	0.21	0.11	-0.18	0.11	0.09
RMS (m)	**East**	0.41	0.15	0.16	0.08	0.08	0.07
	North	0.71	0.18	0.22	0.12	0.16	0.17
	Height	0.31	0.35	0.43	0.48	0.43	0.16
Case-3: 1 to 10		**2001**	**2002**	**2003**	**2004**	**2005**	**2006**
Mean (m)	**East**	0.44	0.00	0.09	-0.09	0.01	-0.01
	North	0.86	-0.19	-0.02	0.11	0.14	0.20
	Height	0.02	0.05	0.07	-0.02	0.13	0.11
RMS (m)	**East**	0.48	0.22	0.12	0.10	0.12	0.17
	North	0.95	0.29	0.13	0.15	0.22	0.25
	Height	0.41	0.50	0.27	0.17	0.31	0.16
Case-4: 1 to 4		**2001**	**2002**	**2003**	**2004**	**2005**	**2006**
Mean (m)	**East**	0.51	-0.01	0.13	-0.12	0.04	0.08
	North	1.12	-0.56	-0.02	0.26	0.32	0.35
	Height	-0.46	-0.08	0.13	-0.15	-0.03	0.06
RMS (m)	**East**	0.54	0.29	0.15	0.13	0.14	0.10
	North	1.16	0.58	0.18	0.31	0.37	0.39
	Height	0.87	0.80	0.31	0.23	0.36	0.16
Case-5: code		**2001**	**2002**	**2003**	**2004**	**2005**	**2006**
Mean (m)	**East**	0.52	0.00	0.15	-0.11	0.04	0.10
	North	1.26	-0.78	0.03	0.37	0.37	0.46
	Height	-0.80	0.05	0.30	-0.31	-0.10	-0.15
RMS (m)	**East**	0.54	0.34	0.17	0.12	0.14	0.11
	North	1.29	0.80	0.25	0.43	0.45	0.48
	Height	1.12	0.92	0.42	0.47	0.49	0.19

High Ionospheric Activity

Low Ionospheric Activity

TOW2							
Case-1: 1 to 100		**2001**	**2002**	**2003**	**2004**	**2005**	**2006**
Mean (m)	**East**	0.13	-0.22	-0.23	-0.35	-0.13	-0.01
	North	0.34	-0.02	0.17	0.10	0.13	-0.08
	Height	0.15	-0.11	-0.47	-0.06	-0.07	0.25
RMS (m)	**East**	0.36	0.43	0.60	0.50	0.58	0.35
	North	0.39	0.20	0.67	0.29	0.38	0.56
	Height	0.54	0.43	1.19	0.82	0.82	0.86
Case-2: 1 to 50		**2001**	**2002**	**2003**	**2004**	**2005**	**2006**
Mean (m)	**East**	0.25	-0.18	-0.26	0.13	-0.01	0.05
	North	0.38	-0.11	0.19	0.11	0.14	0.03
	Height	0.30	0.09	-0.22	-0.26	0.04	0.22
RMS (m)	**East**	0.47	0.24	0.32	0.18	0.25	0.13
	North	0.45	0.30	0.34	0.16	0.23	0.18
	Height	0.59	0.44	0.38	0.49	0.38	0.47
Case-3: 1 to 10		**2001**	**2002**	**2003**	**2004**	**2005**	**2006**
Mean (m)	**East**	0.42	-0.20	-0.41	0.13	0.09	0.02
	North	0.36	-0.29	0.44	0.14	0.24	0.14
	Height	0.56	0.35	-0.13	0.04	0.29	0.34
RMS (m)	**East**	0.63	0.25	0.48	0.22	0.22	0.05
	North	0.48	0.51	0.63	0.24	0.30	0.16
	Height	0.83	0.61	0.31	0.48	0.48	0.46
Case-4: 1 to 4		**2001**	**2002**	**2003**	**2004**	**2005**	**2006**
Mean (m)	**East**	0.44	-0.20	-0.50	0.13	0.11	0.04
	North	0.28	-0.45	0.71	0.24	0.43	0.29
	Height	1.01	0.87	-0.32	0.66	0.81	0.63
RMS (m)	**East**	0.66	0.30	0.60	0.19	0.22	0.07
	North	0.54	0.71	0.89	0.41	0.45	0.30
	Height	1.34	0.96	0.64	0.77	0.90	0.66
Case-5: code		**2001**	**2002**	**2003**	**2004**	**2005**	**2006**
Mean (m)	**East**	0.40	-0.22	-0.59	0.11	0.11	0.07
	North	0.28	-0.52	0.90	0.27	0.53	0.34
	Height	1.32	1.47	-0.85	1.23	1.26	0.98
RMS (m)	**East**	0.63	0.37	0.68	0.17	0.23	0.10
	North	0.55	0.81	1.02	0.47	0.55	0.35
	Height	1.69	1.50	1.58	1.27	1.29	0.99

Appendix B: Different Ionospheric Corrections – Point Positioning Errors

Solar Maximum Period (2001)

- **DARW** – 2001 – No Ionospheric Corrections

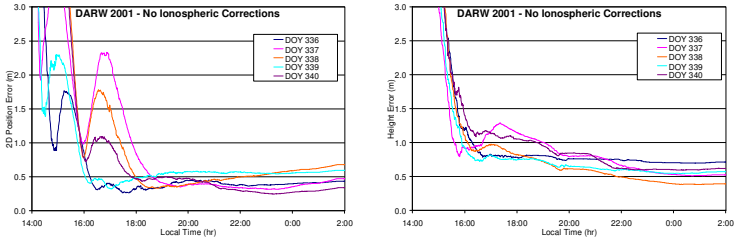

- **DARW** – 2001 – Broadcast model

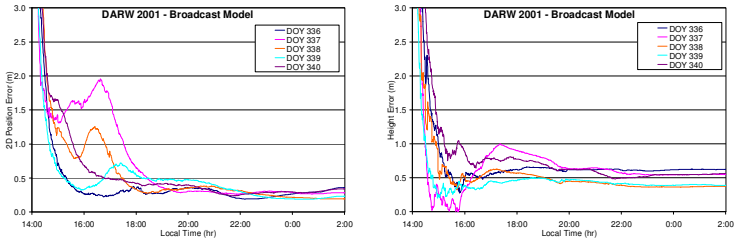

- **DARW** – 2001 – GIMs

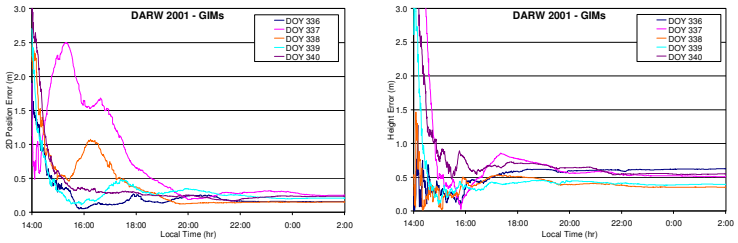

- **DARW** – 2001 – RIMs

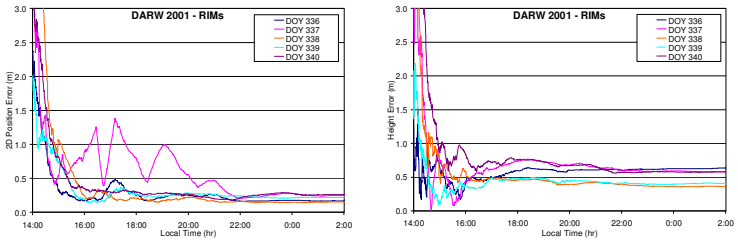

- **DARW** – 2001 – RIMs (1hr)

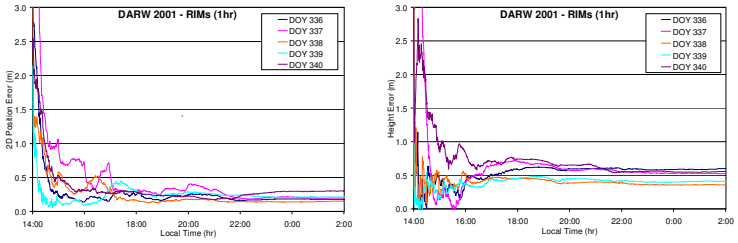

- **TOW2** – 2001 – No Ionospheric Corrections

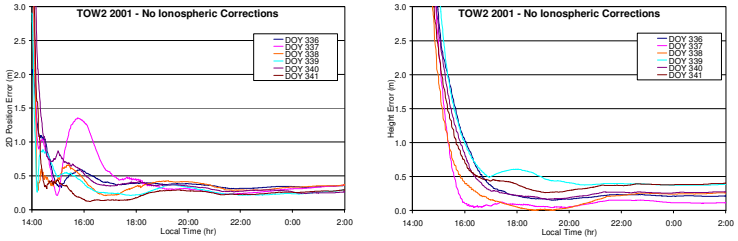

- **TOW2** – 2001 – Broadcast model

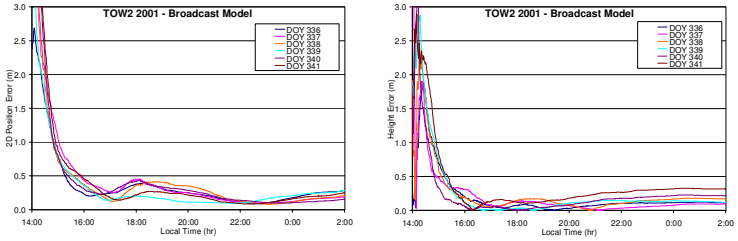

- **TOW2** – 2001 – GIMs

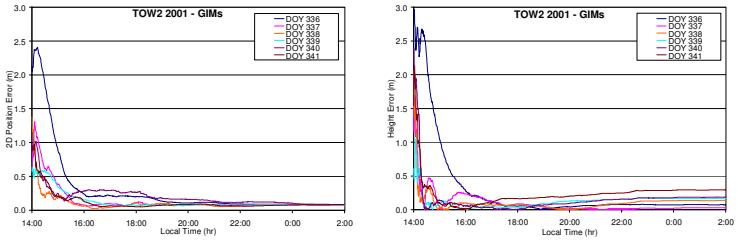

- **TOW2** – 2001 – RIMs

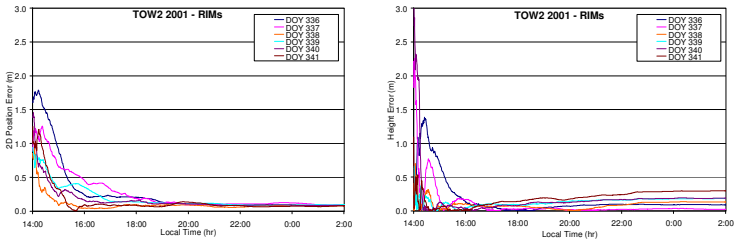

- **TOW2** – 2001 – RIMs (1hr)

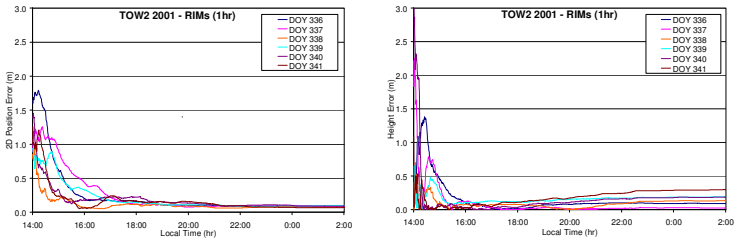

- **ALIC** – 2001 – No Ionospheric Corrections

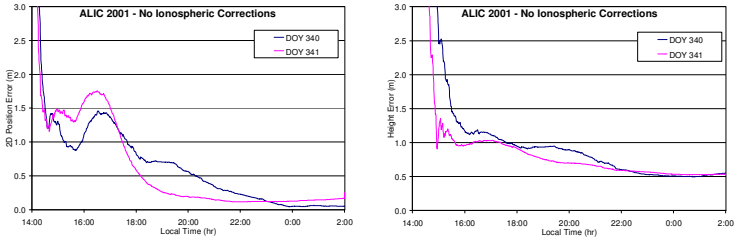

- **ALIC** – 2001 – Broadcast model

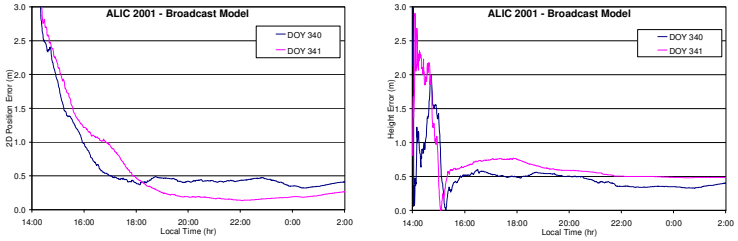

- **ALIC** – 2001 – GIMs

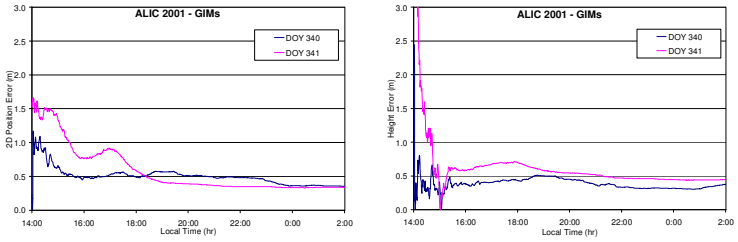

- **ALIC** – 2001 – RIMs

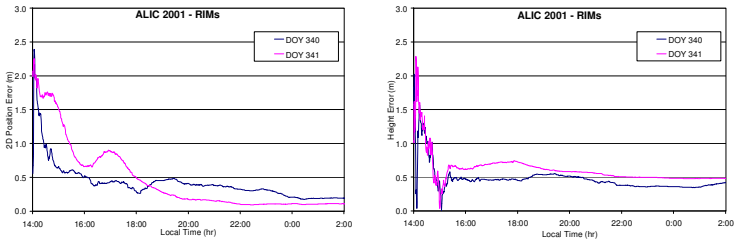

- **ALIC** – 2001 – RIMs (1hr)

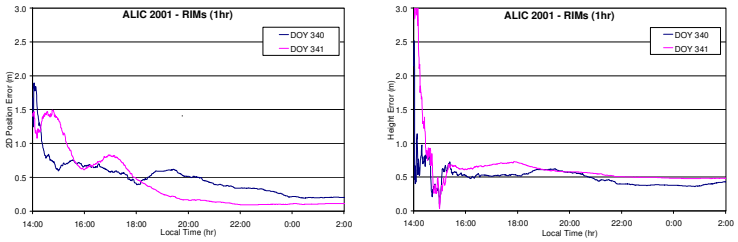

- **STR1** – 2001 – No Ionospheric Corrections

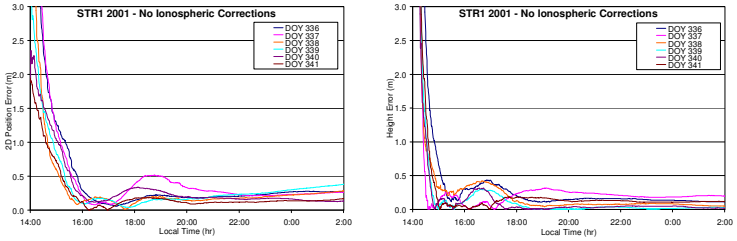

- **STR1** – 2001 – Broadcast model

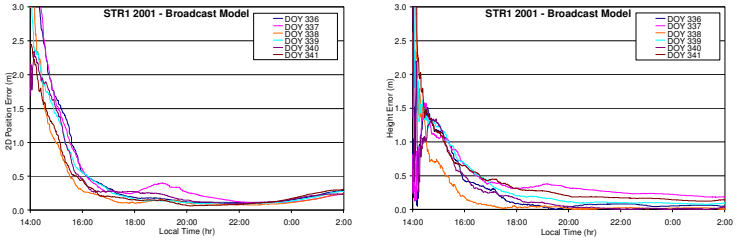

- **STR1** – 2001 – GIMs

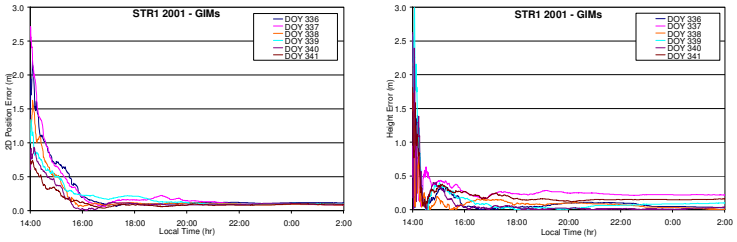

- **STR1** – 2001 – RIMs

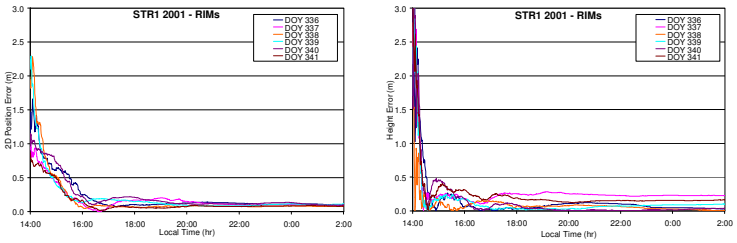

- **STR1** – 2001 – RIMs (1hr)

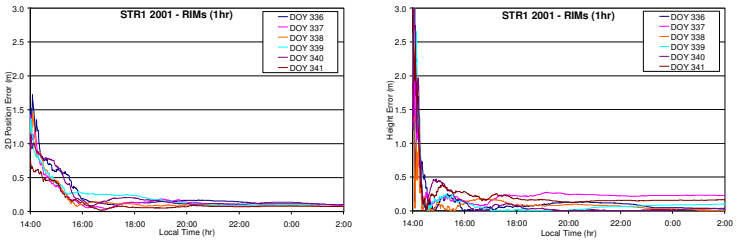

- **HOB2** – 2001 – No Ionospheric Corrections

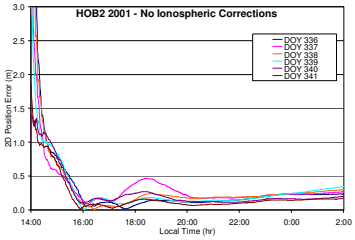

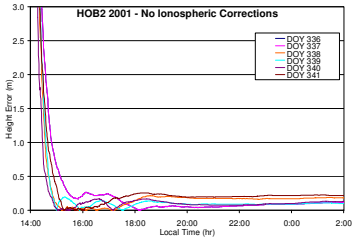

- **HOB2** – 2001 – Broadcast model

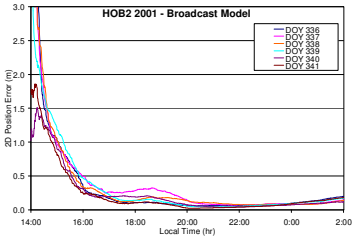

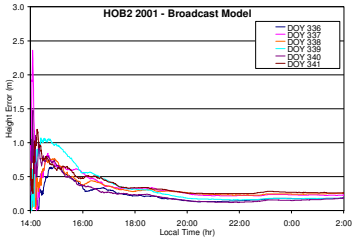

- **HOB2** – 2001 – GIMs

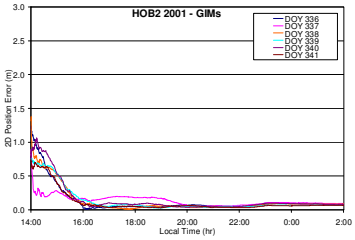

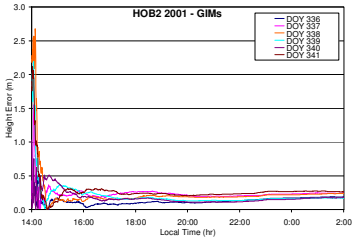

- **HOB2** – 2001 – RIMs

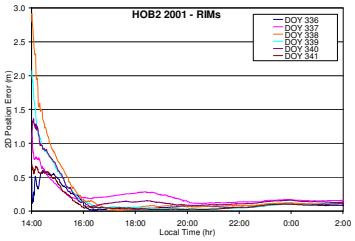

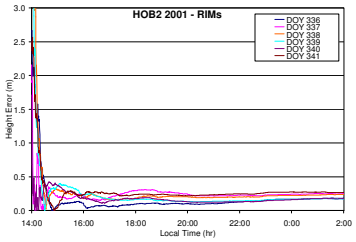

- **HOB2** – 2001 – RIMs (1hr)

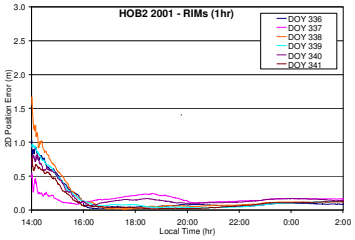

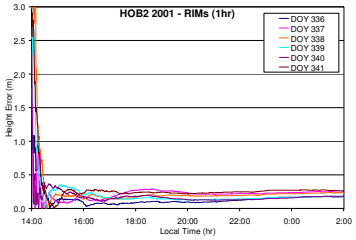

Solar Minimum Period (2006)

- **DARW** – 2006 – No Ionospheric Corrections

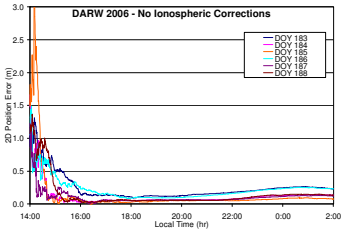

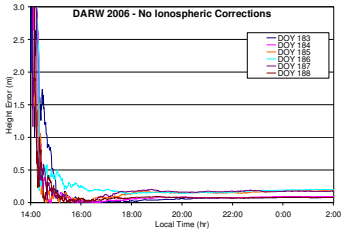

- **DARW** – 2006 – Broadcast model

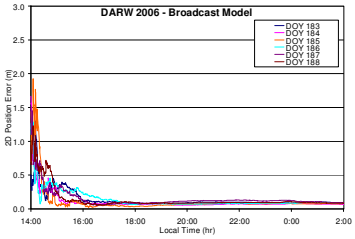

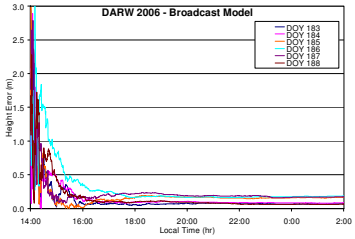

- **DARW** – 2006 – *Rapid* GIMs

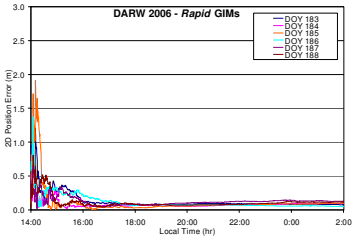

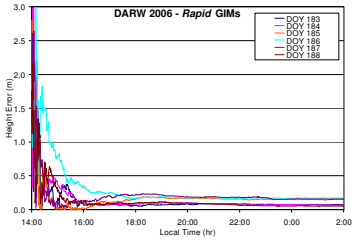

- **DARW** – 2006 – *Final* GIMs

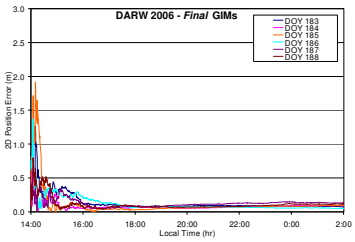

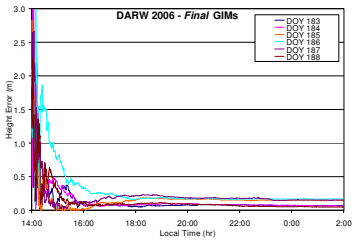

- **DARW** – 2006 – RIMs

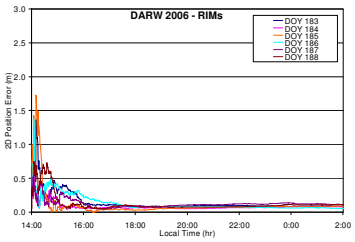

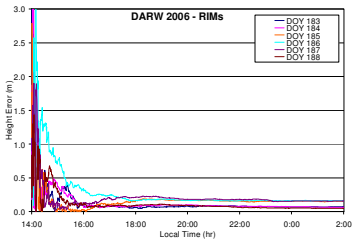

- **DARW** – 2006 – RIMs (1hr)

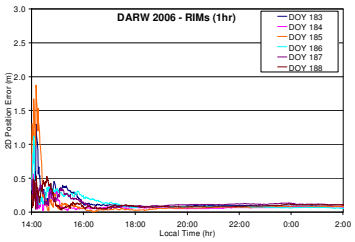

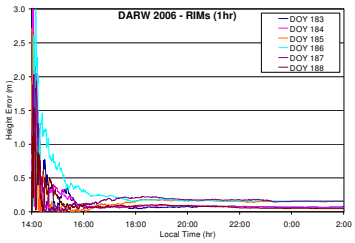

- **TOW2** – 2006 – No Ionospheric Corrections

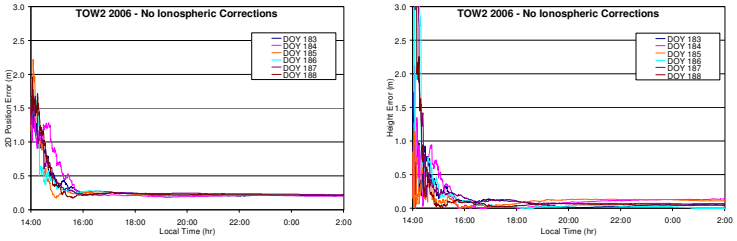

- **TOW2** – 2006 – Broadcast model

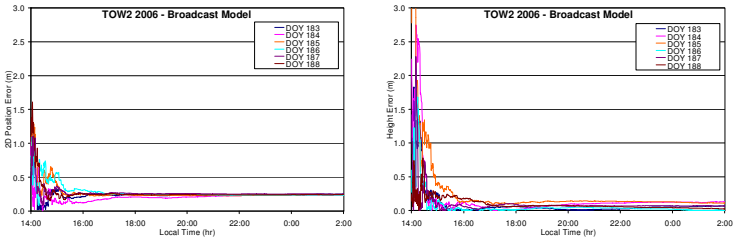

- **TOW2** – 2006 – *Rapid* GIMs

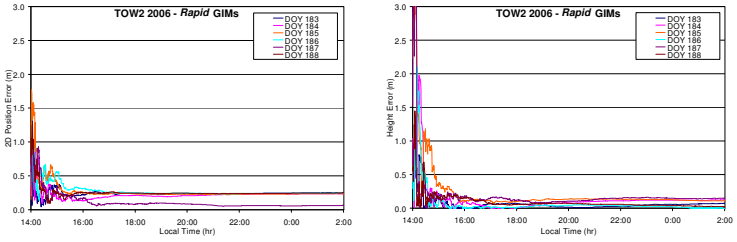

- **TOW2** – 2006 – *Final* GIMs

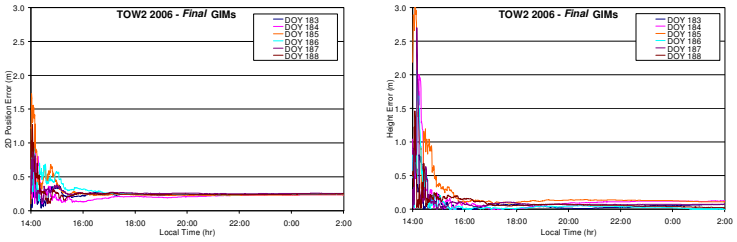

- **TOW2** – 2006 – RIMs

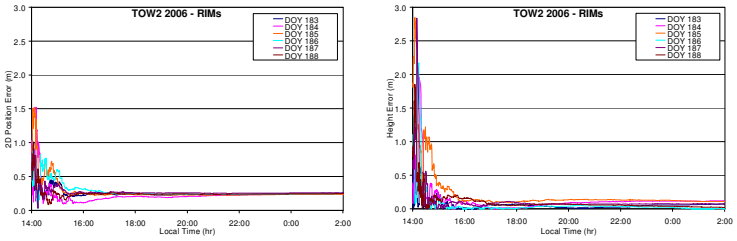

- **TOW2** – 2006 – RIMs (1hr)

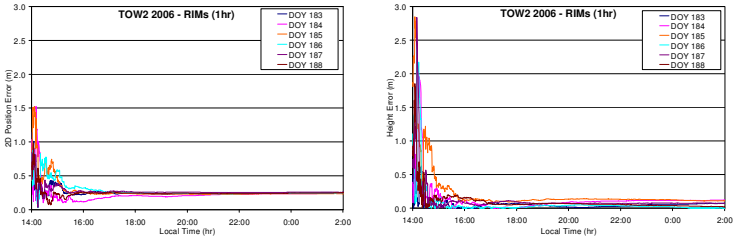

- **ALIC** – 2006 – No Ionospheric Corrections

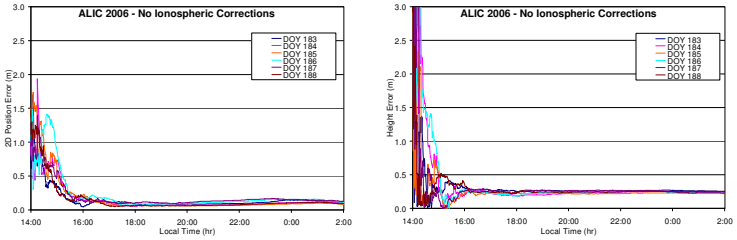

- **ALIC** – 2006 – Broadcast model

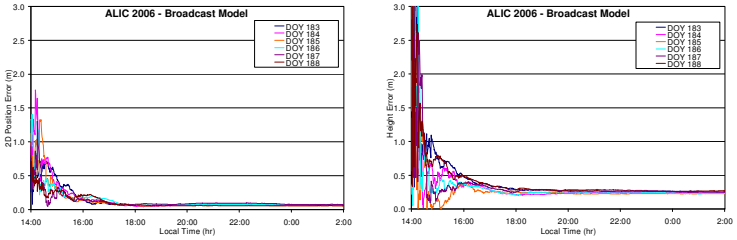

- **ALIC** – 2006 – *Rapid* GIMs

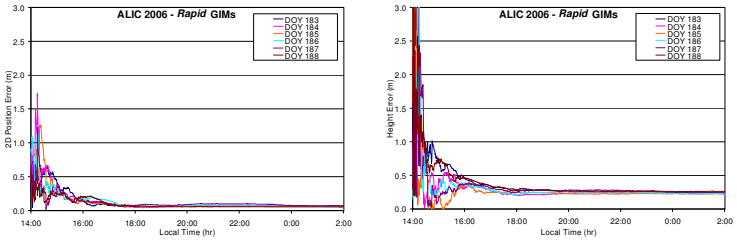

- **ALIC** – 2006 – *Final* GIMs

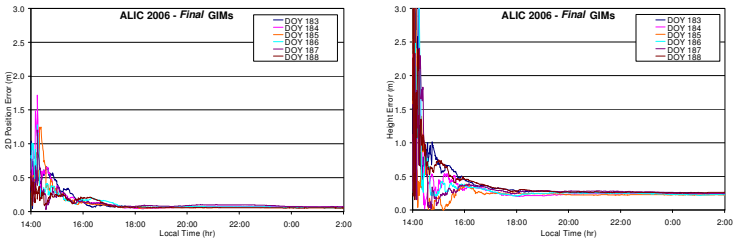

- **ALIC** – 2006 – RIMs

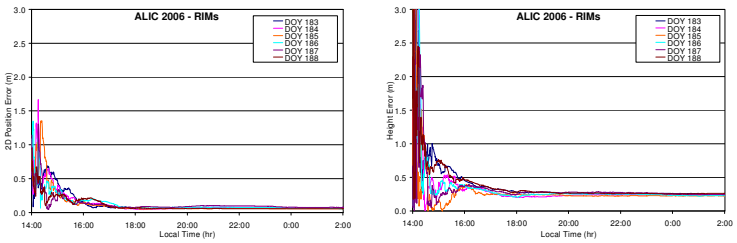

- **ALIC** – 2006 – RIMs (1hr)

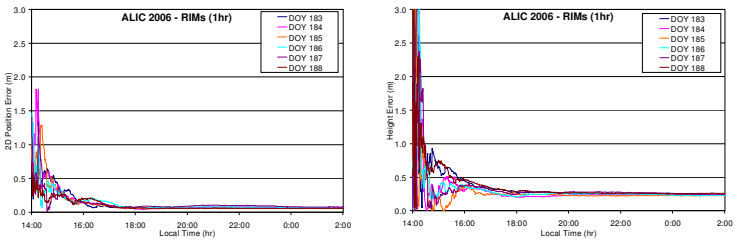

- **STR1** – 2006 – No Ionospheric Corrections

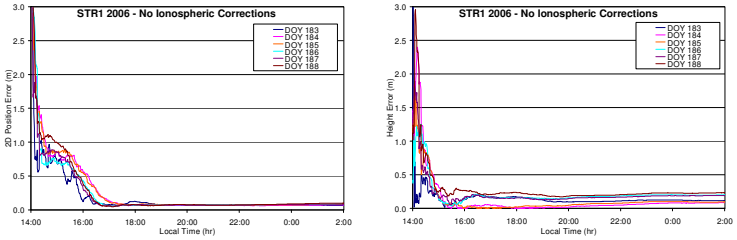

- **STR1** – 2006 – Broadcast model

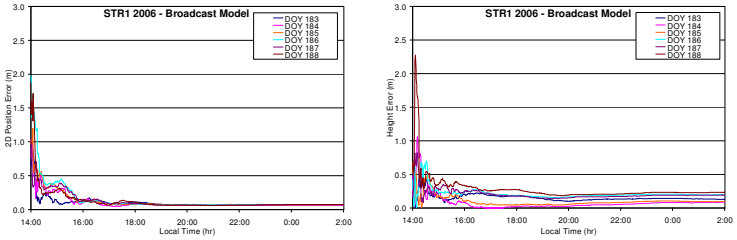

- **STR1** – 2006 – *Rapid* GIMs

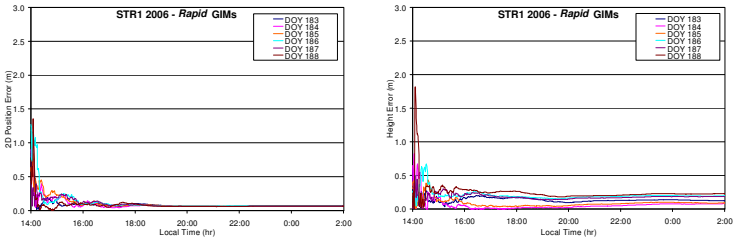

- **STR1** – 2006 – *Final* GIMs

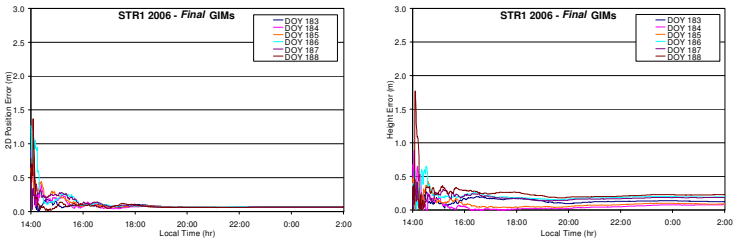

- **STR1** – 2006 – RIMs

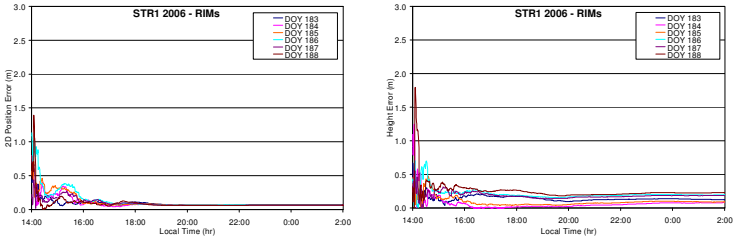

- **STR1** – 2006 – RIMs (1hr)

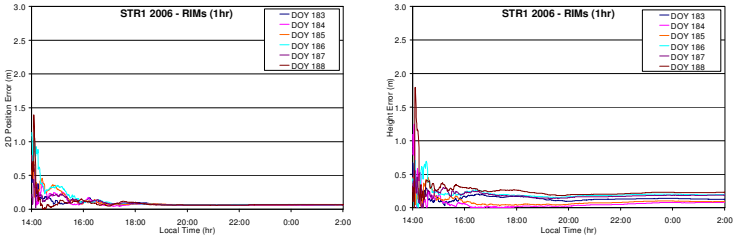

- **HOB2** – 2006 – No Ionospheric Corrections

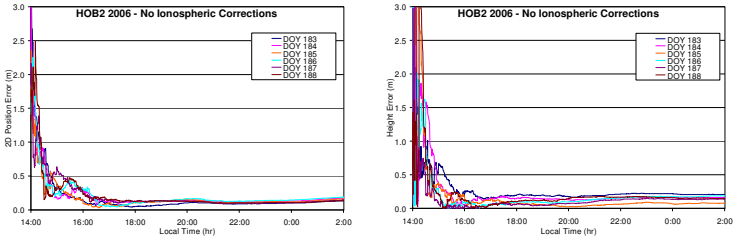

- **HOB2** – 2006 – Broadcast model

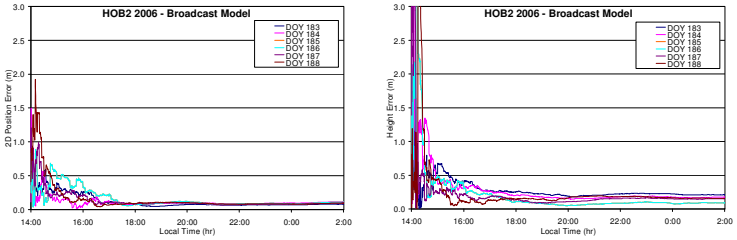

- **HOB2** – 2006 – *Rapid* GIMs

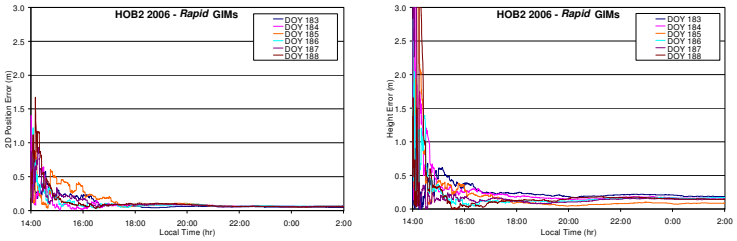

- **HOB2** – 2006 – *Final* GIMs

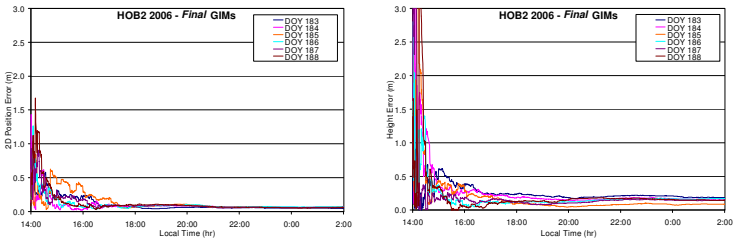

- **HOB2** – 2006 – RIMs

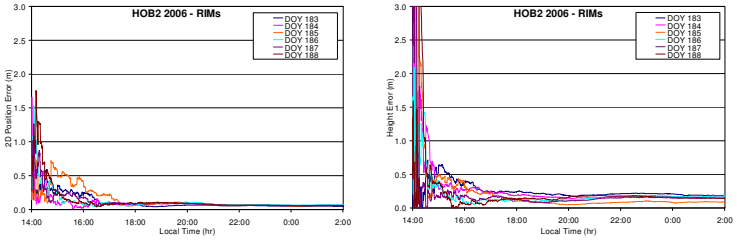

- **HOB2** – 2006 – RIMs (1hr)

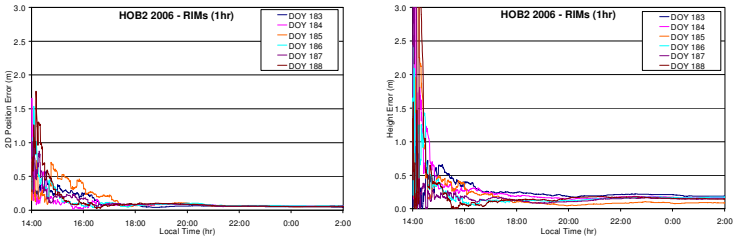

Appendix C: Different IGS Satellite Orbit and Clock Corrections – Point Positioning Errors and Statistical Results

- **DARW** – Broadcast Satellite Orbits and Clocks (code observations)

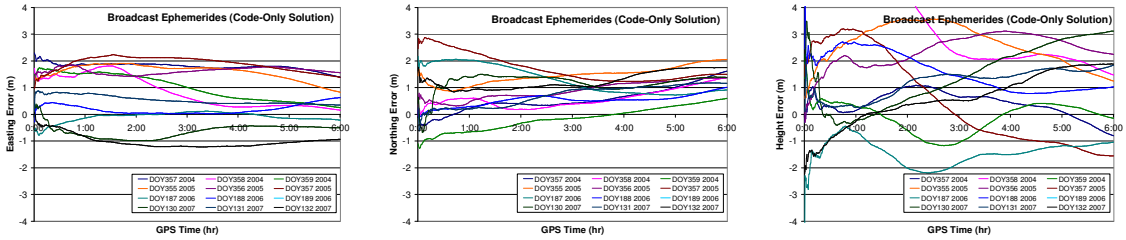

- **DARW** – Broadcast Satellite Orbits and Clocks

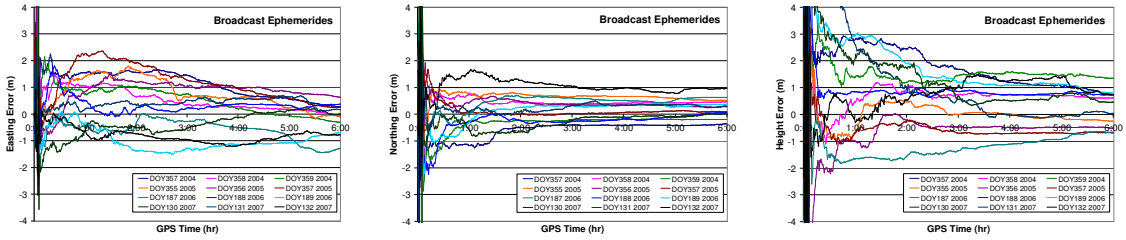

- **DARW** – IGS *Ultra-Rapid (Predicted Half)* Satellite Orbits and Clocks

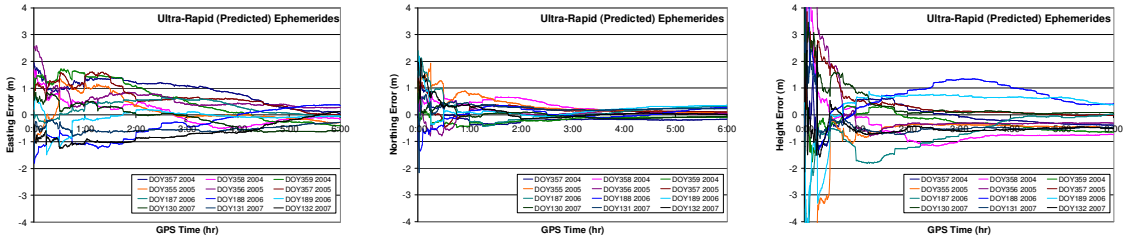

- **DARW** – IGS *Ultra-Rapid (Estimated Half)* Satellite Orbits and Clocks

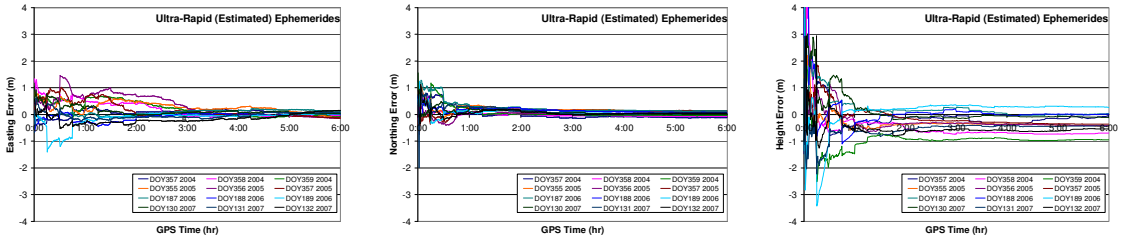

- **DARW** – IGS *Rapid* Satellite Orbits and Clocks

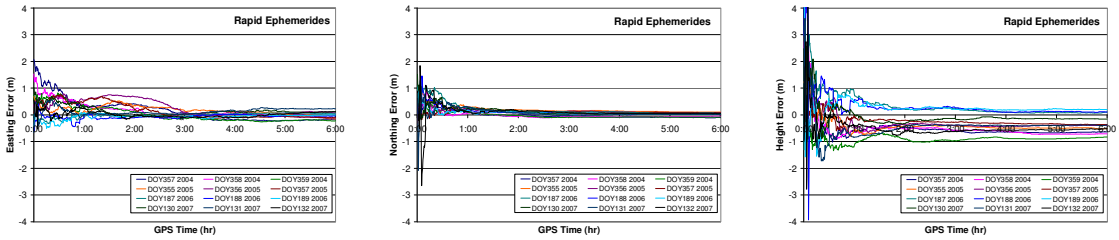

- **DARW** – IGS *Final* Satellite Orbits and Clocks

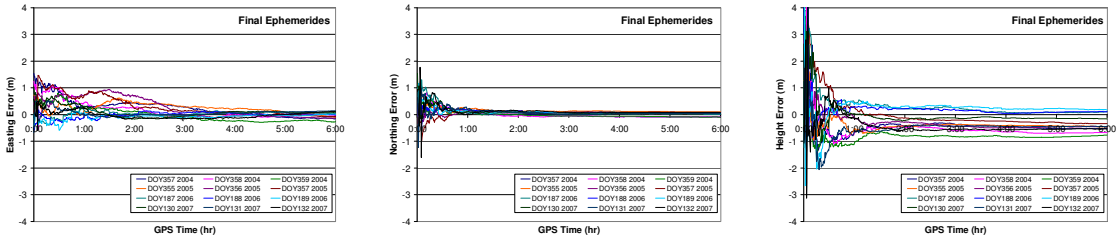

- **TOW2** – Broadcast Satellite Orbits and Clocks (code observations)

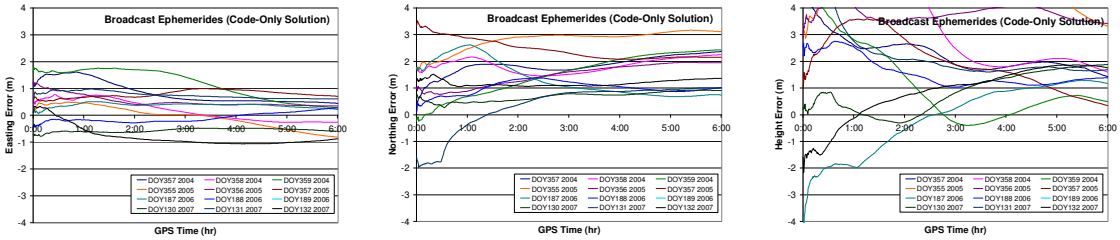

- **TOW2** – Broadcast Satellite Orbits and Clocks

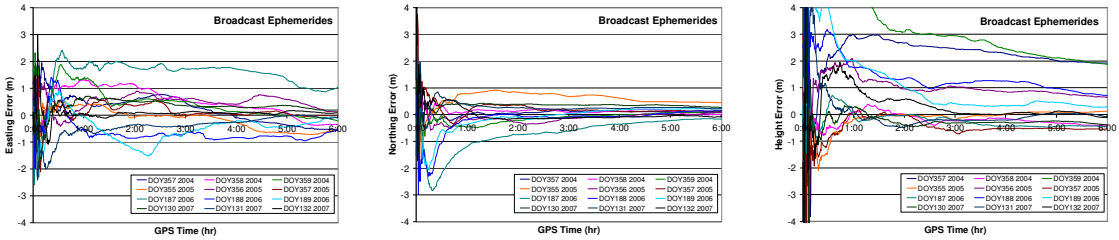

- **TOW2** – IGS *Ultra-Rapid (Predicted Half)* Satellite Orbits and Clocks

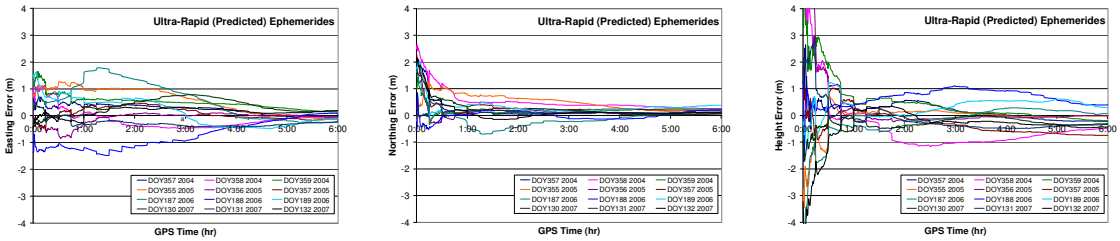

- **TOW2** – IGS *Ultra-Rapid (Estimated Half)* Satellite Orbits and Clocks

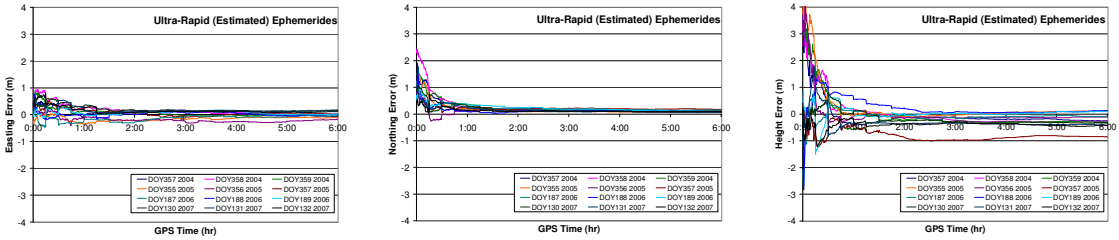

- **TOW2** – IGS *Rapid* Satellite Orbits and Clocks

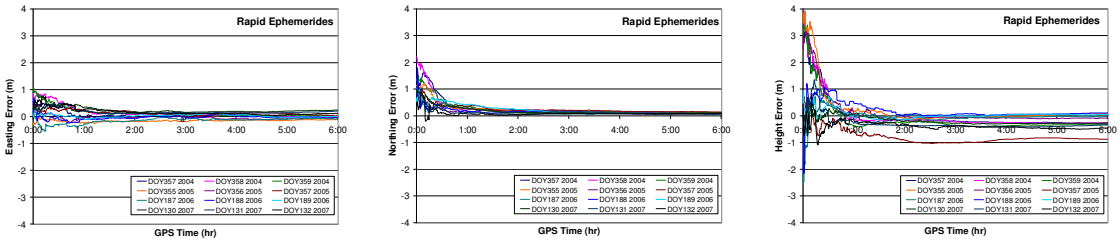

- **TOW2** – IGS *Final* Satellite Orbits and Clocks

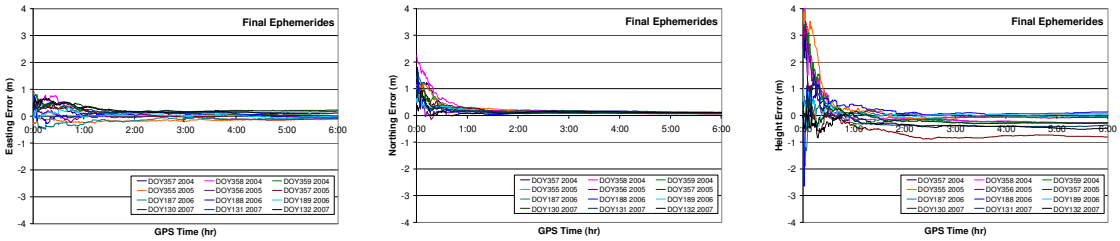

- **ALIC** – Broadcast Satellite Orbits and Clocks (code observations)

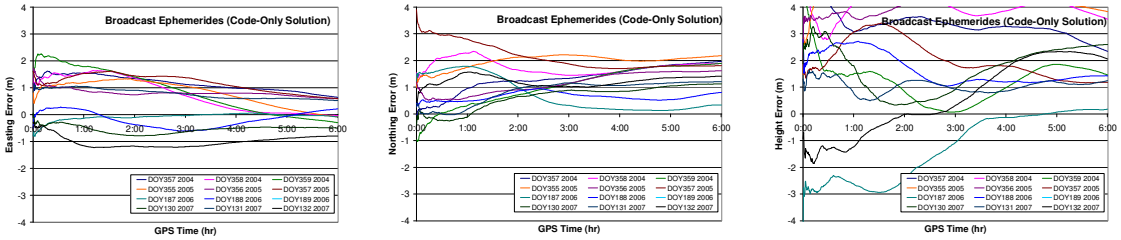

- **ALIC** – Broadcast Satellite Orbits and Clocks

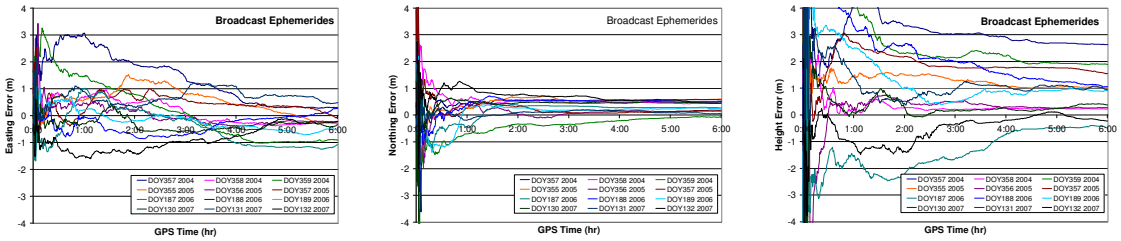

- **ALIC** – IGS *Ultra-Rapid (Predicted Half)* Satellite Orbits and Clocks

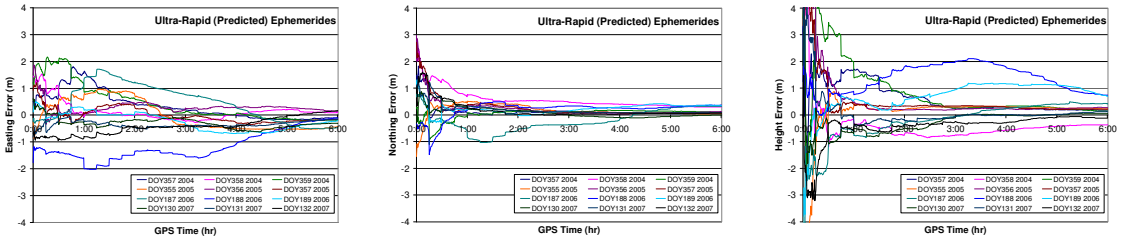

- **ALIC** – IGS *Ultra-Rapid (Estimated Half)* Satellite Orbits and Clocks

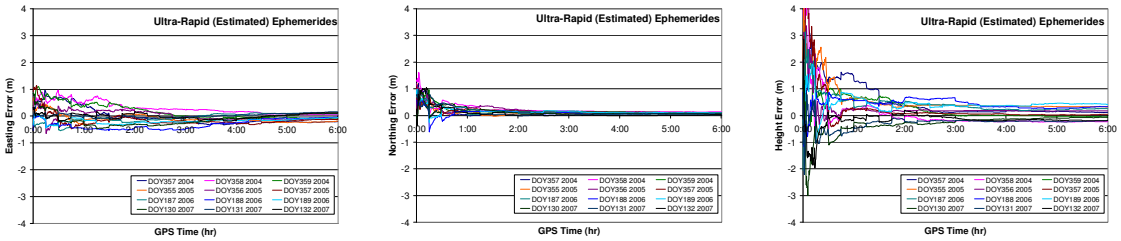

- **ALIC** – IGS *Rapid* Satellite Orbits and Clocks

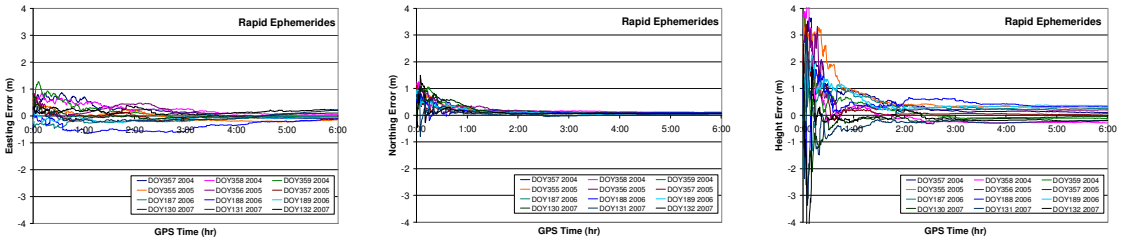

- **ALIC** – IGS *Final* Satellite Orbits and Clocks

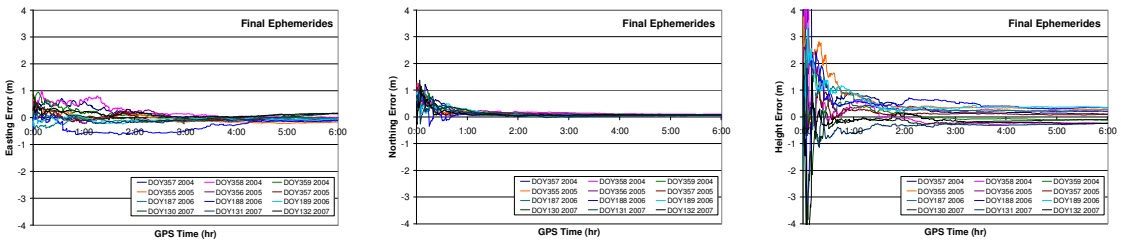

- **STR1** – Broadcast Satellite Orbits and Clocks (code observations)

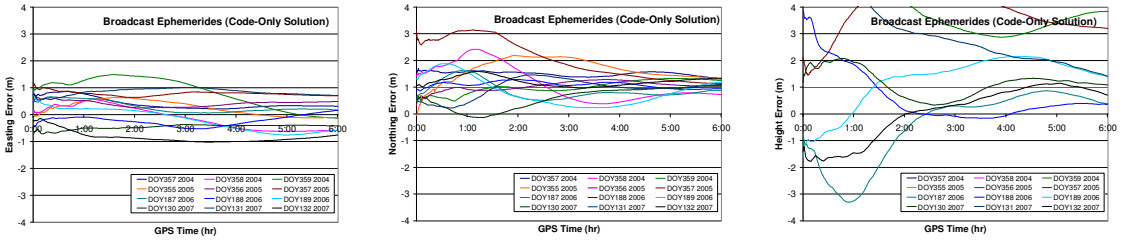

- **STR1** – Broadcast Satellite Orbits and Clocks

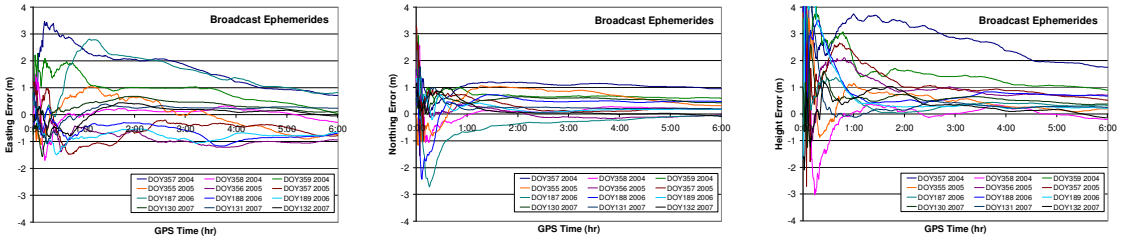

- **STR1** – IGS *Ultra-Rapid (Predicted Half)* Satellite Orbits and Clocks

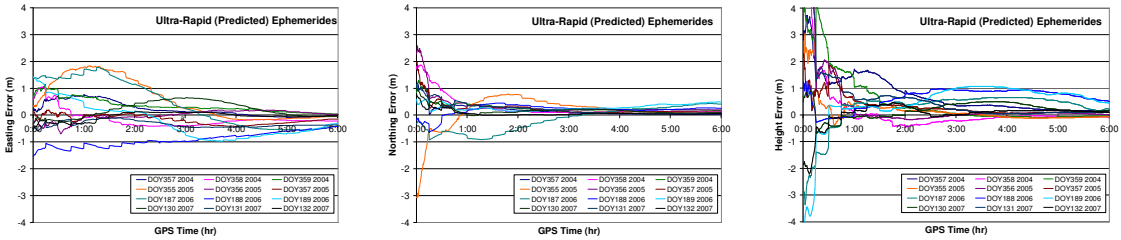

- **STR1** – IGS *Ultra-Rapid (Estimated Half)* Satellite Orbits and Clocks

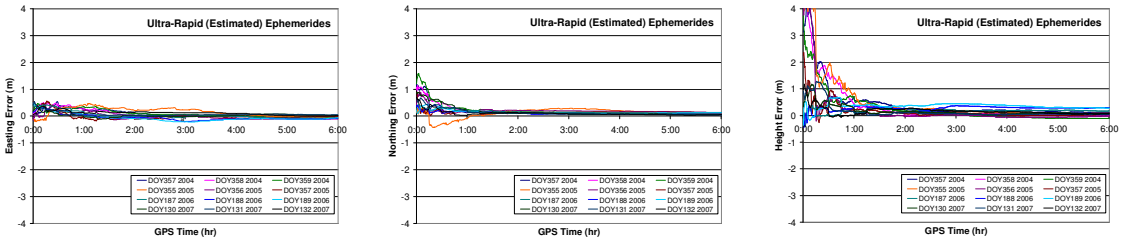

- **STR1** – IGS *Rapid* Satellite Orbits and Clocks

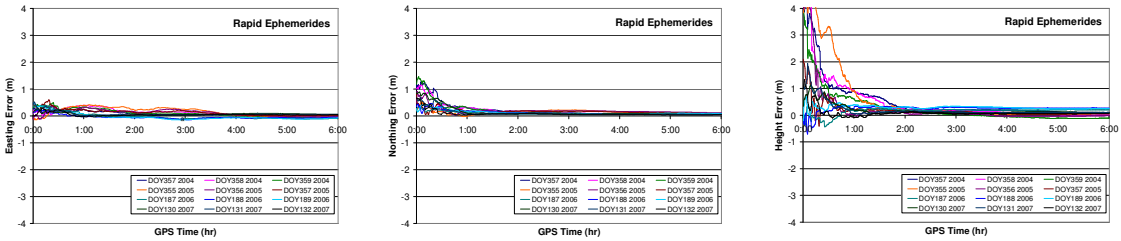

- **STR1** – IGS *Final* Satellite Orbits and Clocks

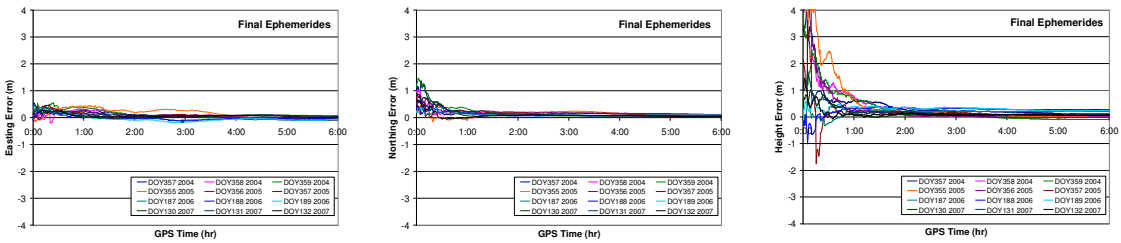

- **HOB2** – Broadcast Satellite Orbits and Clocks (code observations)

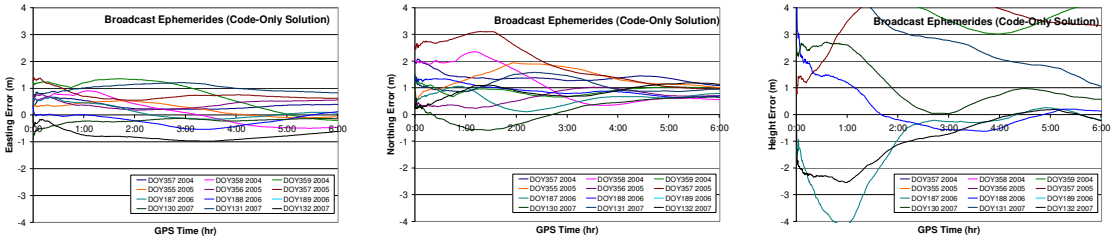

- **HOB2** – Broadcast Satellite Orbits and Clocks

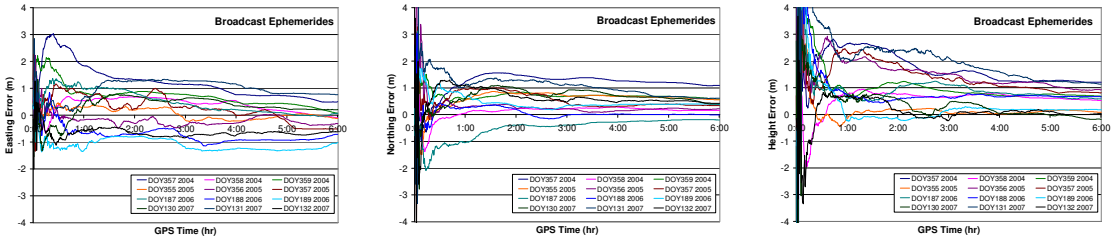

- **HOB2** – IGS *Ultra-Rapid (Predicted Half)* Satellite Orbits and Clocks

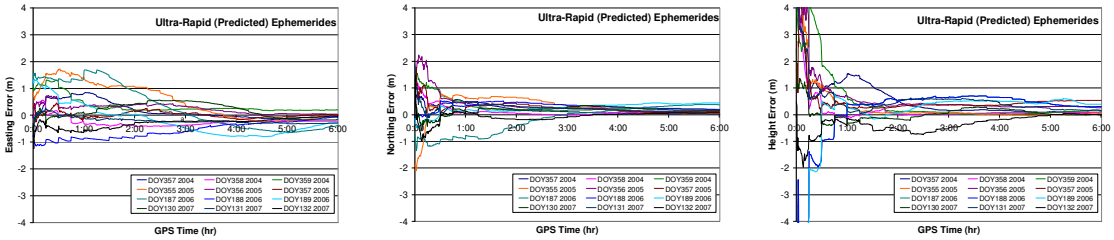

- **HOB2** – IGS *Ultra-Rapid (Estimated Half)* Satellite Orbits and Clocks

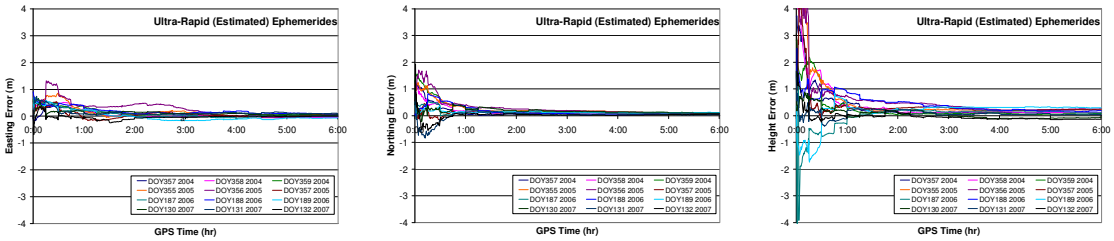

- **HOB2** – IGS *Rapid* Satellite Orbits and Clocks

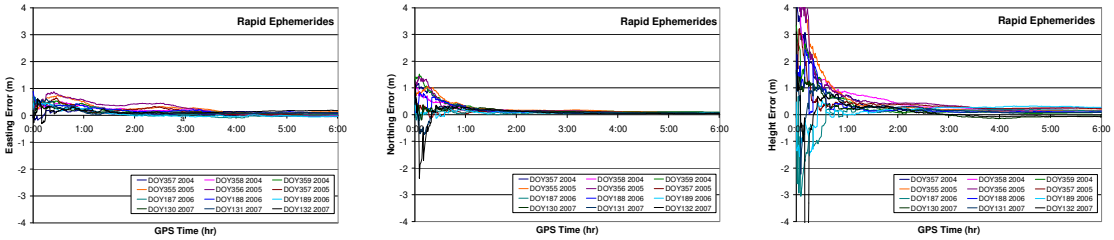

- **HOB2** – IGS *Final* Satellite Orbits and Clocks

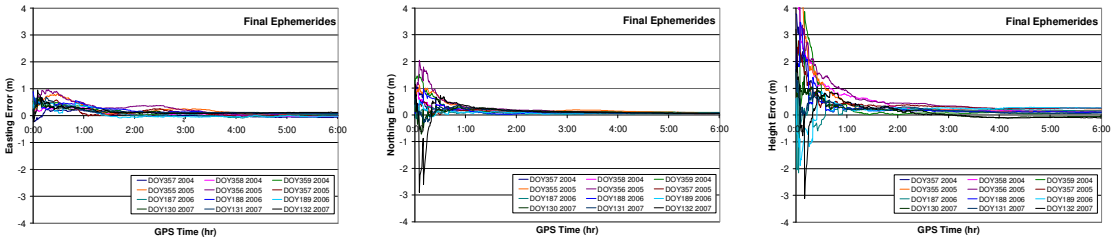

DARW		Mean (m)	RMS (m)
Broadcast Orbit & Clock (code only)	**East**	0.65	1.01
	North	0.89	1.01
	Height	1.09	1.68
Broadcast Orbit & Clock	**East**	0.25	0.86
	North	0.16	0.59
	Height	0.62	1.55
IGS *Ultra-Rapid (Predicted Half)* Orbit & Clock	**East**	0.12	0.62
	North	0.10	0.31
	Height	-0.11	0.94
IGS *Ultra-Rapid (Estimated Half)* Orbit & Clock	**East**	0.08	0.26
	North	0.09	0.18
	Height	-0.16	0.65
IGS *Rapid* Orbit & Clock	**East**	0.09	0.24
	North	0.09	0.18
	Height	-0.25	0.56
IGS *Final* Orbit & Clock	**East**	0.11	0.26
	North	0.08	0.16
	Height	-0.23	0.58

TOW2		Mean (m)	RMS (m)
Broadcast Orbit & Clock (code only)	**East**	0.26	0.63
	North	1.44	1.55
	Height	2.12	2.48
Broadcast Orbit & Clock	**East**	0.17	0.64
	North	0.04	0.41
	Height	0.69	1.29
IGS *Ultra-Rapid (Predicted Half)* Orbit & Clock	**East**	0.12	0.48
	North	0.21	0.36
	Height	0.01	0.72
IGS *Ultra-Rapid (Estimated Half)* Orbit & Clock	**East**	0.04	0.17
	North	0.19	0.26
	Height	-0.12	0.51
IGS *Rapid* Orbit & Clock	**East**	0.06	0.17
	North	0.19	0.27
	Height	-0.10	0.49
IGS *Final* Orbit & Clock	**East**	0.07	0.17
	North	0.17	0.24
	Height	-0.09	0.44

ALIC		Mean (m)	RMS (m)
Broadcast Orbit & Clock (code only)	**East**	0.38	0.79
	North	1.18	1.28
	Height	2.03	2.47
Broadcast Orbit & Clock	**East**	0.11	0.74
	North	0.27	0.50
	Height	1.08	1.78
IGS *Ultra-Rapid (Predicted Half)* Orbit & Clock	**East**	-0.07	0.56
	North	0.17	0.36
	Height	0.29	0.95
IGS *Ultra-Rapid (Estimated Half)* Orbit & Clock	**East**	-0.04	0.23
	North	0.14	0.20
	Height	0.20	0.56
IGS *Rapid* Orbit & Clock	**East**	0.01	0.22
	North	0.14	0.21
	Height	0.20	0.60
IGS *Final* Orbit & Clock	**East**	-0.01	0.19
	North	0.13	0.19
	Height	0.20	0.58

STR1		Mean (m)	RMS (m)
Broadcast Orbit & Clock (code only)	**East**	0.16	0.56
	North	1.16	1.23
	Height	2.96	3.34
Broadcast Orbit & Clock	**East**	0.14	0.80
	North	0.32	0.52
	Height	0.86	1.18
IGS *Ultra-Rapid (Predicted Half)* Orbit & Clock	**East**	-0.01	0.49
	North	0.19	0.35
	Height	0.36	0.82
IGS *Ultra-Rapid (Estimated Half)* Orbit & Clock	**East**	0.04	0.14
	North	0.15	0.20
	Height	0.26	0.51
IGS *Rapid* Orbit & Clock	**East**	0.06	0.13
	North	0.15	0.20
	Height	0.28	0.55
IGS *Final* Orbit & Clock	**East**	0.06	0.13
	North	0.14	0.19
	Height	0.27	0.52

HOB2		Mean (m)	RMS (m)
Broadcast Orbit & Clock (code only)	**East**	0.19	0.53
	North	0.97	1.06
	Height	2.75	3.35
Broadcast Orbit & Clock	**East**	0.15	0.71
	North	0.49	0.70
	Height	0.95	1.33
IGS *Ultra-Rapid (Predicted Half)* Orbit & Clock	**East**	0.02	0.45
	North	0.18	0.35
	Height	0.24	0.92
IGS *Ultra-Rapid (Estimated Half)* Orbit & Clock	**East**	0.10	0.19
	North	0.15	0.23
	Height	0.26	0.56
IGS *Rapid* Orbit & Clock	**East**	0.15	0.20
	North	0.14	0.22
	Height	0.30	0.65
IGS *Final* Orbit & Clock	**East**	0.13	0.20
	North	0.14	0.22
	Height	0.30	0.56